Tampere University

SANNA PITKÄNEN

In Vitro and *in Vivo* Osteogenesis and Vasculogenesis in Synthetic Bone Grafts

SANNA PITKÄNEN née HUTTUNEN

In Vitro and *in Vivo*
Osteogenesis and
Vasculogenesis
in Synthetic Bone Grafts

ACADEMIC DISSERTATION
To be presented, with the permission of
the Faculty of Medicine and Health Technology
of Tampere University,
for public discussion in the Lecture room F114
of the Arvo building, Arvo Ylpön katu 34, Tampere,
on 31 January 2020, at 12 o'clock.

ACADEMIC DISSERTATION
Tampere University, Faculty of Medicine and Health Technology
Finland

Responsible supervisor and Custos	Associate Professor Susanna Miettinen Tampere University Finland	
Supervisor	Docent Suvi Haimi University of Helsinki Finland	
Pre-examiners	Professor Catherine Picart University Grenoble Alpes France	Associate Professor Marco Helder VU University Medical Center The Netherlands
Opponent	Professor Pekka Vallittu University of Turku Finland	

The originality of this thesis has been checked using the Turnitin OriginalityCheck service.

Copyright ©2020 author

Cover design: Roihu Inc.

To my dearest Lilja and Sara,

you can do anything you set your mind to

ACKNOWLEDGEMENTS

ABSTRACT

Bone tissue is the second most common tissue transplant after blood transfusion and as people age, the need for bone transplants is expected to rise even more. Despite the great efforts in biomaterial research and development, autologous bone remains the benchmark among bone grafts whereas synthetic bone grafts are still less-used. Effective and reliable development of synthetic bone grafts require efficient cellular assessments *in vitro* including the evaluation of osteogenic as well as vasculogenic potential of the scaffolds. Adult stem cells, including human adipose stem cells (hASCs) and human bone marrow stem cells (hBMSCs), provide an excellent tool for this as they have been shown to differentiate to bone-forming cells and endothelial cells. However, efficient and cost-effective approaches to induce osteogenic and endothelial differentiation are still needed. This thesis focuses on the study and development of *in vitro* differentiation strategies for hASCs and hBMSCs in 3-dimensional (3D) culture in order to study and verify the feasibility of novel bone substitute materials.

Firstly, two clinically used synthetic bone graft scaffolds, BoneCeramic composed of biphasic calcium phosphate and BioRestore composed of bioactive glass (BaG), were compared in hASC culture and, the effectiveness of commonly used growth factors bone morphogenetic protein (BMP)-2, BMP-7 and vascular endothelial growth factor (VEGF) on hASC osteogenesis were compared to OM. As ceramics are hard and brittle making them difficult to implant and undesirable to load-bearing sites, an elastic β-tricalciumphosphate/poly(L-lactide-co-ε-caprolactone) (β-TCP/PLCL) composite was developed using supercritical CO_2 (scCO$_2$) foaming. The capacity of the composites to support hASC osteogenesis and vasculogenesis were studied *in vitro* in hASC culture and *in vivo* in rabbit femur defect. Finally, 3D printed polycaprolactone (PCL)/copper-doped BaG composites were developed and their osteogenic and vasculogenic potential was studied *in vitro* in hBMSC culture and in a co-culture of hBMSCs and human umbilical vein endothelial cells (HUVECs).

The two biomaterial scaffolds BoneCeramic and BioRestore demonstrated differential effects on hASCs: BoneCeramic induced ALP activity and collagen production of hASCs, while BioRestore stimulated hASC proliferation. In

comparison to the growth factors, OM was more effective in the osteogenic differentiation of hASCs *in vitro* in BoneCeramic and BioRestore. On the other hand, combining the growth factors with OM did not sensitize hASCs to the growth factors.

The β-TCP/PLCL composites supported the viability, proliferation and osteogenic differentiation of hASCs reliably *in vitro*. When studying the osteogenic and endothelial differentiation of hASCs in β-TCP/PLCL composites, hASCs differentiated towards both lineages when cultured in endothelial medium (EM) although the differentiation was left in a premature state. Culture in a cocktail medium of OM and EM supported osteogenic but not endothelial differentiation of hASCs. The *in vivo* study confirmed biocompatibility as well as osteoconductivity of the composite as no inflammation, fibrous tissue or cyst formation was detected and, native bone tissue was able to grow on and in the β-TCP/PLCL composite already at 4 weeks.

In the evaluation of 3D printed PCL/BaG-Cu composites, copper was observed to have a dose-dependent cytotoxic effect on hBMSCs *in vitro*. The PCL/BaG composite induced hBMSC osteogenesis while the addition of copper in BaG had an inhibiting effect on the osteogenic differentiation of hBMSCs. In co-culture of hBMSCs and HUVECs, both PCL/BaG and PCL/BaG-Cu scaffolds supported tubule formation, but the added copper did not boost the vasculogenic effect of the composite.

In conclusion, OM was shown to be a cost-effective osteogenic stimulant in 3D culture as compared to exogenously added growth factors. The feasibility of the scCO$_2$ foamed β-TCP/PLCL composite as potential a bone graft for clinical use was evidenced *in vitro* and *in vivo*. The 3D printed PCL/BaG composite showed promise in supporting osteogenesis *in vitro* whereas the addition of copper hindered the osteogenic effect of the composite. Both PCL/BaG and PCL/BaG-Cu composites supported tubule formation in hBMSC+HUVEC co-culture but the copper did not induce the vasculogenic effect of the composite. To conclude, the elastic and bioactive synthetic polymer -based composites consisting osteoconductive ceramics are highly promising alternatives for synthetic bone grafts when compared to hard ceramics.

TIIVISTELMÄ

Luukudos on heti veren jälkeen maailman käytetyin kudossiirre ja väestön ikääntyessä luusiirteiden tarpeen odotetaan nousevan nykyisestä. Mittavista panostuksista huolimatta biomateriaalikehityksessä ja -tutkimuksessa, potilaiden hoidossa synteettisiä luusiirteitä käytetään huomattavasti vähemmän kuin autologisia luusiirteitä. Uusien synteettisten luusiirteiden kehityksessä tarvitaan tehokkaita ja luotettavia soluviljelymenetelmiä arvioimaan materiaalien kykyä tukea luun ja verisuonien muodostumista. Aikuisen kantasolut, kuten rasvakudoksen ja luuytimen kantasolut, jotka pystyvät erilaistumaan sekä luusoluiksi, että verisuonten endoteelisoluiksi, ovat erinomainen työkalu tähän tarkoitukseen. Toimivia ja kustannustehokkaita menetelmiä luu- ja endoteelierilaistukseen täytyy kuitenkin vielä kehittää. Tämä väitöskirjassa tutkitaan strategioita aikuisen kantasolujen erilaistukseen 3-ulotteisessa ympäristössä, jotta uusien synteettisten luusiirteiden soveltuvuutta voidaan arvioida luotettavasti.

Kahta kliinisessä käytössä olevaa synteettistä luusiirremateriaalia (BoneCeramic kalsiumfosfaatti ja BioRestore bioaktiivinen lasi) verrattiin rasvakudoksen kantasoluviljelmissä. Samalla tutkittiin yleisesti käytettyjen kasvutekijöiden luun morfogeneettisten proteiinien (BMP)-2, BMP-7 ja verisuonen endoteelin kasvutekijän (VEGF) tehokkuutta rasvakudoksen kantasolujen luuerilaistuksessa. Koska kovien ja hauraiden keraamien istuttaminen siirrekohtaan leikkauksen aikana on vaikeaa ja ne sopivat huonosti kuormaakantaviin kohtiin, tutkimuksessa kehitettiin elastinen β-trikalsiumfosfaatti/poly(L-laktidi-ko-ε-kaprolaktoni) (β-TCP/PLCL) komposiitti hyödyntäen ylikriittistä hiilidioksidi prosessointia. Näiden komposiittien kykyä tukea luun ja verisuonten muodostumista tutkittiin sekä rasvakudoksen kantasoluviljelmissä, että kanin reisiluun puutoksessa. Seuraavaksi kehitettiin 3D tulostuksen avulla polykaprolaktoni (PCL)/bioaktiivinen lasi-kupari –komposiitti, jonka soluyhteensopivuutta sekä kykyä tukea luun ja verisuonten muodostumista tutkittiin luuytimen kantasolujen viljelyssä sekä luuytimen kantasolujen ja napanuoran endoteelisolujen yhteisviljelyssä.

BoneCeramic kalsiumfosfaatti ja BioRestore bioaktiivinen lasi vaikuttivat eri tavalla rasvakudoksen kantasoluihin: kalsiumfosfaattirakeet lisäsivät luuerilaistumista, kun taas bioaktiivinen lasi stimuloi solujen jakautumista.

Luuerilaistusliuos oli merkittävästi tehokkaampi luuerilaistaja verrattuna kasvutekijöihin rasvakudoksen kantasolujen erilaistuksessa. Rasvakudoksen kantasolut eivät herkistyneet kasvutekijöille myöskään silloin, kun kasvutekijät yhdistettiin luuerilaistuliuokseen.

Kehitetyt β-TCP/PLCL komposiitit tukivat rasvakudoksen kantasolujen elinkykyä, jakautumista ja luuerilaistumista. Rasvakudoksen kantasolut kykenivät erilaistumaan sekä luu- että endoteelisolujen suuntaan komposiiteilla, kun niitä viljeltiin endoteelierilaistusliuoksessa, mutta erilaistuminen jäi vaillinaiseksi. Luu- ja endoteelierilaistusliuosten sekoituksen näytettiin tukevan solujen luu- mutta ei endoteelierilaistumista. Kun komposiitti istutettiin kanin reisiluun puutokseen, luukudoksen todettiin kasvavan komposiitin pinnalla ja sen sisällä jo 4 viikkoa istutuksen jälkeen. Lisäksi se ei aiheuttanut tulehdusta tai saanut aikaan sidekudoksen tai kystien muodostusta.

Kasvavalla kuparipitoisuudella huomattiin olevan sytotoksinen vaikutus luuytimen kantasoluihin, kun soluja viljeltiin PCL/bioaktiivinen lasi-kupari komposiiteilla. PCL/bioaktiivinen lasi komposiitti tuki hyvin luuerilaistumista, kun taas kuparin lisääminen heikensi komposiitin luun muodostuskykyä. Molemmat komposiitit tukivat verisuonirakenteiden muodostumista luuytimen kantasolujen ja napanuoran endoteelisolujen yhteisviljelyssä; kuparilla ei huomattu olevan merkittävää vaikutusta verisuonittumiseen.

Yhteenvetona luuerilaistusliuos on tehokkaampi luuerilaistaja 3-ulotteisessa ympäristössä kuin yleisesti käytetyt kasvutekijät rasvakudoksen kantasoluille. Huokoinen β-TCP/PLCL komposiitti on lupaava synteettinen luusiirre, sillä se on kudosyhteensopiva, luunkasvua johtava ja sitä on helppo käyttää ja muokata leikkauksen aikana. Lisäksi komposiitti tukee rasvakudoksen kantasolujen endoteelierilaistumista, kun niitä viljellään endoteelierilaistusliuoksessa, mutta solujen erilaistus ei kehity kypsien endoteelisolujen tasolle 3 viikon erilaistuksen aikana. Tulostettu PCL/bioaktiivinen lasi komposiitti tukee luuerilaistumista sekä verisuonittumista, mutta kuparin lisääminen komposiittiin heikentää luuerilaistumista eikä paranna verisuonittumista. Tämä tutkimus osoittaa, että yhdistämällä luunkasvua johtavia keraameja synteettisiin polymeereihin voidaan luoda hyvin lupaavia, elastisia synteettisiä luusiirremateriaaleja verrattuna koviin keraameihin.

CONTENTS

List of Figures

List of Tables

ABBREVIATIONS

ALP	alkaline phosphatase
ASC	adipose stem cell
ATMP	advanced therapeutic medicinal product
BaG	bioactive glass
BCP	biphasic calcium phosphate
BM	basic medium
BMSC	bone marrow stem cell
BMP	bone morphogenetic protein
BTE	bone tissue engineering
CaP	calcium phosphate
CD	cluster of differentiation
CE	Conformité Européenne (CE mark)
COL-1	collagen type 1
DLx5	distal-less homeobox 5
DMEM	Dulbeccos's modified Eagle's medium
EBM-2	endothelial basal medium-2
EC	endothelial cell
ECM	extracellular matrix
EEA	European Economic Area
EGF	endothelial growth factor
EGM-2	endothelial growth medium 2
EM	endothelial medium
EMA	the European Medical Agency
EU	European Union
FBS	fetal bovine serum
FDA	U.S. Food and Drug Administration
FGF-2	fibroblast growth factor 2
HA	hydroxyapatite
hASC	human adipose stem cell
hBMSC	human bone marrow stem cell

hMSC	human mesenchymal stem cell
Hif-1α	hypoxia inducible factor-1 alpha
HUVEC	human umbilical vein endothelial cell
HS	human serum
IGF	insulin growth factor
iPSC	induced pluripotent stem cell
ISCT	International Society for Cellular Therapy
microRNA	micro ribonucleic acid
mRNA	messenger ribonucleic acid
MSC	mesenchymal stem cell
OCN	osteocalcin
OM	osteogenic medium
OSX	osterix
PCL	polycaprolactone
PECAM-1	platelet endothelial cell adhesion molecule-1
PLA	polylactide
PLCL	poly(L-lactide-co-ε-caprolactone)
qRT-PCR	quantitative real-time polymerase chain reaction
RPLP0	acidic ribosomal phosphoprotein large P0
RT	room temperature
Runx2	runt-related transcription factor 2
SD	standard deviation
SBF	simulated body fluid
SMAD	mothers against decapentaplegic homolog protein
scCO$_2$	supercritical CO$_2$
SVF	stromal vascular fraction
TCP	tricalcium phosphate
U.S.	United States
VEGF	vascular endothelial growth factor
VEGFR-2	vascular endothelial growth factor receptor-2
VEGFR3	vascular endothelial growth factor receptor-3
vWF	von Willebrand factor
2D	2-dimensional
3D	3-dimensional
β-TCP	β-tricalcium phosphate

ORIGINAL PUBLICATIONS

This thesis is based on the following original publications referred to in the text by their Roman numbers (I-IV):

Publication I   Tirkkonen L., Haimi S., **Huttunen S.**, Wolff J., Pirhonen E., Sándor G.K., Miettinen S. Osteogenic medium is superior to growth factors in differentiation of human adipose stem cells towards bone forming cells in 3D culture. European Cells and Materials 2013; 25, 144-158.

Publication II   **Pitkänen S.**, Paakinaho K., Vuornos K., Poot A., Leijiten J., Grijpma D., Seppänen-Kaijansinkko R., Kääriäinen M., Kellomäki M., Miettinen S., Kyllönen L.*, Haimi S*. Engineering pre-vascularized bone grafts with adipose stem cells and supercritical carbon dioxide processed composites. *submitted.*

Publication III   **Pitkänen S.**, Paakinaho K., Pihlman H., Ahola N., Hannula M., Asikainen S., Manninen M., Morelius M., Keränen P., Hyttinen J., Kellomäki M., Laitinen-Vapaavuori O., Miettinen S. Characterisation and *in vitro* and *in vivo* evaluation of supercritical-CO_2-foamed β-TCP/PLCL composites for bone applications. European Cells and Materials 2019; 38, 35-55.

Publication IV   Wang X.*, Zhang B.*, **Pitkänen S.***, Ojansivu M., Xu C., Hannula M., Hyttinen J., Miettinen S., Hupa L., Wallace G. 3D scaffolds of PCL/copper-doped bioactive glass: architecture engineering with additive manufacturing and cellular assessments in a co-culture of hBMSCs and endothelial cells. ACS Biomaterials Science & Engineering 2019.

* These authors contributed equally

1 INTRODUCTION

Bone tissue engineering (BTE) is a field of science aiming to create constructs that mimic natural bone tissue and integrate into the skeletal system without conflict allowing and promoting the bone regeneration process. BTE combines biomaterials, cells and signaling molecules to produce constructs that restore, maintain or improve damaged bone tissue. Hence, BTE is a multidisciplinary area of research combining biomaterial engineering, cell biology and medicine. Bone is the second most transplanted tissue worldwide and a bone graft or a bone substitute is used in over 4 million operations annually to treat bone defects (Turnbull *et al.*, 2017). Despite the numerous studies presenting potential scaffold materials and applications during the last few decades, markedly few of them have advanced in to clinical use (de Misquita *et al.*, 2016; Mishra *et al.*, 2016).

Autologous bone transplants remain the gold standard in orthopedic surgeries as they do not cause immune reactions and they have ideal properties to induce bone formation in the defect site (Amini *et al.*, 2012). Autograft is usually harvested from iliac crest, requiring a secondary surgical site and resulting in notable donor site injury, deformity and scarring. However, the amount of autograft bone is limited and there are risks related to the harvesting surgery, such as infection and chronic pain (Freeman & McNamara, 2017; Mishra *et al.*, 2016; Amini *et al.*, 2012). Therefore, autografts are an expensive choice for a bone transplant as well as an unattractive choice for the patient. Allografts on the other hand are donor tissues usually received from cadavers and they are the second most used bone transplants (Amini *et al.*, 2012). Allograft bone is abundantly available in different forms yet its use is hindered by immune reactions, infections, disease transmission and weakened osteoinductivity (Freeman & McNamara, 2017; Amini *et al.*, 2012; Boyce *et al.*, 1999). Consequently, there is an apparent and growing need for reliable synthetic bone transplants and BTE strategies.

Among synthetic bone grafts, calcium phosphates (CaPs) and bioactive glasses (BaGs) are the most used in treating patients. These ceramic materials can bind to bone tissue and even induce bone formation however, they are hard and brittle (Turnbull *et al.*, 2017), making them difficult to implant and undesirable for load-

bearing sites. Synthetic polymers with excellent mechanical properties on the other hand do not have biological binding sites for bone tissue. Hence, composites combining the characteristics of different material types may be the most promising strategy to produce optimal synthetic bone graft materials.

Adipose and bone marrow stem cells (ASCs and BMSCs) are important tools in BTE when studying the interactions between cells and biomaterial scaffolds. As these cells can differentiate towards multiple cell lineages, including osteogenic and endothelial cell (EC) lineages, in addition to cytocompatibility they allow the evaluation of scaffolds' osteogenic as well as vascular potential *in vitro*. Efficient and reliable osteogenic differentiation is highly relevant to enable the *in vitro* study of engineered bone grafts. Reliable *in vitro* characterization ensures that promising scaffolds proceed to animal studies and on the other hand prevents unnecessary animal studies in case of unsuitable scaffolds. Growth factors, such as bone morphogenetic protein-2 (BMP-2), are expensive but commonly used to induce osteogenic differentiation (Gothard *et al.*, 2014). However, their use in patients has resulted in safety concerns (Carragee *et al.*, 2011) and hence safer and more cost-effective differentiation strategies are needed.

The formation of vascular network is crucial for the bone regeneration and therefore the scaffolds' ability to support vascularization is important. In fact, the lack of vascularization has proved to be a significant challenge in BTE (Rouwkema *et al.*, 2008; Rouwkema & Khademhosseini, 2016). The major problem is that nutrients and oxygen are able to diffuse at most to only at a maximum of 2 mm distance, meaning that cells implanted in larger constructs are left to die after implantation (Antonyshyn *et al.*, 2019; Volz *et al.*, 2016). Moreover, angiogenesis of vessels growing into the construct in the defect site is too slow to keep the implanted cells viable. Therefore, *in vitro* methods for vascularization are needed in large tissue engineered constructs for clinical applications as well as in *in vitro* models aiming to mimic live tissues. In addition, modification of materials by adding vasculogenic components, such as copper, is one option to improve vascularization in synthetic bone grafts (*Wu et al.*, 2013).

This thesis aims to study *in vitro* different cell culture methods and strategies, such as medium compositions and supplements, pre-differentiation strategies and co-culture setups, to achieve more efficient and reliable osteogenic differentiation and vascularization in 3-dimensional (3D) culture. Furthermore, the potential of novel composites for BTE applications are evaluated *in vitro* and *in vivo*. This study provides insight on how the osteogenic differentiation and vascularization processes occur interlinked with different synthetic bone graft materials.

2 LITERATURE REVIEW

2.1 Bone tissue

The understanding of the structure and biology of native bone tissue constitute the basis for the field of BTE. Bone is a dynamic tissue with various functions, such as providing support and protection to our body, enabling moving together with muscles, maintaining mineral homeostasis, and homing the biological elements needed for hematopoiesis. (Amini *et al.*, 2012). The pattern arrangement of bone tissue can be either compact (cortical bone) or trabecular (cancellous bone) with a wide range in mechanical strength and modulus. Moreover, the bone matrix is composed of an organic and inorganic part. The organic part of bone matrix is comprised of cells (osteoblasts, osteocytes, and osteoclasts), collagen (mainly collagen type I (COL-1)), proteins (osteocalcin (OCN), osteonectin, osteopontin, bone morphogenetic proteins (BMPs), bone sialoprotein II (BSP II)) and proteoglycans (Florencio-Silva et al., 2015). The inorganic part on the other hand, consist mostly of CaP minerals. The bone matrix has a profound role in regulating bone cell activity via adhesion molecules such as integrins (Florencio-Silva *et al.*, 2015). The combination of flexible collagen fibres reinforced by hydroxyapatite crystals makes bone a nanocomposite with good compressive strength and high fracture toughness (Amini *et al.*, 2012).

Osteoblasts are derived from BMSCs. The expression of transcription factors runt-related transcription factor-2 (Runx2), distal-less homeobox 5 (Dlx5) and, osterix (OSX) is essential for the osteogenic commitment of BMSCs. Mature osteoblasts synthesize the bone matrix in two phases: first osteoblasts secrete the organic matrix including collagen (mainly type I), osteogenic proteins (such as OCN, osteopontin, BSP II and osteonectin) and proteoglycan (Florencio-Silva *et al.*, 2015). In the mineralization phase osteoblasts first release matrix vesicles containing calcium ions and, these vesicles bind to proteoglycans and other organic matrix elements (Florencio-Silva *et al.*, 2015). Osteoblasts also secrete alkaline phosphatase (ALP) that keeps degrading phosphate containing compounds leading to the release of phosphate ions inside the matrix vesicles, leading to phosphate and calcium ion nucleation inside the vesicles forming hydroxyapatite (HA). Finally, the

supersaturation of these ions causes the rupture of the vesicles and the HA crystals are released into the extracellular matrix (Florencio-Silva *et al.*, 2015). Mature osteoblasts can later either undergo apoptosis or, differentiate into osteocytes or, bone lining cells.

Osteocytes are the most abundant cell type (90-95 %) in bone tissue. Osteocytes are situated inside the bone matrix and once a mature osteocyte has been closed into the bone matrix the expression of typical osteoblast markers is downregulated while the expression of osteocyte markers, such as sclerostin, is induced (Florencio-Silva *et al.*, 2015). Tunnels named canaliculi, forming the osteocyte lacunocanalicular system (Florencio-Silva *et al.*, 2015), connect osteocytes to each other. This system is also connected to blood vessels enabling the transport of nutrients and oxygen as well as cell signaling molecules (Florencio-Silva *et al.*, 2015). Osteocytes have mechanosensitive functions affecting osteoblast-osteocyte bone formation (Florencio-Silva *et al.*, 2015).

Osteoclasts are crucial players in bone remodeling, as they can resorb bone. In contrast to osteoblasts, osteoclasts are differentiated from hematopoietic stem cells by influence of factors secreted by BMSCs, osteoblasts and osteocytes, such as macrophage colony-stimulating factor (M-CSF) and receptor activator of nuclear factor kappa-B (RANK) ligand (Florencio-Silva *et al.*, 2015). In addition to bone resorption, osteoclasts have been shown to have regulatory functions with relation to osteoblasts and even hematopoietic stem cells (Florencio-Silva *et al.*, 2015).

2.1.1   Bone healing

In contrast to any other tissue, bone has an innate capacity to regenerate and heal without the formation of scar tissue. The process of fracture healing can be divided in four overlapping phases (Fig. 1). As bone fractures, the trauma initiates inflammatory response and hematoma formation in the fracture site. The hematoma serves as the initial scaffold for the regeneration process and progenitor and inflammatory cells start to migrate into the fracture site where they are activated. The progenitor cells start to differentiate towards chondrocytes, which are the main players in the formation of cartilaginous soft callus containing mainly collagen and proteoglycans. Angiogenesis begins as blood vessels start to grow into the fracture site. After the formation of cartilaginous soft callus, the chondrocytes begin to undergo apoptosis. Additional progenitor cells are then recruited, and they start to differentiate towards osteoblasts. Osteoblast functions lead to the development of

hard callus formed of woven bone. Meanwhile the regeneration of vascular network continues. At the final stage, the bony callus is reshaped and remodeled by osteoclast-osteoblast activity and, eventually resulting in the original bone structure: cortical and trabecular arrangement with a marrow cavity. (Amini *et al.*, 2012; Runyan & Gabrick, 2017.)
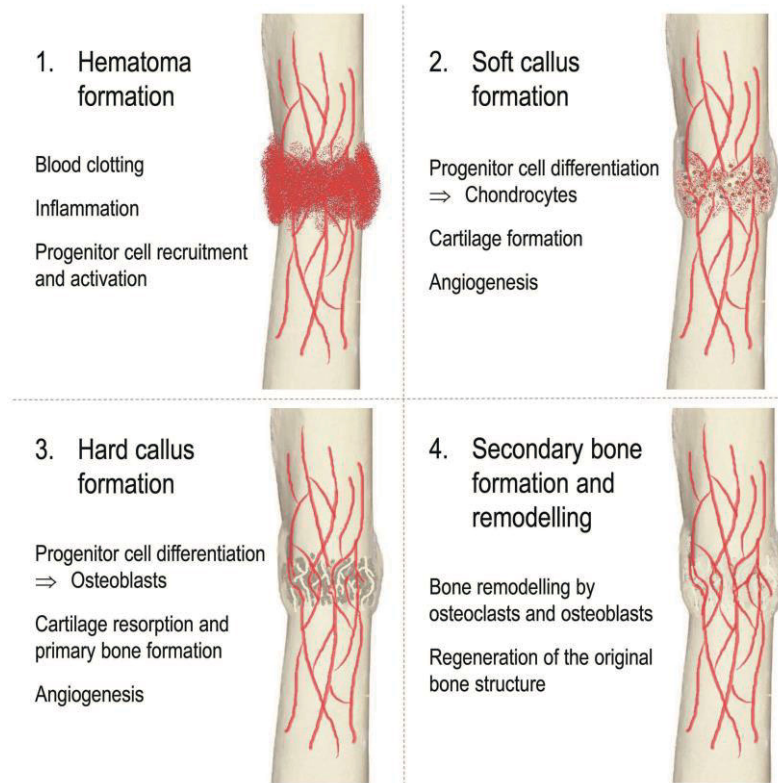
Figure 1. The different stages of bone healing after trauma. (Amini *et al.*, 2012; Runyan & Gabrick, 2017.)

2.2 Vasculogenesis and angiogenesis

In the development of vascularized BTE constructs, it is also important to appreciate the development of vascular networks. Natural vascular networks can form via two different processes: vasculogenesis or angiogenesis (Rouwkema & Khademhosseini, 2016). Vasculogenesis occurs mainly during embryonic development where endothelial progenitor cells differentiate to ECs, which proliferate and organize in a

previously avascular tissue, forming a vascular network (Rouwkema & Khademhosseini, 2016). After extensive trauma, vasculogenesis may also occur in adult tissues, when bone marrow endothelial progenitor cells are recruited to the defect site where they undergo differentiation. However, most of the vascularization and vascular remodeling happen via angiogenesis. In angiogenesis, new vasculature forms from the already existing vessels, which is mainly induced by hypoxia in tissues (Rouwkema & Khademhosseini, 2016). Hypoxic conditions induce the secretion of growth factors and chemokines that stimulate ECs to migrate from the vessel walls to form new capillaries (Rouwkema & Khademhosseini, 2016). Under hypoxic conditions, a proangiogenic transcription factor hypoxia inducible factor-1 alpha (Hif-1α) is activated leading to the activation of numerous proangiogenic genes, such as VEGF (Kütscher *et al.*, 2016). Then, when the oxygen level in the tissue rises, the migration of ECs ceases (Rouwkema & Khademhosseini, 2016). The development of capillaries may continue to arteriogenesis mainly regulated by fluid flow shear stress. Arteriogenesis is a maturation phase where the diameter and wall thickness of the vessels increase (Rouwkema & Khademhosseini, 2016).

2.3   Cells and differentiation in bone tissue engineering

2.3.1   Adult stem cells

Nowadays, many researchers in varying fields have set their hopes on stem cells to provide a treatment or a disease model for their needs. Stem cells are defined as undifferentiated cells that have the capacity to both self-renew and differentiate towards more specialized cell lineages (Choumerianou *et al.*, 2008). Stem cells may be classified according to their origin as embryonic, germinal or, somatic; or according to their differentiation potential as totipotent, pluripotent, multipotent or, unipotent (Choumerianou *et al.*, 2008). A fertilized egg is totipotent with the capacity to differentiate towards all cell types including fetal membranes and placenta. Moreover, pluripotent stem cells can be harvested from the inner cell mass of a blastocyst with the potential to produce cells from all three germ layers (Choumerianou *et al.*, 2008). In addition, pluripotent stem cells can be produced by reprogramming somatic cells into a pluripotent state using different methods, also known as induced pluripotent stem cells (iPSCs). However, while embryonic stem cells and iPSCs have close to an unlimited differentiation potential, their use is

restricted by ethical and political, as well as safety and efficacy issues (Lindroos *et al.*, 2011). Adult stem cells are multipotent stem cells with a limited differentiation capacity, and unipotent stem cells are progenitor cells that only differentiate towards one cell type (Choumerianou *et al.*, 2008).

Mesenchymal stem cells

Adult stem cells are progenitor cells residing in specialized tissues. Mesenchymal stem cells (MSCs) are defined as adult stem cells originating from mesenchymal tissues, such as adipose tissue, bone marrow, skeletal muscle tissue, synovial membranes, dental pulp, cervical tissue, umbilical cord blood, dermal tissue, and lung tissue (Mushahary *et al.*, 2018; Ozkul & Galderisi, 2016). As MSCs lack a specific cell surface marker, the recognition of MSCs during isolation is challenging and inconsistent. In order for more uniform cell characterization, the International Society for Cellular Therapy (ISCT) has generated minimal criteria to identify MSCs: (1) cells must be plastic-adherent in standard culture conditions; (2) cells must express surface markers cluster of differentiation (CD)105, CD73, and CD90, and lack the expression of CD45, CD34, CD14 or CD11b, CD79α or CD19, and HLA-DR and; (3) cells must differentiate into osteoblasts, adipocytes and chondrocytes *in vitro* (Dominici *et al.*, 2006). However, MSCs that meet the above criteria have still been shown to represent a heterogeneous cell population with varying phenotype and functionality (Mo *et al.*, 2016; Mushahary *et al.*, 2018; Strioga *et al.*, 2012; Tormin *et al.*, 2009). Moreover, in some studies a morphologically uniform cell population with uniform surface marker expression has been obtained by long culture period on plastic for several passages most likely effecting the cell properties (Mo *et al.*, 2016).

The differentiation of MSCs is most commonly induced by adding supplements, such as growth factors, into the culture medium. In addition, differentiation can be induced with mechanical signals like vibration loading (Tirkkonen *et al.*, 2011) and stretching (Charoenpanich *et al.*, 2011; Virjula *et al.*, 2017) or, with electrical signals (Björninen *et al.*, 2017). Traditionally MSCs have been considered to differentiate towards mesenchymal cell lineages, such as adipocytes, osteoblasts and chondrocytes. However, MSCs have been shown to differentiate also towards cell lines originating from endo- or ectoderm (Mo *et al.*, 2016), such as pancreatic cells (Chandra *et al.*, 2009), neuronal cells (Zheng *et al.*, 2017) and, ECs (Miranville *et al.*, 2004; Planat-Benard *et al.*, 2004). In addition, MSCs originating from different tissues have presented varying differentiation potential. For instance, ASCs and BMSCs have been demonstrated to differ in differentiation capacity, some studies suggesting

that ASCs differentiate more efficiently towards osteogenic lineage in bioactive glass (BaG) based scaffolds in contrast to BMSCs (Rath *et al.*, 2016), or that ASCs possess better neuronal capacity in comparison to BMSCs (Zheng *et al.*, 2017). However, the culture conditions, differentiation protocols and used biomaterials vary greatly between studies and these elements effect significantly to the fate of these cells (Kyllönen *et al.*, 2013; Strioga *et al.*, 2012). Moreover, Guneta *et al.* (2016) concluded that the microenvironment *in vitro* also guides the differentiation: when ASCs and BMSCs were seeded on adipose tissue (extra cellular matrix (ECM) -coated surface, both cell types differentiated towards adipogenic lineage. However, in a 3-dimensional (3D) environment without biological signals ASCs differentiated towards adipogenic lineage and BMSCs towards osteogenic lineage, suggesting that the cells display an inherent predisposition towards the lineage defined by their native niche (Guneta *et al.*, 2016). In addition, matrix stiffness has been shown to affect human adipose stem cells (hASC) and human BMSC (hBMSC) differentiation (Wen *et al.*, 2014).

Because of the variation between MSCs derived from different tissues there has been debate about the use of the term MSC. Robey (2017) pointed out that not all different MSCs have a common embryonic origin and even though these tissue specific progenitor cells have similar cell surface characteristics, they are not identical. Therefore, it has been suggested that the terminology concerning these cells should be based on the tissue of their origin, such as ASC or BMSC, rather than using the term MSC (Robey, 2017). Regardless of the more limited differentiation potential of MSCs, they have many desirable characteristics, as there are no ethical or political issues related to their isolation and use in contrast to embryonic stem cells and they are more stable and safer in contrast to genetically manipulated iPSCs. Stem cells from adult tissues include a wide range of progenitor cells with different subpopulations expressing varying functionality and phenotype (Mo *et al.*, 2016) therefore providing alternatives for many different applications.

2.3.2 Adipose stem cells

Adipose tissue is a highly active metabolic and endocrine organ of mesodermal origin. Zuk *et al.* (2001) were the first to report that an MSC population later named ASCs can be isolated from the stromal vascular fraction (SVF) based on their ability to attach on plastic. SVF is an aqueous fraction derived from adipose tissue by enzymatic digestion and it contains various cell types, such as pre-adipocytes, ASCs,

ECs and their precursors, macrophages, lymphocytes, smooth muscle cells and pericytes (Bora & Majumdar, 2017; Semon *et al.*, 2013; You *et al.*, 2015). SVF has also attracted attention in the field of regenerative medicine and the advantage in SVF over ASCs lays in the easier acquirement since there is no need for cellular separation. In addition, the more heterogeneous cell population of SVF in contrast to ASCs may be a reason for the better outcomes in comparative animal studies (Bora & Majumdar, 2017; You *et al.*, 2015; Semon *et al.*, 2013). However, the heterogeneous cell population is also a limiting factor as SVF contain cell types known to cause immune reactions and in contrast to ASCs, is therefore suitable only for autologous treatments (Bora & Majumdar, 2017).

Adipose tissue has become a very popular adult stem cell source for research purposes since adipose tissue is an abundant and easily accessible cell source and, can be harvested with minimal donor site morbidity (Bajek *et al.*, 2016; Lindroos *et al.*, 2011). Moreover, the yield of ASCs from an adipose tissue sample can be as high as 34.4 million cells from 100 ml of lipoaspirate (West *et al.*, 2016) and they are stable with minimal chromosomal alterations in *in vitro* culture (Meza-Zepeda *et al.*, 2008). Since clinical treatments usually require a vast number of cells, the high isolation yield and stability in *in vitro* culture make ASCs a promising option also for clinical applications (Bajek *et al.*, 2016).

Adipose stem cell characteristics and culture
ASCs are characterized after isolation usually according to the aforementioned minimal criteria suggested for MSCs by the ISCT (Bourin *et al.*, 2013; Dominici *et al.*, 2006). Shortly, the cells need to attach on plastic and differentiate towards osteogenic, adipogenic and chondrogenic lineages and, the cells need to express a specific surface marker profile. The surface marker profile of ASCs differs slightly from other MSCs; the differences in the surface marker profiles between ASCs and BMSCs, are listed in Table 1. ASCs are positive for markers CD13, CD73, CD90, CD105 and lack the expression of CD11b, CD31, CD45 and, CD106 (Bourin *et al.*, 2013). The expression of CD34 in ASCs varies a lot depending on culture conditions; it is expressed usually in low passage ASCs, the expression declining with continued cell division (Bourin *et al.*, 2013). Markers CD10, CD36 and CD106 can be used in addition to the other markers to better distinguish ASCs from BMSCs, as in contrast to BMSCs, CD10 and CD36 are expressed in ASCs whereas CD106 is not (Bourin *et al.*, 2013). However, similarly to other characteristics of these cells, also the surface marker profile is affected by culture conditions, such as the serum type in the culture medium (Patrikoski *et al.*, 2013).

Another appealing feature in ASCs is their immunomodulatory and immunosuppressing nature. McIntosh and colleagues (2006) demonstrated that ASCs have an immunosuppressive profile *in vitro*, and later ASCs have been shown to be immunosuppressive also *in vivo* (H. Y. Cheng *et al.*, 2014). However, the immunogenicity of ASCs may decrease with passaging of the cells (McIntosh *et al.*, 2006) and with the differentiation of the cells (Niemeyer *et al.*, 2007). Overall, the immunosuppressive nature of ASCs makes these cells good candidates for allogenic cell transplantation (Niemeyer *et al.*, 2008). Allogenic use of ASCs is also supported by the fact that the characteristics, such as proliferation and differentiation capacity, of these cells are significantly affected by donor site variability (Cleal *et al.*, 2017) as well as donor sex (Aksu *et al.*, 2008), age (Alt *et al.*, 2012; Choudhery *et al.*, 2014) and body mass index (Frazier *et al.*, 2013). Therefore, in comparison to autologous treatments, it would be more feasible to select a donor cell line with desirable and well-characterized qualities for the treatment of numerous patients (Patrikoski *et al.*, 2019).

Table 1. A comparison between ASC and BMSC characteristics (Burrow *et al.*, 2017; Vangsness *et al.*, 2015; Bourin *et al.*, 2013).

		Adipose stem cells (ASCs)	Bone marrow stem cells (BMSCs)
Isolated from		stromal vascular fraction (SVF)	bone marrow mononuclear cell fraction
Positive markers	> 70 %	CD10, CD13, CD73, CD90, CD105	CD13, CD73, CD90, CD105
Moderate markers	> 30-70 %	CD36	CD106
	> 2-30 %	CD34, CD106	CD10
Negative markers	< 2 %	CD11b, CD31, CD45, CD106	CD11b, CD34, CD36, CD45
Yield		from 1 mL of tissue: 4 737 - 1 550 000 cells	from 1 mL of tissue: 30 – 317 400 cells
Senescence		reached with higher population doublings	reached with lower population doublings

The culture conditions of ASCs vary between studies, which makes the comparison and translation of results challenging. The ASC expansion conditions need to support the proliferation but not the differentiation of ASCs whereas; the differentiation conditions are designed to induce the desired cell fate effectively. The basic ASC culture medium generally consist of basic medium, such as alpha-modified Eagle's medium (α-MEM) or Dulbecco's modified Eagle's medium/Ham's F12 (DMEM/F-12) with 10 % of serum (Bajek *et al.*, 2016; Patrikoski *et al.*, 2019). Fetal bovine serum (FBS) is widely used in ASC culture however, when the aim is to translate the results to the design of cell therapies, it would be more relevant to use human serum (HS), xeno-free serum or platelet lysate in the culture of human ASCs

(hASCs). In fact, the serum conditions have been shown to affect hASC proliferation and differentiation significantly (Kyllönen *et al.*, 2013; Patrikoski *et al.*, 2013), indicating the importance of choosing a relevant serum type for the purposes of the study. Moreover, when culturing ASCs for cell therapies, all animal-based supplements should be replaced with xeno-free substitutes to avoid infections (Patrikoski *et al.*, 2019).

2.3.3   Bone marrow stem cells

Bone marrow is a soft, semi-solid tissue in the medullary cavities of large bones. Friedenstein and colleagues (1968) were the first to report that in addition to hematopoietic stem cells, bone marrow also contain a stem cell population able to give rise to bone, first referring to these cells as osteogenic progenitor cells. They also demonstrated the basis for mesenchymal stem cell isolation procedure (Friedenstein *et al.*, 1968). The name MSC came to use only in 1991 when Caplan and colleagues (1991) suggested the term based on the differentiation potential of these cells towards multiple mesenchymal cell types.

Bone marrow stem cell characteristics and culture
BMSCs are isolated from bone marrow mononuclear cell fraction, which is harvested in a bone marrow aspiration procedure most commonly from the iliac crest under general anesthesia. This is a painful procedure for the patient with the risk of donor site morbidity. The amount of harvested aspirate is small and the BMSC yield from 1 ml of bone barrow is only 30 – 317 400 cells (Vangsness *et al.*, 2015), which is significantly lower than that of ASCs. Similarly, to ASCs, also BMSCs are characterized after isolation according to the aforementioned criteria set by the ISCT (Bourin *et al.*, 2013; Dominici *et al.*, 2006). The slight differences between ASC and BMSC surface marker expression profiles are presented in Table 1. BMSCs have been shown to be less stable in long time cell culture (Dahl *et al.*, 2008) and reach senescence with lower population doubling number than ASCs (Burrow *et al.*, 2017; Vidal *et al.*, 2012). Burrow and colleagues (2017) compared patient matched hASCs and hBMSCs and demonstrated that although both cell types display deteriorated characteristics in extended *in vitro* culture, hASCs maintain their proliferation and differentiation capacity longer in comparison to hBMSCs. Altogether, hASCs seem to be a more attractive choice for clinical applications when compared to hBMSCs.

However, BMSCs are a highly relevant cell type especially in bone regeneration research, as their native niche is in bone.

Sotiropoulou and colleagues (2006) tested various medium compositions in BMSC culture and concluded that αMEM with 10 % FBS, supplemented with GlutaMAX and fibroblast growth factor-2 (FGF-2), is the most optimal to maintain BMSC proliferation and differentiation capacity during expansion. FGF-2 is used in the BMSC culture to induce proliferation and to maintain differentiation capacity (Sotiropoulou *et al.*, 2006; Tonti & Mannello, 2008). However, FGF-2 supplementation has been evidenced to affect differentiation potential of BMSCs, as it increases osteogenic and slightly adipogenic differentiation capacity of BMSCs (Sotiropoulou *et al.*, 2006). In addition, BMSC characteristics, proliferation and differentiation capacity have been shown to be affected by different serum conditions (Dahl *et al.*, 2008; Tonti & Mannello, 2008).

2.3.4   Osteogenic differentiation

The process of osteogenic differentiation *in vitro* can be divided into three overlapping phases (Fig. 2). Firstly, the osteogenic progenitor cells undergo a proliferation phase. Proliferation is highly important since individual cells cannot produce bone and osteoblasts that secrete the mineralized ECM need a 3D environment (Blair *et al.*, 2017). The cell density needs to be high when cells are cultured on plastic in order for the differentiating cells start to form bone in a nodular form, creating their own 3D microenvironment (Blair *et al.*, 2017). The expression of Runx2 is essential for the osteogenic differentiation to occur, as *Runx2*$^{-/-}$ mice have been shown to totally lack osteoblasts (Komori *et al.*, 1997). During the proliferation phase, also the expression of COL-1 and osteopontin are upregulated. As cell proliferation declines, cell differentiation proceeds into the matrix maturation phase. COL-1 is still produced and secreted into the extracellular space and ALP activity is significantly upregulated (Lian & Stein, 1995). OSX expression also follow the proliferation phase as it has been shown to act downstream of Runx2 (Almalki & Agrawal, 2016). Furthermore, the secretion of OSX is also essential for the mineralization as in the absence of OSX, ossification does not occur (Nakashima *et al.*, 2002). In addition, for the osteogenic differentiation to proceed, the Runx2 expression need to go down as the high Runx2 expression has been demonstrated to inhibit mineralization, leaving the cells in a premature stage (Komori, 2017). As the process proceeds to the mineralization phase, collagenase expression peaks (Lian

& Stein, 1995). Collagenase is needed in the remodeling of the forming bone matrix. As mineralized matrix starts to accumulate, also several proteins typical to bone, such as bone sialoprotein, OCN and osteopontin, can be detected in the ECM (Lian & Stein, 1995). The expression of osteopontin is upregulated in proliferation phase, and then it declines and again peaks during mineralization (Lian & Stein, 1995). OCN, on the other hand, is only expressed by mature osteoblasts (Lian & Stein, 1995). The expression of homeobox protein DLx5 coincides with the expression of OCN and DLx5 has been shown to induce mineralization (Lee *et al.*, 2005).
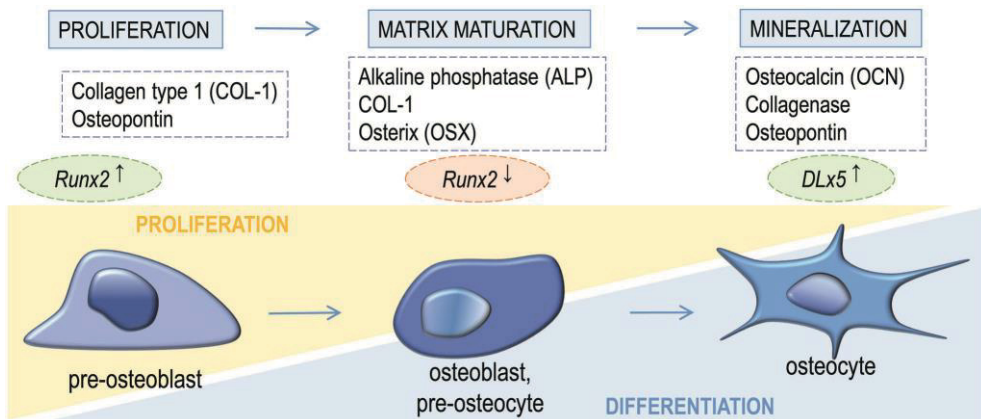
Figure 2. Graphical description of the osteogenic differentiation phases and the most important osteogenic markers expressed during different phases of differentiation. Arrows indicate gene expression (up-regulation↑, down-regulation↓). (Almalki & Agrawal, 2016; Blair *et al.*, 2017; Komori, 2017; Lian & Stein, 1995.)

Growth factors

Bone formation in the body is regulated via various osteogenic factors secreted by the cells and tissues and many of these factors (such as BMP-2, BMP-7 and VEGF) have been used to induce osteogenesis (Gothard *et al.*, 2014). BMPs are a group of cytokines in the transforming growth factor-β superfamily (Bessa *et al.*, 2008). BMPs form a complex with type I and II serine/threonine kinase receptors and these receptors are responsible for phosphorylating receptor-mediated mothers against decapentaplegic homolog protein (SMAD)-proteins (Vanhatupa *et al.*, 2015; Y. K. Wang *et al.*, 2012). SMAD-proteins on the other hand are transcriptional regulators of DNA-binding genes, such as Dlx2 and -5 as well as OSX (Vanhatupa *et al.*, 2015; Y. K. Wang *et al.*, 2012). Recombinant human BMP-2 (rhBMP-2) has been used in the osteogenic induction *in vitro* (Vanhatupa *et al.*, 2015; Waselau *et al.*, 2012b), *in vivo*

(Waselau *et al.*, 2012a) and in clinical treatments (Sandor *et al.*, 2014). In addition, the effect of BMP-7 on bone formation has been studied *in vitro*, *in vivo* and in clinical treatments (Haubruck *et al.*, 2018). Haubrauck and colleagues (2018) concluded that patients who were treated with rhBMP-2 for tibial nonunion had a significantly higher rate of bone healing in comparison to patients treated with rhBMP-7. Furthermore, in addition to promoting vascularization, the potential of VEGF to induce osteogenesis has been studied *in vitro* and *in vivo* (Zhang *et al.*, 2014; Behr *et al.*, 2011). Zhang and colleagues demonstrated that localized VEGF and BMP-2 release induce bone formation via mobilizing and homing of endogenous stem cells (Zhang *et al.*, 2014).

In 2002, the U.S. Food and Drug Administration (FDA) approved two clinical products with recombinant BMP-2 and BMP-7 in resorbable collagen scaffolds intended for spinal fusion and non-unions in long bones (Bessa *et al.*, 2008). However, the large and costly doses of growth factors used in clinical treatments have been shown to be related to a wide range of adverse effects (Bodalia *et al.*, 2016; Carragee *et al.*, 2011). Even though the industry sponsored clinical trials concerning the use of rhBMP-2 reported no adverse events, in 2006 studies started reporting of serious complications associated with rhBMP-2 use in different study settings, including osteolysis, carcinogenesis, nerve root injury and retrograde ejaculation (Carragee *et al.*, 2011). Carragee and colleagues (2011) concluded that the studies regarding the safety and efficacy of rhBMP-2 underestimated the adverse effects of the product and noticed concerns in conflicts of interest in each of the original industry-sponsored publications (Carragee *et al.*, 2011). Nevertheless, rhBPM-2 is still considered a suitable and effective bone graft option for adults suffering for intance from lumbar pseudarthrosis requiring a revision spinal fusion surgery when autologous bone graft is not available (Bodalia *et al.*, 2016; Gothard *et al.*, 2014). However, the case of BMP-2 underlines the need for more cost-effective and safer osteoinductive approaches.

Osteogenic medium

The osteogenic differentiation of both ASCs and BMSCs *in vitro* is most commonly induced using three supplements added into the culture medium: ascorbic acid/ascorbic acid-2-phosphate (AA2P), β-glycerophosphate (β-GP) and dexamethasone (Dex). The most commonly used composition for osteogenic medium (OM) originally developed for BMSC differentiation consist of basal medium with 50 μM of AA2P, 100 nM of Dex and 10 mM of β-GP (Coelho & Fernandes, 2000). Kyllönen and colleagues, (2013) compared three different OM

compositions in hASC differentiation with 10 mM β-GP concentration and varying AA2P and Dex concentrations: OM1 as the composition commonly used in BMSC differentiation (50 µM AA2P, 100 nM Dex;), OM2 (150 µM AA2P, 10 nM Dex) and OM3 (250 µM AA2P, 5 nM Dex). Interestingly, hASCs differentiated more effectively towards osteogenic lineage in OM3, which has a higher AA2P and a lower Dex concentration when compared to the commonly used OM1 composition (Kyllönen *et al.*, 2013). The mode of action of these supplements is well intertwined as they induce osteogenesis most effectively when used together. β-GP contributes to mineralization through the activity of ALP, as ALP is an enzyme cleaving phosphate groups from the added β-GP (Coelho & Fernandes, 2000). Ascorbic acid is important for the correct folding of collagens and it also enhances the secretion of COL-1 into the ECM, which is highly important for the differentiation to proceed. In turn, Dex is a synthetic glucocorticoid inducing proliferation (Coelho & Fernandes, 2000) as well as the transcription of *Runx2*, which is an essential transcription factor in osteogenic differentiation (Langenbach & Handschel, 2013). However, even though glucocorticoids have been shown to have an effect on transcription factor expression and ALP activity (Blair *et al.*, 2017), bone matrix development has been noticed to be more pronounced without glucocorticoids in hBMSC culture (Blair *et al.*, 2017; Chang *et al.*, 2006). This may be one reason for why the lower Dex concentration resulted in a better osteogenic outcome with hASCs in the study of Kyllönen *et al.* (2013). Furthermore, as Dex induce the expression of *Runx2* which in fact need to decline for the osteogenic maturation to proceed, it is tempting to speculate whether Dex would be beneficial in the beginning of the differentiation and its elimination from the OM composition after the initiation of the osteogenic differentiation would benefit the *in vitro* process.

2.3.5   Identification of osteogenic differentiation

Reliable verification of osteogenic differentiation is essential in *in vitro* studies concerning BTE. Analysis of ALP activity is one of the most common markers used to confirm osteogenic differentiation. Even though, ALP activity up-regulation is typical in osteogenic differentiation (Lian & Stein, 1995), ALP activity is not unique for osteoblasts as it is also detected in other tissues such as liver and kidney (Whyte, 2016). Another widely used method to confirm osteogenic differentiation is the staining of mineralized matrix with either alizarin S or Von Kossa stain. Staining of mineralized matrix is a well-established indicator of osteogenic differentiation

however, they are not specific for osteogenic mineralization. Both stains bind to calcium minerals but they cannot distinguish between different calcium deposits: in addition to mineralization resulting from osteogenic differentiation, calcification of cell cultures can be caused by dead cells and, non-apatitic mineralization can be a result of the osteogenic supplement β-GP accumulation (Robey, 2017; Langenbach & Handschel, 2013; Bonewald *et al.*, 2003). Gene expression analysis of osteogenic marker genes is a reliable and widely used method in the verification of differentiation as well. Nevertheless, gene expression analysis should be coupled with protein level analysis, since the mRNA translation in osteogenic differentiation has been shown to be regulated and directly inhibited by microRNAs (Lian *et al.*, 2012). Immunocytochemical staining of osteogenic marker proteins is a reliable, qualitative method for confirming the osteogenic differentiation, if negative and positive controls are used in the process to exclude unspecific staining. Even though the detection of early osteogenic markers, such as ALP activity or *Runx2* gene expression, suggest osteogenesis, the formation of collagenous mineralized matrix with the expression of markers only expressed by mature osteoblasts, such as OCN or DLx5, are the best indicators of successful osteogenesis. In summary, the detection of osteogenic differentiation is the most reliable when various analysis methods are used together, and the differentiation is demonstrated on both gene and protein level in addition to the formation of mineralized bone matrix.

2.3.6 Endothelial differentiation

In vasculogenesis, the differentiation of endothelial progenitor cells into ECs give rise to a vascular network. As endothelial progenitor cells differentiate to ECs, they start to express endothelial proteins, such as vascular endothelial growth factor receptor 2 (VEGFR-2), vascular endothelial cadherin (also known as CD144), von Willebrand factor (vWF) and platelet endothelial cell adhesion molecule-1 (PECAM-1, also known as CD31) (Hristov *et al.*, 2003). vWF is a glycoprotein secreted by ECs and megakaryocytes (Sadler 1998). PECAM-1 is highly expressed by ECs in the cell-cell junctions where it has an important role regulating the EC vascular permeability barrier (Lertkiatmongkol *et al.*, 2016).

The capacity of ASCs to undergo endothelial differentiation was demonstrated already in 2004 (Miranville *et al.*, 2004; Planat-Benard *et al.*, 2004) but still the endothelial differentiation and development of vasculature are not as well known as osteogenic differentiation and there is no established protocol for the differentiation

of MSCs into ECs. Both FGF-2 and VEGF are important signaling molecules in mature EC survival, proliferation and migration (Cross & Claesson-Welsh, 2001). They have also been suggested to be the key signaling molecules in endothelial differentiation however; their mode of action is less understood (Marcelo *et al.*, 2013). Therefore, VEGF (S. Khan *et al.*, 2017; Kukumberg *et al.*, 2017; Zonari *et al.*, 2012; Colazzo *et al.*, 2010) and FGF-2 (S. Khan *et al.*, 2017; Kukumberg *et al.*, 2017; Marino *et al.*, 2012) and their combination have been used in the endothelial differentiation of MSCs *in vitro*. The most used commercial medium in endothelial differentiation is Endothelial Growth Medium-2 (EGM-2) from Lonza originally meant for the culture of mature ECs (Antonyshyn *et al.*, 2019; Correia *et al.*, 2014), which consist growth factors epidermal growth factor (EGF), VEGF and R^3 insulin-like growth factor-1 (R^3-IGF-1) as well as hydrocortisone, ascorbic acid and heparin with 2 % FBS and antibiotics. In addition to supplements added into the medium, also shear stress have been shown to guide BMSCs towards an endothelial lineage (M. Cheng *et al.*, 2013; L. Yuan *et al.*, 2013; Dong *et al.*, 2009) however, it has been suggested that MSCs need VEGF supplementation in addition to shear stress for sufficient endothelial induction (Dan *et al.*, 2015). Furthermore, topographical cues combined with VEGF stimulus have been demonstrated to induce endothelial differentiation of hBMSCs (Kukumberg *et al.*, 2017).

Khan and colleagues (2017) studied the effect of VEGF or FGF-2 and their combination in the endothelial differentiation of hASCs. They concluded that hASCs cultured in medium supplemented with both VEGF and FGF-2 induced the differentiation more towards an endothelial type in contrast to hASCs supplemented only with VEGF or FGF-2 alone (S. Khan *et al.*, 2017). Moreover, they also reported that FGF-2 and VEGF/FGF-2 groups resulted in a more robust differentiation of hASCs in comparison to widely used EGM-2 (S. Khan *et al.*, 2017). Interestingly, Antonyshyn and colleagues (2019) reported that hASCs do not differentiate into mature ECs in the widely used EGM-2 from Lonza. They compared the EGM-2 differentiated hASCs to ECs derived from umbilical vein, coronary artery and dermal microvasculature, and concluded that even though endothelial protein and gene marker levels were up-regulated in hASCs, the levels were still significantly lower in contrast to the ECs (Antonyshyn *et al.*, 2019). Most of the endothelial differentiation studies using human cells are conducted in FBS based media (Antonyshyn *et al.*, 2019; S. Khan *et al.*, 2017; Kukumberg *et al.*, 2017; Correia *et al.*, 2014). However, since proliferation and differentiation of hASCs (Kyllönen *et al.*, 2013; Patrikoski *et al.*, 2013) and hBMSCs (Dahl *et al.*, 2008; Tonti & Mannello, 2008) have been shown

to be affected by serum conditions, the study of endothelial differentiation of human MSCs in HS based media would be important.

2.3.7   Identification of endothelial differentiation

Endothelial differentiation is most commonly verified by immunocytochemical staining of endothelial marker proteins, such as vWF and PECAM-1, as well as on gene expression level of the corresponding endothelial genes. Furthermore, ECs' functionality can be evaluated by a fluorescent-based acetylated low-density lipoprotein (AcLDL) uptake assay. (Antonyshyn *et al.*, 2019.) The assay is based on ECs' ability to uptake the fluorescent-labelled AcLDL inside them and these cells can be imaged with a fluorescence microscope or quantified with flow cytometry. The formation of tubular structures is typical to mature ECs. The formation of tubular structures may be seen in immunocytochemical staining of endothelial marker proteins but also a sprouting assay can be used, where cells are seeded in a basement membrane-like material, such as Matrigel®, where mature ECs start to form tubular structures. The evaluation of EC functionality and tubular formation ability are highly important in addition to endothelial protein and gene expression analyses in order to demonstrate the maturity of the cells reliably. However, it has been suggested that the commonly used endothelial markers are not specific enough, making the verification of endothelial differentiation challenging (Antonyshyn *et al.*, 2019).

2.3.8   Human umbilical vein endothelial cells modelling vasculogenesis

Human umbilical vein endothelial cells (HUVECs) are commonly used to model ECs. In BTE, HUVECs have been used especially in the study and development of vascularized constructs. One reason for this is that umbilical veins are easily accessible for cell harvesting in contrast to other veins (Cao *et al.*, 2017). Another reason for the use of HUVECs as a model EC type in research is that they have been shown to express endothelial markers and signaling molecules typical to ECs (Cao *et al.*, 2017). Furthermore, HUVECs are able to form vascular structures *in vitro* both alone (Da Pozzo *et al.*, 2012) and in co-culture with MSCs (Correia *et al.*, 2011; Tsigkou *et al.*, 2010), as well as *in vivo* (Pirraco *et al.*, 2014). Moreover, they have been demonstrated to be responsive to typical EC stimuli such as shear stress and hypoxia (Lewis *et al.*, 2015). This also makes HUVECs a reliable positive control cell type in

endothelial differentiation studies. However, there are differences for instance in protein expression between ECs isolated from different sites as demonstrated by Antonyshyn and colleagues (2019) and this should be taken into account when choosing an EC model.

2.4   Biomaterials in bone tissue engineering

The requirements for a synthetic bone graft are high, as the ideal scaffold should mimic the properties of natural bone tissue. Firstly, the scaffold needs to be biocompatible with non-toxic degradation products and non-inflammatory components (Turnbull *et al.*, 2017). In addition, the ideal scaffold is biodegradable facilitating the formation of bone ECM as the scaffold degrades and is finally replaced by the host tissue (Turnbull *et al.*, 2017). Importantly, the degradation process should be controlled as a too fast process can lead to mechanical failure of the implant and in contrast, a too slow degradation process may cause an inflammatory response towards the implant material (Turnbull *et al.*, 2017).

Tissue attachment is related to the tissue response caused by the implanted material and all materials induce a response in living tissues when implanted into the body (Hench, 1991). A toxic material causes the surrounding tissues to die whereas, a biologically inactive (nearly inert) material induce the formation of a fibrous capsule around itself (Hench, 1991). On the other hand, a biologically active (bioactive) material can bond directly with the living tissue (Hench, 1991). Furthermore, bone tissue can grow on the surface of an osteoconductive material whereas an osteoinductive material induce bone formation even in an ectopic implant site (Jones, 2013). Therefore an ideal orthopedic implant should be bioactive, osteoconductive and preferably osteoinductive (Turnbull *et al.*, 2017) as well as support vascularization (Amini *et al.*, 2012). In fact, Bohner and Miron (2019) reviewed the body of literature related to osteoinductive materials and proposed a mechanism for materials intrinsic osteoinduction. The authors suggested that the materials intrinsic osteoinductivity is a result of the formation of a biomimetic apatite layer on the material surface, optimal scaffold architecture (total porosity, macro- and microporosity) to allow blood vessel ingrowth and cell migration and finally, of insufficient blood supply to allow a decreased calcium and phosphate ion concentration (Bohner & Miron, 2019). However, the specific biological mechanism of osteoinduction remains unclear.

2.4.1   Scaffold requirements

The structural demands of a bone substitute include high interconnected porosity (porosity for native bone: 60 – 90 %) with the optimal pore size varying between 150-400 μm to allow cell and tissue ingrowth as well as vascularization (Mathieu *et al.*, 2005; Rouwkema *et al.*, 2008; Turnbull *et al.*, 2017). Furthermore, microporosity (pores < 10 μm) of the scaffold induce the surface area for the cells (Turnbull *et al.*, 2017) and have been shown to improve the osteogenic outcome *in vivo* (Habibovic *et al.*, 2005). Unfortunately, the high porosity is in direct conflict with the mechanical stiffness of an implant as the mechanical strength of the material decreases as the total porosity rises. Parameters usually used to asses a bone substitute's mechanical integrity include Young's modulus (also elastic modulus) which describes the stiffness of the material. Compressive strength on the other hand is a parameter describing the capacity of a material to withstand load that tend to reduce its size. In addition, fatigue strength can be used to describe the highest stress a material can withstand without breaking. (Turnbull *et al.*, 2017.) For cortical bone the Young's modulus is 7-30 GPa with a compressive strength of 100-230 MPa whereas for the porous trabecular bone the Young's modulus is 0.05-0.5 GPa with a compressive strength of 2-12 MPa (Kokubo *et al.*, 2003). The mechanical properties of human bone are compared to synthetic bone graft materials in Table 2.

Table 2.   Mechanical properties of synthetic bone graft materials and human bone. Hydroxyapatite (HA); Polycaprolactone (PCL); Polylactide (PLA); Poly(lactide-co-caprolactone) (PLCL); Bioactive glass (BaG)

		Compressive strength (MPa)	Young's modulus (GPa)	Reference
Bioglass® 45S5		-	35	(Kokubo *et al.*, 2003)
Bioglass® 45S6 (porous)		0.3-0.4	-	(Chen *et al.*, 2006)
HA (porous)		6.9-68.9	-	(Owen *et al.*, 2018)
chronOS® (porous β-TCP granule)		~5		chronOS product guide (De Puy Synthes)
PCL (porous)		2-3.2	0.052-0.067	(Williams *et al.*, 2005)
PLA		57.7-70.6	3.4-4.2	(Sarasua *et al.*, 2005)
PLCL+ 50 wt-% BaG		-	0.09	(Tainio *et al.*, 2017)
Human bone	Trabecular	2-12	0.05-0.5	(Kokubo *et al.*, 2003)
	Cortical	100-230	7-30	

The user-friendliness and easy intra-operative tailoring are yet another significant factor in the development of a bone substitute, as the surgeon is the one who chooses the implant material and not the patient. From an industrial point of view,

large-scale manufacturing with reasonable costs and a long shelf life would also be desirable traits for a bone substitute (Amini et al., 2012). As a result of this long list of demands, the development of a bone substitute often requires some compromising between achieving an optimal cell and tissue response, architecture as well as mechanical integrity.

2.4.2   Calcium phosphates

Calcium phosphates (CaPs) are a widely used bioactive biomaterial type in BTE because they are so like the native bone mineral. CaPs are crystalline, bioactive and osteoconductive bioceramics with good corrosion resistance. However, they are hard and brittle making them challenging to tailor and undesirable for load-bearing sites (Turnbull *et al.*, 2017). CaP ceramics commonly comprise of hydroxyapatite (HA) or tricalcium phosphate (TCP) or both known as biphasic CaP (BCP) (Campana *et al.*, 2014; Turnbull *et al.*, 2017). Beta-TCP (β-TCP) on the other hand has a significantly higher degradation rate in contrast to HA, which is the most stable and least soluble of CaPs (Samavedi *et al.*, 2013). Different CaPs have been successfully used to treat patients(Prins *et al.*, 2016; Sandor *et al.*, 2014; Mesimäki *et al.*, 2009) and there are many CaPs among clinically used bone fillers, such as Endobon® HA granules from Zimmer Biomet Dental, chronOS® β-TCP granules from De Puy Synthes and, BoneCeramic® HA/β-TCP (60/40%) granules from Straumann.

Osteoinductivity
Whereas the osteoconductivity of CaPs is clear, there are contradicting results concerning the osteoinductive properties of CaPs (Owen *et al.*, 2018). A few *in vitro* studies have demonstrated the induction of osteogenic markers in hASCs cultured on β-TCP (Marino *et al.*, 2010) and of hBMSCs cultured on HA (Muller *et al.*, 2008) even without the addition of osteogenic supplements. Some studies have also demonstrated the osteoinductive properties of CaPs *in vivo* (Duan *et al.*, 2017; L. Wang *et al.*, 2014; Kondo *et al.*, 2006). The osteoinductive properties of CaPs are based on the ions released from the material as well as on focal adhesion mediated signals arising from protein adsorption and cell attachment (Samavedi *et al.*, 2013; Muller *et al.*, 2008) however, the ion dissolution from CaPs is relatively slow when compared to that from BaGs. Fig. 3 gives an overview on the different material features affecting the biological processes on the surface of CaPs. The

osteoinductive capacity of CaPs has been shown to be influenced by the macrostructure (dimension, geometry, and porosity), micro- and nanostructure (microporosity, grain size, surface topography) as well as by the chemical composition of the CaP (Chai *et al.*, 2012).
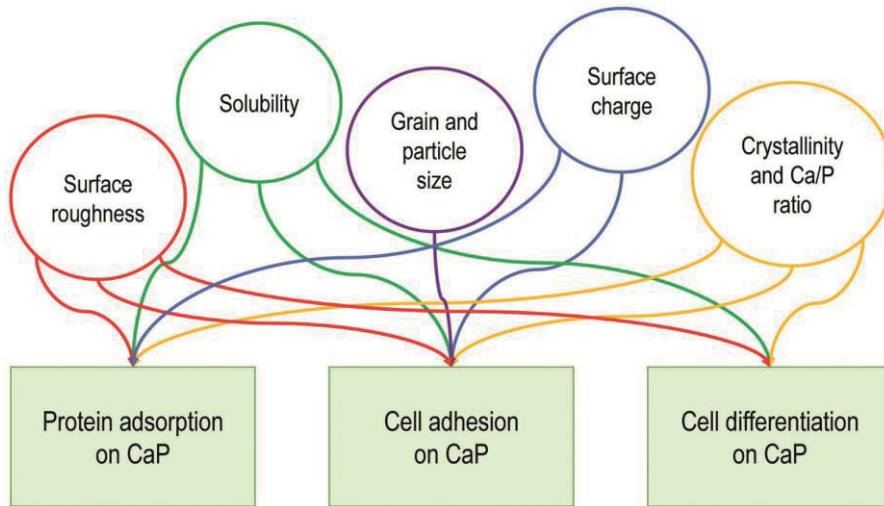
Figure 3. CaP characteristics effecting protein adsorption, cell adhesion and differentiation, adapted from Samavedi *et al.* (2013).

Duan and colleagues (2017) compared the ectopic bone formation capacity of six commercial CaPs as well as two TCP granules with either a micron-scale or a submicron-scale surface structure in a dog model. The chemical composition of CaPs alone did not explain the ectopic bone formation capacity as a silicon-substituted HA (Si-HA) named Actifuse®, MBCP comprised of BCP and, the self-manufactured submicron- scale surface structured TCP granules all induced ectopic bone formation (Duan *et al.*, 2017). Moreover, the amount of proteins adsorbed onto the surface of the materials or, the release of calcium or phosphate ions did not fully explain the osteoinductive properties of the CaPs either (Duan *et al.*, 2017). However, they showed that the submicron-scale surface structure is more beneficial for material-driven bone formation when compared to nanoscale or micron scale surface -structures (Duan *et al.*, 2017). Furthermore, later Duan and co-workers (2018) studied three chemically identical TCP granules with the same granule size but different crystal grain size in a rabbit condyle defect -model. They concluded that the submicron structured TCP (crystal grain size 0.77 ± 0.21 µm) induced bone formation more and resorbed more when compared to TCP ceramics with larger

crystal grains during the 26-week follow-up (Duan *et al.*, 2018). Having the largest surface area, the small crystal grain TCP released more calcium ions in comparison to TCPs with a larger grain size. Although the fast degradation is beneficial for osteogenesis, also a stable surface is important for the basis of bone formation (Owen *et al.*, 2018). In contrast to their earlier study conducted in an ectopic site, Duan and colleagues (2018) concluded that the induced protein adsorption on the surface as well as the higher calcium and phosphate ion release induce the bone formation capacity of the TCP granules. The mechanism behind the effect of surface structure and topography on osteogenic induction may be the differentiation of cells and recruitment of stem cells via mechanotransduction referring to the translation of mechanical signals eliciting from the cell-surface interaction, into cellular responses (Duan *et al.*, 2017; Gattazzo *et al.*, 2014; Dupont *et al.*, 2011). In addition, macrophages and osteoclasts, which derive from the monocyte-macrophage lineage, have been shown to be sensitive to surface topography and their activity and secretion of cytokines have been evidenced to be beneficial for bone formation on CaP surfaces (Duan *et al.*, 2017; Davison *et al.*, 2014; Kondo *et al.*, 2006).

Effects on angiogenesis

The degradation of CaPs result in the release of calcium and inorganic phosphate to liquid phase (Malhotra & Habobovic, 2016). Although these ions are important for osteogenesis and their circulation is crucial for homeostasis (Malhotra & Habobovic, 2016), their elevated levels have been connected to vascular smooth muscle cell apoptosis (Shanahan *et al.*, 2011), EC oxidative stress (DiMarco *et al.*, 2013) and apoptosis (*DiMarco et al.*, 2008). CaPs are not inherently angiogenic however different modifications have been tested to increase their angiogenic effect, such as addition of copper to CaP cement (Zhang *et al.*, 2019) or integration of growth factors to CaP scaffolds (Malhotra & Habobovic, 2016). Furthermore, combining CaPs with BaGs, which has angiogenic potential, to form ceramic composites is an intriguing alternative to produce more optimal bone filler materials to combine the good properties of both materials (Karadjian *et al.*, 2019).

2.4.3 Bioactive glasses

The whole BaG research field is based on the development of the first BaG, later named Bioglass® 45S5, by Hench and colleagues at the beginning of 1970s (Hench, 2006). The 45S5 is a degradable BaG composed of 45 wt-% SiO_2, 24.5 wt-% Na_2O,

24.5 wt-% CaO and 6 wt-% P_2O_5 (Hench, 1991). Bioglass 45S5 binds to bone tissue with chemical bonds and induces bone formation away from the implant and in an ectopic site making it osteoinductive (Hench, 1991; Jones, 2013). A Finnish-developed BaG type S53P4 (later named BonAlive®) is highly like the original 45S5, only with a slower reactivity. In addition to traditional silicate-based BaGs, such as 45S5 and S53P4, also phosphate-based BaGs and borate-based BaGs have been developed (Jones, 2013). Silicate-based BaGs have a slow resorption rate in the body and BaG granules have been shown to preserve in the implant site for years without degrading (Lindfors *et al.*, 2010). The partial replacement of silicate with borate in S53P4 BaG composition has been proposed as one solution to induce the degradation rate of the silicate-based S53P4 BaG (Ojansivu, Mishra *et al.*, 2018).

Osteoinductive properties

The mechanism of osteoinduction by BaGs is based on the formation of a polycrystalline hydroxyl carbonate apatite bi-layer on the glass surface when implanted in living tissues (Hench, 2006). The formed bi-layer induce the adsorption of growth factors as well as the attachment and proliferation of osteoblasts (Hench, 2006). Rath and colleagues (2016) studied the osteogenic differentiation of ASCs and BMSCs in 45S5 BaG scaffolds with and without osteogenic supplements in the culture medium. Interestingly, they concluded that ASCs seeded in the BaG scaffold differentiated towards osteogenic lineage even without the addition of osteogenic supplements whereas BMSCs needed the osteogenic supplements in addition to the BaG scaffold in order to differentiate (Rath *et al.*, 2016). Furthermore, BaGs have an effect also on cells that are not seeded on its surface, as BaGs have been shown to induce bone formation via ionic dissolution products. Ojansivu and colleagues (2015) studied the effect of four BaG extract media on osteogenic differentiation of hASCs. Intriguingly, they concluded that the ionic dissolution products of S53P4 BaG and of three experimental BaGs alone did not induce osteogenesis of hASCs but the addition of osteogenic supplements into the culture medium was needed for osteoinduction of hASCs (Ojansivu *et al.*, 2015). However, the BaG extract in OM induced hASC osteogenesis significantly more in contrast to OM alone (Ojansivu *et al.*, 2015). On the other hand, the ionic dissolution from BaGs induces a rise in pH. Monfoulet and colleagues (2014) studied the effect of pH on osteogenic differentiation of hBMSCs *in vitro* and on bone formation *in vivo* using BCP, coral and BaG granules. They showed *in vitro* that there is a pH range of 7.9–8.27 where hBMSC proliferation is not affected, but the osteogenic differentiation of hBMSCs is inhibited (Monfoulet *et al.*, 2014). Furthermore, they implanted the cell seeded

constructs in mouse subcutis and concluded that bone formation declined 20–30 fold as pH rose from 7.5 to 7.8 and, bone formation was completely inhibited as pH reached 8 (Monfoulet *et al.*, 2014).

Angiogenic and antibacterial properties

In addition to osteoinduction, BaGs have been evidenced to have a pro-angiogenic effect both *in vitro* and *in vivo* (Gorustovich *et al.*, 2010). Bioglass 45S5 induce the release of VEGF and FGF-2 in human fibroblasts as well as proliferation and vessel sprouting of ECs *in vitro* (Day, 2005). In addition, S53P4 have been shown to induce the release of VEGF in human fibroblasts *in vitro* (Detsch *et al.*, 2014). During the recent years, the addition of angiogenic ions, such as copper, in BaG compositions have been studied in order to develop a BaG type to support both osteogenesis as well as angiogenesis (Bari *et al.*, 2017; Wu *et al.*, 2013). Wu and colleagues (2013) manufactured mesoporous copper doped BaG, which was demonstrated to induce the osteogenic differentiation of hBMSCs and the expression of VEGF and hypoxia-inducible factor (HIF)-1α in hBMSCs. In addition, the S53P4 based borosilicate BaGs have also been shown to induce the expression of endothelial genes *PECAM-1* and *vWF* (Ojansivu *et al.*, 2018).

On top of everything else, BaGs have presented antibacterial properties in various studies (Lindfors *et al.*, 2017; Bari *et al.*, 2017; Wu *et al.*, 2013; Hu *et al.*, 2009). In an aqueous environment BaGs undergo surface reactions resulting in ion release, which causes a rise in the pH (Hu *et al.*, 2009) as well as induces the osmotic pressure around the BaG (Lindfors *et al.*, 2017). Both of these phenomena have been shown to contribute to the antibacterial effect of BaGs (Lindfors *et al.*, 2017; Hu *et al.*, 2009). Hu and co-workers (2009) evidenced the antibacterial effect of 45S5 *in vitro* using three pathogenic bacteria that could be related to wound healing. Furthermore, Romano and colleagues (2014) compared S53P4 in two antibiotic-loaded calcium-based bone fillers in the treatment of chronic osteomyelitis and concluded that S53P4 resulted in an equally good outcome as the antibiotic-loaded bone fillers. In fact, a multinational and multicenter study evidenced that S53P4 can be used alone without antibiotics in the treatment chronic osteomyelitis (Lindfors *et al.*, 2017).

Although BaGs are osteoinductive, pro-angiogenic as well as antibacterial, they are brittle with low toughness, which make them difficult to tailor and undesirable for load-bearing sites (Jones, 2013). As a result, most commercial BaGs are in granule or cement form (Jones, 2013). The mechanical properties of 45S5 (Chen *et al.*, 2006) are compared to those of other biomaterials and native bone in Table 2. The hard and brittle nature of BaGs has limited their clinical use however, due to the superior

biological effects of BaGs they are excellent components to be combined for instance with synthetic polymers to form composite materials for vascularized bone applications.

2.4.4 Aliphatic polyesters

Aliphatic polyesters are a biodegradable biomaterial group with highly tailorable mechanical and structural characteristics even though they are not bioactive. This class include polymers such as polylactide acid (PLA), polyglycolic acid and poly-ε-caprolactone (PCL). The properties of these polymers can be further modulated by blending them or, co-polymerization with other monomers resulting in copolymers, such as poly (lactide-co-glycolic acid) or poly (lactide-co-caprolactone) (PLCL) (Narayanan *et al.*, 2016). Co-polymerization and blending have been demonstrated to affect the polymer properties significantly, such as ionic property, crystallinity, solubility, and degradation (Dash & Konkimalla, 2012). Furthermore, PLA, PCL, polyglycolic acid and their copolymers are biocompatible and they have been demonstrated to support osteogenic differentiation of stem cells *in vitro* (Z. Wang *et al.*, 2016; Campana *et al.*, 2014; Temple *et al.*, 2014; Jeong *et al.*, 2008).

PLA is a non-toxic, biodegradable, FDA approved material obtained from renewable resources with low costs (Gritsch *et al.*, 2019). PLA is processed from lactic acid monomers. Lactic acid has a chiral carbon atom and therefore it has two stereoisomers: L-lactic acid and D-lactic acid resulting in either poly (L-lactide) or poly (D-lactide) or a copolymer of both monomers (Gritsch *et al.*, 2019; Sarasua *et al.*, 2005). In addition, PLA can be processed using different techniques, such as extrusion, fiber spinning, gas foaming or film casting; allowing the production of various structures with varying properties (Gritsch *et al.*, 2019). However, the degradation rate of PLA is relatively slow, and the hydrophobic and inert material interacts poorly with cells and tissues inducing an inflammatory response when implanted into the body (Gritsch *et al.*, 2019).

PCL is also a biocompatible, biodegradable and FDA approved polymer with slow and close to linear hydrolytic degradation profile within a period of 18-24 months (Teoh *et al.*, 2019). PCL is a highly versatile and tailorable polymer, which is why it has been studied and trialed widely both in the field of tissue engineering and drug delivery (Dash & Konkimalla, 2012). Moreover, PCL has high mechanical strength making it a potential candidate to load-bearing sites as well (Turnbull *et al.*, 2017).

Poly(L-lactide-co-ε-caprolactone (PLCL) is a copolymer of L-lactide and ε-caprolactone with attractive properties for a BTE implant material: flexible and elastic with high tensile strength, controllable degradation rate as well as good biocompatibility (Z. Wang *et al.*, 2016; Holmbom *et al.*, 2005). Higher ε-caprolactone amount results in a polymer with more flexible and elastic properties (Sartoneva *et al.*, 2018; Ahola *et al.*, 2013). However, PLCL is hydrophobic and inert and even though it has been used in BTE, it still lacks biological binding sites and therefore its interaction with cells or tissues is not optimal *in vitro* or *in vivo* (Z. Wang *et al.*, 2016; Jeong *et al.*, 2008). Therefore, PLCL has been combined with other bioactive materials, such as gelatin (Jeong *et al.*, 2008) or silk-fibroin (Z. Wang *et al.*, 2016), to improve its interaction with cells and tissues.

2.4.5   Composites

Bone is a natural composite with excellent mechanical properties. Individual biomaterial types alone have not been able to reproduce the properties of bone tissue (Turnbull *et al.*, 2017) and therefore, combining different material types to form a synthetic composite may be the best strategy to develop an optimal bone substitute material. Aliphatic polyesters and their copolymers provide a versatile basis for a bone composite material in terms of mechanical properties and ductility, to be further reinforced with bioactive components such as CaPs (Akkouch *et al.*, 2014; Haimi *et al.*, 2009), BaGs (Xiao *et al.*, 2017; Haimi *et al.*, 2009) or silk-fibroin (Z. Wang *et al.*, 2016). The most used synthetic polymers in composites in BTE are PLA, PCL, polyglycolic acid and poly(lactide-co-glycolic acid) (Turnbull *et al.*, 2017).

Haimi and colleagues (2009) compared hASC attachment, proliferation and early osteogenic commitment on PLA/BaG and PLA/β-TCP composites with 10- or 20 % bioceramic content. Interestingly, the composites did not result in a more robust proliferation when compared to plain PLA scaffold (Haimi *et al.*, 2009). Moreover, they observed that hASCs proliferated more on PLA/β-TCP composites in contrast to PLA/BaG composites although; the PLA/BaG composites induced ALP activity of hASCs more when compared to PLA/β-TCP composites (Haimi *et al.*, 2009). Akkouch *et al.* (2014) studied a porous composite consisting COL-1, HA and PLCL by culturing and differentiating human dental pulp stem cells on them. The authors concluded that ALP activity, osteogenic gene expression and secretion of mineralized matrix were notably higher in human dental pulp stem cells cultured on the composites in contrast to plain PLCL scaffolds (Akkouch *et al.*, 2014).

Montjovent and colleagues (2007) on the other hand fabricated porous PLA/HA and PLA/ β-TCP (5 % ceramic content) composites with supercritical CO_2 (scCO$_2$) foaming and tested their biocompatibility and osteoconductivity in a rat cranial defect model. The composites were shown to be biocompatible, but they did not result in as good bone formation as the β-TCP scaffold used as a control (Montjovent *et al.*, 2007). A reason for this may be the low ceramic content of the composites or the insufficient display of the ceramic content on the surface.

The high ceramic content in composites designed for BTE is desirable although it may affect processing. Furthermore, the high ceramic content may also affect the creation of a porous structure into a composite material. For instance, with scCO$_2$ processing, a higher ceramic content has been shown to decrease total porosity and increase average pore size of the foamed composite (Mathieu *et al.*, 2006).

2.5   Bone *in vitro* models

In addition to contributing to the development of clinical BTE applications, the study of vascularized bone is highly relevant for the development of bone *in vitro* models. The development of relevant 3D *in vitro* models is important because animal models mimic the functions of human body differentially and therefore, fail to predict the clinical outcome (Rossi *et al.*, 2018; Salamanna *et al.*, 2016; Pearce *et al.*, 2007). Functional human cell based *in vitro* models of bone could decrease the need for animal experiments, which would be significant as the *in vivo* experiments related to bone are often painful, time consuming and, expensive. However, the creation of a reliable *in vitro* bone model is challenging, as it requires the formation of mineralized bone matrix and inclusion of vascularization and other relevant cell types in the specific study, such as osteoclasts and/or immunocytes.

One highly relevant research area in need of an *in vitro* bone model is cancer (Bersini *et al.*, 2016). Bone tissue is the third most common metastatic site for cancer and once bone metastasis has occurred patient survival reduces dramatically (Salamanna *et al.*, 2016). As cell-cell and cell-matrix interactions have a key role in cancer metastasis, it is not ideal to study bone metastasis in a conventional 2-dimensional (2D) culture setup (Salamanna *et al.*, 2016). Moreover, as spontaneous bone metastases are rare in rodents, cats and dogs in most tumor types (Simmons *et al.*, 2015), the need for human cell based vascularized bone *in vitro* models is evident in order to bring further insight to bone metastasis mechanisms. A bone *in vitro* model would also provide an opportunity to study the safety of BTE transplants

related to cancer development. In addition to cancer research, bone *in vitro* model has been utilized in the study of Alzheimer disease when studying the role of triggering receptor expressed on myeloid cells-2 in bone homeostasis (Rossi *et al.*, 2018). To create the *in vitro* bone model, Rossi and colleagues (2018) used hBMSCs and differentiated them towards an osteogenic lineage in a perfusion bioreactor on porous cross-linked COL-1 scaffolds for 3 weeks. Then, they seeded monocytes into the constructs and supplemented the culture system with medium guiding the monocytes towards an osteoclast lineage for another 3 weeks (Rossi *et al.*, 2018). The created bone model was able to demonstrate the bone matrix deposition and remodeling, successfully providing the basis for their study related to bone homeostasis (Rossi *et al.*, 2018).

2.6   Animal models in bone tissue engineering

The safety and efficacy of a bone substitute or a BTE construct must be evidenced *in vitro*, *in vivo* and in a clinical trial before it can become a clinically used product or a treatment. *In vitro* models are not able to recreate the complex *in vivo* environment and therefore animal models are needed to test and verify the biocompatibility and osteoinductivity of BTE constructs and, to model bone healing of fractures and critical defects to study the effect of the used construct (Schindeler *et al.*, 2018; Muschler *et al.*, 2010). A major challenge in the *in vivo* studies related to BTE applications, is the lack of standardization related to the used parameters (de Misquita *et al.*, 2016). This means that the parameters between studies testing and evaluating similar properties vary greatly, which makes translation and interpretation of the results challenging. Such parameters include for instance animal species, defect site and size, duration of the study as well as time points, chosen surgical techniques and instruments, fixation methods, preservation or removal of periosteum or local marrow, and the methods used to analyze the results of the study (Gothard *et al.*, 2014; Muschler *et al.*, 2010).

There are three different experimental animal models for BTE applications: firstly, an ectopic model with a subcutaneous implantation site, which can be used to assess the materials intrinsic osteoinductivity in an environment without osteogenic resident cells or other osteoinductive factors in proximity (de Misquita *et al.*, 2016). Secondly, an orthotopic model with a calvarial implantation site that allows the study of osteoinductivity and bone formation in a non-load bearing site

(de Misquita *et al.*, 2016). Finally, an orthotopic model in long bones enabling also the study of load bearing of the used implant (de Misquita *et al.*, 2016).

Small mammals, such as mice and rats, are the most used models in BTE, mostly due to their low cost and easy accessibility (Schindeler *et al.*, 2018). Mice and rats are useful models in the initial testing of biocompatibility and safety however; when aiming at clinical trials larger animals demonstrate a more relevant environment in terms of bone structure and load bearing (Muschler *et al.*, 2010). In contrast to human, rodents' skeleton grows and reshapes throughout their lives, as their growth plates remain open. In addition, they have a very limited amount of trabecular bone and the process of bone remodeling differs significantly (Muschler *et al.*, 2010). Rabbits on the other hand, have more trabecular bone when compared to rodents and, the bone remodeling process is more like human bone (Muschler *et al.*, 2010). However, the bone biology and composition of sheep, dog and pig are highly like human bone (Muschler *et al.*, 2010). In addition, larger animals allow the drilling of larger defects enabling the evaluation of tissue ingrowth and vascularization, as in some cases it is important to exceed the diffusion limit of approximately 200 μm (Muschler *et al.*, 2010). The selection of an animal model may be crucial for the outcome of the study as noticed by Wang and colleagues (2014). They evaluated the osteoinductivity of three CaPs in an ectopic site in rats, rabbits and dogs and concluded that ectopic bone formation was detected in dogs, whereas in rabbits and rats, only osteoid formation was noted (L. Wang *et al.*, 2014). The authors discussed that the differences in osteoinduction between species may be related to differences between metabolism, which affects degradation and adsorption kinetics, level of growth factors and other secreted factors near the implantation site (L. Wang *et al.*, 2014).

2.6.1   Bone formation *in vivo*

Different approaches to treat bone defects effectively have been studied in animal models. These approaches include the use of a biomaterial scaffold alone, a scaffold combined with cells such as ASCs, a scaffold combined with growth factors or, a scaffold combined with both cells and growth factors.

The use of only a biomaterial scaffold is the simplest BTE approach with less potential risks. Furthermore, a biomaterial-based application is subjected to a lower level of regulation during commercialization when compared to approaches using cells or growth factors. However, for a biomaterial to be effective alone it needs to

be osteoconductive or osteoinductive. As demonstrated in a number of *in vivo* studies, CaPs and BaGs alone (Duan *et al.*, 2018; Duan *et al.*, 2017; L. Wang *et al.*, 2014; H. Yuan *et al.*, 2010) or, combined with synthetic or natural polymers in a composite (Fennema *et al.*, 2018; Pihlman *et al.*, 2018; Xiao *et al.*, 2017) have the ability to induce bone formation even without the addition of cells or inductive factors.

Yuan and colleagues (2010) compared β-TCP to autologous bone transplant and to rhBMP-2 delivered in a collagen sponge (Infuse® Bone Graft, Medtronic) in a critical sized bilateral iliac wing defect in sheep. The authors concluded that the β-TCP resulted in a more pronounced bone formation when compared to Infuse® and in an equal level of bone formation as the autologous bone transplant (H. Yuan *et al.*, 2010). Furthermore, the use of cells in an aggregated form in contrast to individual cells has been shown to result in increased cell viability, anti-inflammatory effect as well as tissue formation (Gionet-Gonzales & Leach, 2018). Fennema and colleagues (2018) on the other hand compared the osteogenic potential of aggregated hASCs, hBMSCs and SVF cells with and without rhBMP-2 delivered with CaP microparticles and enveloped in a plateletrich plasma hydrogel in an ectopic site in immunodeficient mice. The authors concluded that hBMSCs combined with CaP microparticles and enveloped in a plateletrich plasma induced bone formation and showed a higher bone maturity when compared to hASCs, SVF cells or rhBMP-2 (Fennema *et al.*, 2018). Moreover, rhBMP-2 induced ectopic bone formation more in contrast to hASCs (Fennema *et al.*, 2018).

2.7 Clinical landscape in bone engineering

Majority of tissue engineering and biomaterial research justify the importance of their research with the clinical need of novel treatments, materials or strategies. Although numerous strategies and materials have been studied during the last few decades in the field of BTE, only a fraction of these have been translated into clinical use (de Misquita *et al.*, 2016; Mishra *et al.*, 2016). Tissue engineering combines a scaffold, cells and bioactive molecules (such as growth factors) however, in 2016 Mishra and colleagues reported that there were no clinical BTE applications consisting all three elements. There are most likely different reasons behind this lack of translation of conducted preclinical research, which we may speculate. Firstly, novel inventions may require patenting, which needs to be well timed, prior to publishing the research behind the invention. Moreover, patenting is expensive, and the inventors rarely

have the expertise to follow-through the patenting process whereas they may have more interest to publish their results quickly. Furthermore, the pathway of a BTE application from bench to clinic is strongly regulated. In fact, it has been proposed that the unawareness of the regulatory requirements as well as the high cost of the whole translation process of new BTE products is a major reason for the difference between the amount and investment for preclinical research and clinical BTE applications (Mishra *et al.*, 2016).

The pathway of clinical translation for a BTE application is described in Fig. 4. A BTE application may be cell-based, biomaterial-based, growth factor based or, be a combination of two or three of these. After demonstrating its effectiveness and safety in preclinical studies (*in vitro* and *in vivo*), depending on the regulative authorities the effectiveness and safety may need to be evidenced in clinical trials. If the clinical trials are successful, the product may be approved for market. Depending on the product and the requirements of the regulative authorities, the manufacturer may also need to conduct post-approval studies to further demonstrate the long-term safety and behavior of the application. (Mishra *et al.*, 2016.)
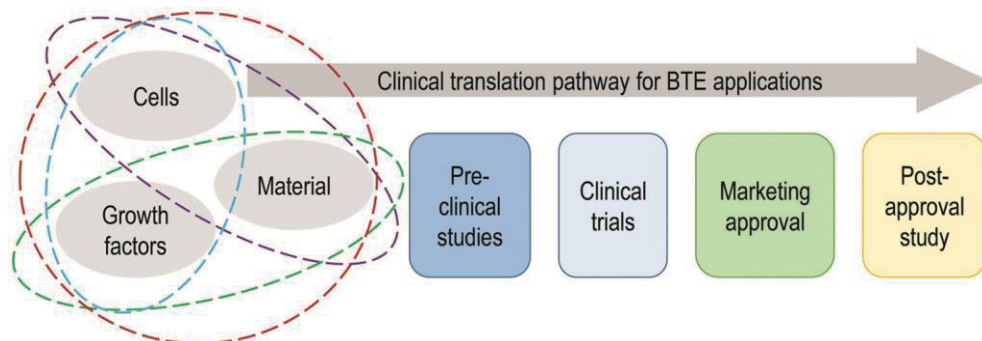
Figure 4. The clinical translation pathway for BTE applications. A BTE application may comprise of all three tissue engineering components (cells, material, growth factors), or of two of them or of only one of them. After successful preclinical studies, the next step is clinical trials before a product may receive marketing approval. Thereafter, post-approval studies may be required to show the long-term effects and behavior of the product. (Mishra *et al.*, 2016.)

2.7.1   Regulation related to commercialization of medical devices

The safety and efficacy of a bone substitute need to be demonstrated on different levels before it can be approved for clinical use. The European Medical Agency

(EMA) classifies a bone substitute material as a medical device. Medical devices as products are regulated on national level, such as by VALVIRA in Finland, and the EMA is involved in the assessment of medical devices under European Union (EU) legislation. The regulation of medical devices confirms that only safe and functional devices are on the market. Stem cell -based products are classified as advanced therapeutic medicinal products (ATMP) and their translation is notably more regulated as compared to medical devices (Ho-Shui-Ling *et al.*, 2018).

In order to introduce a new product into the market the manufacturer needs to provide a Declaration of Conformity and place a CE (Conformité Européenne) mark onto the product to indicate the conformity. CE marking is a certification mark that indicates the accordance with safety, health and environmental product standards that are required of products sold in the European Economic Area (EEA). Furthermore, for the product the CE marking enables freedom of movement, as no additional authoritative approval is required from the CE marked products within Europe. In order to receive a CE mark, medical devices must undergo a conformity assessment to show that they fulfil the legal requirements, verify their safety and, to show that they perform as intended. At the same time, the ISO 13485 –standard (International Organization for Standardization, 2016) defines the requirements for a quality management system for the different stages of medical device's life cycle, such as design, development, production, storage and distribution, installation and maintenance. For instance, European Union (EU) -directive for medical devices (Medical Devices Directive – 93/42/EEC) refers to the ISO 13485 -standard as a part of their approval process.

To select the correct compliance route for a specific medical device, the device needs to be classified according to the classification provided by the European Commission. The conformity assessment is carried out in a graduated level of control, by categorizing the devices based on their inherent risk level (class I, class IIa, class IIb and class III) as described in the guidelines related to the application of the council directive 93/42/EEC on medical devices (European Commission, 2015). This means that a more rigorous assessment is applied to devices with a higher risk level. For instance, wound dressings that serve as mechanical barriers are classified as class I devices. In turn, an osteoconductive bone substitute material without any biological or animal-based additives is classified as a class III device, as it is implanted surgically, it remains long term (> 30 days) in the body and it absorbs fully or mainly in the body (European Commission, 2015). Moreover, a class III bone substitute material that has shown potential in preclinical studies needs to evidence its safety and functionality in a clinical trial to receive a CE mark, as stated in the regulation

(EU) 2017/745 of the European Parliament and of the Council of 5 April 2017 on medical devices.

On the other hand, when aiming to the United States (U.S.) market, medical devices need to abide by the regulation set by the FDA. According to the classification of FDA, a bone filler without any biological or animal-based additives may be classified as a class II device (U.S. Food and Drug Administration, 2018a). Class II medical devices require a Premarket Notification 510(k), which "must demonstrate that the device is substantially equivalent to one legally in commercial distribution in the United States: (1) before May 28, 1976; or (2) to a device that has been determined by FDA to be substantially equivalent" (U.S. Food and Drug Administration, 2018b). Approximately only 10-15 % of class II medical devices are required a clinical trial.

Altogether, the translation of new BTE applications is highly regulated on different levels. This means that the whole translation process takes a long time and therefore it must be well planned and organized. Furthermore, the relevant developmental steps need to be conducted according to relevant standards, such as the ISO 13485 –standard for medical devices, for the acquired results to be acceptable by the regulative authorities.

3   AIMS OF THE STUDY

The aim of this study was to assess the suitability of synthetic bone grafts for BTE. Furthermore, to combine the clinically used bioactive ceramics to synthetic polymers and assess the potential of novel composites in BTE *in vitro* and *in vivo*. In addition, the study aimed to develop effective differentiation strategies for osteogenesis and vasculogenesis *in vitro*. The specific aims of the studies I-IV are listed below:

I   The aim was to compare the effect of two commercially available clinical bone substitutes BioRestore and BoneCeramic in hASC culture *in vitro*. In addition, to achieve osteogenic differentiation efficiently in the biomaterial scaffold commonly used growth factors BMP-2, BMP-7 and VEGF are compared.

II   The hard and brittle ceramic phase is combined to an elastic polymer to create an easier-to-use composite scaffold. The osteogenic and vasculogenic potential of a novel β-TCP/PLCL composite are evaluated in hASC culture *in vitro*. Furthermore, to analyze different differentiation strategies and medium compositions to achieve both osteogenic and endothelial differentiation of hASCs in the same composite.

III   The study aim was to further develop the structure and composition of the β-TCP/PLCL composite and characterize its properties. In addition, to analyze the cytocompatibility and osteogenic capacity of the composite in hASC culture *in vitro*. Finally, to evaluate the biocompatibility and osteoconductivity of the composite *in vivo* by implanting them in a rabbit femur defect.

IV   The aim was to use 3D printing to create PCL/BaG and PCL/BaG-Cu composites for vascularized BTE and analyze their properties and bioactivity. In addition, to evaluate the effect of the composites on proliferation, osteogenesis and vasculogenesis in hBMSC culture and in a co-culture of hBMSCs and HUVECs *in vitro*.

4   MATERIALS AND METHODS

4.1   Biomaterial scaffolds used in the study

4.1.1   Commercial scaffolds

In study I, two commercial biomaterials, Straumann® BoneCeramic granules (Straumann AG, Basel, Switzerland) and Inion BioRestore™ BaG scaffolds (Inion Oy, Tampere, Finland), were compared. The granular BoneCeramic is a BCP with 60 % HA (100 % crystalline) and 40 % β-TCP. The composition of BioRestore BaG scaffold is described in Table 3. The porous BioRestore scaffolds were manufactured as described in the original publication. Details of biomaterial characteristics are listed in Table 4. Prior to cell seeding, the granules and scaffolds were incubated in corresponding medium for 48 h.

4.1.2   ScCO$_2$ foaming of β-TCP/PLCL composites

The β-TCP/PLCL composites with 40 wt-% ceramic content in study II and with 50 wt-% ceramic content used in study III, were manufactured by using scCO$_2$ as described in patent by Paakinaho and Kellomäki (2019) and in original publications. Briefly, the composite material was processed by melt-mixing PLCL (70L/30CL; Purasorb PLC7015, Corbion Purac Biomaterials, Gorinchem, the Netherlands) with 50 wt-% β-TCP (Plasma Biotal Ltd., Buxton, UK). Then, the composite was foamed with scCO$_2$, by using a Supercritical Carbon Dioxide Reactor System (SFE250, Waters Ltd., MA, USA).

Composite characteristics are presented in Table 4. In study III, a dynamic compression treatment was conducted for the composites in an aqueous environment at 37°C for minimum of 20 cycles with a compression level of at least 50 % prior to *in vitro* and *in vivo* studies. For the *in vitro* studies in studies II and III, the composites were incubated in basic medium (BM; Table 5) for 24 h before

seeding the cells. For the *in vivo* study in study III, the composites were pre-compressed in blood collected from the bony defect site.

4.1.3   3D printing of Cu^{2+} doped BaG/PCL composites

The Cu^{2+} doped BaG/PCL composites in study IV were 3D printed by direct ink writing as described in the original publication. The 2 BaG compositions used in the composites are described in Table 3. In brief, the BaG batches were melted in a Pt crucible at 1360 °C for 3 h, cast, annealed, crushed, and remelted to ensure their homogeneity. The annealed glass block was crushed and gradually fractionated and the finest powder fraction ($\emptyset \leq 45$ µm) was further grinded to obtain the finest particles for ink formulation. To obtain a viscous solution, PCL was dissolved in acetone, which was used as a carrier for BaG particles in ink formulation. The BaG particles were dispersed into the viscose PCL solution homogeneously with a planetary centrifugal mixer (ARE-250, Thinky Corporation). The compositional ratios (wt-%) between PCL and BaG or BaG-Cu were 4:1, 2:1, or 1:1. Scaffold fabrication via direct ink writing was conducted using an adapted Korean Institute for Machinery and Materials (KIMM) Bioplotter. The ink was loaded into a fluid dispensing system (Optimum by Nordson EFD) and a stainless steel precision tip (25GA, Nordson EFD) was used as the dispensing nozzle. The scaffolds were printed layer-by-layer by extruding the ink into a cold ethanol bath. Then, the scaffolds were soaked in absolute ethanol for 24 h and the ethanol was changed every 8 h. Finally, the scaffolds were left to dry prior to further characterizations. For sterilization before cell culture experiments, the scaffolds were incubated 2 x 10 min in 70 % ethanol and then left to dry for 2 h. The scaffolds were incubated for 48 h in BM (Table 5) prior to cell seeding.

Table 3.   Composition of BaGs in studies I and IV.

| | wt-% | | | | | | | | |
	Na_2O	K_2O	MgO	CaO	P_2O_5	B_2O_3	SiO_2	TiO_2	CuO
BioRestore	11.1-12	15-17.1	2.8-3.3	12.7- 15.2	2.7-3.8	1-1.4	48.5-52	0- 0.6	-
S53P4	23	-	-	20	4	-	53	-	-
S53P4-Cu	23	-	-	19	4	-	53	-	1

Table 4. Biomaterials used in studies I-IV.

Biomaterials in studies I-IV		Sterilization	Composition	Dimensions/ sample size	Porosity, pore size
Straumann® BoneCeramic granules	I	sterile package	60 % HA and 40 % β-TCP	0.25 g of 0.5-1.0 mm sized granules	90 % 100-500 µm
Inion BioRestore™ BaG scaffold	I	70 % ethanol	BaG	square 7x7x3 mm	70 %
40 wt-% β-TCP in PLCL	II	γ-irradiation	40 wt-% β-TCP in PLCL	Ø=10mm, h=3mm	67 % 340 ± 130 µm
50 wt-% β-TCP in PLCL	III	γ-irradiation	50 wt-% β-TCP in PLCL	**in vitro:** Ø=8mm, h=3mm **in vivo:** Ø=3.2mm, h=10mm Ø=4mm, h=10mm	65-67 % 380 ± 130 µm
PCL/ BaG(S53P4)- Cu composites	IV	70 % ethanol	PCL/BaG or PCL/BaG-Cu in ratios 1:1, 2:1 or 4:1	square 10x10x1-4 mm	60 %

4.1.4 Scaffold characterization

The morphology and surface topography of the Straumann® BoneCeramic granules and Inion BioRestore™ bioactive glass scaffolds in study I and, the $scCO_2$ processed β-TCP/PLCL composites in study III, were imaged by using a scanning electron microscopy (SEM; Philips XL-30; Philips, Eindhoven, The Netherlands) as described in the original publications. In addition, even though not included in the original publication of study II, the $scCO_2$ processed β-TCP/PLCL composites used in study II were also imaged using SEM (Jeol JSM T-100, Freising Germany).

The $scCO_2$ processed β-TCP/PLCL composites (studies II and III) and the PCL/BaG scaffolds (study IV) were imaged by using an Xradia MicroXCT-400 x-ray imaging system (Carl Zeiss X-ray Microscopy Inc., Pleasanton, USA) as described in the original publications.

In study IV, the PCL/BaG-Cu scaffolds were evaluated by using a LEICA M205A optical microscope. The bioactivity of the PCL/BaG-Cu composites in study IV was analyzed for 30 days in SBF and the formation of CaP precipitates was confirmed with a SEM-EDXA (EDXA, LEO Gemini 1530 with a Thermo Scientific UltraDry Silicon Drift Detector, X-ray detector by Thermo Scientific).

4.1.5   Mechanical testing of scaffolds

In study III, the mechanical testing of scCO$_2$ processed β-TCP/PLCL composites was conducted for both intact and pre-compressed scaffolds (Ø = 8 mm, h = 3.5 ± 0.6 mm) as dry at RT and in an aqueous solution at 37 °C with Instron Electropuls E1000 (High Wycombe, UK) as described in the original publication. The elastic modulus was calculated based on the linear section of the stress-strain curve, between 0 and 20 % strain.

The compressive response of the BaG-Cu/PCL scaffolds in study IV was analyzed with a Shimadzu EZ-L Universal Mechanical Tester as described in the original publication. The compressive modulus was determined based on the stress versus engineering strain curves.

4.1.6   Hydrolytic degradation of composites *in vitro* and *in vivo*

In study III, the hydrolytic degradation of the porous β-TCP/PLCL composites was studied *in vitro* and *in vivo* at 4-, 12- and, 24-week time points as described in the original publication. The *in vitro* study was conducted at 37 °C in SBF and the *in vivo* study as intramuscular implantation in rabbit supraspinatus muscle. As a reference, a porous PLCL (70/30) polymer scaffold was used. The number average molecular weight (M_n), weight-average molecular weight (M_w) and polydispersity of the scaffold samples were calculated against polystyrene standards at RT.

4.1.7   Ion release from PCL/BaG-Cu composites

The ion release profile of PCL/BaG and PCL/BaG-Cu composites in study IV was determined in SBF at 37 °C as described in the original publication. The samples were incubated in SBF for 30 days and analyzed at 6 h, 24 h, 3 d, 7 d, 14 d, 22 d and 30 d. The Ca, P, Si and Cu ion concentrations in samples were determined with an inductively coupled plasma optical emission spectrometer (ICP-OES) (Optima 5300 DV, Perkin Elmer, Shelton, CT).

The Cu^{2+} release was also analyzed from the culture medium during the 14-day hBMSC culture as described in the original publication. The Cu^{2+} concentration in medium was analyzed by utilizing the ICP-OES analysis and the aforementioned protocol.

4.2   Cell isolation, characterization and culture

4.2.1   Human adipose stem cells

hASCs were used in studies I, II and III and the cells were isolated from adipose tissue samples received from surgeries at the Department of Plastic Surgery, Tampere University Hospital with the patients' consent. The hASCs used in studies were obtained from (I) 11 donors (mean age 50 ± 14 years), (II) six donors (mean age 44 ± 14 years) and, (III) three donors (mean age 40 ± 11 years). The studies were carried out under authorization of the Ethics Committee of the Pirkanmaa Hospital District, Tampere (R15161). Isolation of hASCs was conducted using a mechanical and enzymatic protocol as described in the original publications. Isolated hASCs were expanded in BM (composition described in Table 5). The hASC culture experiments were conducted at passages 2 to 5 in studies I-III.

4.2.2   Human bone marrow stem cells

The hBMSCs used in study IV were extracted from a bone marrow aspirate obtained from a surgical procedure at the Department of Orthopedics and traumatology, Tampere University Hospital with the patient's consent. The donor was an 80-year-old female. The study was carried out in agreement with the Ethics Committee of the Pirkanmaa Hospital District, Tampere (R15174). The hBMSCs were isolated using centrifugation through a Ficoll gradient as described in the original publication. Isolated hBMSCs were expanded in BM (composition described in Table 5) and the experiments were conducted at passage 3.

4.2.3   Human umbilical vein endothelial cells

HUVECs used in study IV were isolated from an umbilical cord received from a planned Cesarean section at the Department of Obstetrics and Gynecology, Tampere University Hospital with the patient's consent. The study was conducted under authorization of the Ethics Committee of the Pirkanmaa Hospital District, Tampere (R13019). The HUVEC extraction procedure is described in the original publication. The isolated HUVECs were cultured in EGM-2 (Lonza; composition presented in Table 5) and the experiments were conducted at passage 3.

Table 5. Different media compositions used in studies I-IV. Basal medium (BM), osteogenic medium (OM), endothelial medium (EM), endothelial growth factor (EGF).

	Medium	Composition
BM	BM for hASCs in study I	DMEM-F12 with 5-10 % (v/v) FBS, 1 % (v/v) antibiotics and 1 % (v/v) L-alanyl-L-glutamine
	BM for hASCs in study II and III	DMEM-F12 with 5-10 % (v/v) HS, 1 % (v/v) antibiotics and 1 % (v/v) L-alanyl-L-glutamine
	BM for hBMSCs in study IV	MEM Alpha Medium with 5 % HS and 1 % antibiotics with 5 ng/mL of human FGF-2
OM	OM for hASCs	BM with 250 µM ascorbic acid 2-phosphate (AA2P), 10 mM β-glycerophosphate (β-GP) and 5 nM dexamethasone (Dex)
	OM for hBMSCs	BM with 200 µM ascorbic acid 2-phosphate (AA2P), 10 mM β-glycerophosphate (β-GP) and 5 nM dexamethasone (Dex)
EM	EGM-2	Endothelial basal medium (EBM)-2 supplemented with GA-1000, EGF, VEGF, FGF-2, R^3-IGF-1, heparin, hydrocortisone, ascorbic acid and 2 % (v/v) FBS
	EM	EBM-2 supplemented with GA-1000, EGF, VEGF, FGF-2, R^3-IGF-1, and 2 % (v/v) HS

4.2.4   Cell characterization

To verify the mesenchymal origin of hASCs (studies I-III) and of hBMSCs (study IV) and to characterize the isolated HUVECs, the surface marker expression of the cells was determined by a fluorescent-activated cell sorter (FACSAria; BD Biosciences, Erembodegem, Belgium) at passage 1-3 as described in the original publications.

The surface marker expression of hASCs and hBMSCs are presented in Table 6. Their surface marker profile verified the mesenchymal origin of the isolated cells (Bourin *et al.*, 2013; Dominici *et al.*, 2006). The HUVECs were positive for markers CD31 (99.5 %), CD73 (99.9 %), CD105 (99.9 %), CD146 (99.9%), whereas the expression of CD90 (5.7 %) and VEGFR2 (3.8 %) was low. Furthermore, the expression of CD34 (42.9 %), CD36 (12.2 %), CD144 (12.9 %), CD202B (35.6 %) and VEGFR3 (27.8 %) was moderate in the isolated HUVECs.

4.3   Optimization of endothelial medium for hASCs

In study II, 2 medium compositions were compared in order to optimize EM for hASC differentiation. hASCs were cultured in BM, EGM-2 (Lonza) or in a HS-based version of EGM-2 (EM; described in Table 5). The comparison was repeated with 3 hASC lineages at passage 2. The optimization is described in the original publication.

Based on the results of the comparison described in more detail in the original publication, EM was selected for the 3D experiments in study II.

Table 6.   Surface marker expression of hASCs and hBMSCs cultured in HS or FBS used in studies I-IV. Results are expressed as mean ± SD.

Surface markers		Study I	Study II	Study IV	Study III
		hASCs (FBS)	hASCs (HS)	hASCs (HS)	hBMSCs (HS)
CD14	Serum lipopolysaccharide binding protein	0.96 ± 0.63	0.6 ± 0.6	1.5 ± 0.6	0.4
CD19	B lymphocyte-lineage differentiation antigen	0.7 ± 0.4	0.4 ± 0.2	1.1 ± 0.2	1
CD34	Sialomucin-like adhesion molecule	19.8 ± 21.1	34.8 ± 32.2	15.2 ± 11.1	0.1
CD45	Leukocyte common antigen	1.4 ± 0.4	1.6 ± 0.3	1.4 ± 0.5	1.8
CD73	Ecto-50-nucleotidase	96.5 ± 3.4	98.2 ± 1.3	97.8 ± 0.7	99.8
CD90	Thy-1 (T-cell surface glycoprotein)	99.6 ± 0.2	99.8 ± 0.1	99.5 ± 0.1	85.1
CD105	SH-2 endoglin	87.1 ± 21.7	98.3 ± 1.2	98.8 ± 0.5	99.8
HLA-DR	Major histocompatibility class II antigens	0.8 ± 0.5	0.6 ± 0.1	1.2 ± 0.7	97.2

4.4   Cell culture in different scaffolds

In study I, the hASCs were seeded at a density of 9.7×10^4 cells per BoneCeramic granule sample or BioRestore scaffold, in a 50 μl medium drop. The cells were left to attach for 3 h before adding 1 mL of corresponding medium. In the first part of study I, rhBMP-2 (Genscript, Pisataway, NJ, USA), rhBMP-7 (Sigma-Aldrich), and VEGF (rhVEGF165; R&D Systems) were added to BM and compared with OM. In the second part of study I, the growth factors were added to OM. The concentrations of rhBMP-2, rhBPM-7 and VEGF were respectively 50 ng/mL, 100 ng/mL and, 20ng/mL.

In study II, the differentiation of hASCs in β-TCP/PLCL composites was studied in 2 parts. Firstly, hASCs were cultured in 2 experimental groups: OM and EM while BM served as a control. Before seeding the cells into the scaffolds, hASCs were cultured for 5 days in BM, EM or OM in polystyrene. In Part I of the study, 120 000 hASCs (510 cells/ mm³) were seeded at day 0 per scaffold in 50 μL of medium. Cells were allowed to attach for 3 h prior to adding 1 mL of corresponding medium. Secondly, the differentiation of hASCs in the composites was studied in 2 additional experimental groups: OM-cocktail and EM-cocktail. In OM-cocktail group, hASCs were cultured for 5 days in OM before seeding 60 000 cells into the scaffolds at day

0. Then, hASCs seeded constructs were supplemented with OM for 7 days. At day 7, another 60 000 cells were seeded into the scaffolds. The hASCs seeded at day 7 were cultured for 5 days in EM before cell seeding in scaffolds. After the day 7 cell seeding, the cell seeded constructs were supplemented with a cocktail medium of OM and EM (1:1) for the rest of the experiment. In EM-cocktail group, hASCs were cultured for 5 days in EM before cell seeding 60 000 cells into the scaffolds at day 0. Thereafter, hASCs seeded in scaffolds were supplemented with EM for 7 days. At day 7, another 60 000 cells were seeded into the scaffolds. The hASCs seeded at day 7 were cultured for 5 days in OM prior to cell seeding at day 7. After the day 7 cell seeding, the cell seeded constructs were supplemented with a cocktail medium of OM and EM (1:1) for the rest of the experiment. In Part II of the study (OM-cocktail and EM-cocktail), 60 000 hASCs (255 cells/mm^3) were seeded per scaffold in a 50 µL volume of medium at day 0 and day 7. Cells were allowed to attach for 3 h prior to adding 1 mL of corresponding medium.

In study III, the hASCs were seeded in β-TCP/PLCL composites at a density of 510 cells/ mm^3 in 50 µL of medium. Cells were allowed to attach for 2-3 h before adding 500 µL of BM or OM per well. In alizarin red staining, a 2D control was used: 500 cells were seeded in 1 ml of BM or OM in a 24-well plate (Nunc, Roskilde, Denmark).

In the first part of study IV, the PCL/BaG and PCL/BaG-Cu scaffolds' ability to support hBMSC viability, proliferation and early osteogenic differentiation were assessed. 50 000 hBMSCs were seeded in a 50 µL volume of OM per scaffold. Cells were allowed to attach for 3 h prior to adding 2 mL of OM per well. Secondly, the ability of PCL, PCL/BaG (4:1) and PCL/BaG-Cu (4:1) to support vascularization was evaluated in co-culture of hBMSCs and HUVECs. Due to the detected inhibitory effect of high copper content caused by PCL/BaG-Cu (2:1) and (1:1), they were excluded from the co-culture experiments. The printed scaffolds (10x10x1mm) were cut in quarters and 20 000 hBMSCs were seeded per scaffold quarter. hBMSCs were cultured for 6 d in OM. Thereafter, 20 000 HUVECs were seeded into the scaffolds and the medium was changed to EGM-2 (Lonza, Basel, Switzerland) for the rest of the experiment.

4.5   Cell viability and proliferation

Cell viability was evaluated qualitatively in studies I, III and IV by staining the cells with fluorescent live/dead-staining probes (Molecular Probes/ Invitrogen, Eugene,

OR, USA) as described in the original publications. Representative images of living cells (green fluorescence) and dead cells (red fluorescence) were acquired with an Olympus IX51 phase contrast microscope with fluorescence optics and Olympus DP30BW camera (Olympus, Tokyo, Japan).

In study IV, hBMSC viability was also quantitatively assessed by using a lactate dehydrogenase (LDH) activity assay (Abcam, Cambridge, UK) as described in the original publication. Absorbance was determined at 450 nm with a microplate reader (Victor 1420 Multilabel Counter; Wallac; Turku, Finland).

Proliferation was analyzed quantitatively in studies I-IV at different time points by determining the total amount of DNA by CyQUANT Cell Proliferation Assay Kit (Molecular Probes, Eugene, OR, USA; Invitrogen) as described in the original publications. Fluorescence in samples was measured at 480/520 nm with a microplate reader (Victor 1420 Multilabel Counter).

4.6   Analysis of osteogenic and endothelial differentiation *in vitro*

Osteogenic differentiation of hASCs and hBMSCs was analyzed using various osteogenic markers and methods in studies I-IV as presented in Table 7. Endothelial differentiation of hASCs in study III and, vascularization in co-culture of hBMSCs and HUVECs in study IV were analyzed with different techniques as presented in Table 8.

ALP activity in samples was determined in studies I-IV at various time points as described in the original publications. The ALP activity was determined from the same cell lysates as total DNA content. Absorbance was measured at 405 nm (Victor 1420 Multilabel Counter). Absorbance values were normalized to cell amount in study IV.

Soluble total collagen in samples was quantified in studies I and III by using Sircol Soluble Collagen Assay (Biocolor, Carrickfergus, United Kingdom) as described in the original publication. Absorbance in samples was measured from two parallel 100 µl samples in a 96-well plate (Nunc) using a microplate reader (Victor 1420 Multilabel Counter) at 540 nm.

Alizarin red staining after 14 and 21 days in studies II and III was used to assess the formation of mineralized matrix in samples as described in the original publications. Stained scaffolds were photographed, then the stain was extracted, and the intensity of the dye was determined by measuring absorbance at 540 nm (Victor 1420 Multilabel Counter).

Endothelial (PECAM-1, vWF and CD144) and osteogenic marker proteins (COL-1 and OCN) were detected with immunocytochemistry using an indirect staining method in studies II-IV as described in the original publications. The used primary and secondary antibodies as well as their dilutions are presented in the original publications. The stained samples were imaged using an Olympus IX51 phase contrast microscope with fluorescence optics and Olympus DP30BW camera (Olympus, Tokyo, Japan). Images were edited and constructed by using Adobe Photoshop. In the 2D medium optimization experiments in study III, the samples were imaged with fluorescence optics using a digital inverted microscope (AMG EVOS).

Quantitative real-time reverse transcription polymerase chain reaction (qRT-PCR) analysis was used to evaluate the relative expression of osteogenic and endothelial genes in studies II-IV as described in the original publications. The primer sequences and accession numbers for *RPLP0* (human acidic ribosomal phosphoprotein large P0) and osteogenic genes *ALP*, *COL-1*, *Runx2a*, *OSX*, *DLx5* are presented in the original publications. For analysis of endothelial gene *vWF* a commercial primer assay was used. The reactions were carried out with ABIPRISM® 7300 Sequence Detection System. qRT-PCR data was normalized to the expression of *RPLP0*. The results were processed by using AbiPrism 7300 Sequence Detection System -software (Applied Biosystems).

Table 7.   Markers, methods and time points used to analyze the osteogenic differentiation of hASCs (I-III) and hBMSCs (IV).

Study	Marker for osteogenic differentiation	Detection technique	Time points
I	ALP activity	ALP activity assay	7 d, 14 d
	Soluble total collagen amount	Sircol soluble collagen assay	7 d, 14 d
II	ALP activity	ALP activity assay	14 d, 21 d
	Mineralized matrix formation	Alizarin red staining	14 d, 21 d
	Gene expression of *ALP, COL-1, Runx2a, OSX and DLx5*	qRT-PCR	14 d, 21 d
III	ALP activity	ALP activity assay	7 d, 14 d, 21 d
	Soluble total collagen amount	Sircol soluble collagen assay	7 d, 14 d, 21 d
	Mineralized matrix formation	Alizarin red staining	14 d, 21 d
	Protein expression of COL-1 and osteocalcin	Immunocytochemical staining and fluorescence microscopy	7 d, 14 d, 21 d
	Gene expression of *Runx2a, OSX and DLx5*	qRT-PCR	14 d, 21 d
IV	ALP activity	ALP activity assay	7 d, 14 d
	Gene expression of *Runx2a, osteocalcin and DLx5*	qRT-PCR	11d, 20 d

Table 8.   Markers, methods and time points used to analyze endothelial differentiation and vascularization in studies III and IV.

Study	Marker for endothelial differentiation	Detection technique	Time points
III	Vessel formation in Matrigel	Sprouting assay	20 d
	Protein expression of PECAM-1, vWF and CD144	Immunocytochemical staining and fluorescence microscopy	14 d, 21 d
	Gene expression of *PECAM-1* and *vWF*	qRT-PCR	14 d, 21 d
IV	Protein expression of PECAM-1 and vWF	Immunocytochemical staining and fluorescence microscopy	13 d, 20 d
	Gene expression of *PECAM-1* and *vWF*	qRT-PCR	6 d, 11d, 20 d

4.7   Analysis of bone formation *in vivo*

The animal study in study III was conducted in accordance with The Animal Experiment Board in Finland (ESAVI/5398/04.10.07/2014). In the *in vivo* experiment, 20 female New Zealand white rabbits were used and handling of rabbits as well as the surgeries are described in detail in the original publication. Briefly, a 3.2 mm diameter and 10 mm deep hole was drilled above the lateral collateral ligament of the right femoral condyle. The β-TCP/PLCL composite scaffolds (3.2 x 10 mm) were pre-compressed in blood collected from the drilling hole and placed into the defect. For the analysis hydrolytic degradation *in vivo*, a skin incision was made midline over the spine between the scapulae and two β-TCP/PLCL composites (4 x 10 mm) were implanted into the right supraspinatus muscle and two PLCL scaffolds (4 x 10 mm) into the left supraspinatus muscle. The rabbits were randomly divided in groups and euthanized 4-, 12- and, 24 weeks after the procedure.

Micro-CT analysis (MicroXCT-400, Zeiss) was performed on all the harvested femoral condyles before histological preparation as described in study II. Thereafter, histological preparation was carried out and the sectioned samples were histologically stained (Masson-Goldner's Trichrome (MGT) staining). The intramuscular implants were collected for the hydrolytic degradation analysis.

4.8   Statistical testing

In study I, the statistical testing was conducted with SPSS version 19 (IBM, Armonk, NY, USA). Depending on the comparison, a one-way analysis of variance (ANOVA) with a Tukey *post hoc* test or, a Student's *t*-test for independent samples were used. The statistical testing is described in more detail in the original publication. Statistical

analyses in studies II-IV were conducted with SPSS version 22 or 23 (IBM, Armonk, NY, USA) using non-parametric tests due to low sample size and non-linearly distributed data. In studies II and III, a Mann-Whitney U-test with Bonferroni correction were used as described in the original publications. In study IV, a Kruskal-Wallis test with Mann-Whitney U *post hoc* test and Bonferroni correction were used as described in the original publication. The results were considered significant when $p < 0.05$.

5   RESULTS

5.1   Scaffold characterization

5.1.1   Scaffold architecture and surface topography

All scaffolds used in studies I-IV were imaged using SEM and a summary panel of the results is presented in Fig. 5. When comparing the SEM images of the scaffolds, they exhibit distinctly different surface architecture for the seeded cells.

In study I, both BoneCeramic granules and BioRestore scaffold were shown to have a high porosity. Furthermore, BioRestore exhibited a larger surface area, as it is composed of small sized fibers. BoneCeramic on the other hand demonstrated more surface roughness when compared to BioRestore.
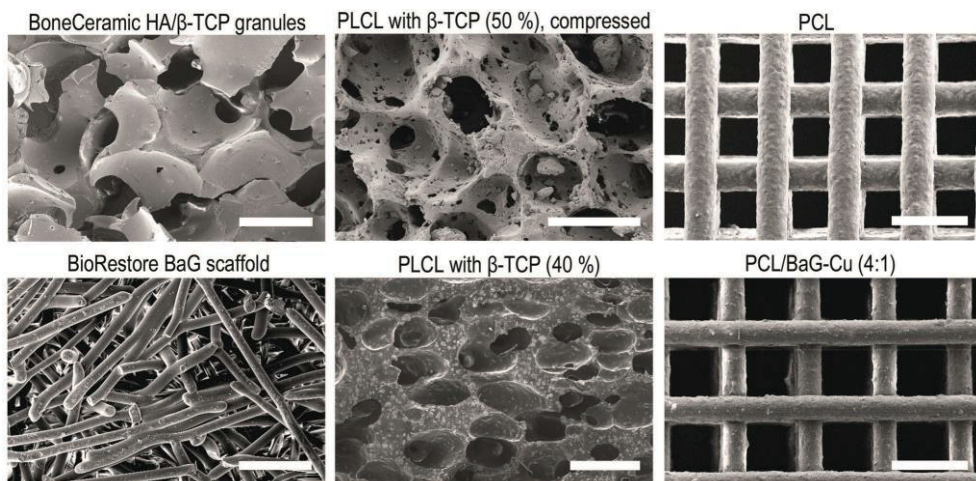
Figure 5.   Representative SEM images of the different biomaterials used in the study. Scale bars 500 μm.

In study II, scCO$_2$ processed PLCL composites with 40 wt-% β-TCP were used. The micro-CT analysis gave a scaffold porosity of 67 % with an average pore size of 340 ± 130 μm. In study III, in addition to the scaffold architecture the SEM images

exhibited the effect of the used pre-compression treatment on the scCO$_2$ processed β-TCP/PLCL (50 wt-% ceramic content) composites as presented in the original publication. The used β-TCP granules had a larger particle size as compared to composites in study II. Prior to the pre-compression treatment β-TCP was mainly visible on the cutting surface on the composite whereas a PLCL film mostly covered the β-TCP granules elsewhere. After the pre-compression the PLCL surface ruptured and the β-TCP granules protruded on display. Moreover, the pre-compression treatment tore additional holes into the polymer surfaces. According to the micro-CT analysis scaffold porosity was 65-67 % with an average pore size of 380 $\pm$ 130 μm and, the micro-CT imaging confirmed the effect of the pre-compression treatment. The structure of the composite in study III is notably different as compared to the composite used in study II (Fig. 5).

In study IV, the SEM imaging showed that the surface roughness of the PCL-based composites increased as the BaG-Cu content in the composites elevated as shown in the original publication. All the scaffolds in study IV had a total porosity of 60 % according to the micro-CT analysis.

5.1.2   Mechanical properties of the scaffolds

In study III, the compressive stress at 20- and 50 % strain as well as the modulus were determined. The compression treatment and the physiological temperature of 37 °C had a significant effect on the mechanical properties of the scCO$_2$ processed PLCL with 50 wt-% β-TCP composite as shown in the original publication. As dry, the pre-compression decreased the modulus significantly when compared to an intact composite however, the difference was diminished after 1h at 37 °C in aqueous solution. Furthermore, the same phenomenon was observed in the analysis of compressive stress at 20- and 50 % strain. In addition, the warming and wetting of the intact composite decreased the modulus significantly when compared to dry intact composite. The modulus and strength increased between 1h and 7 d when analyzed at 37 °C in an aqueous environment.

In study IV, the printed PCL/BaG-Cu composites (4:1, 2:1 and 1:1) demonstrated reinforced mechanical properties as compared to PCL scaffold. The compressive Young's modulus for PCL scaffold was 5.9 MPa. Among the PCL/BaG-Cu composites with compositional ratios 4:1, 2:1 and 1:1; PCL/BaG-Cu (2:1) demonstrated the highest E value (12.5 MPa) whereas PCL/BaG-Cu (1:1) had the lowest E value (7.19 MPa).

5.1.3 Hydrolytic degradation of β-TCP/PLCL composites

In study III, the M_n and M_w change during the 24-week follow-up showed that the *in vitro* degradation is a lot like the degradation *in vivo* for both β-TCP/PLCL (50 wt-%) composites and PLCL polymer scaffolds. The molecular weight of the scaffolds decreased significantly already during the first 4 weeks. The polymer scaffold had a higher initial M_n and M_w in comparison to the composite, but the difference was evened out during the degradation already in 4 weeks. After the 4-week time point, no clear differences between the degradation of the two scaffold types or between the in *vitro* or in *vivo* environments were observed. The residual L-lactide monomer content after processing for the PLCL scaffold was 0.09 wt-% and for the β-TCP/PLCL composite 0.06 wt-%.

5.1.4 Bioactivity and ion dissolution profile of PCL/BaG-Cu composites

In study IV, notable CaP precipitation on the strut surfaces was only observed after 7 d of immersion. After 30 days, a clear CaP layer had formed on the surfaces of PCL/BaG-Cu (2:1) and PCL/BaG-Cu (1:1) composites while only small aggregates of CaP were observed on PCL/BaG-Cu (4:1). The CaP precipitates had a characteristic cauliflower-like morphology with a Ca/P ratio of 1.56, which is close to that of natural bone mineral (1.67).

When considering Si release, a burst release was observed within 3 days of immersion with all composites, which is most likely associated to the initial dissolution of BaG-Cu particles exposed on the surface of the composites. After 3 days, the BaG-Cu dissolution slowed down. With PCL/BaG-Cu (4:1), a low level of Si was detected most likely due to the low BaG-Cu content. With PCL/BaG-Cu (2:1), a continuous Si release at a close to constant level was observed for the rest of the immersion. Whereas with PCL/BaG-Cu (1:1), after 7 d of immersion the released Si reached a saturation level at ~ 60 mg/L in SBF. The release trend of Cu was similar to that of Si. A higher Cu^{2+} concentration in SBF was measured with PCL/BaG-Cu (1:1) as compared to the other composites. The ion concentration profiles of Ca and P in SBF were reflected on the CaP precipitation on the surfaces of the composites. With PCL/BaG-Cu (2:1) and PCL/BaG-Cu (1:1) the P ion concentration decreased immediately during the first few days of immersion most likely due to formation of a CaP layer. In contrast, the P concentration remained high with PCL/BaG-Cu (4:1) composite during the first two weeks. This was in line

with the fact that CaP precipitation was observed only after 14 days of immersion with PCL/BaG-Cu (4:1).

The Cu^{2+} concentration was also analyzed from culture medium during the *in vitro* experiment. At 0 d, the scaffolds had been pre-incubated for 48h in BM and the Cu^{2+} concentration in PCL/BaG-Cu composites in compositional ratios (4:1), (2:1) and (1:1) were 35 µM, 70 µM and 117 µM, respectively. hBMSC amount was low in PCL/BaG-Cu (4:1) at day 7 but as the Cu^{2+} concentration decreased to 20 µM as a result of medium changes and dissolution slowdown, hBMSC proliferation was enhanced. Most likely due to high Cu^{2+} concentrations, hBMSC proliferation was inhibited in PCL/BaG-Cu (2:1) and PCL/BaG-Cu (1:1) composites during the 14-day experiment.

5.2   Cell viability and proliferation

In study I, hASCs seeded on both BioRestore and BoneCeramic materials were viable and proliferated well for the whole 2-week culture period as demonstrated by live/dead staining in the original publication and proliferation assay (Fig. 6). BioRestore supported hASC proliferation better as compared to BoneCeramic, as cell number was significantly higher in BioRestore than in BoneCeramic in BM and OM at day 14. Furthermore, hASCs proliferated significantly more in OM in contrast to BM in both BioRestore and BoneCeramic. Concerning the growth factors, BMP-2 and VEGF in BM resulted in similar proliferation levels as BM in both BioRestore and BoneCeramic. In turn, BMP-7 resulted in a lower cell number as compared to BM in BioRestore. In contrast, in BoneCeramic BMP-7 did not inhibit proliferation. Overall, OM demonstrated superior potential to induce proliferation and osteogenic differentiation of hASCs when compared to the tested growth factors. The viability and cell number with OM + growth factors were comparable to those with plain OM, although slightly higher than with BM + growth factors. In BioRestore the slight hindering effect of BMP-7 on proliferation was observed even when combined with OM.

In study II, EM induced hASC proliferation significantly less than OM at both time points (Fig. 7B). In addition, cell number in EM group was at the same level as that in BM group. The effect of OM on hASC proliferation was evident, as hASCs proliferated significantly more in OM when compared to BM and EM at 14- and 21 days (Fig. 7B). Concerning the effect of the cocktail medium, both OM-cocktail and EM-cocktail groups resulted in significantly higher cell numbers than BM.

Figure 6. Proliferation of hASCs in study I at 3-, 7-, and 14-day time points on BioRestore and BoneCeramic. hASCs are cultured in BM, OM or BM + growth factors. Results are expressed as mean + SD ($n = 6$; $^*p < 0.05$ between the indicated groups; $^\#p < 0.05$ when compared to other groups within that time point).
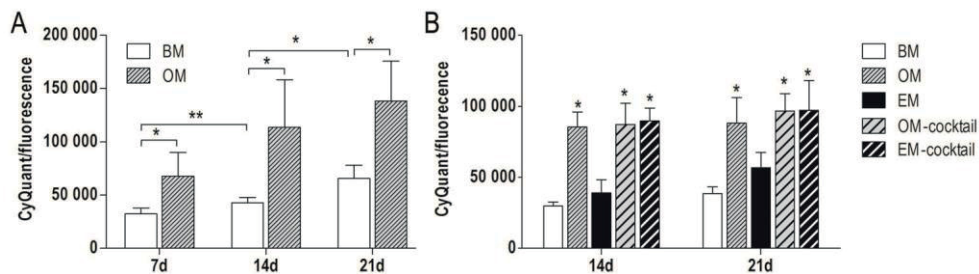
Figure 7. Proliferation of hASCs in scCO$_2$-foamed β-TCP/PLCL composites in study **A)** III (50 wt-% β-TCP in PLCL) at 7-, 14- and 21-day time points and, **B)** II (40 wt-% β-TCP in PLCL) at 14- and 21-day time points. Results are expressed as mean ± SD ($n = 9$; $^*p < 0.001$, $^{**}p < 0.05$).

According to live/dead staining in study III, hASC viability on β-TCP/PLCL composites was good in both BM and OM and, OM seemed to support hASC proliferation better in contrast to BM. In concordance with live/dead staining, the cell amount was significantly higher in OM in contrast to BM at all time points (Fig. 7A).

In study IV, hBMSC viability was good in all scaffolds at 14-day time point, as the number of dead cells was low (Fig. 8A). When compared to the plain PCL scaffold, the elevating BaG content in composites seemed to induce hBMSC proliferation. According to live/dead staining, the higher copper content had an inhibitory effect on hBMSC amount on scaffolds (Fig. 8A). Overall, the LDH activity was at a relatively low and constant level with all the scaffolds during the first

9 days, indicating low cytotoxicity of the studied scaffolds as shown in the original publication. In contrast to live/dead staining results, the Cu^{2+} released from PCL/BaG-Cu (2:1) and PCL/BaG-Cu (1:1) composites did not induce elevated LDH levels in the culture medium. The addition of BaG in PCL had an increasing effect on hBMSC proliferation with all BaG contents at both time points (Fig. 8B). Regarding the role of Cu^{2+} in the composites, also the cell amount results supported the inhibitory effect of rising Cu^{2+} concentration. The amount of hBMSCs in PCL/BaG-Cu (4:1) was low at day 7 however, the cell amount elevated to a similar level as that in PCL/BaG (4:1) at 14 days.
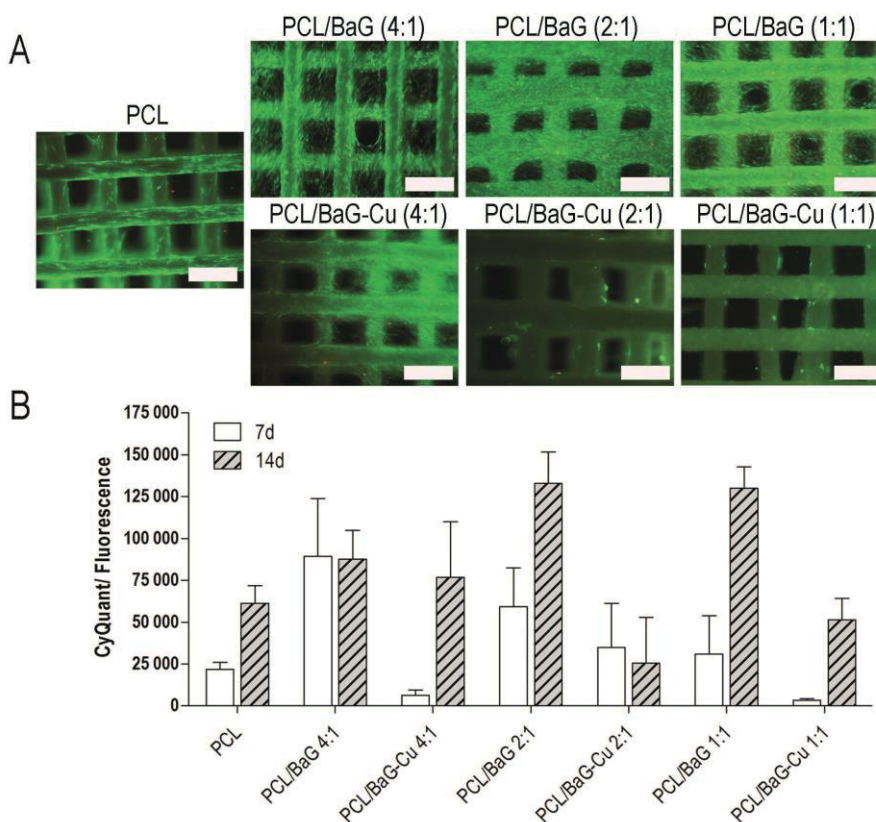
Figure 8. Viability and proliferation of hBMSCs in study IV in PCL, PCL/BaG and PCL/BaG-Cu composites cultured in OM. **A)** Live/dead staining at 14 d (live cells stained green and dead cells stained red). Scale bars 500 μm. **B)** Total DNA amount in samples at 7- and 14 days expressed as mean ± SD (n = 4).

This is most likely connected to the initial burst release of Cu^{2+} as demonstrated in Cu^{2+} concentration analysis from the culture medium. When the Cu^{2+} concentration

decreased to 20 µM, the cells retained their proliferative capacity. The Cu^{2+} concentration remained at a high level during the 14 days with PCL/BaG-Cu (2:1) and (1:1) composites indicating a clear inhibitory effect of higher Cu^{2+} concentration on hBMSC proliferation.

5.3 Osteogenic differentiation

5.3.1 Alkaline phosphatase activity

In study I, both BioRestore and BoneCeramic in BM supported ALP activity in hASCs. However, with BoneCeramic, the effect of OM was more significant and consistent when compared to BM or growth factors, as OM + BoneCeramic combination induced significantly higher ALP activity when compared to all other groups (Fig. 9). Concerning ALP activity of hASCs in BioRestore, OM induced ALP activity significantly more than BMP-2 or BMP-7, but not when compared to BM.
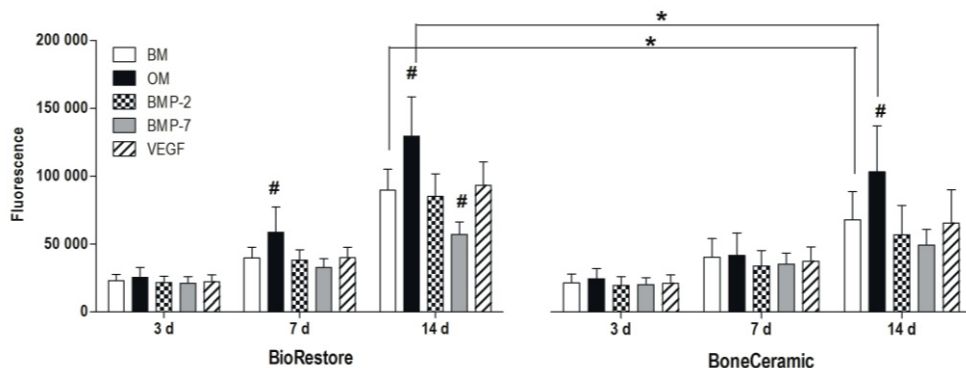

Figure 9. ALP activity of hASCs in study I at 3-, 7-, and 14-day time points on BioRestore or BoneCeramic. hASCs are cultured in BM, OM or BM + growth factors. Results are expressed as mean + SD ($n = 6$; *$p < 0.05$ between the indicated groups; #$p < 0.05$ when compared to other groups within that time point).

In turn, BMP-2 and VEGF resulted in a comparable level of ALP activity as BM with both BoneCeramic and BioRestore. In addition, BMP-7 induced a clearly lower level of ALP activity in comparison to BM in BioRestore. The effects of growth factors on ALP activity were mostly similar in both BoneCeramic and BioRestore.

However, in BoneCeramic the negative effect of BMP-7 on ALP activity was significant. On the other hand, VEGF induced ALP activity significantly more than BMP-7, but not more than BM. Interestingly, adding growth factors in OM did not result in enhanced ALP activity in comparison to plain OM as shown in the original publication. However, the negative effect of BMP-7 on ALP activity was diminished when combined with OM.

In study II, ALP activity analysis demonstrated significant induction in EM group when compared to BM or OM at 14- and 21 days. At 21-day time point, ALP activity in OM was significantly higher when compared to BM. Furthermore, ALP activity was significantly enhanced in EM-cocktail in contrast to BM at both time points.

In study III, ALP activity was significantly higher in OM than in BM after 7 and 14 days in culture. In addition, ALP activity in both BM and OM elevated significantly from 7 days to 14 days whereas the rise from 14 days to 21 days in BM or OM was modest. ALP activity was donor-dependent and especially hASCs from one donor gave higher ALP activity results than the other donor cells.

In study IV, ALP activity increased in all scaffold types from 7 d to 14 d. In turn, ALP activity decreased with rising BaG and BaG-Cu content. Surprisingly, the plain PCL induced ALP activity more than in any of the composites. In turn, PCL/BaG-Cu (4:1) gave a higher ALP activity result than PCL/BaG (4:1).

5.3.2   Total soluble collagen quantification

In study I, BoneCeramic induced collagen production of hASCs significantly more when compared to BioRestore (Fig. 10). Furthermore, collagen production of hASCs in BoneCeramic in BM or BM combined with growth factors was significantly higher than in BioRestore at 7 and 14 days (Fig. 10). Moreover, OM elevated collagen production in both biomaterials at 14 d, with the highest collagen level in BoneCeramic combined with OM. Equally low collagen production was induced by all growth factors and BM in hASCs cultured in BioRestore. In contrast, in BoneCeramic at 7 days BMP-2 induced significantly higher collagen amount when compared to BM and OM. Also, VEGF induced significantly higher collagen amount in comparison to BMP-7 but not higher than BM. In turn, combining growth factors with OM did not increase total collagen production as compared to OM alone as shown in the original publication.

In study III, the total collagen production did not notably differ between BM and OM groups after 7-, 14-, or 21 days in culture as presented in the original publication.

Total collagen amount elevated slightly in both BM and OM from 7 to 14 days whereas, the soluble collagen amount declined from 14 d to 21 d.

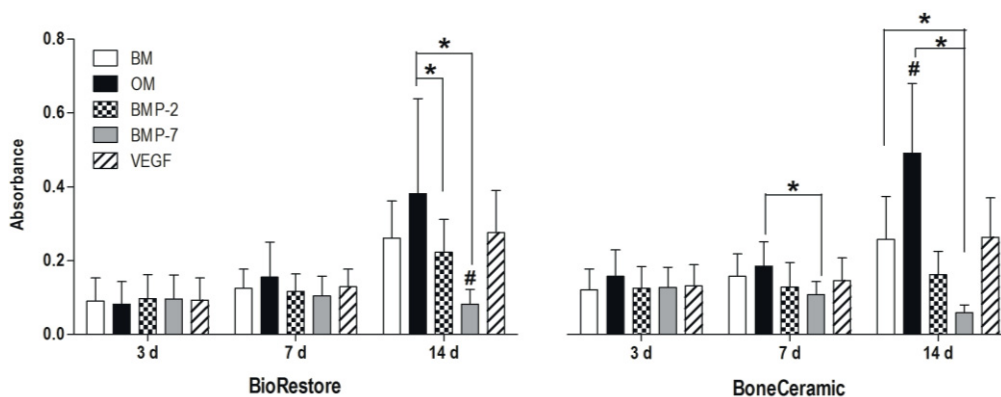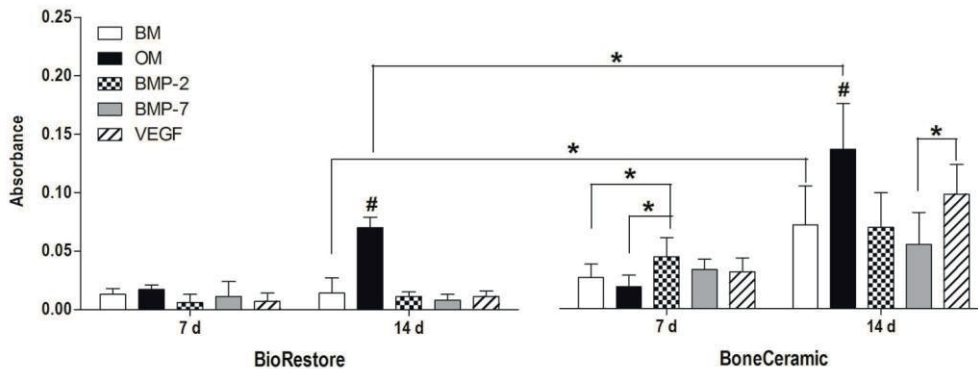**Figure 10.** Soluble collagen amount in study I at 7- and 14-day time points on BioRestore or BoneCeramic. hASCs are cultured BM, OM or BM + growth factors. Results are expressed as mean + SD (n = 6; *p < 0.05 between the indicated groups; #p < 0.05 when compared to other groups within that time point).

5.3.3 Production of mineralized matrix

In study II, hASCs were able to produce mineralized matrix on the β-TCP/PLCL composite surface in all groups already at 14 d (Fig. 11). As observed at both 14 d and 21 d, larger strongly stained areas of mineralized matrix were present in OM in contrast to BM or EM. In addition, OM-cocktail and EM-cocktail induced mineralized matrix formation more when compared to BM (Fig. 11). Quantitative results demonstrated that mineralization was the strongest in OM whereas EM induced the lowest mineralization at both time points as shown in the original publication. However, there were no significant differences between the groups in mineral amount. Furthermore, no significant increase in the calcium mineral amount from 14 d to 21 d was observed in any of the groups.

In study III, hASCs produced a dense mineralized matrix on the β-TCP/PLCL composite surface in both BM and OM already at 14 days (Fig. 12A). Furthermore, hASCs produced a notably thicker mineralized matrix on the scaffold when compared to hASCs cultured on cell culture plastic (2D) at 21 d. As the staining of mineralized matrix was quantified, there was no difference between BM and OM at 14 d whereas, after 21 days of culture the mineral amount in OM was significantly higher when compared to that in BM (Fig. 12B).

When comparing the effect of the 50 wt-% β-TCP/PLCL (study III) composite to that of the 40 wt-% β-TCP/PLCL (study II) composite on mineralization by hASCs, the composite with 50 wt-% ceramic content seems to induce more mineralization in both BM and OM conditions.
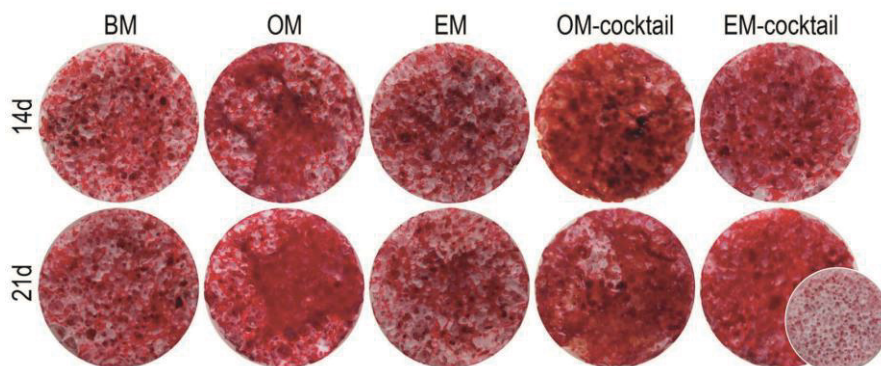
Figure 11. Representative images of mineralized matrix staining of hASC seeded β-TCP/PLCL composites with 40 wt-% mineral content in study II after 14- and 21 days in experimental groups (scaffold Ø = 10 mm). Stained blank scaffold without seeded cells presented on the right lower corner.
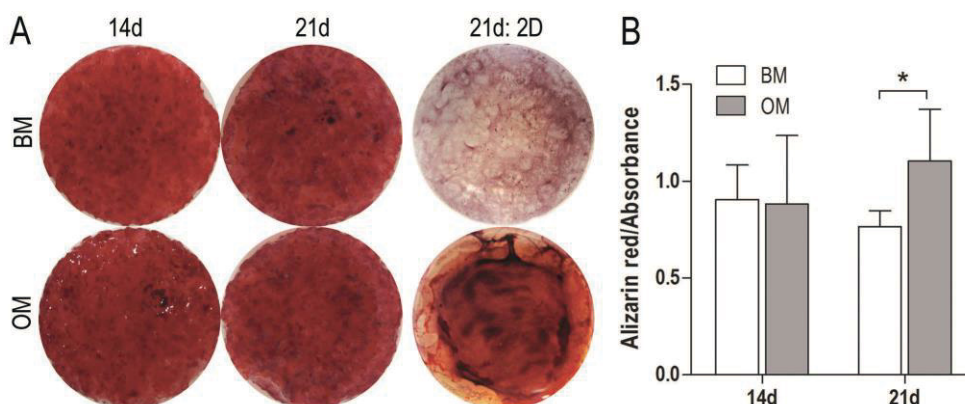
Figure 12. Staining of mineralized matrix in study III in hASC seeded β-TCP/PLCL composites with 50 wt-% mineral content. **A)** Representative images of Ca-mineral stained cell-scaffold constructs after 14- and 21 days and, of hASC cultures on cell culture plastic (2D) after 21 days. Stained blank scaffold without seeded cells is presented on the left of 21 d OM scaffold (scaffold Ø = 8 mm; well Ø = 1.55 cm). **B)** Quantitative Ca-mineral amount after 14- and 21 days expressed as mean ± SD. Statistical significance indicated as $p^* < 0.05$ ($n = 9$).

5.3.4 Immunocytochemical staining of osteogenic markers

In study II, COL-1 staining was carried out at 7 d, 14 d, and 21 d. When considering the COL-1 expression in BM, the induction was modest at all time points (Fig. 13A). However, the COL-1 staining in OM revealed the development of a collagenous matrix during the 3-week experiment: at 7 d cells were producing COL-1 intracellularly; at 14 d the cells were still producing COL-1 intracellularly but they were also secreting COL-1 into the extracellular space; and finally, at 21 d the intracellular production had ceased and a dense extracellular COL-1 matrix can be seen in the representative image (Fig. 13A). In addition to COL-1, ASCs expressed OCN in both BM and OM conditions at both time points however; the intensity of the staining was stronger in OM at both time points (Fig. 13B).
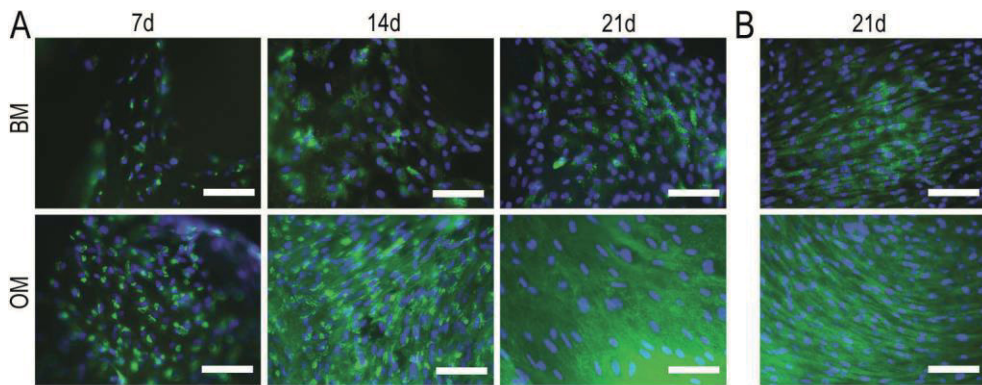
Figure 13. Immunocytochemical staining of osteogenic marker proteins in hASC seeded in β-TCP/PLCL composites in study II. **A)** COL-1 at 7-, 14 and, 21 days and; **B)** OCN at 21 d time point. COL-1 and OCN are stained green and nuclei are stained blue. Scale bar 100 μm.

5.3.5 Osteogenic gene expression

In study II, similar to ALP enzymatic activity results the gene expression of *ALP* was significantly elevated in EM when compared to BM at 14 d and at 21 d. Moreover, the *ALP* expression in EM-cocktail group was significantly higher than that in BM at 14 d. However, the effect of OM was seen in *Runx2a* gene expression, which was significantly induced in OM when compared to BM and EM, and in both cocktail groups relative to BM. On the other hand, *COL-1* expression did not differ significantly between experimental groups. In turn, the expression of *OSX* was

higher in EM relative to BM and OM at day 14. However, the cocktail groups did not have a notable effect on *OSX* expression when compared to BM. Then again, *DLx5* expression was elevated in OM when compared to BM and EM at day 14 and, the expression was also elevated in both cocktail groups when compared to BM at day 21. qRT-PCR analysis of genes *OSX* and *DLx5* were repeated with only 2 donor lines and due to small sample size statistical testing was not carried out.

In study III, the relative expression of osteogenic genes *ALP*, *Runx2a*, *OSX* and *DLx5* did not differ significantly between BM and OM at any of the time points (Fig 15A-D). However, the expression of *Runx2a* and *OSX* were elevated in OM when compared to BM at all time points.

In study IV in hBMSC culture, the gene expression of *Runx2a* was higher in PCL and PCL/BaG-Cu (4:1) in contrast to PCL/BaG (4:1) at days 11 and 20 (Fig. 16A). Then again, in hBMSC+HUVEC co-culture PCL/BaG (4:1) promoted *Runx2a* expression more at both time points when compared to PCL and PCL/BaG-Cu (4:1) scaffolds. The copper containing composite seemed to decrease the expression of *OCN* (Fig. 16B) and *DLx5* (Fig. 16C) while, the PCL/BaG (4:1) scaffold induced the expression of those at both time points and both culture setups. Overall, the expression of osteogenic genes was higher in hBMSC culture than in the co-culture setup.
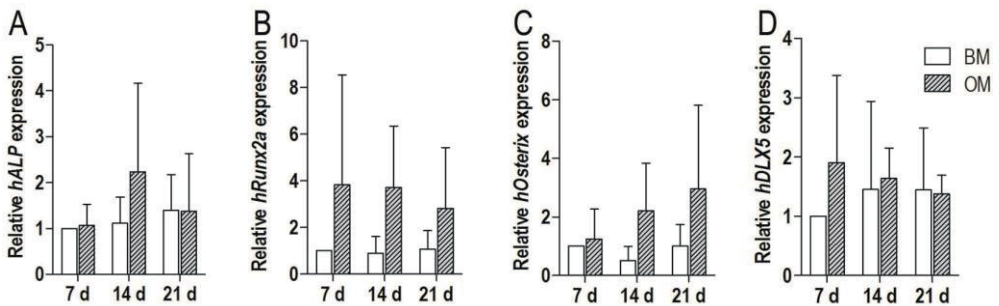
Figure 14. Relative osteogenic gene expression of **A)** *ALP*, **B)** *Runx2a*, **C)** *OSX* and, **D)** *DLx5* in hASCs in study III at 7-, 14- and 21-day time points. Results are expressed as mean ± SD.
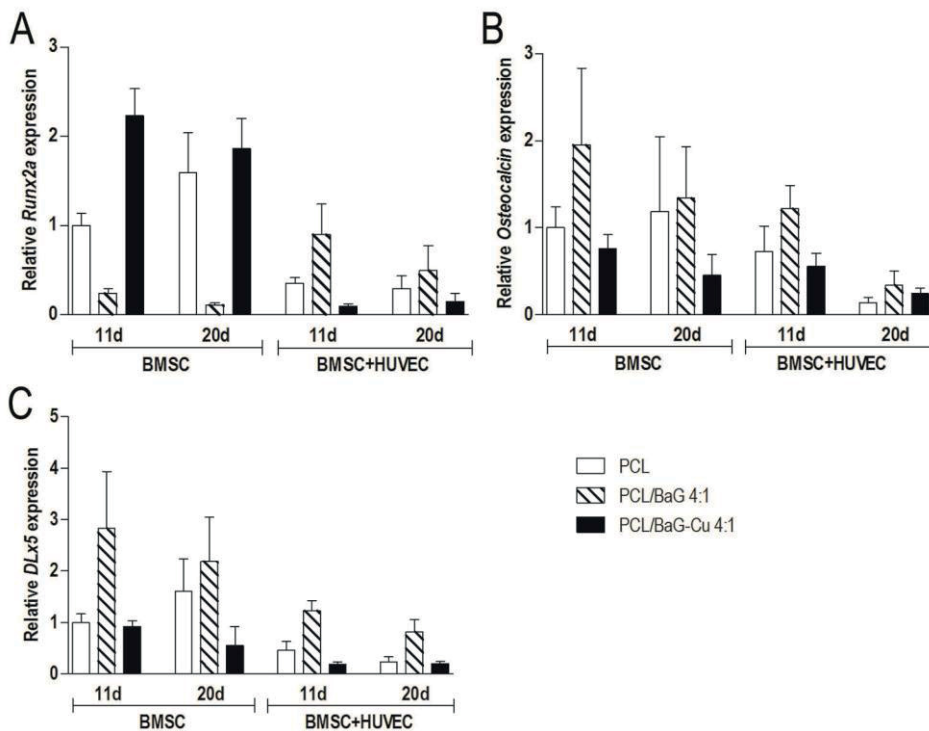
Figure 15. Relative gene expression of osteogenic marker genes **A)** *Runx2a*, **B)** *OCN* and, **C)** *DLx5* in hBMSC and hBMSC+HUVEC culture setups at 13 d and 20 d time points in study IV. Results are expressed relative to hBMSCs cultured for 6 days on PCL scaffold (*n* = 3, mean + SD).

5.4 Endothelial differentiation of hASCs in β-TCP/PLCL composites

In study II, endothelial induction in hASCs in β-TCP/PLCL composites was achieved when cultured in EM for 3 weeks. The expression of endothelial proteins CD31, CD144, and vWF were detected in EM-cultured cells at 14 and 21 days (Fig. 16A, B). However, the cells expressing the vascular markers were not organized as no tubular formation was observed. While according to the immunocytochemical staining the expression of CD31 and vWF was clear in EM, in EM-cocktail the expression of those went down from day 14 to 21. Furthermore, endothelial proteins CD31, CD144 or vWF were not expressed in BM, OM, or OM-cocktail groups during the 3-week experiment, as shown in the original publication.

The gene expression of *vWF* varied between donors but the trend between them was similar: the expression of *vWF* was elevated in EM and EM-cocktail as compared to the other groups at 14 and 21-day time points (Fig. 16C). Like immunocytochemical staining, *vWF* gene expression in EM-cocktail decreased from 14 to 21 days.
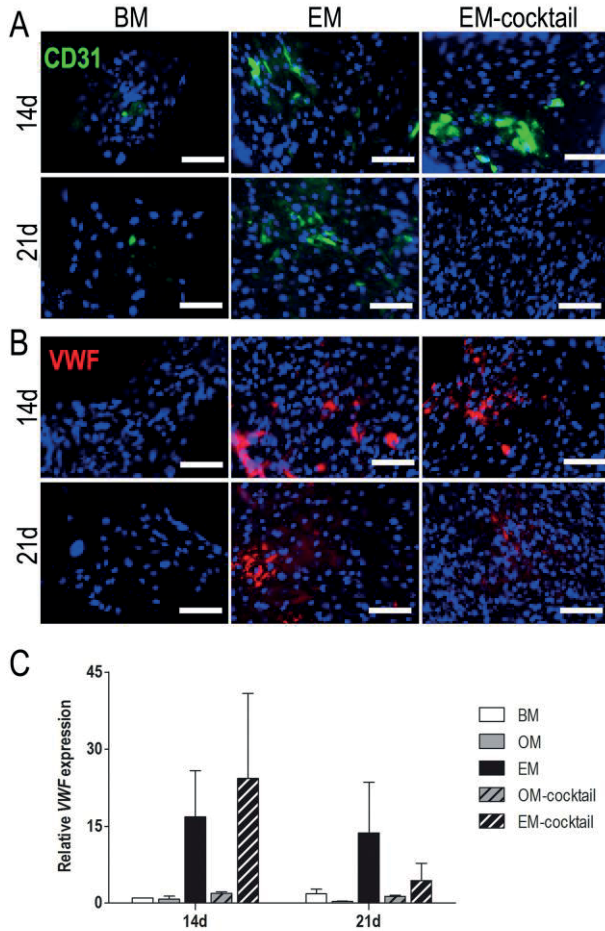
Figure 16. Endothelial differentiation of hASCs in β-TCP/PLCL composites in study III. Protein expression of **A)** CD31 and, **B)** vWF in BM, EM and EM-cocktail groups at 14 d and 21 d time-points. **C)** Relative *vWF* gene expression in experimental groups at 14 d and 21 d time points. Results are expressed as mean ± SD (*n* = 6).

5.5   Vascularization in PCL/BaG-Cu composites

In study IV in hBMSC culture, CD31 protein was expressed in PCL/BaG (4:1) and PCL/BaG-Cu (4:1) composites, whereas cells cultured in PCL did not induce CD31 expression, as demonstrated in the original publication. Furthermore, the CD31 expression in hBMSCs in both PCL/BaG (4:1) and PCL/BaG-Cu (4:1) composites seemed more pronounced at 13 d than at 20 d. In contrast to immunocytochemical staining, the qRT-PCR of *PECAM* demonstrated higher expression in PCL than in the composites at all time points (Fig. 17A). In turn, vWF was not notably expressed at protein level in any of the scaffolds in hBMSC culture during the experiment. Moreover, qRT-PCR demonstrated low *vWF* expression in all scaffolds in hBMSC culture (Fig. 17B).

In immunocytochemical staining of hBMSC+HUVEC co-cultures, CD31 was expressed in all scaffold types at 13- and 20-day time points (Fig. 18). Moreover, visible tubule formation was observed in all scaffold types. In PCL scaffold, the tubular structures were thick but relatively sparse, while the BaG-containing scaffold induced the formation of a denser network of thinner tubes. In turn, the BaG-Cu containing composite induced tubule formation to a lesser extent when compared to the BaG-containing composite (Fig. 18). Considering the staining of vWF, tubular formation was seen in PCL and the BaG containing composite already at 13 d and, the amount of the formed tubes increased from 13 d to 20 d especially with the BaG containing composite. The BaG-Cu containing composite did not induce vWF protein expression in the co-culture setup. In turn, the gene expression of *PECAM* was highly upregulated in the co-culture when compared with the hBMSC culture in all scaffolds, however no clear differences were observed between the scaffolds in either culture setup (Fig. 17A). Still, in the co-culture setup, the *PECAM* gene expression elevated from 11d to 20 d in all scaffolds. The relative *vWF* gene expression followed a highly similar pattern as *PECAM*; the expression level was higher in the co-culture and differences between the scaffolds were minimal (Fig. 17B). In addition, the *vWF* gene expression increased from 11 to 20 days in the co-culture setup. Furthermore, the *vWF* expression level was slightly elevated in BaG-Cu containing composite when compared to PCL and BaG containing composite.
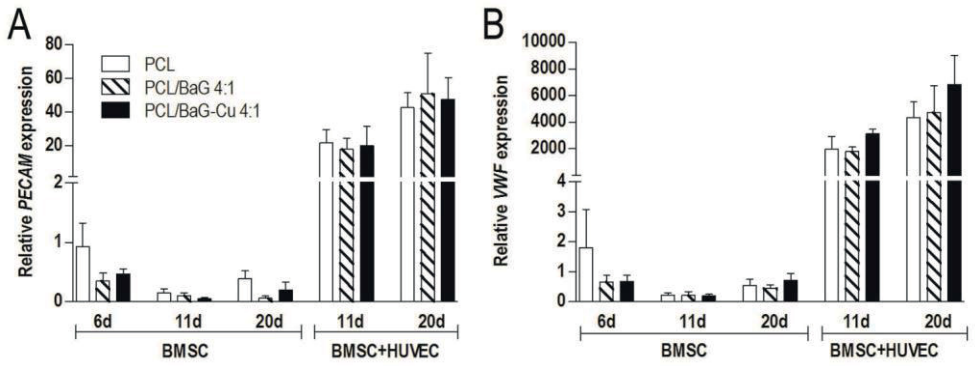
Figure 17. Gene expression results of endothelial marker genes **A)** *PECAM* and, **B)** *vWF* in hBMSC and hBMSC+HUVEC culture setups at 6 d, 13 d and 20 d time points in study IV. Results are expressed relative to hBMSCs cultured for 6 days on PCL scaffold (mean + SD, *n* = 3).
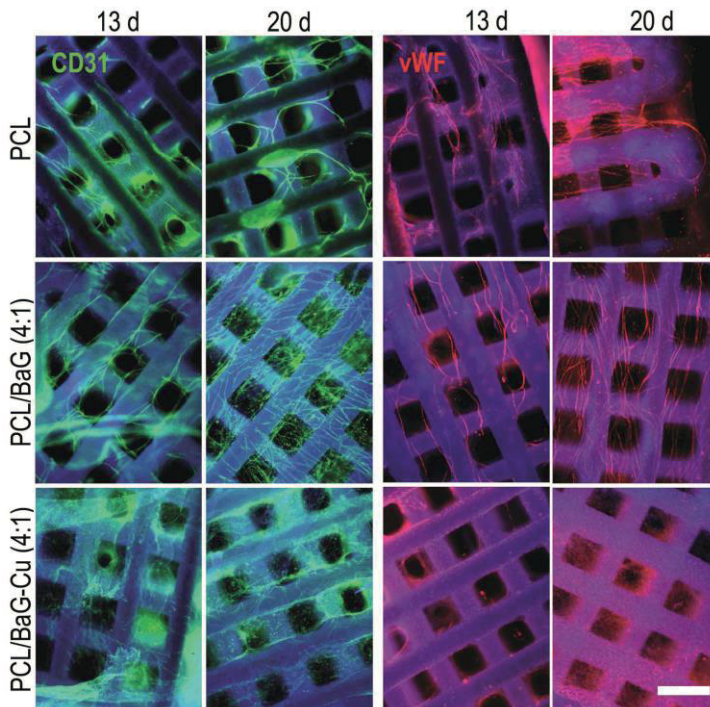
Figure 18. Expression of endothelial proteins CD31 and vWF in study IV in PCL, PCL/BaG (4:1) and PCL/ BaG-cu (4:1) scaffolds at 13- and 20-day time points. Scale bar 500μm.

5.6 The effect of β-TCP/PLCL composites on bone formation *in vivo*

The ability of the PLCL with 50 wt-% β-TCP on bone formation in rabbit distal femur defect was evaluated in study III with histological MGT staining and micro-CT imaging 4-, 12- and 24 weeks after implantation. At 4 weeks, the MGT staining revealed that bone was able to grow on the surface of the composite and, bone formation was also detected inside the composite. Furthermore, the bone growth on the surface and inside the composite increased with time as seen at 12- and 24 weeks. Importantly, the MGT staining demonstrated that no induction of inflammation, formation of fibrous tissue or cysts during the 24 weeks were detected. The micro-CT imaging confirmed the MGT staining results. Furthermore, especially the representative micro-CT images reveal how the composite degraded during the 24-week experiment in rabbit femur.

6   DISCUSSION

6.1   Scaffold architecture and properties affect cell and tissue response in BTE

The current study includes the evaluation of two commercially available BoneCeramic materials that have shown potential in bone regeneration *in vivo* and in patients: BioRestore BaG scaffold (Lappalainen, Karhula *et al.*, 2016a; Clozza *et al.*, 2014; Clozza *et al.*, 2012) and BoneCeramic BCP granules (Beger *et al.*, 2018; Lappalainen *et al.*, 2016a; Schmitt *et al.*, 2013). In addition, the effect of PLCL and PCL based composites consisting either β-TCP, BaG or BaG-Cu on osteogenic differentiation and bone formation were evaluated. A summary of the effects of the scaffolds used in this study on bone formation *in vitro* are presented in Fig. 19. Furthermore, the biomaterials are all manufactured via different methods resulting in different scaffold architectures and surface topographies. As CaPs and BaGs are the most relevant bioactive components in bone substitutes, this study provides an opportunity to evaluate the characteristics, feasibility and performance of plain bioceramics and composites consisting them in BTE.

A major difference between BoneCeramic granules and BioRestore scaffold used in study I was their ability to enhance hASC proliferation, as BioRestore induced hASC proliferation significantly more than BoneCeramic. This phenomenon is most likely related to the difference in 3D architecture of the scaffolds as the fibre-formed BioRestore provides a larger surface area for the seeded cells in contrast to the BoneCeramic granules. Secondly, BoneCeramic enhanced collagen production in hASCs significantly more when compared to BioRestore in BM, and the effect was even more notable in OM. A previous study compared β-TCP to autologous bone graft and commercial Infuse® Bone Graft (rhBMP-2 delivered in a collagen sponge) in a critical sized bone defect in sheep, concluding that β-TCP resulted in an equal bone formation as autograft and to superior bone formation when compared to Infuse® (H. Yuan *et al.*, 2010). Furthermore, as Duan and colleagues (2017; 2018) reported that in CaPs the grain size and micropore size at the submicron scale are connected to an induced bone formation *in vivo,* the rougher micron-scale surface of

BoneCeramic to BioRestore may also have benefitted the better performance of BoneCeramic.

A similar positive effect to BoneCeramic is seen with another CaP in studies II and III with β-TCP/PLCL composites. In study III the composite contained 50 wt-% and in study II 40 wt-% of β-TCP in PLCL. In addition, the composites in study III were pre-compressed resulting in increased β-TCP display on the composite surface as compared to an intact composite. When comparing the representative alizarin red staining images in studies II and III, the effect of β-TCP is evident. The composite's higher ceramic content and display of β-TCP in study III resulted in the formation of an intensely stained and continuous mineralized matrix on the composite surface even in BM. Whereas in study II, only separate areas of well-stained mineralized matrix were observed on the composite surfaces even in the best performing group OM. Also, like BoneCeramic in study I, the β-TCP/PLCL composites in study III induced the secretion of soluble collagen well and, the immunocytochemical staining further demonstrated the formation of a continuous COL-1 matrix on the surface of the scaffolds especially in OM. The formation of a collagenous matrix, consisting mostly of type I collagen, is strongly related to the early phase of bone formation. In fact, dense collagenous matrix itself has been shown to induce osteogenic differentiation of MSCs *in vitro* (Buxton *et al.*, 2008). The more rapid and robust collagen production may be an advantage in more rapid and effective bone formation, as the formation of the organic matrix including collagen needs to occur prior to the mineralization phase (Florencio-Silva *et al.*, 2015).

BioRestore and BoneCeramic scaffolds have later been compared also in a rabbit cranial defect model either alone (Lappalainen, Karhula *et al.*, 2016b) or combined with ASCs (Lappalainen *et al.*, 2016a). Both studies by Lappalainen and colleagues concluded that the BoneCeramic granules resulted in more pronounced bone formation as compared to BioRestore during the 6-week follow-ups (Lappalainen *et al.*, 2016a; Lappalainen *et al.*, 2016b). In contrast to study I where BioRestore induced hASC proliferation, in study IV hBMSC proliferation in PCL/BaG composites was reduced with higher BaG content during the first week but the difference was evened out after that, which is most likely a result of the initial burst release of BaG ions. A reason for this is most likely the different composition of the BaGs. The composition of BioRestore is more similar to an experimental BaG 1-06 than S53P4 used in study IV, and 1-06 has been shown to be less reactive as compared to S53P4 in hASC culture (Ojansivu, Hyväri *et al.*, 2018). Furthermore, ALP activity was elevated with the decreasing BaG content in the PCL-based composites. Similarly, Haimi and colleagues (2009) compared PLA/β-TCP and PLA/BaG composites in

hASC culture and concluded that the PLA/β-TCP composite induced hASC proliferation and ALP activity more as compared to the PLA/BaG composite. One reason for the weaker performance of BaG and BaG consisting composites may be the pH rise caused by BaGs as Monfoulet and colleagues (2014) demonstrated when comparing the osteogenic capacity of BaG to BCP based on pH values both *in vitro* and *in vivo*.
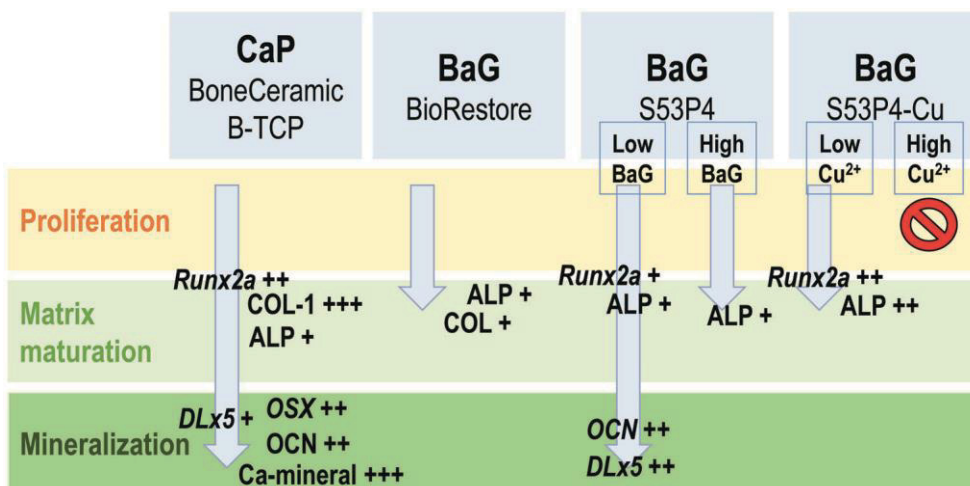
Figure 19. Summary of the effect of the used CaPs and BaGs on bone formation *in vitro*. CaPs (BoneCeramic and β-TCP in PLCL) demonstrated better osteogenic potential as compared to BaGs. In PCL/S53P4 and PCL/S53P4-Cu scaffolds lower BaG and Cu content resulted in a better osteogenic outcome. High Cu-content had a cytotoxic effect. (+++ high expression/secretion; ++ moderate expression/secretion; + low expression/secretion)

When considering the ability to support vascularization, hASCs were able to express endothelial markers when cultured in β-TCP/PLCL composite in study II. Nevertheless, the study setup failed to induce the formation of tubular structures, but this may also be the result of the limited endothelial potential of EM as well as hASCs as discussed later. However, the β-TCP/PLCL composites have previously been shown to support vascularization in a rabbit cranial defect (Pihlman *et al.*, 2018). The osteogenic potential of CaPs has in fact been linked to ECs and vascularization as osteogenic differentiation of MSCs first occurs near capillaries and the internal ceramic surfaces of porous CaPs (Tang *et al.*, 2018). Furthermore, it has been proposed that pericytes associated to capillaries undergo osteogenic differentiation near CaPs (Tang *et al.*, 2018). In study IV, both PCL/BaG and PCL/BaG-Cu composites supported the formation of tubular structures in hBMSC+HUVEC co-

culture in EGM-2. BaGs have been demonstrated to have a vasculogenic effect *in vitro* and *in vivo* (Gorustovich *et al.*, 2010). Furthermore, in study IV the use of a commonly used, mature EC type as a tool in the evaluation of the scaffolds' vascular potential was a more reliable strategy as compared to study II, where only hASCs were used as a cell source. HUVECs are known to form tubular structures when cultured in EGM-2, which is developed specifically for EC culture while the endothelial differentiation capacity of hASCs has been under debate (Antonyshyn *et al.*, 2019).

6.2 The relevance of mechanical properties of BTE scaffolds and the significance of the polymer phase in composite strength

Many times, the development of novel bone substitutes aims to create materials that would mimic the mechanical properties of bone so well that the defect site could bear load or that the treated defect site would not require additional metallic fixation. Even though this would be ideal, the requirements for a scaffold material are so manifold that the development of a bone substitute material may need compromising between achieving a good cell and tissue response, user-friendliness and ideal mechanical properties (Turnbull *et al.*, 2017).

The developed β-TCP/PLCL composite in study III was created to serve as a synthetic scaffold for the regeneration of native bone similarly, as the formed callus serves as a natural scaffold for the bone regeneration process during bone healing. Therefore, the modulus of the composite (as dry 9.0 MPa or 1.2 MPa after pre-compression) is closer to the modulus of cartilage (2.4-10 MPa) (Beck *et al.*, 2016) than to modulus of trabecular bone (10.75-13.66 GPa) (Peters *et al.*, 2018). Among clinical products, the closest comparable composite bone void filler to the β-TCP/PLCL composite is chronOS™ Strip (DePuy Synthes), also manufactured from PLCL and β-TCP granules. The compressive strength of the β-TCP/PLCL composite analyzed dry at room temperature was 1.1 MPa at 20 % strain and 3 MPa at 50 % strain. To compare, the compression strength of trabecular bone has been reported to vary from 2 to 12 MPa (Kokubo *et al.*, 2003). To our knowledge the mechanical properties of chronOS™ Strip composite has not been reported however; the compressive strength of the chronOS® β-TCP granules is of the same order as the strength of the β-TCP/PLCL composite (5 MPa; product manual of chronOS®). Moreover, aliphatic polyester based composites consisting β-TCP have

demonstrated compression strengths of 5.4 MPa (Shikinami *et al.*, 2006) and 3.5 MPa (Mathieu *et al.*, 2006), which are also highly similar to that of the developed β-TCP/PLCL composite.

In contrast to hard and brittle ceramic bone substitutes, the elasticity of the composite allows the dense and tight fitting of the material into a defect. This can be considered a significant advantage firstly for the operating surgeon, as the composite material is easier to implant and mold even by cutting intraoperatively, when compared to most clinically available bone substitute materials as concluded by Pihlman and colleagues (2018). Secondly, in contrast to many clinically used hard ceramic granules that can be poured or placed into a defect site, the elastic composite material can be tightly pushed and fitted into the defect, which ensures that the composite remains immobile in its place. This is highly important, as a common complication in bone fracture healing is a non-union of the bone defect, which the FDA defines as the incomplete healing of a fracture within 9 months after injury (Panteli *et al.*, 2015). A major factor contributing to the development of a non-union is insufficient stabilization as the bone regeneration process is disturbed if the defect site is not mechanically stabile (Panteli *et al.*, 2015).

When considering the mechanical properties of synthetic polymer-based composites, these results suggest that the mechanical properties of the polymer phase are more significant than those of the incorporated ceramic phase. In study III, the modulus and compression strength of the 50 wt-% β -TCP in PLCL were analyzed both dry at RT and in physiological environment (aqueous solution at 37 °C). The compression treatment lowered the modulus and strength significantly at 20- and 50 % strain, when the samples were tested dry at RT. Intriguingly, the difference was diminished in the physiological environment. The glass transition temperature of PLCL is between 21 °C and 22 °C (Ahola *et al.*, 2013) which is why at 37 °C the polymer chains are mobile making the composite elastic whereas the β-TCP particles do not reinforce the composite matrix. Even though CaPs have been reported to be able to form weak chemical bonding to PLA, at least in a BCP-PLA composite this kind of bonding has been shown to be negligible (Bleach *et al.*, 2002). When incubated at 37 °C there was a rise from 1h at 37 °C to 7 d at 37 °C in modulus and strength, demonstrating that the β-TCP/PLCL composites started to recover after the initial decrease in mechanical properties. This increase in modulus may be caused by the reorganization of the polymer chains in aqueous environment at 37 °C, such as crystallization or aging of the material, allowing the polymer chains to organize into energetically more stable conformations (Pan *et al.*, 2007; Zong *et al.*, 1999). Contradictory to our results, van der Pol and colleagues (2010) suggested that

increasing the β-TCP content over 5 wt-% in a scCO$_2$ processed composite would make the P$_L$LA-based (intrinsic viscosity of raw material 1.6 dL/g) composite more brittle and make it lose its ability to recover after deformation. In addition, Mathieu and colleagues (2005; 2006) reported that higher than 5 wt-% HA content in P$_L$LA (intrinsic viscosity of raw material 1.6 dL/g) made the composite fragile. In the β-TCL/PLCL composite, the addition of the elastic caprolactone in lactide polymer backbone makes the polymer phase more elastic and therefore the higher filler content does not cause the same problems as with the P$_L$LA based composites. However, the effect of rising filler content on mechanical properties of polymer-based composite is seen in study IV with PCL/BaG-Cu composites. The addition of BaG-Cu enhances the compressive modulus of the PCL-based composites up to approximately 30 % filler content. Nevertheless, as the filler content rises to approximately 50 %, the modulus decreases notably. One reason for the negative effect of rising filler content in polymer-based composites is the agglomeration of filler particles and void formation in the composite matrix as the particles are not chemically bonded to the polymer matrix and are able to move (Bleach *et al.*, 2002). Overall, it seems that to improve the mechanical properties of synthetic polymer-based composites, the development needs to focus on tuning the polymer composition and chemistry rather than trying to improve the mechanical properties by increasing the ceramic content.

Polymer degradation kinetics may be affected by different parameters, such as processing method, so that the molecular degradation profile *in vitro* may model the degradation *in vivo* relatively well (Weir *et al.*, 2004) or they may differ considerably (Koepp *et al.*, 2004). In study II, the hydrolytic degradation of β-TCP/PLCL composites was shown to be highly similar both *in vitro* and *in vivo*. This finding enables the study and observation of the degradation process as well as the following structural changes of the composite in *in vitro* in the future. The differences between the degradation rates of PLCL and the composite during the first 4 weeks are related to the β-TCP filler, which slows down the hydrolytic degradation of the polymer by neutralizing acidic degradation products of the lactide-based polymer phase (Niemelä, 2005). Previously, non-foamed scaffolds of PLCL and β-TCP/PLCL composite, with different initial molecular weight but with similar residual monomer content, were studied *in vitro* (Ahola *et al.*, 2013). To compare, the molecular weight of the non-foamed scaffolds was at an equal level after 12 weeks incubation at 37 °C as with the foamed scaffolds (Ahola *et al.*, 2013).

6.3 OM induction is more effective than exogenously added BMP-2, BMP-7 or, VEGF in the osteogenic differentiation of hASCs

In BTE, the osteoinductive effect of BMPs has been widely trusted (Lappalainen *et al.*, 2016a; Sandor *et al.*, 2014; Sandor *et al.*, 2013; Mesimäki *et al.*, 2009) however, the safety and effectiveness of them has been challenged (Young & Mirarchi, 2015; P. Zuk *et al.*, 2011; Carragee *et al.*, 2011; Garrison *et al.*, 2007). Therefore, in study I, OM was studied as a cost-effective alternative to growth factors to induce the osteogenic differentiation of hASCs. The used OM supplemented with AA2P, β-GP and Dex has previously been optimized for hASC differentiation (Kyllönen *et al.*, 2013).

Study I was the first report to show the advantage of OM over exogenously added BMP-2, BMP-7 or VEGF in the osteogenic differentiation of hASCs in 3D culture. The addition of BMP-2 or VEGF in BM did not induce the osteogenic differentiation of hASC more than BM alone with either BoneCeramic or BioRestore scaffolds. Furthermore, BMP-7 significantly reduced hASC proliferation and ALP activity with both scaffolds. To study the effects of these growth factors further, they were also combined to OM. Intriguingly, the combination of BMP-2, BMP-7 or VEGF with OM did not boost the osteogenic effect of OM, indicating that plain OM is enough for the osteogenic differentiation of hASCs *in vitro*. When considering the negative effect of BMP-7 on hASC osteoinduction, its combination with OM diminished the inhibitory effect.

In contrast to the results in study I, exogenously added BMP-2 (Song *et al.*, 2011; Knippenberg *et al.*, 2006) (Knippenberg *et al.*, 2006; Song *et al.*, 2011), BMP-7 (Al-Salleeh *et al.*, 2008) and VEGF (Behr *et al.*, 2011) have been proposed to induce the osteogenic differentiation of hASCs. In turn, it has been suggested that growth factors separately are not as effective as a combination of them. For instance, the use of BMP-2, FGF-2 and VEGF synergistically and sequentially was shown to induce osteogenesis of rat osteoblasts significantly more than using the growth factors separately (P. Li *et al.*, 2014).

Among the studied growth factors, BMP- 2 is the most widely studied in the differentiation ASCs (Vanhatupa *et al.*, 2015; Mehrkens *et al.*, 2012; Waselau *et al.*, 2012b; P. Zuk *et al.*, 2011; Song *et al.*, 2011; Knippenberg *et al.*, 2006). Some studies have proposed concentrations between 50-100 ng/mL to be osteoinductive with ASCs (Song *et al.*, 2011; Knippenberg *et al.*, 2006) and, others have reported that ASCs are not responsive to BMP-2 concentrations between 10-100 ng/mL (Mehrkens *et al.*, 2012; Waselau *et al.*, 2012b; P. Zuk *et al.*, 2011). In turn, a short and

low concentration treatment (15 min; 10 ng/mL) with BMP-2 has been shown to induce osteogenic differentiation of ASCs (Knippenberg *et al.*, 2006). Vanhatupa and colleagues (2015) studied the effects of BMP-2 in hASCs and discovered that BMP-2 enhance both osteogenic and adipogenic differentiation of hASCs in a donor-dependent way. The donor variation may be one reason for the contradicting results between different studies. The authors also demonstrated that hASCs were more sensitive to BMP-2 when cultured in HS-based medium in contrast to FBS-based medium (Vanhatupa *et al.*, 2015). Study I was conducted in FBS-based medium, which may have contributed to the ineffectiveness of the growth factors. Moreover, the conformation of BMP-2 was shown to affect its functionality, as hASCs were more responsive to mammalian-produced rhBMP-2 than to that produced in *E. coli* (Vanhatupa *et al.*, 2015). In study I, the rhBMP-2 was produced in *E. coli*, which also partly explain the lack of its effect on hASCs. In addition, other factors may explain the different outcomes between studies, such as animal-derived ASCs (Knippenberg *et al.*, 2006), differences between 3D (Waselau *et al.*, 2012b) and 2D culture, cell densities as well as medium compositions. Evidently, the BMP-2 related cell signaling is a complex interaction of various factors and all the reciprocal actions are not yet known.

Similar to study I, BMP-7 has been shown to have a negative effect on osteogenic differentiation of rat BMSCs (Wongwitwichot & Kaewsrichan, 2017). Another study observed a negative effect of BMP-7 on osteogenic differentiation of human periodontal ligament stem cells however, they also noticed an inductive effect of BMP-7 on the osteogenic differentiation hMSCs (Ern *et al.*, 2017). On the other hand, BMP-7 has been observed to induce signaling routes related to tenogenesis more than those related to osteogenesis or chondrogenesis in the culture of primary human tenocyte-like cells (Klatte-Schulz *et al.*, 2016). Overall, the cell signaling events related to BMP-7 use still require more elucidation although it appears that BMP-7 is not an optimal candidate for osteogenic differentiation.

6.4 scCO$_2$ processed β-TCP/PLCL composite is cytocompatible and osteogenic *in vitro* and biocompatible and osteoconductive *in vivo*

Synthetic polymer-based composites filled with CaPs have shown promise in BTE and among biomaterials composites may be the most promising strategy for a synthetic bone graft with most optimal properties (de Misquita *et al.*, 2016). ScCO$_2$

foaming is an excellent processing method for polymer-based tissue engineering scaffolds. The method only uses CO_2 and is therefore non-toxic, cost effective, and requires low critical parameters (T_C 304 K, P_C 7.5 MPa) allowing the addition of biomolecules, such as growth factors, into the material during processing (Duarte *et al.*, 2013).

Previously, Mathieu and colleagues (2006) concluded that in scCO$_2$ processing a higher ceramic content reduce porosity and increase average pore size of the composite (Mathieu *et al.*, 2006). Furthermore, the authors also suggested that 5 wt-% β-TCP content is an upper limit to achieve an interconnected and homogenous pore structure (Mathieu *et al.*, 2006). Contradictory to this report, study III presents a composite with 50 wt-% β-TCP content with high porosity (65-67 %) and average pore size of 380 μm processed by using scCO$_2$. Previously, PLA/β-TCP composites with 10 % ceramic content and 74 % porosity (Mathieu *et al.*, 2006) and, PCL/fibroin/hydroxyapatite (70/20/10 %) composites with average porosity of 69.7 % (Diaz-Gomez *et al.*, 2017) have been manufactured with scCO$_2$ foaming. Study II also reports a solution to uncover the ceramic granules covered by a polymer surface – a problem related to scCO$_2$ processing of polymer-ceramic composites. The reported pre-compression treatment resulted in the tearing of the polymer surface, enabling the display of the β-TCP granules. This is highly important in the early interaction of cells and tissues with the composite, as PLCL is not bioactive and lacks biological binding sites (Jeong *et al.*, 2008; Z. Wang *et al.*, 2016) while β-TCP is bioactive and osteoconductive (Barrere *et al.*, 2006; Chatterjea *et al.*, 2013). In addition, the additional holes in the PLCL pore surfaces, which gave rise during the pre-compression, enhanced interconnectivity and micro-porosity of the composites.

Study III demonstrated the cytocompatibility of the novel composite *in vitro*. ALP activity was induced in BM and OM, although the level of ALP activity was significantly enhanced in OM when compared to BM during the first 2 weeks. Both ALP activity and *ALP* gene expression were highest at 14 days, which is logical as high ALP expression occurs in matrix maturation phase of the osteogenic differentiation (Lian *et al.*, 2012). The total soluble collagen amount was comparable in both BM and OM but unexpectedly the soluble collagen amount decreased from 14 to 21 days. This may be caused by the mineralization of collagen fibrils that are the basic building blocks on bone ECM (Nair *et al.*, 2013) as the mineralization may hinder the solubility of collagen. Alizarin red staining confirmed the high level of mineralization of hASC culture in the scaffolds in both BM and OM and, as the immunocytochemical staining demonstrated the formation of COL-1 matrix in the composites as well, we may conclude that hASCs were able to develop a mineralized

collagen matrix typical to bone when cultured in the β-TCP/PLCL composites. The expression of late osteogenic marker protein OCN and also of osteogenic genes was in agreement with literature related bone formation as *ALP* and *Runx2a* expression peaks occurred at the early phase of differentiation while *OSX* expression peaked later (Lian *et al.*, 2012). In studies II and III, the presence of OM enhanced the osteogenic effect of the composite material. In study II, the gene expression of *Runx2a* was significantly higher in OM and OM-cocktail groups compared to BM and EM. The trend in *ALP* and *Runx2a* gene expression as well as in quantified mineralization results in BM and OM were very similar in both studies II and III. Although, there were more significant differences in study II between BM and OM conditions than in study III, and a reason may be the higher β-TCP content of the composite in study III as well as enhanced display of the ceramic granules as a result of the pre-compression treatment. In study III, the comparison of mineralization in the composite and on cell culture plastic (2D) in BM further underlines the composite's inherent osteogenic potential *in vitro*. Also, in study II, concurrent enhancement of ALP activity and *ALP* gene expression with mineral formation was detected in EM, also indicating the composite's inherent osteogenic potential. Previously, a nanocomposite of poly-(lactic-co-glycolicacid) with 40 wt-% of amorphous calcium was shown to support the co-culture and further differentiation of hASC derived endothelial and osteogenic cells (Gao *et al.*, 2014). Furthermore, a composite consisting of 60 % β-TCP in PLLA has been shown to perform similarly to plain β-TCP in osteogenesis *in vivo* (Aunoble *et al.*, 2006).

The osteoconductivity of the β-TCP/PLCL composites was demonstrated in study III in a rabbit femur defect model. Previously, PLA implants (Pihlajamäki *et al.*, 2006) have induced an inflammatory reaction caused by acidic degradation products, leading to the formation of fibrous tissue surrounding the implant. In contrast, the β-TCP/PLCL composite was shown to be biocompatible as no fibrous tissue formation, cysts or inflammation were observed during the 24-week follow-up. Furthermore, the composite was demonstrated to be osteoconductive as based on the representative MGT staining and micro-CT images, bone tissue grew on the composite surface and was able to penetrate the porous composite already 4 weeks after implantation. In a previous study, a PLA/β-TCP (95/5 wt-%) composite foamed by using $scCO_2$ caused the formation of a clear fibrous layer between the composite and mineralized tissue after 8- and 16 weeks in sheep femur defects (van der Pol *et al.*, 2010). Similarly to the results in study III, Pihlman and colleagues (2018) implanted the same porous β-TCP/PLCL composites in a rabbit calvarial defect, demonstrating the osteoconductivity and ingrowth of both bone and vascular tissue.

The authors also reported that the β-TCP/PLCL composite provided structural support in the defect site by blocking the bulging soft tissues around the defect (Pihlman *et al.*, 2018).

6.5   hASC endothelial differentiation potential may be limited

Tissue engineered synthetic bone grafts are still limitedly used in the clinic while autologous and allogeneic bone grafts remain the gold standard in treating large bone defects. One reason for the weak success of BTE grafts is that the implanted cells die without proper vasculature to transport them oxygen and nutrients (Pirosa *et al.*, 2018; Rouwkema *et al.*, 2008). As hASCs have been shown to have the potential to differentiate towards both osteogenic and endothelial lineages, the hypothesis was that hASCs could provide a single cell source for engineering vascularized bone grafts.

In study II, hASCs demonstrated to have ability to differentiate towards an endothelial phenotype in 2D culture conditions when cultured in a modified version of EGM-2 based on HS instead of FBS and excluding hydrocortisone and ascorbic acid from the supplements. hASCs formed tubular structures in EM more extensively when compared to EGM-2 however, the vessel network was not as organized as that formed by HUVECs. Previously, endothelially differentiated ASCs have been shown to remain less matured in contrast to mature ECs (Antonyshyn *et al.*, 2019; Volz *et al.*, 2016). Furthermore, Antonyshyn and colleagues (2019) reported that even though differentiated hASCs express the commonly used endothelial markers and even demonstrate EC functionality in an AcLDL uptake assay, their expression levels remain in a significantly lower level when compared to those of mature ECs. The authors proposed that the endothelial differentiation potential of hASCs is limited however, they used EGM-2 in the differentiation of hASCs (Antonyshyn *et al.*, 2019) even though FGF-2 and a combination of VEGF/FGF-2 have been shown to be more effective in the endothelial induction of hASCs (S. Khan *et al.*, 2017). In turn, DNA methylation reduction was shown to increase endothelial marker expression, suggesting that ASC endothelial potential is epigenetically restricted (Culmes *et al.*, 2013). Furthermore, Cheng and colleagues converted hASCs into functional endothelial-like cells via lentiviral transduction (F. Cheng *et al.*, 2018). Nevertheless, epigenetic modification and viral transduction are not safe enough methods to be used in clinical treatments. It is also debatable whether the implanted cells used for treating patients would need to be mature, as it

has been suggested that undifferentiated MSCs have a higher angiogenic capacity than endothelially differentiated MSCs (Guo *et al.*, 2016). Furthermore, the endothelial potential of ASCs has been under debate and different studies have suggested that the endothelial potential of hASCs is related to a hASC subpopulation such as CD34+/CD31- hASCs (Miranville *et al.*, 2004), SSEA-4+ hASCs (Mihaila *et al.*, 2013) or CD45-/CD31- hASCs (Antonyshyn *et al.*, 2019). In addition, as human SVF consist approximately 20 % of ECs (Kanthilal & Darling, 2014), it has been speculated whether the endothelial capacity of hASCs gives rise from the proliferation of this EC population or from differentiation. Ell and colleagues (2017) cultured hASCs from 18 different donors in a co-culture, seeding the hASCs on top of endothelial progenitor cells. The authors demonstrated that the intrinsic endothelial potential of hASCs could be evoked merely by culturing hASCs in contact with ECs (Ell *et al.*, 2017). Furthermore, they observed notable donor variation in hASC endothelial potential and discussed that diseases and conditions, such as diabetes type 2, metabolic syndrome and obesity, may have a fundamental impact on hASCs. Also, alarmingly maternal obesity has been shown to result in epigenetic modifications in adipose tissue gene expression of the offspring (Ell *et al.*, 2017; Attig *et al.*, 2013). Low-level inflammation, which is related to insulin resistance as well as metabolic syndrome, leads to adipose tissue fibrosis and hindered neoangiogenesis eventually causing hypoxia (Ell *et al.*, 2017; T. Khan *et al.*, 2009). Pro-longed inflammation may lead to epigenetic changes in the adipose tissue and cause the harvested cells to behave differently even in non-hypoxic conditions (Ell *et al.*, 2017; Stenvinkel *et al.*, 2007).

When cultured in the β-TCP/PLCL composites in EM in study II, hASCs were able to differentiate towards an EC phenotype, as the cells expressed endothelial proteins CD31 and vWF and, the relative expression of *vWF* was enhanced. However, as tubular formation was not observed, the differentiation remained in a pre-mature state. The expression of CD31 and vWF was clear in EM at 14 and 21 d whereas in EM-cocktail their expression went down from 14 to 21 d. Similarly, the gene expression of *vWF* in EM-cocktail declined from 14 to 21 d. A reason for this may be the OM components including β-GP added after 7 days of culture. ALP cleaves inorganic phosphate from β-GP and high inorganic phosphate levels have been shown to impair angiogenesis, EC migration, tube formation, and EC survival (Di Marco *et al.*, 2013; Di Marco *et al.*, 2008). Therefore, β-GP may have limited or even inhibited the endothelial differentiation of hASCs. Then again, endothelial differentiation of hASCs has been shown to occur in semi-solid or gel-like materials such as fibrin (Correia *et al.*, 2014; Hutton *et al.*, 2013) or Matrigel (Planat-Benard *et*

al., 2004). Considering the endothelial differentiation of hASCs, seeding them in fibrin into the β-TCP/PLCL composites may have resulted in a better endothelial outcome. Based on the results of study II and IV and the debate related to hASC endothelial capacity, a mature EC type, such as HUVECs, would be a more attractive choice for the evaluation of angiogenic potential of novel biomaterial scaffolds.

6.5.1 hASCs alone are not a promising cell-source for the engineering of vascularized bone

In study II the aim was to induce both endothelial and osteogenic differentiation of hASCs in the same culture in β-TCP/PLCL composites. hASCs have the potential to differentiate towards both lineages however, an efficient and controllable method to induce hASC differentiation towards both lineages have not been reported. Differentiation of hASCs towards both osteogenic and endothelial lineages was achieved in EM in β-TCP/PLCL composites. Endothelial marker proteins CD31, CD144 and, vWF and relative *vWF* gene expression as well as ALP activity and relative *ALP* and *OSX* gene expressions were elevated in EM. However, when considering the endothelial differentiation, tubular formation was not observed. In addition, hASCs produced mineralized matrix in EM although, to a lesser extent than in other groups. In contrast to study II, previously osteogenic supplements were needed for osteogenic differentiation of hASCs following the endothelial induction (Correia *et al.*, 2014). Furthermore, Gardin and colleagues (2012) required osteogenic supplements in addition to endothelial supplements for hASC osteogenic induction even though they used a HA scaffold. The osteogenic induction in EM is most likely a result of β-TCP/PLCL composite as it was shown to induce osteogenic differentiation of hASCs even in BM in both studies II and III. Overall, the differentiation pathways were still in a premature state after 3-week culture in EM. As mechanical stimulation enhance both osteogenic (Virjula *et al.*, 2017; Tirkkonen *et al.*, 2011) as well as endothelial differentiation (Colazzo *et al.*, 2014) of hASCs, a mechanical stimulus may have benefitted the *in vitro* setup in study II.

The induction of both osteogenic and endothelial differentiation paths in the same cell culture *in vitro* has been shown to be challenging also by other authors (Correia *et al.*, 2014; Hutton *et al.*, 2013). In fact, it has been proposed that osteogenic and endothelial differentiation pathways may be mutually inhibitory (Correia *et al.*, 2011; Hutton *et al.*, 2013). One reason may be the negative effect of inorganic phosphate related to osteogenic supplements on ECs (Di Marco *et al.*, 2013; Di

Marco *et al.*, 2008). In study II, the cocktail medium of EM and OM supported the osteogenic differentiation, but not the endothelial differentiation of hASCs. In contrast, Gardin and colleagues (2012) reported that a medium consisting osteogenic supplements (β-GP, DEX and ascorbic acid) as well as FGF-2 and endothelial cell growth factor induced the expression of both osteogenic and endothelial genes in hASCs cultured in a HA scaffold. When comparing the simultaneous differentiation of hASCs towards both osteogenic and endothelial lineages in cocktail groups similar to study II the best strategy was to start with osteogenic differentiation of hASCs for 3 weeks followed by addition of undifferentiated hASCs and a 2-week culture in EGM-2 (Correia *et al.*, 2014). In contrast, Hutton and colleagues (2013) cultured hASCs in fibrin gel and concluded that the best strategy for achieving both osteogenic and endothelial pathways in the same culture is to induce first a strong endothelial population and then continue with the osteogenic differentiation.

As the inorganic phosphate causes problems in the endothelial differentiation of hASCs, it may be more feasible to first produce a well-established tubular network and then add the osteogenic precursors and continue with osteogenic differentiation. In addition, as the endothelial differentiation capacity of hASCs has been questioned, it may be more beneficial to choose another cell source to provide ECs for a vascularized bone model. Altogether, the results between studies concerning the simultaneous osteogenic and endothelial differentiation of hASCs differ greatly, underlining the complexity of the study area. The parameters of the studies, such as medium composition, scaffold type, culture period, used analysis methods, vary greatly, which makes it challenging to reach conclusions.

6.6 Incorporation of copper in PCL/BaG composite does not provide benefit for vascularized bone engineering

The dissolution of Si, Ca, P and Na induce both intra- and extracellular responses in cells at the BaG interface contributing to both osteogenesis and angiogenesis. In study IV, the incorporation of Cu into S53P4 was designed to release the Cu^{2+} locally to even more enhance vascularization. However, the specific mechanisms of Cu^{2+} affecting hBMSCs and HUVECs were observed to be complex.

In line with previous studies, the ionic dissolution products from S53P4 did not strongly affect the proliferation of hBMSCs (Qazi *et al.*, 2017; Weng *et al.*, 2017). However, the Cu^{2+} released from the PCL/BaG composites had a dose-dependent inhibitory effect on hBMSC proliferation. The cytotoxic effect of Cu^{2+} *in vitro* is

mainly based on the generation of reactive oxygen species. Weng and colleagues (2017) reported a dose- and exposure duration dependent cytotoxicity of Cu^{2+} released from Cu-BaG nanofibers using different cell types, including HUVECs, ASCs and BMSCs. Furthermore, a high Cu^{2+} concentration produced by mesoporous BaG-Cu microparticles incorporated in nanocellulose hydrogel was shown to be cytotoxic for 3T3 fibroblasts (X. Wang *et al.*, 2016). In turn, Wu and colleagues (2013) compared mesoporous BaG-Cu scaffolds and their extracts with varying amounts of Cu^{2+} and, demonstrated that a high Cu^{2+} concentration significantly decreased proliferation of hBMSCs. In study IV, the highest Cu^{2+} concentration in the culture medium varied from 50 µM (PCL/BaG-Cu 4:1) to 140 µM (PCL/BaG-Cu 1:1). In study IV, hBMSCs were able to maintain their proliferative capacity when the Cu^{2+} concentration was lower than 20 µM. Furthermore, study IV was conducted in a static model with fixed medium change intervals resulting in accumulation of Cu^{2+} between the medium changes. Altogether, these Cu^{2+} concentrations are still clearly lower than the 157 µM level, which Wu and colleagues (2013) proposed to be inhibitory for hBMSC proliferation. In turn, another study reported that a 50 µM Cu^{2+} concentration reduces hBMSC proliferation while increasing their osteogenic and adipogenic differentiation potential (Rodriguez *et al.*, 2002). Importantly, when considering the osteogenic differentiation process, the proliferation phase is followed by matrix maturation and mineralization phases during which the high proliferation has already ceased (Lian & Stein, 1995).

Even though the PCL/BaG and PCL/BaG-Cu scaffolds supported ALP activity in hBMSCs, the rising BaG and BaG-Cu content had a lowering effect on ALP activity. The study of Wu and colleagues (2013) demonstrated that rising Cu^{2+} concentration had a slight increasing effect on ALP activity in hBMSCs, but the difference was not significant. Similarly, Rath and colleagues (2014) detected no significant effect by Cu^{2+} concentration on ALP activity in hBMSCs cultured in the Cu-doped 45S5 BaG scaffolds. In fact, it may be sufficient to have a distinct induction of ALP activity, rather than trying to achieve a high ALP activity level, as the function of ALP in osteogenic differentiation is to ensure the presence of Pi and decrease pyrophosphate concentration to allow mineralization (Ojansivu *et al.*, 2015).

The osteogenic differentiation of hBMSCs was also evaluated based on osteogenic gene expression in both hBMSC culture and hBMSC+HUVEC co-culture setups using PCL, PCL/BaG 4:1 and PCL/BaG-Cu 4:1 scaffolds. Intriguingly, the copper containing composite enhanced the expression of early osteogenic marker gene *Runx2a* evidently more when compared to PCL/BaG

composite in hBMSC culture. The expression is *Runx2* is required for the osteogenic differentiation to occur. Nevertheless, for the differentiation to proceed to maturation the high *Runx2* expression needs to decrease, because the high *Runx2* expression inhibits osteogenic maturation maintaining the cells in a premature stage (Komori, 2017). For this reason, the late and high expression of *Runx2a* at 20-day time point together with the low expression of late osteogenic marker genes *OCN* and *DLx5* in PCL/BaG-Cu 4:1 scaffold suggests that osteogenesis is in a stagnant state. PCL/BaG 4:1 induced the gene expression of *OCN* and *DLx5* more when compared to PCL/BaG-Cu 4:1 at both time points, pointing out the negative effect of Cu^{2+} on hBMSC osteogenesis. Similarly, a previous study concluded that copper supplementation decreased the expression of ALP activity, expression of osteogenic genes and formation of bone nodules in rat BMSCs *in vitro* (S. Li *et al.*, 2014). In an animal model the authors also demonstrated that Cu^{2+} ions induce vascularization while inhibiting collagen type I formation and accumulation *in vivo* (S. Li *et al.*, 2014). The hBMSC+HUVEC co-cultures were supplemented with EGM-2 after the HUVECs were seeded at day 6, explaining the lower osteogenic gene expression levels when compared to hBMSC culture setup.

Both PCL/BaG 4:1 and PCL/BaG-Cu 4:1 scaffolds enhanced the expression of endothelial proteins vWF and CD31 and, induced the formation of tubular network more in both hBMSC and hBMSC+HUVEC culture setups when compared to plain PCL scaffold. Previously, 45S5 BaG was demonstrated to support the tubular formation in fibroblast and EC cultures (Gorustovich *et al.*, 2010) and, the dissolution products of S53P4 have been shown to enhance VEGF secretion of human fibroblasts (Detsch *et al.*, 2014). Proteins CD31 and vWF were more strongly expressed in the co-culture setup than in hBMSC culture. In agreement with this, the Cu-doped 45S5 scaffolds have been shown to enhance the VEGF secretion and tubular formation in a co-culture of hBMSCs with human dermal microvascular ECs (Rath *et al.*, 2014). In addition, the authors observed that copper alone did not enhance the VEGF secretion in ECs but the presence of hBMSCs was also required (Rath *et al.*, 2014) suggesting that BaG has a paracrine effect on hBMSCs such as to secrete factors that influence the ECs. Predictably, the endothelial gene expression of *PECAM* and *vWF* were elevated in co-culture setup when compared to hBMSC culture with all scaffold types (PCL, PCL/BaG 4:1 and PCL/BaG-Cu 4:1). Because several previous reports have proposed that copper ions induce vascularization (X. Wang *et al.*, 2016; Rath *et al.*, 2014; Wu *et al.*, 2013), it was surprising to detect so little difference between PCL/BaG 4:1 and PCL/BaG-Cu 4:1 scaffolds. Only the *vWF* gene expression in the co-culture was slightly elevated in the Cu-containing scaffold

when compared to PCL/BaG 4:1. The conflicting conclusions between studies may result from different scaffold design including BaG composition, used cell type or medium composition. For instance, Detsch and colleagues (2014) demonstrated that that BaG granule size had a significant effect on VEGF release in fibroblasts: granule sizes of 0.5-0.8 mm and 1.0-2.0 mm induced VEGF secretion while granule sizes of 2.0–3.15 mm inhibited it. Altogether, PCL/BaG-Cu 4:1 scaffold supported vasculogenesis and tubular formation in the co-culture setup but the angiogenic effect of Cu^{2+} was not significant as compared to PCL/BaG composite. The angiogenic effect of S53P4 itself may be enough and the addition of copper does not significantly boost this effect.

7 CONCLUSIONS

In this thesis, the effect of different synthetic bone graft materials on bone formation *in vitro* and *in vivo* were evaluated. Ceramic components commonly used as bone grafts were firstly studied *in vitro* and then successfully integrated in PLCL- and PCL-based composites. The study focused on analyzing how osteogenesis and vasculogenesis occur with the biomaterial scaffolds *in vitro* and *in vivo*. The main conclusions of the four studies included in this thesis are described below:

I Both biomaterials BioRestore and BoneCeramic support the viability and proliferation of hASCs *in vitro*. However, the materials affect hASCs differentially: BioRestore promotes hASC proliferation while BoneCeramic enhances the osteogenic differentiation. Furthermore, osteogenic medium enhances hASC osteogenesis in 3D culture significantly more as compared to the traditionally used growth factors BMP-2, BMP-7 and VEGF. By contrast, growth factors combined with either biomaterial do not stimulate proliferation or osteogenic differentiation as compared to basal medium. Furthermore, BMP-7 consistently inhibits proliferation and osteogenic differentiation of hASCs in 3D culture. In turn, the addition of growth factors in OM does not significantly benefit the hASC osteoinduction. The most robust osteogenic outcome with hASCs is achieved with BoneCeramic combined with OM.

II The elastic scCO$_2$-processed β-TCP/PLCL composite supports both osteogenic and endothelial differentiation of hASCs *in vitro* when cultured in endothelial medium. As no tubular formation was observed, the combination of endothelial medium and the composite cannot induce mature endothelial differentiation during the 3-week protocol. Cocktail medium of osteogenic medium and endothelial medium (1:1) supports osteogenic but not endothelial differentiation of hASCs.

III A highly porous, biodegradable, elastic and easy-to-handle β-TCP/PLCL composite was developed to serve as a synthetic bone graft. The study is the first to report a scCO$_2$ processed composite with a high ceramic content (50 wt-%) and high

porosity (65-67 %) for bone tissue engineering. To increase the bioactivity of the composite, the otherwise polymer embedded β-TCP particles can be uncovered by a dynamic compression treatment. The β-TCP/PLCL composite is cytocompatible and supports hASC proliferation and osteogenic differentiation *in vitro*. Furthermore, the composite is biocompatible and osteoconductive *in vivo* as demonstrated in a rabbit femur defect.

IV   The incorporation of BaG-Cu to PCL enhances the mechanical properties of the printed scaffolds as compared to PCL scaffold. The composites provide sustained release of biologically relevant inorganic ions and, a bioactive CaP precipitate layer forms on the surface of the PCL/BaG-Cu composites in SBF *in vitro*. However, copper released from PCL/BaG-Cu composites has a dose-dependent inhibitory effect on hBMSC proliferation. PCL/BaG composite supports hBMSC osteoinduction while the incorporation of copper diminishes the osteogenic effect. Both PCL/BaG and PCL/BaG-Cu composites support the formation of tubular structures in hBMSC+HUVEC co-culture showing that the added copper does not enhance the vasculogenic potential of the composite.

These findings demonstrate that by adding β-TCP or BaG in an inert synthetic polymer phase, bioactive composites can be created with scCO$_2$ foaming and 3D printing. Especially the developed osteoconductive β-TCP/PLCL composite is a promising synthetic bone graft for clinical use. Both hASCs and hBMSCs serve reliably as tools in the *in vitro* study of synthetic bone graft materials. Furthermore, these cells are differentiated cost-effectively and efficiently to bone-forming cells with OM *in vitro*. However, considering the evaluation of vasculogenic effect of the materials, HUVECs provide a more consistent cell type for *in vitro* studies.

8 REFERENCES

Ahola, N., Veiranto, M., Rich, J., Efimov, A., Hannula, M., Seppala, J., & Kellomäki, M. (2013). Hydrolytic degradation of composites of poly(L-lactide-co-epsilon-caprolactone) 70/30 and beta-tricalcium phosphate. *Journal of Biomaterials Applications, 28*(4), 529-543.

Akkouch, A., Zhang, Z., & Rouabhia, M. (2014). Engineering bone tissue using human dental pulp stem cells and an osteogenic collagen-hydroxyapatite-poly (L-lactide-co-epsilon-caprolactone) scaffold. *Journal of Biomaterials Applications, 28*(6), 922-936.

Aksu, A. E., Rubin, J. P., Dudas, J. R., & Marra, K. G. (2008). Role of gender and anatomical region on induction of osteogenic differentiation of human adipose-derived stem cells. *Annals of Plastic Surgery, 60*(3), 306-322.

Almalki, S. G., & Agrawal, D. K. (2016). Key transcription factors in the differentiation of mesenchymal stem cells. *Differentiation; Research in Biological Diversity, 92*(1-2), 41-51.

Al-Salleeh, F., Beatty, M. W., Reinhardt, R. A., Petro, T. M., & Crouch, L. (2008). Human osteogenic protein-1 induces osteogenic differentiation of adipose-derived stem cells harvested from mice. *Archives of Oral Biology, 53*(10), 928-936.

Alt, E. U., Senst, C., Murthy, S. N., Slakey, D. P., Dupin, C. L., Chaffin, A. E., . . . Izadpanah, R. (2012). Aging alters tissue resident mesenchymal stem cell properties. *Stem Cell Research, 8*(2), 215-225.

Amini, A. R., Laurencin, C. T., & Nukavarapu, S. P. (2012). Bone tissue engineering: Recent advances and challenges. *Critical Reviews in Biomedical Engineering, 40*(5), 363-408.

Antonyshyn, J. A., McFadden, M. J., Gramolini, A. O., Hofer, S. O. P., & Santerre, J. P. (2019). Limited endothelial plasticity of mesenchymal stem cells revealed by quantitative phenotypic comparisons to representative endothelial cell controls. *Stem Cells Translational Medicine, 8*(1), 35-45.

Attig, L., Vige, A., Gabory, A., Karimi, M., Beauger, A., Gross, M. S., . . . Junien, C. (2013). Dietary alleviation of maternal obesity and diabetes: Increased resistance to diet-induced obesity transcriptional and epigenetic signatures. *PloS One, 8*(6), e66816.

Aunoble, S., Clement, D., Frayssinet, P., Harmand, M. F., & Le Huec, J. C. (2006). Biological performance of a new beta-TCP/PLLA composite material for applications in spine surgery: In vitro and in vivo studies. *Journal of Biomedical Materials Research.Part A, 78*(2), 416-422.

Bajek, A., Gurtowska, N., Olkowska, J., Kazmierski, L., Maj, M., & Drewa, T. (2016). Adipose-derived stem cells as a tool in cell-based therapies. *Archivum Immunologiae Et Therapiae Experimentalis, 64*(6), 443-454.

Bari, A., Bloise, N., Fiorilli, S., Novajra, G., Vallet-Regi, M., Bruni, G., . . . Vitale-Brovarone, C. (2017). Copper-containing mesoporous bioactive glass nanoparticles as multifunctional agent for bone regeneration. *Acta Biomaterialia, 55*, 493-504.

Barrere, F., van Blitterswijk, C. A., & de Groot, K. (2006). Bone regeneration: Molecular and cellular interactions with calcium phosphate ceramics. *International Journal of Nanomedicine, 1*(3), 317-332.

Beck, E. C., Barragan, M., Tadros, M. H., Gehrke, S. H., & Detamore, M. S. (2016). Approaching the compressive modulus of articular cartilage with a decellularized cartilage-based hydrogel. *Acta Biomaterialia, 38*, 94-105.

Beger, B., Blatt, S., Pabst, A. M., Hansen, T., Goetz, H., Al-Nawas, B., & Ziebart, T. (2018). Biofunctionalization of synthetic bone substitutes with angiogenic stem cells: Influence on regeneration of critical-size bone defects in an in vivo murine model. *Journal of Cranio-Maxillo-Facial Surgery : Official Publication of the European Association for Cranio-Maxillo-Facial Surgery, 46*(9), 1601-1608.

Behr, B., Tang, C., Germann, G., Longaker, M. T., & Quarto, N. (2011). Locally applied vascular endothelial growth factor A increases the osteogenic healing capacity of human adipose-derived stem cells by promoting osteogenic and endothelial differentiation. *Stem Cells (Dayton, Ohio), 29*(2), 286-296.

Bersini, S., Gilardi, M., Arrigoni, C., Talò, G., Zamai, M., Zagra, L., . . . Moretti, M. (2016). Human in vitro 3D co-culture model to engineer vascularized bone-mimicking tissues combining computational tools and statistical experimental approach. *Biomaterials, 76*, 157-172.

Bessa, P. C., Casal, M., & Reis, R. L. (2008). Bone morphogenetic proteins in tissue engineering: The road from the laboratory to the clinic, part I (basic concepts). *Journal of Tissue Engineering and Regenerative Medicine, 2*(1), 1-13.

Björninen, M., Gilmore, K., Pelto, J., Seppänen-Kaijansinkko, R., Kellomäki, M., Miettinen, S., . . . Haimi, S. (2017). Electrically stimulated adipose stem cells on polypyrrole-coated scaffolds for smooth muscle tissue engineering. *Annals of Biomedical Engineering, 45*(4), 1015-1026.

Blair, H. C., Larrouture, Q. C., Li, Y., Lin, H., Beer-Stoltz, D., Liu, L., . . . Nelson, D. J. (2017). Osteoblast differentiation and bone matrix formation in vivo and in vitro. *Tissue Engineering.Part B, Reviews, 23*(3), 268-280.

Bleach, N. C., Nazhat, S. N., Tanner, K. E., Kellomaki, M., & Tormala, P. (2002). Effect of filler content on mechanical and dynamic mechanical properties of particulate biphasic calcium phosphate--polylactide composites. *Biomaterials, 23*(7), 1579-1585.

Bodalia, P. N., Balaji, V., Kaila, R., & Wilson, L. (2016). Effectiveness and safety of recombinant human bone morphogenetic protein-2 for adults with lumbar spine pseudarthrosis following spinal fusion surgery. *Bone & Joint Research, 5*(4), 145-152.

Bohner, M., & Miron, R. J. (2019). A proposed mechanism for material-induced heterotopic ossification. *Materials Today, 22*, 132-141.

Bonewald, L. F., Harris, S. E., Rosser, J., Dallas, M. R., Dallas, S. L., Camacho, N. P., . . . Boskey, A. (2003). Von kossa staining alone is not sufficient to confirm that mineralization in vitro represents bone formation. *Calcified Tissue International, 72*(5), 537-547.

Bora, P., & Majumdar, A. S. (2017). Adipose tissue-derived stromal vascular fraction in regenerative medicine: A brief review on biology and translation. *Stem Cell Research & Therapy, 8*(1), 145-017-0598-y.

Bourin, P., Bunnell, B. A., Casteilla, L., Dominici, M., Katz, A. J., March, K. L., . . . Gimble, J. M. (2013). Stromal cells from the adipose tissue-derived stromal vascular fraction and culture expanded adipose tissue-derived stromal/stem cells: A joint statement of the international federation for adipose therapeutics and science (IFATS) and the international society for cellular therapy (ISCT). *Cytotherapy, 15*(6), 641-648.

Boyce, T., Edwards, J., & Scarborough, N. (1999). Allograft bone. the influence of processing on safety and performance. *The Orthopedic Clinics of North America, 30*(4), 571-581.

Burrow, K. L., Hoyland, J. A., & Richardson, S. M. (2017). Human adipose-derived stem cells exhibit enhanced proliferative capacity and retain multipotency longer than donor-matched bone marrow mesenchymal stem cells during expansion in vitro. *Stem Cells International, 2017*, 2541275.

Buxton, P. G., Bitar, M., Gellynck, K., Parkar, M., Brown, R. A., Young, A. M., . . . Nazhat, S. N. (2008). Dense collagen matrix accelerates osteogenic differentiation and rescues the apoptotic response to MMP inhibition. *Bone, 43*(2), 377-385.

Campana, V., Milano, G., Pagano, E., Barba, M., Cicione, C., Salonna, G., . . . Logroscino, G. (2014). Bone substitutes in orthopaedic surgery: From basic science to clinical practice. *Journal of Materials Science.Materials in Medicine, 25*(10), 2445-2461.

Cao, Y., Gong, Y., Liu, L., Zhou, Y., Fang, X., Zhang, C., . . . Li, J. (2017). The use of human umbilical vein endothelial cells (HUVECs) as an in vitro model to assess the toxicity of nanoparticles to endothelium: A review. *Journal of Applied Toxicology : JAT, 37*(12), 1359-1369.

Caplan, A. I. (1991). Mesenchymal stem cells. *Journal of Orthopaedic Research : Official Publication of the Orthopaedic Research Society, 9*(5), 641-650.

Carragee, E. J., Hurwitz, E. L., & Weiner, B. K. (2011). A critical review of recombinant human bone morphogenetic protein-2 trials in spinal surgery: Emerging safety concerns and lessons learned. *The Spine Journal, 11*(6), 471-491.

Chai, Y. C., Carlier, A., Bolander, J., Roberts, S. J., Geris, L., Schrooten, J., . . . Luyten, F. P. (2012). Current views on calcium phosphate osteogenicity and the translation into effective bone regeneration strategies. *Acta Biomaterialia, 8*(11), 3876-3887.

Chandra, V., G, S., Phadnis, S., Nair, P. D., & Bhonde, R. R. (2009). Generation of pancreatic hormone-expressing islet-like cell aggregates from murine adipose tissue-derived stem cells. *Stem Cells (Dayton, Ohio), 27*(8), 1941-1953.

Chang, P. L., Blair, H. C., Zhao, X., Chien, Y. W., Chen, D., Tilden, A. B., . . . Hicks, P. (2006). Comparison of fetal and adult marrow stromal cells in osteogenesis with and without glucocorticoids. *Connective Tissue Research, 47*(2), 67-76.

Charoenpanich, A., Wall, M. E., Tucker, C. J., Andrews, D. M., Lalush, D. S., & Loboa, E. G. (2011). Microarray analysis of human adipose-derived stem cells in three-dimensional collagen culture: Osteogenesis inhibits bone morphogenic protein and wnt signaling pathways, and cyclic tensile strain causes upregulation of proinflammatory cytokine regulators and angiogenic factors. *Tissue Engineering.Part A, 17*(21-22), 2615-2627.

Chatterjea, A., van der Stok, J., Danoux, C. B., Yuan, H., Habibovic, P., van Blitterswijk, C. A., . . . de Boer, J. (2013). Inflammatory response and bone healing capacity of two porous calcium phosphate ceramics in critical size cortical bone defects. *Journal of Biomedical Materials Research.Part A,*

Chen, Q. Z., Thompson, I. D., & Boccaccini, A. R. (2006). 45S5 bioglass-derived glass-ceramic scaffolds for bone tissue engineering. *Biomaterials, 27*(11), 2414-2425.

Cheng, F., Zhang, Y., Wang, Y., Jiang, Q., Zhao, C. J., Deng, J., . . . Deng, H. (2018). Conversion of human adipose-derived stem cells into functional and expandable endothelial-like cells for cell-based therapies. *Stem Cell Research & Therapy, 9*(1), 350-018-1088-6.

Cheng, H. Y., Ghetu, N., Huang, W. C., Wang, Y. L., Wallace, C. G., Wen, C. J., . . . Wei, F. C. (2014). Syngeneic adipose-derived stem cells with short-term immunosuppression induce vascularized composite allotransplantation tolerance in rats. *Cytotherapy, 16*(3), 369-380.

Cheng, M., Guan, X., Li, H., Cui, X., Zhang, X., Li, X., . . . Avsar, E. (2013). Shear stress regulates late EPC differentiation via mechanosensitive molecule-mediated cytoskeletal rearrangement. *PloS One, 8*(7), e67675.

Choudhery, M. S., Badowski, M., Muise, A., Pierce, J., & Harris, D. T. (2014). Donor age negatively impacts adipose tissue-derived mesenchymal stem cell expansion and differentiation. *Journal of Translational Medicine, 12*, 8-5876-12-8.

Choumerianou, D. M., Dimitriou, H., & Kalmanti, M. (2008). Stem cells: Promises versus limitations. *Tissue Engineering.Part B, Reviews, 14*(1), 53-60.

Cleal, L., Aldea, T., & Chau, Y. Y. (2017). Fifty shades of white: Understanding heterogeneity in white adipose stem cells. *Adipocyte, 6*(3), 205-216.

Clozza, E., Biasotto, M., Cavalli, F., Moimas, L., & Di Lenarda, R. (2012). Three-dimensional evaluation of bone changes following ridge preservation procedures. *The International Journal of Oral & Maxillofacial Implants, 27*(4), 770-775.

Clozza, E., Pea, M., Cavalli, F., Moimas, L., Di Lenarda, R., & Biasotto, M. (2014). Healing of fresh extraction sockets filled with bioactive glass particles: Histological findings in humans. *Clinical Implant Dentistry and Related Research, 16*(1), 145-153.

Coelho, M. J., & Fernandes, M. H. (2000). Human bone cell cultures in biocompatibility testing. part II: Effect of ascorbic acid, beta-glycerophosphate and dexamethasone on osteoblastic differentiation. *Biomaterials, 21*(11), 1095-1102.

Colazzo, F., Alrashed, F., Saratchandra, P., Carubelli, I., Chester, A. H., Yacoub, M. H., . . . Somers, P. (2014). Shear stress and VEGF enhance endothelial differentiation of human adipose-derived stem cells. *Growth Factors (Chur, Switzerland), 32*(5), 139-149.

Colazzo, F., Chester, A. H., Taylor, P. M., & Yacoub, M. H. (2010). Induction of mesenchymal to endothelial transformation of adipose-derived stem cells. *The Journal of Heart Valve Disease, 19*(6), 736-744.

Correia, C., Grayson, W. L., Park, M., Hutton, D., Zhou, B., Guo, X. E., . . . Vunjak-Novakovic, G. (2011). In vitro model of vascularized bone: Synergizing vascular development and osteogenesis. *PloS One, 6*(12), e28352.

Correia, C., Grayson, W., Eton, R., Gimble, J. M., Sousa, R. A., Reis, R. L., & Vunjak-Novakovic, G. (2014). Human adipose-derived cells can serve as a single-cell source for the in vitro cultivation of vascularized bone grafts. *Journal of Tissue Engineering and Regenerative Medicine, 8*(8), 629-639.

Cross, M. J., & Claesson-Welsh, L. (2001). FGF and VEGF function in angiogenesis: Signalling pathways, biological responses and therapeutic inhibition. *Trends in Pharmacological Sciences, 22*(4), 201-207.

Culmes, M., Eckstein, H., Burgkart, R., Nüssler, A. K., Guenther, M., Wagner, E., & Pelisek, J. (2013). Endothelial differentiation of adipose-derived mesenchymal stem cells is improved by epigenetic modifying drug BIX-01294. *European Journal of Cell Biology, 92*(2), 70-79.

Da Pozzo, E., Barsotti, M. C., Bendinelli, S., Martelli, A., Calderone, V., Balbarini, A., . . . Di Stefano, R. (2012). Differential effects of fondaparinux and bemiparin on angiogenic and vasculogenesis-like processes. *Thrombosis Research, 130*(3), e113-e122.

Dahl, J. A., Duggal, S., Coulston, N., Millar, D., Melki, J., Shahdadfar, A., . . . Collas, P. (2008). Genetic and epigenetic instability of human bone marrow mesenchymal stem

cells expanded in autologous serum or fetal bovine serum. *The International Journal of Developmental Biology, 52*(8), 1033-1042.

Dan, P., Velot, E., Decot, V., & Menu, P. (2015). The role of mechanical stimuli in the vascular differentiation of mesenchymal stem cells. *Journal of Cell Science, 128*(14), 2415-2422.

Dash, T. K., & Konkimalla, V. B. (2012). Poly-c-caprolactone based formulations for drug delivery and tissue engineering: A review. *Journal of Controlled Release : Official Journal of the Controlled Release Society, 158*(1), 15-33.

Davison, N. L., Gamblin, A. L., Layrolle, P., Yuan, H., de Bruijn, J. D., & Barrere-de Groot, F. (2014). Liposomal clodronate inhibition of osteoclastogenesis and osteoinduction by submicrostructured beta-tricalcium phosphate. *Biomaterials, 35*(19), 5088-5097.

Day, R. M. (2005). Bioactive glass stimulates the secretion of angiogenic growth factors and angiogenesis in vitro. *Tissue Engineering, 11*(5-6), 768-777.

de Misquita, M. R., Bentini, R., & Goncalves, F. (2016). The performance of bone tissue engineering scaffolds in in vivo animal models: A systematic review. *Journal of Biomaterials Applications, 31*(5), 625-636.

Detsch, R., Stoor, P., Grunewald, A., Roether, J. A., Lindfors, N. C., & Boccaccini, A. R. (2014). Increase in VEGF secretion from human fibroblast cells by bioactive glass S53P4 to stimulate angiogenesis in bone. *Journal of Biomedical Materials Research.Part A, 102*(11), 4055-4061.

Di Marco, G. S., Hausberg, M., Hillebrand, U., Rustemeyer, P., Wittkowski, W., Lang, D., & Pavenstadt, H. (2008). Increased inorganic phosphate induces human endothelial cell apoptosis in vitro. *American Journal of Physiology.Renal Physiology, 294*(6), F1381-7.

Di Marco, G. S., König, M., Stock, C., Wiesinger, A., Hillebrand, U., Reiermann, S., . . . Brand, M. (2013). High phosphate directly affects endothelial function by downregulating annexin II. *Kidney International, 83*(2), 213-222.

Diaz-Gomez, L., Garcia-Gonzalez, C. A., Wang, J., Yang, F., Aznar-Cervantes, S., Cenis, J. L., . . . Alvarez-Lorenzo, C. (2017). Biodegradable PCL/fibroin/hydroxyapatite porous scaffolds prepared by supercritical foaming for bone regeneration. *International Journal of Pharmaceutics, 527*(1-2), 115-125.

Dominici, M., Le Blanc, K., Mueller, I., Slaper-Cortenbach, I., Marini, F., Krause, D., . . . Horwitz, E. (2006). Minimal criteria for defining multipotent mesenchymal stromal cells. the international society for cellular therapy position statement. *Cytotherapy, 8*(4), 315-317.

Dong, J. D., Gu, Y. Q., Li, C. M., Wang, C. R., Feng, Z. G., Qiu, R. X., . . . Zhang, J. (2009). Response of mesenchymal stem cells to shear stress in tissue-engineered vascular grafts. *Acta Pharmacologica Sinica, 30*(5), 530-536.

Duan, R., Barbieri, D., de Groot, F., de Bruijn, J. D., & Yuan, H. (2018). Modulating bone regeneration in rabbit condyle defects with three surface-structured tricalcium phosphate ceramics. *ACS Biomaterials Science & Engineering, 4*(9), 3347-3355.

Duan, R., Barbieri, D., Luo, X., Weng, J., Bao, C., de Bruijn, J. D., & Yuan, H. (2017). Variation of the bone forming ability with the physicochemical properties of calcium phosphate bone substitutes. *Biomaterials Science, 6*(1), 136-145.

Duarte, A. R. C., Santo, V. E., Alves, A., Silva, S. S., Moreira-Silva, J., Silva, T. H., . . . Mano, J. F. (2013). Unleashing the potential of supercritical fluids for polymer processing in tissue engineering and regenerative medicine. *The Journal of Supercritical Fluids, 79*, 177-185.

Dupont, S., Morsut, L., Aragona, M., Enzo, E., Giulitti, S., Cordenonsi, M., . . . Piccolo, S. (2011). Role of YAP/TAZ in mechanotransduction. *Nature, 474*, 179.

Ell, J., Regn, S., Buchberger, A. M., von Bomhard, A., Stark, T., Schantz, J. T., & Storck, K. (2017). Donor-dependent variances of human adipose-derived stem cells in respect to the in-vitro endothelial cell differentiation capability. *Adipocyte, 6*(1), 20-32.

Ern, C., Berger, T., Frasheri, I., Heym, R., Hickel, R., & Folwaczny, M. (2017). Differentiation of hMSC and hPDLSC induced by PGE2 or BMP-7 in 3D models. *Prostaglandins, Leukotrienes and Essential Fatty Acids, 122*, 30-37.

European Commission. (2015). Guidance document - classification of medical devices. Retrieved from https://ec.europa.eu/docsroom/documents/10337/attachments/1/translations

Fennema, E. M., Tchang, L. A. H., Yuan, H., van Blitterswijk, C. A., Martin, I., Scherberich, A., & de Boer, J. (2018). Ectopic bone formation by aggregated mesenchymal stem cells from bone marrow and adipose tissue: A comparative study. *Journal of Tissue Engineering and Regenerative Medicine, 12*(1), e150-e158.

Florencio-Silva, R., Sasso, G. R., Sasso-Cerri, E., Simoes, M. J., & Cerri, P. S. (2015). Biology of bone tissue: Structure, function, and factors that influence bone cells. *BioMed Research International, 2015*, 421746.

Frazier, T. P., Gimble, J. M., Devay, J. W., Tucker, H. A., Chiu, E. S., & Rowan, B. G. (2013). Body mass index affects proliferation and osteogenic differentiation of human subcutaneous adipose tissue-derived stem cells. *BMC Cell Biology, 14*, 34-2121-14-34.

Freeman, F. E., & McNamara, L. M. (2017). Endochondral priming: A developmental engineering strategy for bone tissue regeneration. *Tissue Engineering.Part B, Reviews, 23*(2), 128-141.

Friedenstein, A. J., Petrakova, K. V., Kurolesova, A. I., & Frolova, G. P. (1968). Heterotopic of bone marrow. analysis of precursor cells for osteogenic and hematopoietic tissues. *Transplantation, 6*(2), 230-247.

Gao, S., Calcagni, M., Welti, M., Hemmi, S., Hild, N., Stark, W. J., . . . Buschmann, J. (2014). Proliferation of ASC-derived endothelial cells in a 3D electrospun mesh: Impact of bone-biomimetic nanocomposite and co-culture with ASC-derived osteoblasts. *Injury, 45*(6), 974-980.

Gardin, C., Bressan, E., Ferroni, L., Nalesso, E., Vindigni, V., Stellini, E., . . . Zavan, B. (2012). In vitro concurrent endothelial and osteogenic commitment of adipose-derived stem cells and their genomical analyses through comparative genomic hybridization array: Novel strategies to increase the successful engraftment of tissue-engineered bone grafts. *Stem Cells & Development, 21*(5), 767-777.

Garrison, K. R., Donell, S., Ryder, J., Shemilt, I., Mugford, M., Harvey, I., & Song, F. (2007). Clinical effectiveness and cost-effectiveness of bone morphogenetic proteins in the non-healing of fractures and spinal fusion: A systematic review. *Health Technology Assessment (Winchester, England), 11*(30), 1-150, iii-iv.

Gattazzo, F., Urciuolo, A., & Bonaldo, P. (2014). Extracellular matrix: A dynamic microenvironment for stem cell niche. *Biochimica Et Biophysica Acta, 1840*(8), 2506-2519.

Gionet-Gonzales, M. A., & Leach, J. K. (2018). Engineering principles for guiding spheroid function in the regeneration of bone, cartilage, and skin. *Biomedical Materials (Bristol, England), 13*(3), 034109-605X/aab0b3.

Gorustovich, A. A., Roether, J. A., & Boccaccini, A. R. (2010). Effect of bioactive glasses on angiogenesis: A review of in vitro and in vivo evidences. *Tissue Engineering.Part B, Reviews, 16*(2), 199-207.

Gothard, D., Smith, E., Kanczler, J., Rashidi, H., Qutachi, O., Henstock, J., . . . Oreffo, R. (2014). Tissue engineered bone using select growth factors: A comprehensive review of animal studies and clinical translation studies in man. *Eur.Cell.Mater., 28*, 166-208.

Gritsch, L., Conoscenti, G., La Carrubba, V., Nooeaid, P., & Boccaccini, A. R. (2019). Polylactide-based materials science strategies to improve tissue-material interface without the use of growth factors or other biological molecules. *Materials Science & Engineering.C, Materials for Biological Applications, 94*, 1083-1101.

Guneta, V., Tan, N. S., Chan, S. K., Tanavde, V., Lim, T. C., Wong, T. C., & Choong, C. (2016). Comparative study of adipose-derived stem cells and bone marrow-derived stem cells in similar microenvironmental conditions. *Experimental Cell Research, 348*(2), 155-164.

Guo, L. Z., Kim, T. H., Han, S., & Kim, S. W. (2016). Angio-vasculogenic properties of endothelial-induced mesenchymal stem cells derived from human adipose tissue. *Circulation Journal : Official Journal of the Japanese Circulation Society, 80*(4), 998-1007.

Habibovic, P., Yuan, H., van, d. V., Meijer, G., van Blitterswijk, C. A., & de Groot, K. (2005). 3D microenvironment as essential element for osteoinduction by biomaterials. *Biomaterials, 26*(17), 3565-3575.

Haimi, S., Suuriniemi, N., Haaparanta, A. M., Ellä, V., Lindroos, B., Huhtala, H., . . . Suuronen, R. (2009). Growth and osteogenic differentiation of adipose stem cells on PLA/bioactive glass and PLA/beta-TCP scaffolds. *Tissue Engineering.Part A, 15*(7), 1473-1480.

Haubruck, P., Tanner, M. C., Vlachopoulos, W., Hagelskamp, S., Miska, M., Ober, J., . . . Schmidmaier, G. (2018). Comparison of the clinical effectiveness of bone morphogenic protein (BMP) -2 and -7 in the adjunct treatment of lower limb nonunions. *Orthopaedics & Traumatology, Surgery & Research : OTSR, 104*(8), 1241-1248.

Hench, L. L. (2006). The story of bioglass. *Journal of Materials Science.Materials in Medicine, 17*(11), 967-978.

Hench, L. L. (1991). Bioceramics: From concept to clinic. *Journal of the American Ceramic Society, 74*(7), 1487-1510.

Holmbom, J., Sodergard, A., Ekholm, E., Martson, M., Kuusilehto, A., Saukko, P., & Penttinen, R. (2005). Long-term evaluation of porous poly(epsilon-caprolactone-co-L-lactide) as a bone-filling material. *Journal of Biomedical Materials Research.Part A, 75*(2), 308-315.

Ho-Shui-Ling, A., Bolander, J., Rustom, L. E., Johnson, A. W., Luyten, F. P., & Picart, C. (2018). Bone regeneration strategies: Engineered scaffolds, bioactive molecules and stem cells current stage and future perspectives. *Biomaterials, 180*, 143-162.

Hristov, M., Erl, W., & Weber, P. C. (2003). Endothelial progenitor cells: Isolation and characterization. *Trends in Cardiovascular Medicine, 13*(5), 201-206.

Hu, S., Chang, J., Liu, M., & Ning, C. (2009). Study on antibacterial effect of 45S5 bioglass. *Journal of Materials Science.Materials in Medicine, 20*(1), 281-286.

Hutton, D. L., Moore, E. M., Gimble, J. M., & Grayson, W. L. (2013). Platelet-derived growth factor and spatiotemporal cues induce development of vascularized bone tissue by adipose-derived stem cells. *Tissue Engineering.Part A, 19*(17-18), 2076-2086.

International Organization for Standardization. (2016). ISO 13485:2016 medical devices - quality management systems - requirements for regulatory purposes. Retrieved from https://www.iso.org/standard/59752.html

Jeong, S. I., Lee, A. Y., Lee, Y. M., & Shin, H. (2008). Electrospun gelatin/poly(L-lactide-co-epsilon-caprolactone) nanofibers for mechanically functional tissue-engineering scaffolds. *Journal of Biomaterials Science.Polymer Edition, 19*(3), 339-357.

Jones, J. R. (2013). Review of bioactive glass: From hench to hybrids. *Acta Biomaterialia, 9*(1), 4457-4486.

Kanthilal, M., & Darling, E. M. (2014). Characterization of mechanical and regenerative properties of human, adipose stromal cells. *Cellular and Molecular Bioengineering, 7*(4), 585-597.

Karadjian, M., Essers, C., Tsitlakidis, S., Reible, B., Moghaddam, A., Boccaccini, A. R., & Westhauser, F. (2019). Biological properties of calcium phosphate bioactive glass composite bone substitutes: Current experimental evidence. *International Journal of Molecular Sciences, 20*(2), 10.3390/ijms20020305.

Khan, S., Villalobos, M. A., Choron, R. L., Chang, S., Brown, S. A., Carpenter, J. P., . . . Zhang, P. (2017). Fibroblast growth factor and vascular endothelial growth factor play a critical role in endotheliogenesis from human adipose-derived stem cells. *Journal of Vascular Surgery, 65*(5), 1483-1492.

Khan, T., Muise, E. S., Iyengar, P., Wang, Z. V., Chandalia, M., Abate, N., . . . Scherer, P. E. (2009). Metabolic dysregulation and adipose tissue fibrosis: Role of collagen VI. *Molecular and Cellular Biology, 29*(6), 1575-1591.

Klatte-Schulz, F., Giese, G., Differ, C., Minkwitz, S., Ruschke, K., Puts, R., . . . Wildemann, B. (2016). An investigation of BMP-7 mediated alterations to BMP signalling components in human tenocyte-like cells. *Scientific Reports, 6*, 29703.

Knippenberg, M., Helder, M. N., Zandieh Doulabi, B., Wuisman, P. I., & Klein-Nulend, J. (2006). Osteogenesis versus chondrogenesis by BMP-2 and BMP-7 in adipose stem cells. *Biochemical and Biophysical Research Communications, 342*(3), 902-908.

Koepp, H. E., Schorlemmer, S., Kessler, S., Brenner, R. E., Claes, L., Günther, K., & Ignatius, A. A. (2004). Biocompatibility and osseointegration of β-TCP: Histomorphological and biomechanical studies in a weight-bearing sheep model. *Journal of Biomedical Materials Research Part B: Applied Biomaterials, 70B*(2), 209-217.

Kokubo, T., Kim, H. M., & Kawashita, M. (2003). Novel bioactive materials with different mechanical properties. *Biomaterials, 24*(13), 2161-2175.

Komori, T. (2017). Roles of Runx2 in skeletal development. *Advances in Experimental Medicine and Biology, 962*, 83-93.

Komori, T., Yagi, H., Nomura, S., Yamaguchi, A., Sasaki, K., Deguchi, K., . . . Kishimoto, T. (1997). Targeted disruption of Cbfa1 results in a complete lack of bone formation owing to maturational arrest of osteoblasts. *Cell, 89*(5), 755-764.

Kondo, N., Ogose, A., Tokunaga, K., Umezu, H., Arai, K., Kudo, N., . . . Endo, N. (2006). Osteoinduction with highly purified beta-tricalcium phosphate in dog dorsal muscles and the proliferation of osteoclasts before heterotopic bone formation. *Biomaterials, 27*(25), 4419-4427.

Kukumberg, M., Yao, J. Y., Neo, D. J. H., & Yim, E. K. F. (2017). Microlens topography combined with vascular endothelial growth factor induces endothelial differentiation of human mesenchymal stem cells into vasculogenic progenitors. *Biomaterials, 131*, 68-85.

Kütscher, C., Lampert, F. M., Kunze, M., Markfeld-Erol, F., Stark, G. B., & Finkenzeller, G. (2016). Overexpression of hypoxia-inducible factor-1 alpha improves vasculogenesis-related functions of endothelial progenitor cells. *Microvascular Research, 105*, 85-92.

Kyllönen, L., Haimi, S., Mannerström, B., Huhtala, H., Rajala, K. M., Skottman, H., . . . Miettinen, S. (2013). Effects of different serum conditions on osteogenic differentiation of human adipose stem cells in vitro. *Stem Cell Research & Therapy, 4*(1), 17.

Langenbach, F., & Handschel, J. (2013). Effects of dexamethasone, ascorbic acid and beta-glycerophosphate on the osteogenic differentiation of stem cells in vitro. *Stem Cell Research & Therapy, 4*(5), 117.

Lappalainen, O. P., Karhula, S., Haapea, M., Kyllonen, L., Haimi, S., Miettinen, S., . . . Sandor, G. K. (2016a). Bone healing in rabbit calvarial critical-sized defects filled with stem cells and growth factors combined with granular or solid scaffolds. *Child's Nervous System : ChNS : Official Journal of the International Society for Pediatric Neurosurgery, 32*(4), 681-688.

Lappalainen, O. P., Karhula, S. S., Haapea, M., Kauppinen, S., Finnila, M., Saarakkala, S., . . . Sandor, G. K. (2016b). Micro-CT analysis of bone healing in rabbit calvarial critical-sized defects with solid bioactive glass, tricalcium phosphate granules or autogenous bone. *Journal of Oral & Maxillofacial Research, 7*(2), e4.

Lee, M. H., Kim, Y. J., Yoon, W. J., Kim, J. I., Kim, B. G., Hwang, Y. S., . . . Ryoo, H. M. (2005). Dlx5 specifically regulates Runx2 type II expression by binding to homeodomain-response elements in the Runx2 distal promoter. *The Journal of Biological Chemistry, 280*(42), 35579-35587.

Lertkiatmongkol, P., Liao, D., Mei, H., Hu, Y., & Newman, P. J. (2016). Endothelial functions of platelet/endothelial cell adhesion molecule-1 (CD31). *Current Opinion in Hematology, 23*(3), 253-259.

Lewis, D. M., Abaci, H. E., Xu, Y., & Gerecht, S. (2015). Endothelial progenitor cell recruitment in a microfluidic vascular model. *Biofabrication, 7*(4), 045010-5090/7/4/045010.

Li, P., Bai, Y., Yin, G., Pu, X., Huang, Z., Liao, X., . . . Yao, Y. (2014). Synergistic and sequential effects of BMP-2, bFGF and VEGF on osteogenic differentiation of rat osteoblasts. *Journal of Bone and Mineral Metabolism, 32*(6), 627-635.

Li, S., Wang, M., Chen, X., Li, S., Li-Ling, J., & Xie, H. (2014). Inhibition of osteogenic differentiation of mesenchymal stem cells by copper supplementation. *Cell Proliferation, 47*(1), 81-90.

Lian, J. B., & Stein, G. S. (1995). Development of the osteoblast phenotype: Molecular mechanisms mediating osteoblast growth and differentiation. *The Iowa Orthopaedic Journal, 15*, 118-140.

Lian, J. B., Stein, G. S., van Wijnen, A. J., Stein, J. L., Hassan, M. Q., Gaur, T., & Zhang, Y. (2012). MicroRNA control of bone formation and homeostasis. *Nature Reviews.Endocrinology, 8*(4), 212-227.

Lindfors, N., Geurts, J., Drago, L., Arts, J. J., Juutilainen, V., Hyvänen, P., . . . Romanó, C. L. (2017). Antibacterial bioactive glass, S53P4, for chronic bone infections: A multinational study. In L. Drago (Ed.), *A modern approach to biofilm-related orthopaedic implant infections: Advances in microbiology, infectious diseases and public health volume 5* (pp. 81-92). Cham: Springer International Publishing.

Lindfors, N., Koski, I., Heikkila, J. T., Mattila, K., & Aho, A. J. (2010). A prospective randomized 14-year follow-up study of bioactive glass and autogenous bone as bone

graft substitutes in benign bone tumors. *Journal of Biomedical Materials Research.Part B, Applied Biomaterials, 94*(1), 157-164.

Lindroos, B., Suuronen, R., & Miettinen, S. (2011). The potential of adipose stem cells in regenerative medicine. *Stem Cell Reviews, 7*(2), 269-291.

Malhotra, A., & Habibovic, P. (2016). Calcium phosphates and angiogenesis: Implications and advances for bone regeneration. *Trends in Biotechnology, 34*(12), 983-992.

Marcelo, K. L., Goldie, L. C., & Hirschi, K. K. (2013). Regulation of endothelial cell differentiation and specification. *Circulation Research, 112*(9), 1272-1287.

Marino, G., Rosso, F., Cafiero, G., Tortora, C., Moraci, M., Barbarisi, M., & Barbarisi, A. (2010). Beta-tricalcium phosphate 3D scaffold promote alone osteogenic differentiation of human adipose stem cells: In vitro study. *Journal of Materials Science.Materials in Medicine, 21*(1), 353-363.

Marino, G., Rosso, F., Ferdinando, P., Grimaldi, A., De Biasio, G., Cafiero, G., . . . Barbarisi, A. (2012). Growth and endothelial differentiation of adipose stem cells on polycaprolactone. *Journal of Biomedical Materials Research.Part A, 100*(3), 543-548.

Mathieu, L. M., Montjovent, M. O., Bourban, P. E., Pioletti, D. P., & Manson, J. A. (2005). Bioresorbable composites prepared by supercritical fluid foaming. *Journal of Biomedical Materials Research.Part A, 75*(1), 89-97.

Mathieu, L. M., Mueller, T. L., Bourban, P. E., Pioletti, D. P., Muller, R., & Manson, J. A. (2006). Architecture and properties of anisotropic polymer composite scaffolds for bone tissue engineering. *Biomaterials, 27*(6), 905-916.

McIntosh, K., Zvonic, S., Garrett, S., Mitchell, J. B., Floyd, Z. E., Hammill, L., . . . Gimble, J. M. (2006). The immunogenicity of human adipose-derived cells: Temporal changes in vitro. *Stem Cells (Dayton, Ohio), 24*(5), 1246-1253.

Mehrkens, A., Saxer, F., Guven, S., Hoffmann, W., Muller, A. M., Jakob, M., . . . Scherberich, A. (2012). Intraoperative engineering of osteogenic grafts combining freshly harvested, human adipose-derived cells and physiological doses of bone morphogenetic protein-2. *European Cells & Materials, 24*, 308-319.

Mesimäki, K., Lindroos, B., Tornwall, J., Mauno, J., Lindqvist, C., Kontio, R., . . . Suuronen, R. (2009). Novel maxillary reconstruction with ectopic bone formation by GMP adipose stem cells. *International Journal of Oral and Maxillofacial Surgery, 38*(3), 201-209.

Meza-Zepeda, L. A., Noer, A., Dahl, J. A., Micci, F., Myklebost, O., & Collas, P. (2008). High-resolution analysis of genetic stability of human adipose tissue stem cells cultured to senescence. *Journal of Cellular and Molecular Medicine, 12*(2), 553-563.

Mihaila, S. M., Frias, A. M., Pirraco, R. P., Rada, T., Reis, R. L., Gomes, M. E., & Marques, A. P. (2013). Human adipose tissue-derived SSEA-4 subpopulation multi-differentiation potential towards the endothelial and osteogenic lineages. *Tissue Engineering.Part A, 19*(1-2), 235-246.

Miranville, A., Heeschen, C., Sengenes, C., Curat, C. A., Busse, R., & Bouloumie, A. (2004). Improvement of postnatal neovascularization by human adipose tissue-derived stem cells. *Circulation, 110*(3), 349-355.

Mishra, R., Bishop, T., Valerio, I. L., Fisher, J. P., & Dean, D. (2016). The potential impact of bone tissue engineering in the clinic. *Regenerative Medicine, 11*(6), 571-587.

Mo, M., Wang, S., Zhou, Y., Li, H., & Wu, Y. (2016). Mesenchymal stem cell subpopulations: Phenotype, property and therapeutic potential. *Cellular and Molecular Life Sciences : CMLS, 73*(17), 3311-3321.

Monfoulet, L. E., Becquart, P., Marchat, D., Vandamme, K., Bourguignon, M., Pacard, E., . . . Logeart-Avramoglou, D. (2014). The pH in the microenvironment of human

mesenchymal stem cells is a critical factor for optimal osteogenesis in tissue-engineered constructs. *Tissue Engineering.Part A, 20*(13-14), 1827-1840.

Montjovent, M. O., Mathieu, L., Schmoekel, H., Mark, S., Bourban, P. E., Zambelli, P. Y., . . . Pioletti, D. P. (2007). Repair of critical size defects in the rat cranium using ceramic-reinforced PLA scaffolds obtained by supercritical gas foaming. *Journal of Biomedical Materials Research.Part A, 83*(1), 41-51.

Muller, P., Bulnheim, U., Diener, A., Luthen, F., Teller, M., Klinkenberg, E. D., . . . Rychly, J. (2008). Calcium phosphate surfaces promote osteogenic differentiation of mesenchymal stem cells. *Journal of Cellular and Molecular Medicine, 12*(1), 281-291.

Muschler, G. F., Raut, V. P., Patterson, T. E., Wenke, J. C., & Hollinger, J. O. (2010). The design and use of animal models for translational research in bone tissue engineering and regenerative medicine. *Tissue Engineering.Part B, Reviews, 16*(1), 123-145.

Mushahary, D., Spittler, A., Kasper, C., Weber, V., & Charwat, V. (2018). Isolation, cultivation, and characterization of human mesenchymal stem cells. *Cytometry.Part A : The Journal of the International Society for Analytical Cytology, 93*(1), 19-31.

Nair, A. K., Gautieri, A., Chang, S. W., & Buehler, M. J. (2013). Molecular mechanics of mineralized collagen fibrils in bone. *Nature Communications, 4*, 1724.

Nakashima, K., Zhou, X., Kunkel, G., Zhang, Z., Deng, J. M., Behringer, R. R., & de Crombrugghe, B. (2002). The novel zinc finger-containing transcription factor osterix is required for osteoblast differentiation and bone formation. *Cell, 108*(1), 17-29.

Narayanan, G., Vernekar, V. N., Kuyinu, E. L., & Laurencin, C. T. (2016). Poly (lactic acid)-based biomaterials for orthopaedic regenerative engineering. *Advanced Drug Delivery Reviews, 107*, 247-276.

Niemelä, T. (2005). Effect of b-tricalcium phosphate addition on the in vitro degradation of self-reinforced poly-L,D-lactide. *Polymer Dedradation and Stability, Polym Degrad Stab, 89*, 492-500.

Niemeyer, P., Kornacker, M., Mehlhorn, A., Seckinger, A., Vohrer, J., Schmal, H., . . . Krause, U. (2007). Comparison of immunological properties of bone marrow stromal cells and adipose tissue-derived stem cells before and after osteogenic differentiation in vitro. *Tissue Engineering, 13*(1), 111-121.

Niemeyer, P., Vohrer, J., Schmal, H., Kasten, P., Fellenberg, J., Suedkamp, N. P., & Mehlhorn, A. T. (2008). Survival of human mesenchymal stromal cells from bone marrow and adipose tissue after xenogenic transplantation in immunocompetent mice. *Cytotherapy, 10*(8), 784-795.

Ojansivu, M., Hyväri, L., Kellomaki, M., Hupa, L., Vanhatupa, S., & Miettinen, S. (2018). Bioactive glass induced osteogenic differentiation of human adipose stem cells is dependent on cell attachment mechanism and mitogen-activated protein kinases. *European Cells & Materials, 35*, 54-72.

Ojansivu, M., Mishra, A., Vanhatupa, S., Juntunen, M., Larionova, A., Massera, J., & Miettinen, S. (2018). The effect of S53P4-based borosilicate glasses and glass dissolution products on the osteogenic commitment of human adipose stem cells. *PloS One, 13*(8), e0202740.

Ojansivu, M., Vanhatupa, S., Björkvik, L., Häkkänen, H., Kellomäki, M., Autio, R., . . . Miettinen, S. (2015). Bioactive glass ions as strong enhancers of osteogenic differentiation in human adipose stem cells. *Acta Biomaterialia, 21*, 190-203.

Owen, G., Dard, M., & Larjava, H. (2018). Hydoxyapatite/beta-tricalcium phosphate biphasic ceramics as regenerative material for the repair of complex bone defects. *Journal of Biomedical Materials Research.Part B, Applied Biomaterials, 106*(6), 2493-2512.

Ozkul, Y., & Galderisi, U. (2016). The impact of epigenetics on mesenchymal stem cell biology. *Journal of Cellular Physiology, 231*(11), 2393-2401.

Paakinaho and Kellomäki. (2019). Method for producing porous composite material. FI 127762B.

Pan, P., Zhu, B., & Inoue, Y. (2007). Enthalpy relaxation and embrittlement of poly(l-lactide) during physical aging. *Macromolecules, 40*(26), 9664-9671.

Panteli, M., Pountos, I., Jones, E., & Giannoudis, P. V. (2015). Biological and molecular profile of fracture non-union tissue: Current insights. *Journal of Cellular and Molecular Medicine, 19*(4), 685-713.

Patrikoski, M., Mannerström, B., & Miettinen, S. (2019). Perspectives for clinical translation of adipose stromal/stem cells. *Stem Cells International, 2019*, 21.

Patrikoski, M., Juntunen, M., Boucher, S., Campbell, A., Vemuri, M. C., Mannerström, B., & Miettinen, S. (2013). Development of fully defined xeno-free culture system for the preparation and propagation of cell therapy-compliant human adipose stem cells. *Stem Cell Research & Therapy, 4*(2), 27.

Pearce, A. I., Richards, R. G., Milz, S., Schneider, E., & Pearce, S. G. (2007). Animal models for implant biomaterial research in bone: A review. *European Cells & Materials, 13*, 1-10.

Peters, A. E., Akhtar, R., Comerford, E. J., & Bates, K. T. (2018). The effect of ageing and osteoarthritis on the mechanical properties of cartilage and bone in the human knee joint. *Scientific Reports, 8*(1), 5931-018-24258-6.

Pihlajamäki, H., Böstman, O., Tynninen, O., & Laitinen, O. (2006). Long-term tissue response to bioabsorbable poly-l-lactide and metallic screws: An experimental study. *Bone, 39*(4), 932-937.

Pihlman, H., Keranen, P., Paakinaho, K., Linden, J., Hannula, M., Manninen, I. K., . . . Laitinen-Vapaavuori, O. (2018). Novel osteoconductive beta-tricalcium phosphate/poly(L-lactide-co-e-caprolactone) scaffold for bone regeneration: A study in a rabbit calvarial defect. *Journal of Materials Science.Materials in Medicine, 29*(10), 156-018-6159-9.

Pirosa, A., Gottardi, R., Alexander, P. G., & Tuan, R. S. (2018). Engineering in-vitro stem cell-based vascularized bone models for drug screening and predictive toxicology. *Stem Cell Research & Therapy, 9*(1), 112-018-0847-8.

Pirraco, R. P., Iwata, T., Yoshida, T., Marques, A. P., Yamato, M., Reis, R. L., & Okano, T. (2014). Endothelial cells enhance the in vivo bone-forming ability of osteogenic cell sheets. *Laboratory Investigation; a Journal of Technical Methods and Pathology, 94*(6), 663-673.

Planat-Benard, V., Silvestre, J. S., Cousin, B., Andre, M., Nibbelink, M., Tamarat, R., . . . Casteilla, L. (2004). Plasticity of human adipose lineage cells toward endothelial cells: Physiological and therapeutic perspectives. *Circulation, 109*(5), 656-663.

Prins, H. J., Schulten, E. A., Ten Bruggenkate, C. M., Klein-Nulend, J., & Helder, M. N. (2016). Bone regeneration using the freshly isolated autologous stromal vascular fraction of adipose tissue in combination with calcium phosphate ceramics. *Stem Cells Translational Medicine, 5*(10), 1362-1374.

Qazi, T. H., Hafeez, S., Schmidt, J., Duda, G. N., Boccaccini, A. R., & Lippens, E. (2017). Comparison of the effects of 45S5 and 1393 bioactive glass microparticles on hMSC behavior. *Journal of Biomedical Materials Research.Part A, 105*(10), 2772-2782.

Rath, S. N., Brandl, A., Hiller, D., Hoppe, A., Gbureck, U., Horch, R. E., . . . Kneser, U. (2014). Bioactive copper-doped glass scaffolds can stimulate endothelial cells in co-culture in combination with mesenchymal stem cells. *PloS One, 9*(12), e113319.

Rath, S. N., Nooeaid, P., Arkudas, A., Beier, J. P., Strobel, L. A., Brandl, A., . . . Kneser, U. (2016). Adipose- and bone marrow-derived mesenchymal stem cells display different osteogenic differentiation patterns in 3D bioactive glass-based scaffolds. *Journal of Tissue Engineering and Regenerative Medicine, 10*(10), E497-E509.

Robey, P. (2017). "Mesenchymal stem cells": Fact or fiction, and implications in their therapeutic use [version 1; peer review: 2 approved]. *F1000Research, 6*, 524.

Rodriguez, J. P., Rios, S., & Gonzalez, M. (2002). Modulation of the proliferation and differentiation of human mesenchymal stem cells by copper. *Journal of Cellular Biochemistry, 85*(1), 92-100.

Romano, C. L., Logoluso, N., Meani, E., Romano, D., De Vecchi, E., Vassena, C., & Drago, L. (2014). A comparative study of the use of bioactive glass S53P4 and antibiotic-loaded calcium-based bone substitutes in the treatment of chronic osteomyelitis: A retrospective comparative study. *The Bone & Joint Journal, 96-B*(6), 845-850.

Rossi, E., Mracsko, E., Papadimitropoulos, A., Allafi, N., Reinhardt, D., Mehrkens, A., . . . Scherberich, A. (2018). An in vitro bone model to investigate the role of triggering receptor expressed on myeloid cells-2 in bone homeostasis. *Tissue Engineering Part C: Methods, 24*(7), 391-398.

Rouwkema, J., & Khademhosseini, A. (2016). Vascularization and angiogenesis in tissue engineering: Beyond creating static networks. *Trends in Biotechnology, 34*(9), 733-745.

Rouwkema, J., Rivron, N. C., & van Blitterswijk, C. A. (2008). Vascularization in tissue engineering. *Trends in Biotechnology, 26*(8), 434-441.

Runyan, C. M., & Gabrick, K. S. (2017). Biology of bone formation, fracture healing, and distraction osteogenesis. *The Journal of Craniofacial Surgery, 28*(5), 1380-1389.

Salamanna, F., Contartese, D., Maglio, M., & Fini, M. (2016). A systematic review on in vitro 3D bone metastases models: A new horizon to recapitulate the native clinical scenario? *Oncotarget, 7*(28), 44803-44820.

Samavedi, S., Whittington, A. R., & Goldstein, A. S. (2013). Calcium phosphate ceramics in bone tissue engineering: A review of properties and their influence on cell behavior. *Acta Biomaterialia, 9*(9), 8037-8045.

Sandor, G. K., Numminen, J., Wolff, J., Thesleff, T., Miettinen, A., Tuovinen, V. J., . . . Ohman, J. (2014). Adipose stem cells used to reconstruct 13 cases with cranio-maxillofacial hard-tissue defects. *Stem Cells Translational Medicine, 3*(4), 530-540.

Sandor, G. K., Tuovinen, V. J., Wolff, J., Patrikoski, M., Jokinen, J., Nieminen, E., . . . Miettinen, S. (2013). Adipose stem cell tissue-engineered construct used to treat large anterior mandibular defect: A case report and review of the clinical application of good manufacturing practice-level adipose stem cells for bone regeneration. *Journal of Oral and Maxillofacial Surgery : Official Journal of the American Association of Oral and Maxillofacial Surgeons, 71*(5), 938-950.

Sarasua, J. R., Arraiza, A. L., Balerdi, P., & Maiza, I. (2005). Crystallinity and mechanical properties of optically pure polylactides and their blends. *Polymer Engineering & Science, 45*(5), 745-753.

Sartoneva, R., Nordback, P. H., Haimi, S., Grijpma, D. W., Lehto, K., Rooney, N., . . . Lahdes-Vasama, T. (2018). Comparison of poly(l-lactide-co-varepsilon-caprolactone) and poly(trimethylene carbonate) membranes for urethral regeneration: An in vitro and in vivo study. *Tissue Engineering.Part A, 24*(1-2), 117-127.

Schindeler, A., Mills, R. J., Bobyn, J. D., & Little, D. G. (2018). Preclinical models for orthopedic research and bone tissue engineering. *Journal of Orthopaedic Research : Official Publication of the Orthopaedic Research Society, 36*(3), 832-840.

Schmitt, C. M., Doering, H., Schmidt, T., Lutz, R., Neukam, F. W., & Schlegel, K. A. (2013). Histological results after maxillary sinus augmentation with straumann(R) BoneCeramic, bio-oss(R), puros(R), and autologous bone. A randomized controlled clinical trial. *Clinical Oral Implants Research, 24*(5), 576-585.

Semon, J. A., Zhang, X., Pandey, A. C., Alandete, S. M., Maness, C., Zhang, S., . . . Bunnell, B. A. (2013). Administration of murine stromal vascular fraction ameliorates chronic experimental autoimmune encephalomyelitis. *Stem Cells Translational Medicine, 2*(10), 789-796.

Shanahan, C. M., Crouthamel, M. H., Kapustin, A., & Giachelli, C. M. (2011). Arterial calcification in chronic kidney disease: Key roles for calcium and phosphate. *Circulation Research, 109*(6), 697-711.

Shikinami, Y., Okazaki, K., Saito, M., Okuno, M., Hasegawa, S., Tamura, J., . . . Nakamura, T. (2006). Bioactive and bioresorbable cellular cubic-composite scaffolds for use in bone reconstruction. *Journal of the Royal Society, Interface, 3*(11), 805-821.

Simmons, J. K., Hildreth, B. E.,3rd, Supsavhad, W., Elshafae, S. M., Hassan, B. B., Dirksen, W. P., . . . Rosol, T. J. (2015). Animal models of bone metastasis. *Veterinary Pathology, 52*(5), 827-841.

Song, I., Kim, B. S., Kim, C. S., & Im, G. I. (2011). Effects of BMP-2 and vitamin D3 on the osteogenic differentiation of adipose stem cells. *Biochemical and Biophysical Research Communications, 408*(1), 126-131.

Sotiropoulou, P. A., Perez, S. A., Salagianni, M., Baxevanis, C. N., & Papamichail, M. (2006). Characterization of the optimal culture conditions for clinical scale production of human mesenchymal stem cells. *Stem Cells (Dayton, Ohio), 24*(2), 462-471.

Stenvinkel, P., Karimi, M., Johansson, S., Axelsson, J., Suliman, M., Lindholm, B., . . . Schalling, M. (2007). Impact of inflammation on epigenetic DNA methylation – a novel risk factor for cardiovascular disease? *Journal of Internal Medicine, 261*(5), 488-499.

Strioga, M., Viswanathan, S., Darinskas, A., Slaby, O., & Michalek, J. (2012). Same or not the same? comparison of adipose tissue-derived versus bone marrow-derived mesenchymal stem and stromal cells. *Stem Cells and Development, 21*(14), 2724-2752.

Tainio, J., Paakinaho, K., Ahola, N., Hannula, M., Hyttinen, J., Kellomaki, M., & Massera, J. (2017). In vitro degradation of borosilicate bioactive glass and poly(l-lactide-co-epsilon-caprolactone) composite scaffolds. *Materials (Basel, Switzerland), 10*(11), 1274.

Tang, Z., Li, X., Tan, Y., Fan, H., & Zhang, X. (2018). The material and biological characteristics of osteoinductive calcium phosphate ceramics. *Regenerative Biomaterials, 5*(1), 43-59.

Temple, J. P., Hutton, D. L., Hung, B. P., Huri, P. Y., Cook, C. A., Kondragunta, R., . . . Grayson, W. L. (2014). Engineering anatomically shaped vascularized bone grafts with hASCs and 3D-printed PCL scaffolds. *Journal of Biomedical Materials Research.Part A, 102*(12), 4317-4325.

Teoh, S. H., Goh, B. T., & Lim, J. (2019). 3D printed polycaprolactone scaffolds for bone regeneration-success and future perspective. *Tissue Engineering.Part A,*

Tirkkonen, L., Halonen, H., Hyttinen, J., Kuokkanen, H., Sievänen, H., Koivisto, A. M., . . . Haimi, S. (2011). The effects of vibration loading on adipose stem cell number, viability and differentiation towards bone-forming cells. *Journal of the Royal Society, Interface / the Royal Society,*

Tonti, G. A., & Mannello, F. (2008). From bone marrow to therapeutic applications: Different behaviour and genetic/epigenetic stability during mesenchymal stem cell

expansion in autologous and foetal bovine sera? *The International Journal of Developmental Biology, 52*(8), 1023-1032.

Tormin, A., Brune, J. C., Olsson, E., Valcich, J., Neuman, U., Olofsson, T., . . . Scheding, S. (2009). Characterization of bone marrow-derived mesenchymal stromal cells (MSC) based on gene expression profiling of functionally defined MSC subsets. *Cytotherapy, 11*(2), 114-128.

Tsigkou, O., Pomerantseva, I., Spencer, J. A., Redondo, P. A., Hart, A. R., O'Doherty, E., . . . Neville, C. (2010). Engineered vascularized bone grafts. *Proceedings of the National Academy of Sciences of the United States of America, 107*(8), 3311-3316.

Turnbull, G., Clarke, J., Picard, F., Riches, P., Jia, L., Han, F., . . . Shu, W. (2017). 3D bioactive composite scaffolds for bone tissue engineering. *Bioactive Materials, 3*(3), 278-314.

U.S. Food and Drug Administration. (2018a). Department of health and human services - subchapter H - medical devices - part 888 - orthopedic devices. Retrieved from https://www.accessdata.fda.gov/scripts/cdrh/cfdocs/cfcfr/CFRSearch.cfm?CFRPart=888

U.S. Food and Drug Administration. (2018b). Overview of device regulation. Retrieved from https://www.fda.gov/medical-devices/device-advice-comprehensive-regulatory-assistance/overview-device-regulation

van der Pol, U., Mathieu, L., Zeiter, S., Bourban, P. E., Zambelli, P. Y., Pearce, S. G., . . . Pioletti, D. P. (2010). Augmentation of bone defect healing using a new biocomposite scaffold: An in vivo study in sheep. *Acta Biomaterialia, 6*(9), 3755-3762.

Vangsness, C. T.,Jr, Sternberg, H., & Harris, L. (2015). Umbilical cord tissue offers the greatest number of harvestable mesenchymal stem cells for research and clinical application: A literature review of different harvest sites. *Arthroscopy : The Journal of Arthroscopic & Related Surgery : Official Publication of the Arthroscopy Association of North America and the International Arthroscopy Association, 31*(9), 1836-1843.

Vanhatupa, S., Ojansivu, M., Autio, R., Juntunen, M., & Miettinen, S. (2015). Bone morphogenetic protein-2 induces donor-dependent osteogenic and adipogenic differentiation in human adipose stem cells. *Stem Cells Translational Medicine, 4*(12), 1391-1402.

Vidal, M. A., Walker, N. J., Napoli, E., & Borjesson, D. L. (2012). Evaluation of senescence in mesenchymal stem cells isolated from equine bone marrow, adipose tissue, and umbilical cord tissue. *Stem Cells and Development, 21*(2), 273-283.

Virjula, S., Zhao, F., Leivo, J., Vanhatupa, S., Kreutzer, J., Vaughan, T. J., . . . Miettinen, S. (2017). The effect of equiaxial stretching on the osteogenic differentiation and mechanical properties of human adipose stem cells. *Journal of the Mechanical Behavior of Biomedical Materials, 72*, 38-48.

Volz, A. C., Huber, B., & Kluger, P. J. (2016). Adipose-derived stem cell differentiation as a basic tool for vascularized adipose tissue engineering. *Differentiation; Research in Biological Diversity, 92*(1-2), 52-64.

Wang, L., Zhang, B., Bao, C., Habibovic, P., Hu, J., & Zhang, X. (2014). Ectopic osteoid and bone formation by three calcium-phosphate ceramics in rats, rabbits and dogs. *PloS One, 9*(9), e107044.

Wang, X., Cheng, F., Liu, J., Smatt, J. H., Gepperth, D., Lastusaari, M., . . . Hupa, L. (2016). Biocomposites of copper-containing mesoporous bioactive glass and nanofibrillated cellulose: Biocompatibility and angiogenic promotion in chronic wound healing application. *Acta Biomaterialia, 46*, 286-298.

Wang, Y. K., Yu, X., Cohen, D. M., Wozniak, M. A., Yang, M. T., Gao, L., . . . Chen, C. S. (2012). Bone morphogenetic protein-2-induced signaling and osteogenesis is regulated by cell shape, RhoA/ROCK, and cytoskeletal tension. *Stem Cells and Development, 21*(7), 1176-1186.

Wang, Z., Lin, M., Xie, Q., Sun, H., Huang, Y., Zhang, D., . . . Fan, X. (2016). Electrospun silk fibroin/poly(lactide-co-epsilon-caprolactone) nanofibrous scaffolds for bone regeneration. *International Journal of Nanomedicine, 11*, 1483-1500.

Waselau, M., Patrikoski, M., Mannerström, B., Raki, M., Bergström, K., von Rechenberg, B., & Miettinen, S. (2012a). In vivo effects of bioactive glass S53P4 or beta tricalcium phosphate on osteogenic differentiation of human adipose stem cells after incubation with BMP-2. *Journal of Stem Cell Research &Therapy, 2*(4)

Waselau, M., Patrikoski, M., Juntunen, M., Kujala, K., Kääriäinen, M., Kuokkanen, H., . . . Miettinen, S. (2012b). Effects of bioactive glass S53P4 or beta-tricalcium phosphate and bone morphogenetic protein-2 and bone morphogenetic protein-7 on osteogenic differentiation of human adipose stem cells. *Journal of Tissue Engineering, 3*(1)

Weir, N. A., Buchanan, F. J., Orr, J. F., & Dickson, G. R. (2004). Degradation of poly-L-lactide. part 1: In vitro and in vivo physiological temperature degradation. *Proc Inst Mech Eng H, 218*(5), 307-319.

Wen, J. H., Vincent, L. G., Fuhrmann, A., Choi, Y. S., Hribar, K. C., Taylor-Weiner, H., . . . Engler, A. J. (2014). Interplay of matrix stiffness and protein tethering in stem cell differentiation. *Nature Materials, 13*(10), 979-987.

Weng, L., Boda, S. K., Teusink, M. J., Shuler, F. D., Li, X., & Xie, J. (2017). Binary doping of strontium and copper enhancing osteogenesis and angiogenesis of bioactive glass nanofibers while suppressing osteoclast activity. *ACS Applied Materials & Interfaces, 9*(29), 24484-24496.

West, C. C., Hardy, W. R., Murray, I. R., James, A. W., Corselli, M., Pang, S., . . . Peault, B. (2016). Prospective purification of perivascular presumptive mesenchymal stem cells from human adipose tissue: Process optimization and cell population metrics across a large cohort of diverse demographics. *Stem Cell Research & Therapy, 7*, 47-016-0302-7.

Whyte, M. P. (2016). Hypophosphatasia - aetiology, nosology, pathogenesis, diagnosis and treatment. *Nature Reviews.Endocrinology, 12*(4), 233-246.

Williams, J. M., Adewunmi, A., Schek, R. M., Flanagan, C. L., Krebsbach, P. H., Feinberg, S. E., . . . Das, S. (2005). Bone tissue engineering using polycaprolactone scaffolds fabricated via selective laser sintering. *Biomaterials, 26*(23), 4817-4827.

Wongwitwichot, P., & Kaewsrichan, J. (2017). Osteogenic differentiation of mesenchymal stem cells is impaired by bone morphogenetic protein 7. *Advances in Medical Sciences, 62*(2), 266-272.

Wu, C., Zhou, Y., Xu, M., Han, P., Chen, L., Chang, J., & Xiao, Y. (2013). Copper-containing mesoporous bioactive glass scaffolds with multifunctional properties of angiogenesis capacity, osteostimulation and antibacterial activity. *Biomaterials, 34*(2), 422-433.

Xiao, W., Zaeem, M. A., Li, G., Bal, B. S., & Rahaman, M. N. (2017). Tough and strong porous bioactive glass-PLA composites for structural bone repair. *Journal of Materials Science, 52*(15), 9039-9054.

You, D., Jang, M. J., Kim, B. H., Song, G., Lee, C., Suh, N., . . . Kim, C. S. (2015). Comparative study of autologous stromal vascular fraction and adipose-derived stem cells for erectile function recovery in a rat model of cavernous nerve injury. *Stem Cells Translational Medicine, 4*(4), 351-358.

Young, A., & Mirarchi, A. (2015). Soft tissue swelling associated with the use of recombinant human bone morphogenetic protein-2 in long bone non-unions. *Journal of Orthopaedic Case Reports, 5*(3), 18-21.

Yuan, H., Fernandes, H., Habibovic, P., de Boer, J., Barradas, A. M., de Ruiter, A., . . . de Bruijn, J. D. (2010). Osteoinductive ceramics as a synthetic alternative to autologous bone grafting. *Proceedings of the National Academy of Sciences of the United States of America, 107*(31), 13614-13619.

Yuan, L., Sakamoto, N., Song, G., & Sato, M. (2013). High-level shear stress stimulates endothelial differentiation and VEGF secretion by human mesenchymal stem cells. *Cellular and Molecular Bioengineering, 6*(2), 220-229.

Zhang, J., Wu, H., He, F., Wu, T., Zhou, L., & Ye, J. (2019). Concentration-dependent osteogenic and angiogenic biological performances of calcium phosphate cement modified with copper ions. *Materials Science and Engineering: C, 99*, 1199-1212.

Zhang, W., Zhu, C., Wu, Y., Ye, D., Wang, S., Zou, D., . . . Jiang, X. (2014). VEGF and BMP-2 promote bone regeneration by facilitating bone marrow stem cell homing and differentiation. *European Cells & Materials, 27*, 1-11; discussion 11-2.

Zheng, Y., Huang, C., Liu, F., Lin, H., Yang, X., & Zhang, Z. (2017). Comparison of the neuronal differentiation abilities of bone marrowderived and adipose tissuederived mesenchymal stem cells. *Molecular Medicine Reports, 16*(4), 3877-3886.

Zonari, A., Novikoff, S., Electo, N. R., Breyner, N. M., Gomes, D. A., Martins, A., . . . Goes, A. M. (2012). Endothelial differentiation of human stem cells seeded onto electrospun polyhydroxybutyrate/polyhydroxybutyrate-co-hydroxyvalerate fiber mesh. *PloS One, 7*(4), e35422.

Zong, X., Wang, Z., Hsiao, B. S., Chu, B., Zhou, J. J., Jamiolkowski, D. D., . . . Dormier, E. (1999). Structure and morphology changes in absorbable poly(glycolide) and poly(glycolide-co-lactide) during in vitro degradation. *Macromolecules, 32*(24), 8107-8114.

Zuk, P., Chou, Y. F., Mussano, F., Benhaim, P., & Wu, B. M. (2011). Adipose-derived stem cells and BMP2: Part 2. BMP2 may not influence the osteogenic fate of human adipose-derived stem cells. *Connective Tissue Research, 52*(2), 119-132.

Zuk, P. A., Zhu, M., Mizuno, H., Huang, J., Futrell, J. W., Katz, A. J., . . . Hedrick, M. H. (2001). Multilineage cells from human adipose tissue: Implications for cell-based therapies. *Tissue Engineering, 7*(2), 211-228.

PUBLICATIONS

PUBLICATION
I

Osteogenic medium is superior to growth factors in differentiation of human adipose stem cells towards bone forming cells in 3D culture

Tirkkonen L., Haimi S., Huttunen S., Wolff J., Pirhonen E., Sándor G.K., Miettinen S.

OSTEOGENIC MEDIUM IS SUPERIOR TO GROWTH FACTORS IN DIFFERENTIATION OF HUMAN ADIPOSE STEM CELLS TOWARDS BONE-FORMING CELLS IN 3D CULTURE

L. Tirkkonen[1,2,3], S. Haimi[1,2,3,4,*], S. Huttunen[1,2], J. Wolff[1,2,5], E. Pirhonen[6], G.K. Sándor[1,2,3,7] and S. Miettinen[1,2,3]

[1]Adult Stem Cells, Institute of Biomedical Technology, University of Tampere, FI-33014 Tampere, Finland
[2]BioMediTech, FI-33520 Tampere, Finland
[3]Science Centre, Tampere University Hospital, FI-33521 Tampere, Finland
[4]Department of Biomaterials Science and Technology, University of Twente, 7500 AE Enschede, The Netherlands
[5]Oral and Maxillofacial Unit, Department of Otorhinolaryngology, Tampere University Hospital,
FI-33520 Tampere, Finland.
[6]Onbone Oy, FI-00521 Helsinki, Finland
[7]Department of Oral and Maxillofacial Surgery, Institute of Dentistry, University of Oulu, FI-90014 Oulu, Finland

Abstract

Human adipose stem cells (hASCs) have been recently used to treat bone defects in clinical practice. Yet there is a need for more optimal scaffolds and cost-effective approaches to induce osteogenic differentiation of hASCs. Therefore, we compared the efficiency of bone morphogenetic proteins (BMP-2 and BMP-7), vascular endothelial growth factor (VEGF), and osteogenic medium (OM) for the osteo-induction of hASCs in 3D culture. In addition, growth factors were tested in combination with OM. Commercially available bioactive glass scaffolds (BioRestore) and biphasic calcium phosphate granules (BoneCeramic) were evaluated as prospective carriers for hASCs. Both biomaterials supported hASC-viability, but BioRestore resulted in higher cell number than BoneCeramic, whereas BoneCeramic supported more significant collagen production. The most efficient osteo-induction was achieved with plain OM, promoting higher alkaline phosphatase activity and collagen production than growth factors. In fact, treatment with BMP-2 or VEGF did not increase osteogenic differentiation or cell number significantly more than maintenance medium with either biomaterial. Moreover, BMP-7 treatment consistently inhibited proliferation and osteogenic differentiation of hASCs. Interestingly, there was no benefit from growth factors added to OM. This is the first study to demonstrate that OM enhances hASC-differentiation towards bone-forming cells significantly more than growth factors in 3D culture.

Keywords: Adipose stem cells; mesenchymal stem cells; bone tissue engineering; bioactive glass; biphasic calcium phosphate; growth factors; osteogenic differentiation; *in vitro* culture; 3D scaffolds.

*Address for correspondence:
Suvi Haimi
Department of Biomaterials Science and Technology
University of Twente
P.O. Box 217, 7500 AE Enschede, The Netherlands
              Telephone Number: + 358 40 190 1771
              E-mail: suvi.haimi@uta.fi

Introduction

Tissue engineered bone has emerged as a potential alternative to meet the increasing need for bone replacements in clinical medicine and to overcome the limitations of autologous grafts as well as the risks related to allogeneic bone grafts (Betz, 2002). Specifically, bone regeneration *via* autologous stem cell transplantation is a promising approach to treat large bone defects. For example, patient's own multipotent mesenchymal stem cells (MSCs) can be isolated from adipose tissue, expanded *ex vivo*, and transplanted to the defect site using biomaterial scaffold as a carrier (Mesimaki *et al.*, 2009; Thesleff *et al.*, 2011). Among adult stem cells, human adipose stem cells (hASCs) are readily available multipotent cells having the potential to differentiate into lineages of mesenchymal tissues, including bone, cartilage, fat, tendon, muscle, and marrow stroma (Zuk *et al.*, 2001; Zuk *et al.*, 2002; Park *et al.*, 2010; Choi *et al.*, 2012). The osteogenic capacity of ASCs has been demonstrated in both *in vitro* (Zuk *et al.*, 2002; De Girolamo *et al.*, 2007) and *in vivo* studies (Cowan *et al.*, 2004; Hicok *et al.*, 2004; Hattori *et al.*, 2006; Di Bella *et al.*, 2008; Behr *et al.*, 2011). In addition, our group has reported several clinical cases, where autologous hASCs combined with biomaterials have been used to repair cranio-maxillofacial defects (Mesimaki *et al.*, 2009; Thesleff *et al.*, 2011).

In order to enhance the bone formation capacity, a number of inducing factors have been tested in combination with biomaterials and cells. Based on the fact that bone formation is modulated by a number of osteogenic factors released from the bone and surrounding tissues during the repair process, recombinant bone morphogenetic protein (BMP)-2 and BMP-7 have been utilised in clinical applications in order to stimulate bone healing (Samartzis *et al.*, 2005; Garrison *et al.*, 2007; Clokie and Sandor, 2008). Similar to BMPs, vascular endothelial growth factor A (VEGF-A) has been used to promote angiogenesis and osteogenesis of MSCs *in vitro* (Behr *et al.*, 2011; D'Alimonte *et al.*, 2011) and *in vivo* (Roldan *et al.*, 2010; Behr *et al.*, 2011). However, critical views on the use of BMPs have been emerging lately due to their short half-lives, expensiveness and ineffectiveness (Garrison *et al.*, 2007; Garrison *et al.*, 2010; Zuk *et al.*,

Table 1. The compositions of different media used in the study.

	Medium	Supplements
	Maintenance medium (MM)	DMEM/F-12, 10 % FBS, 1 % L-glutamine, 1 % antibiotics
	Osteogenic medium (OM)	5 nM dexamethasone, 250 µM L-ascorbic acid 2-phosphate, 10 mM β-glycerophoshate (Sigma-Aldrich, MO, USA) in MM
Part I	MM + BMP-2	50 ng/mL bone morphogenetic protein-2 (Genscript, NJ, USA) in MM
	MM + BMP-7	100 ng/mL bone morphogenetic protein-7 (Sigma-Aldrich) in MM
	MM + VEGF	20 ng/mL vascular endothelial growth factor (R&D Systems Inc, MN, USA) in MM
Part II	OM + BMP-2	50 ng/mL BMP-2 (Genscript, NJ, USA) in OM
	OM + BMP-7	100 ng/mL BMP-7 (Sigma-Aldrich) in OM
	OM + VEGF	20 ng/mL VEGF (R&D Systems Inc, MN, USA) in OM

2011). The clinical use of growth factors has been hindered by the significantly large, and hence costly, doses needed in humans. Large doses of exogenous growth factors may cause unexpected physiological effects ranging from bone resorption (Giannoudis *et al.*, 2007) to heterotopic ossification (Wysocki and Cohen, 2007; Axelrad *et al.*, 2008). Hence, alternative methods for effective osteo-induction of MSCs are under investigation (Kim *et al.*, 2003; Kim *et al.*, 2005; McCullen *et al.*, 2010; Tirkkonen *et al.*, 2011).

For example, osteogenic medium (OM) supplemented with L-ascorbic acid 2-phosphate (AsA2-P), dexamethasone (Dex) and β-glycerophosphate (β-GP) has been commonly used for the osteogenic differentiation of MSCs *in vitro* (Zuk *et al.*, 2001; Ogawa *et al.*, 2004; Giusta *et al.*, 2010; Rada *et al.*, 2011). The *in vivo* studies have also shown the advantage of OM-induction in ASC-based bone regeneration; significantly greater bone healing was detected with the OM-induced ASCs compared to the non-induced ASCs (Dudas *et al.*, 2006; Yoon *et al.*, 2007; Di Bella *et al.*, 2008; Schubert *et al.*, 2011). However, the osteo-induction efficiency of OM has not been systematically compared to BMP-2, BMP-7 and VEGF with hASCs *in vivo* or *in vitro*. Although *in vivo* studies are required in the future to demonstrate the utility of OM over growth factors, obtaining sufficient *in vitro* data is of fundamental importance before it is reasonable to initiate *in vivo* studies.

In addition to effective osteo-induction, suitable biomaterial carriers for supporting the hASC proliferation and differentiation are required for successful bone regeneration. Bioactive glass and biphasic calcium phosphate, both biomaterials currently used in cranio-maxillofacial (Peltola *et al.*, 2006; Peltola *et al.*, 2008; Frenken *et al.*, 2010; Clozza *et al.*, 2012b) and orthopaedic surgery (Lindfors *et al.*, 2010; Garrido *et al.*, 2011), were compared as prospective carriers for hASCs in the current study. Synthetic bioceramics are among the most promising biomaterials for the use of bone tissue engineering largely due to their capacity to form bone-like apatite layers in contact with physiological fluids, a reaction which facilitates their strong bonding to bone (Hench, 1998; Kokubo *et al.*, 2003). Furthermore, bioactive glass and calcium phosphate biomaterials are capable of promoting

bone formation through the dissolution of Ca and P ions (Xynos *et al.*, 2000; E *et al.*, 2010). Essential characteristics for silicate bioactive glasses include high Na_2O and CaO content, high CaO/P_2O_5 ratio, and SiO_2 content less than 60 mol%. Biphasic calcium phosphates, in turn, consist of varying ratios of hydroxyapatite (HA) and beta-tricalcium phosphate (β-TCP). With slowly resorbing HA and more soluble β-TCP, the ratio 60/40 wt% of HA/β-TCP has been widely used as it offers controlled degradation and optimal osseous substitution (Frenken *et al.*, 2010; Ghanaati *et al.*, 2012).

While searching for an optimal approach to treat patients with adipose stem cells, the aim of the present study was to compare the efficiency of BMP-2, BMP-7, VEGF and OM for the osteogenic differentiation of hASCs in clinically relevant 3D environment. In addition, BMP-2, BMP-7 and VEGF were tested in combination with OM.

Materials and Methods

Biomaterial characterisation and preparation

Two commercially available biomaterials, Straumann® BoneCeramic granules (Straumann AG, Basel, Switzerland) and Inion BioRestore™ (Inion Oy, Tampere, Finland) bioactive glass scaffolds were compared as 3D carriers for hASCs in this study. The morphology and surface topography of both materials was examined using scanning electron microscopy (SEM; Philips XL-30; Philips, Eindhoven, The Netherlands). The biomaterial samples were air-dried and sputter coated with gold prior to analysis with SEM.

The fully synthetic, granular form Straumann® BoneCeramic composed of biphasic calcium phosphate with 60 % hydroxyapatite (HA; 100 % crystalline) and 40 % β-tricalcium phosphate (β-TCP) was used in this study. BoneCeramic has a porosity of 90 %, and a granule size between 0.5 and 1.0 mm with interconnected pores of 100-500 µm in diameter. For cell culturing, 0.25 g aliquots of sterile BoneCeramic granules were transferred onto 24-well plates (Nunc, Roskilde, Denmark) using an analytical balance that was placed inside a laminar hood. The granules were incubated in 1 mL of corresponding medium (Table 1) for 48 h prior to cell seeding.

The Inion BioRestore™ bioactive glass scaffolds used in this study had a nominal composition of 11.1-12.0 wt% Na_2O, 15.0-17.1 wt% K_2O, 2.8-3.3 wt% MgO, 12.7-15.2 wt% CaO, 2.7-3.8 wt% P_2O_5, 1.0-1.4 wt% B_2O_3, 0.0-0.6 wt% TiO_2 and 48.5-52 wt% SiO_2. The porous bioactive glass scaffolds were manufactured from fibres as described previously (Moimas *et al.*, 2006). Briefly, bioactive glass fibres of 75 μm diameter and 3 mm length were produced by melt spinning. The fibres were sintered under defined conditions to obtain desired structural and mechanical properties. Scaffolds with porosity of 70 % and dimensions of 7 x 7 x 3 mm were used in this study.

Before cell seeding, the bioactive glass scaffolds were sterilised with 70 % ethanol followed by several steps of washing with Dulbecco's phosphate-buffered saline (DPBS; Lonza Biowhittaker; Verviers, Belgium), and incubated in 1 mL of corresponding medium (Table 1) for 48 h.

Cell isolation, characterisation and culture
Adipose tissue samples were acquired from surgical procedures in the Department of Plastic Surgery, Tampere University Hospital with the patients' written consent. The study was conducted in accordance with the Ethics Committee of the Pirkanmaa Hospital District, Tampere, Finland (R03058). The adipose tissue samples were obtained from 11 donors (mean age 50 ± 14 years).

The adipose tissue was manually chopped into small fragments and digested with collagenase type I (1.5 mg/mL; Invitrogen/Life Technologies, Carlsbad, CA, USA) in a water bath at 37 °C for 60 min, and the hASCs were isolated by centrifugation. Following isolation, the hASCs were expanded in T75 cm² polystyrene flasks (Nunc) in maintenance medium (MM) consisting of Dulbecco's modified Eagle's medium: nutrient mixture F-12 (DMEM/F-12 1:1) (Invitrogen, Paisley, UK), 10 % foetal bovine serum (PAA Laboratories, Pasching, Austria), 1 % antibiotics (100 U/mL penicillin; 100 U/mL streptomycin; Lonza Biowhittaker, Basel, Switzerland) and 1 % L-glutamine (GlutaMAX I; Invitrogen). After expansion hASCs were cryo-preserved in gas phase nitrogen in freezing solution consisting of 10 % dimethyl sulphoxide (Hybri-Max; Sigma-Aldrich, St. Louis, MO, USA) in foetal bovine serum (PAA Laboratories, Pasching, Austria).

After primary cell culture (at passage 1-2) the hASCs were characterised by a fluorescent-activated cell sorter (FACSAria; BD Biosciences, Erembodegem, Belgium). Monoclonal antibodies against CD14-PE, CD19-PE, CD49d-PE, CD73-PE, CD90-APC, CD106-PE, (BD Biosciences); CD45-FITC (Miltenyi Biotech, Bergisch Gladbach, Germany); CD34-APC, HLA-ABC-PE, HLA-DR-PE (Immunotools, Friesoythe, Germany); and CD105-PE (R&D Systems, Minneapolis, MN, USA) were used. The analysis was performed on 10,000 cells per sample and unstained cell samples were used to compensate for the background autofluorescence levels.

The hASCs needed for the study were thawed and expanded in maintenance medium in T75 cm² polystyrene flasks (Nunc). At passage 2-4, the hASCs were seeded onto

BoneCeramic granules at a density of 9.7 x 10⁴ cells per well, and similarly to the BioRestore scaffolds at a density of 9.7 x 10⁴ cells per scaffold, using a small volume (50 μL) of MM. The cells were let to attach at +37 °C for 3 h before adding 1 mL of corresponding medium (Table 1). Fresh medium was changed 3 times per week. During each medium change the growth factors were freshly added to the medium from frozen aliquots avoiding multiple freeze-thaw cycles in order to keep the growth factors active. The experiments were repeated 3-6 times using one donor cell line per each repeat.

In the first part of this study, recombinant human BMP-2 (rhBMP-2; Genscript, Pisataway, NJ, USA), BMP-7 (rhBMP-7; Sigma-Aldrich), and VEGF-A (rhVEGF₁₆₅; R&D Systems) were added to MM and compared with osteogenic medium (OM). In the second part of the study, the growth factors were combined with OM. The compositions of the different media used in the study are described in Table 1. The concentrations of BMP-2 (Barr *et al.*, 2010), BMP-7 (Shen *et al.*, 2010) and VEGF (Behr *et al.*, 2011) used in this study were based on literature.

Cell viability
Cell attachment and viability were evaluated qualitatively using Live/dead-staining probes (Molecular Probes/Invitrogen, Eugene, OR, USA) at day 3, 7 and 14. The hASCs were incubated for 45 min at room temperature with a mixture of 0.5 μM calcein acetoxymethyl ester (Molecular Probes) and 0.25 μM ethidium homodimer-1 (Molecular Probes). Images of the viable cells (green fluorescence) and dead cells (red fluorescence) were obtained using an Olympus IX51 phase contrast microscope with fluorescence optics and Olympus DP30BW camera (Olympus, Tokyo, Japan).

Cell number
The cell number of the samples was studied at 3-, 7- and 14-day time points by determining the amount of total DNA by CyQUANT Cell Proliferation Assay Kit (CyQUANT; Molecular Probes) according to the manufacturer's protocol. CyQUANT GR dye expresses fluorescence when bound to cellular nucleic acids.

The cells were washed with DPBS and lysed with 500 μL of 0.1 % Triton-X 100 buffer (Sigma-Aldrich). The Triton cell lysates were frozen and stored at -70 °C until analysis. After thawing three parallel 20 μL samples of each cell lysate were pipetted on a 96-well plate (Nunc) and mixed with 180 μL of working solution containing CyQUANT GR dye. Fluorescence was measured at 480/520 nm with a microplate reader (Victor 1420 Multilabel Counter; Wallac, Turku, Finland).

Alkaline phosphatase activity
Alkaline phosphatase (ALP) activity was analysed at 3-, 7- and 14-day time points. ALP cleaves phosphate groups from *p*-nitrophenol phosphates at pH 10.4 liberating yellow-coloured *p*-nitrophenol and phosphate. The rate of *p*-nitrophenol formation is proportional to the catalytic concentration of ALP in the sample. The ALP activity was determined from the same Triton-X 100 cell lysates as the cell number.

Table 2. Surface marker expression of undifferentiated hASCs at passage 1-2. The results are displayed as mean percentage of the surface marker expression ($n = 11$).

Antigen	Surface protein	Mean	SD	Expression
CD14	serum lipopolysaccharide binding protein	1.8	1.1	negative
CD19	B lymphocyte-lineage differentiation antigen	0.8	0.7	negative
CD34	sialomucin-like adhesion molecule	17.4	8.3	moderate
CD45	leukocyte common antigen	1.4	1.1	negative
CD49d	integrin a2, VLA-4	41.7	20.0	moderate
CD73	ecto-50-nucleotidase	90.4	9.4	positive
CD90	Thy-1 (T cell surface glycoprotein)	99.3	0.6	positive
CD105	SH-2, endoglin	95.7	4.4	positive
CD106	VCAM-1 (vascular cell adhesion molecule)	1.1	1.1	negative
HLA-ABC	major histocompatibility class I antigens	42.0	24.6	moderate
HLA-DR	major histocompatibility class II antigens	0.9	0.8	negative

Three parallel 20 µL samples were pipetted on a MicroAmp™ Optical 96-well plate (Applied Biosystems, CA, USA). The reaction was started by pipetting 90 µL of working solution per well, containing 50 % of alkaline buffer solution (2-amino-2-methyl propanol; 1.5 M; pH 10.3; Sigma-Aldrich) and 50 % of stock substrate solution (*p*-nitrophenol phosphate; Sigma-Aldrich) and incubated for 15 min at 37 °C. The reaction was stopped by adding 50 µL of NaOH (1 M, Sigma-Aldrich) and the colour intensity was determined with a microplate reader (Victor 1420) at 405 nm.

Collagen assay

The amount of collagen was determined at 7- and 14-day time points by Sircol Soluble Collagen Assay (Biocolor, Carrickfergus, Northern Ireland). The basis of the assay was binding of Sirius red dye to [Gly-X-Y] peptide sequence of mammalian collagen types I-V. Production of collagenous matrix was measured, as it was not possible to analyse mineralisation due to the calcium containing 3D-scaffolds.

For the measurement, acid-soluble collagen was extracted from the cultures by 0.5 M acetic acid (Merck, Darmstadt, Germany) containing 0.1 mg/mL pepsin (Sigma-Aldrich) for 2 h at 4 °C. The collagen content was determined from 100 µL samples, with 1 mL of Sircol Dye reagent (Sirius Red in picric acid; Biocolor) added to each aliquot and incubated with gentle shaking for 30 min. The samples were centrifuged at 12,000 rpm for 10 min, and the collagen-dye pellet was washed once to remove unbound dye with 750 µL of ice-cold Acid-Salt Wash Reagent (acetic acid, sodium chloride and surfactants; Biocolor). After centrifugation, the supernatant was discarded and the collagen-bound dye was released by adding 250 µL of Alkali Reagent (0.5 M sodium hydroxide; Biocolor). The dye intensity was measured from two parallel 100 µL samples on a 96-well plate (Nunc) with a microplate reader (Victor 1420) at 540 nm.

Statistical analysis

Statistical analyses were performed with SPSS version 19 (IBM, Armonk, NY, USA). Data were reported as mean and standard deviation (SD). The effects of different culture conditions on cell number, ALP activity, and collagen content were compared using a one-way analysis of variance (ANOVA) with Tukey *post hoc* test. The results were considered significant when $p < 0.05$. The effect of culture duration was analysed using a Student's *t*-test for independent samples for collagen content (day 7 *versus* day 14), and one-way ANOVA for cell number and ALP activity for comparing 3-, 7- and 14-day time points. In the first part of this study growth factors were added to control medium and compared with OM, the experiments for cell number and ALP activity were repeated using 6 donor lines ($n = 6$), and the analysis of collagen content was repeated with 3 donor lines ($n = 3$). In the second part, where growth factors were tested in combination with OM, all experiments were repeated using 3 donor lines ($n = 3$).

Results

Scanning electron microscopy

The scanning electron microscopy (SEM) images (Fig. 1) illustrated the macro structure (Fig. 1a,b) and surface roughness (Fig. 1e,f) of the biomaterials. Based on SEM images a larger surface area may be expected for BioRestore that is composed of small sized fibres (Fig. 1, left side). Regarding surface topography, BoneCeramic exhibited more surface roughness than BioRestore (Fig. 1e,f). Overall, the SEM images confirmed the high porosity of both biomaterials. More detailed information on material characteristics of BioRestore scaffold has been provided previously (Haimi *et al.*, 2009a).

Flow cytometric surface marker expression analysis

The flow cytometric analysis (Table 2) demonstrated that the hASCs used in this study expressed the surface markers CD73, CD90, CD105, and lacked the expression of the CD14, CD19, HLA-DR, the haematopoietic marker CD45, and the vascular cell adhesion molecule CD106. The expression of CD34, CD49d and HLA-ABC, was moderate. Overall, the surface marker analysis confirmed the mesenchymal origin of the cells in agreement with literature (Dominici *et al.*, 2006; McIntosh *et al.*, 2006; Lindroos *et al.*, 2010).
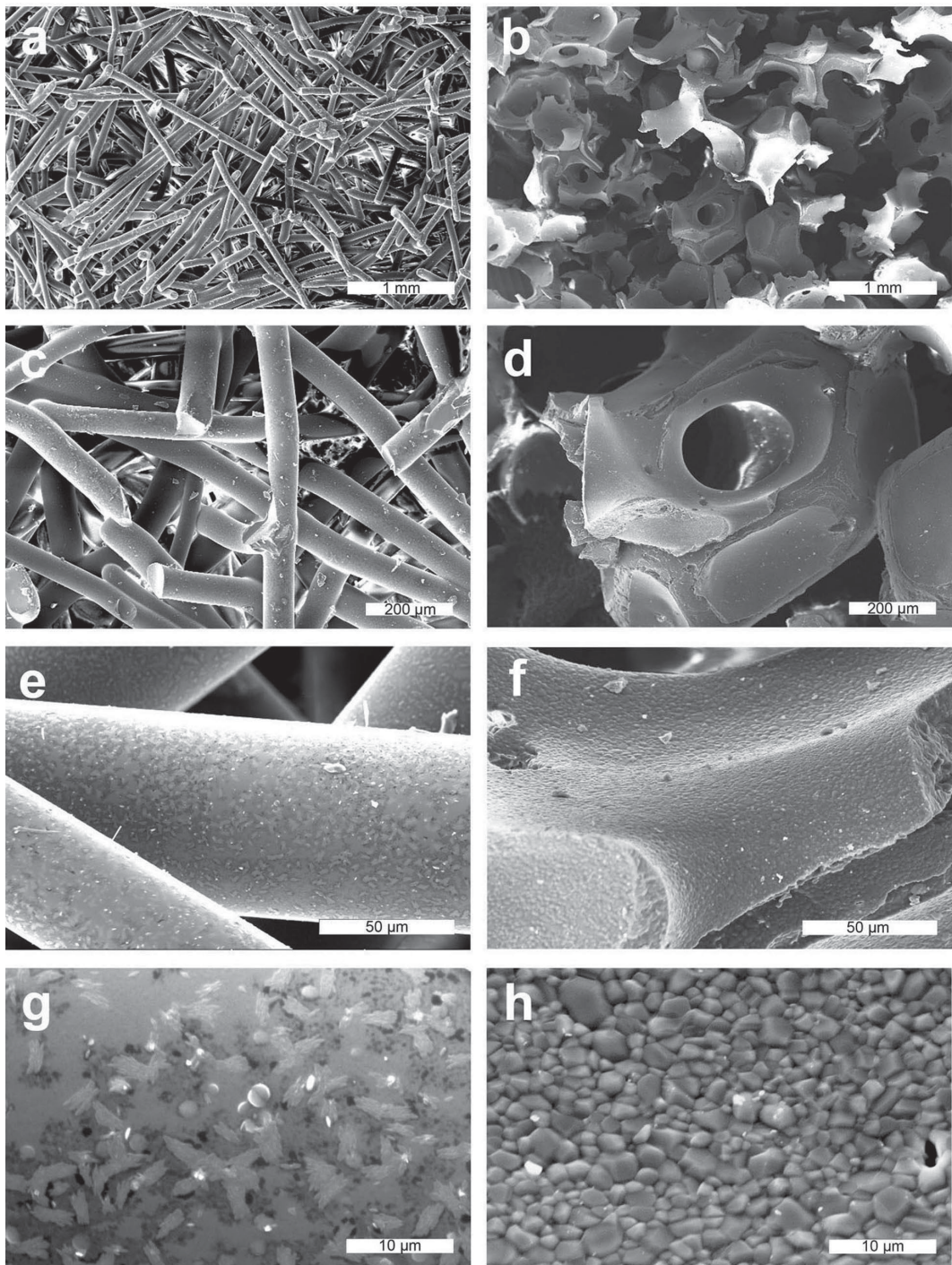
Fig. 1. Scanning electron micrographs of BioRestore (left; **a**, **c**, **e**, **g**) and BoneCeramic (right; **b**, **d**, **f**, **h**) at magnification of 20x (**a**, **b**), 80x (**c**, **d**), 500x (**e**, **f**), and 2000x (**g**, **h**). Scale bars in the lower right corner of the micrographs.
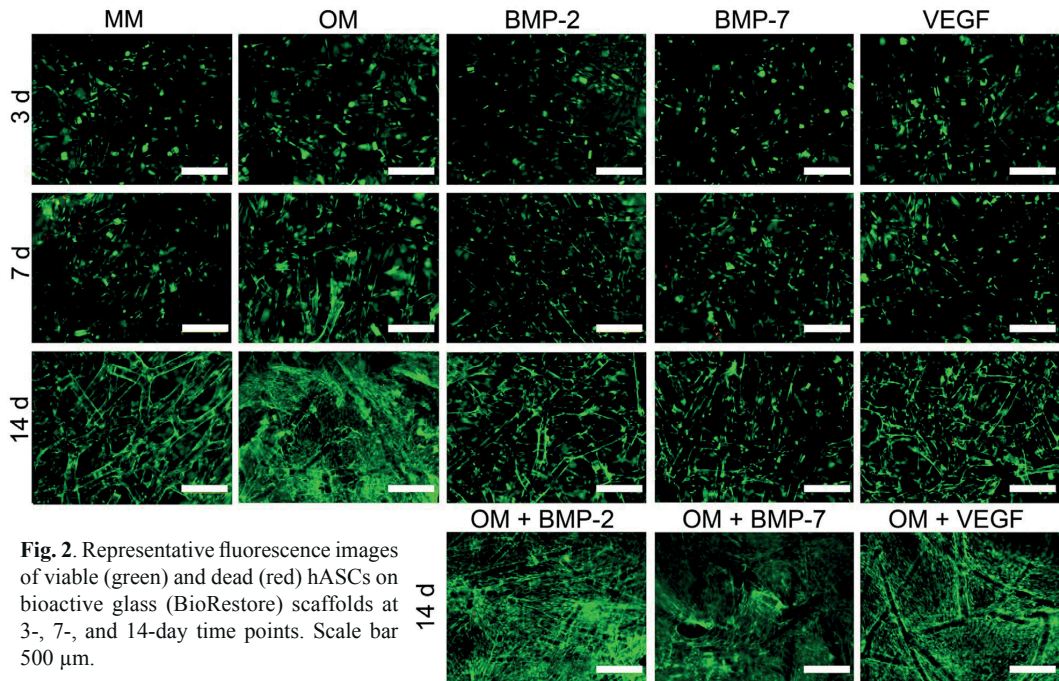
Fig. 2. Representative fluorescence images of viable (green) and dead (red) hASCs on bioactive glass (BioRestore) scaffolds at 3-, 7-, and 14-day time points. Scale bar 500 μm.
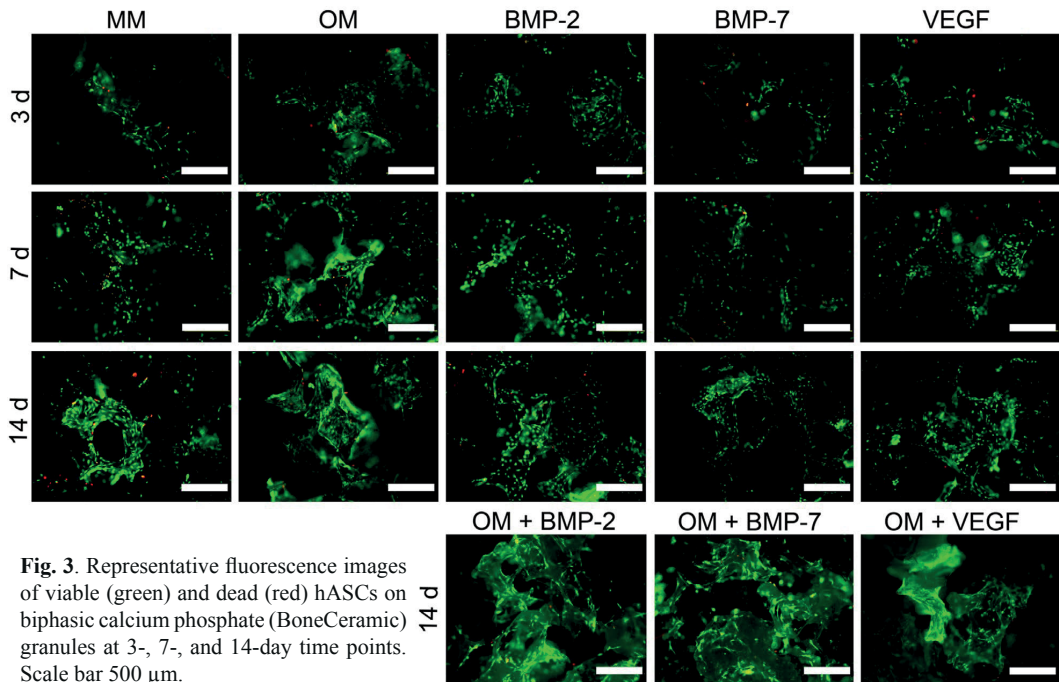

Fig. 3. Representative fluorescence images of viable (green) and dead (red) hASCs on biphasic calcium phosphate (BoneCeramic) granules at 3-, 7-, and 14-day time points. Scale bar 500 μm.

Comparison of BioRestore and BoneCeramic biomaterials

The hASCs seeded on both BioRestore (Fig. 2) and BoneCeramic (Fig. 3) were viable and proliferated steadily under control conditions during the whole 14-day culturing period as monitored by qualitative Live/dead Cell Viability (Fig. 2 and 3) and quantitative CyQuant Cell Proliferation (Fig. 4) assays. According to Live/dead assay, BioRestore supported cell proliferation more than BoneCeramic. This was confirmed by the quantitative analysis of cell number (Fig. 4a), which showed 1.4-fold higher cell number with BioRestore than BoneCeramic in MM ($p = 0.026$), and 1.3-fold in OM ($p = 0.002$) at day 14.
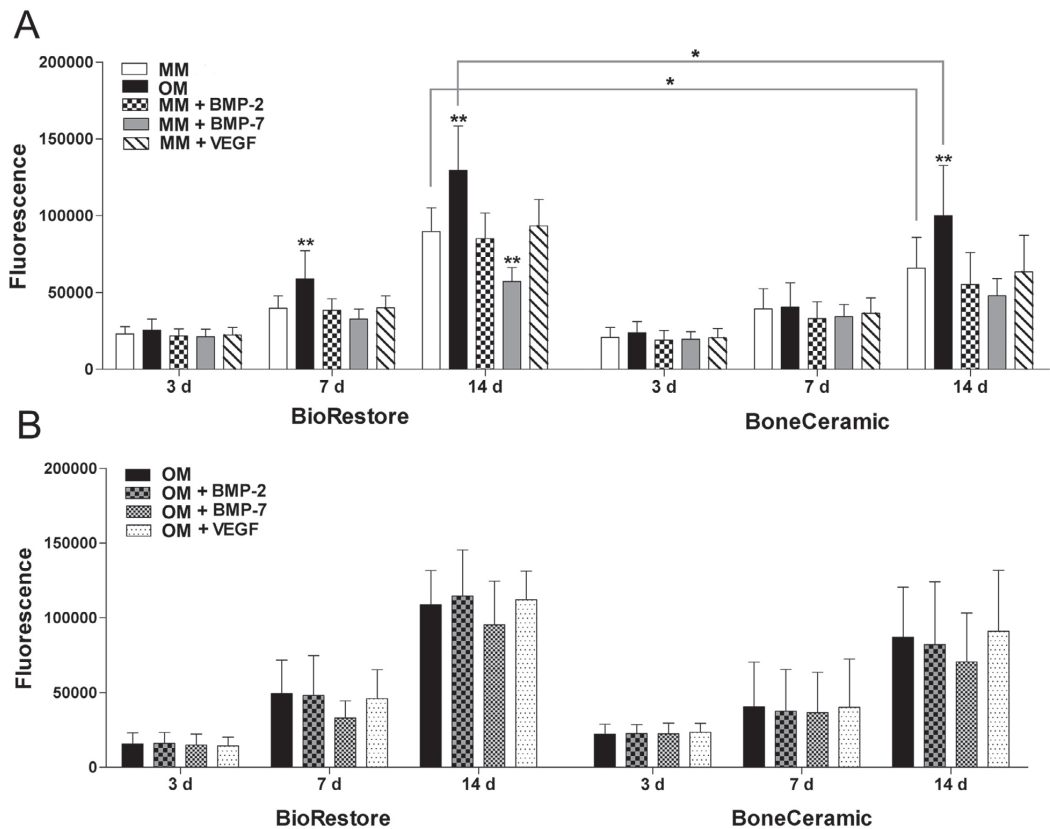
Fig. 4. Cell number at 3-, 7-, and 14-day time points on BioRestore or BoneCeramic. (**A**) Growth factors in MM*: Number of hASCs cultured with MM, OM or growth factors in MM. *$p < 0.05$ between the indicated groups. **$p < 0.05$ with respect to other groups within that time point. (**B**) Growth factors in OM: Number of hASCs cultured with OM or growth factors in OM. No significant differences in panel B. Results are expressed as mean fluorescence + SD.

The ALP activity of hASCs (Fig. 5) was supported equally by both biomaterials in MM, but the induction by OM was more significant and consistent in BoneCeramic. For example, with BoneCeramic the ALP activity was enhanced by OM 2-fold when compared to MM, 3-fold to BMP-2, 8-fold to BMP-7, and 2-fold to VEGF ($p < 0.05$ in all). In BioRestore, the ALP activity induced by OM was higher than with BMP-2 (1.7-fold) and BMP-7 (4.5-fold), but not when compared to MM.

Furthermore, BoneCeramic supported the collagen production of hASCs significantly more than BioRestore (Fig. 6a). Collagen production by hASCs grown on BoneCeramic in MM or MM + growth factors was significantly higher when compared to BioRestore both at day 7 and day 14. At day 14, the amount of collagen was 5-fold higher in BoneCeramic MM than in BioRestore MM ($p < 0.05$). In fact, BoneCeramic combined with MM produced comparable collagen levels to that made by osteo-induced hASCs grown on BioRestore. Induction by OM resulted in increased collagen production on both biomaterials at day 14 with the highest levels of collagen being produced by hASCs induced in OM on

BoneCeramic. However, the enhancement of collagen production was more intense in the case of BioRestore; OM resulted in 5 times more collagen than MM in BioRestore, but only a 1.9-fold induction in BoneCeramic – due to the high level of collagen present under control conditions. When compared to MM control, growth factor treatment did not increase collagen production on either biomaterial.

Comparison of OM induction to MM

Overall, OM resulted in higher cell numbers and collagen production than MM with both biomaterials. When comparing the effect of OM to MM in BioRestore, a significant stimulation was detected on proliferation of hASCs (Fig. 4a). OM increased the cell number 1.5-fold on day 7 and 14 when compared to MM ($p < 0.05$). Live/dead analysis confirmed the high growth rate of OM-cultured hASCs in BioRestore (Fig. 2). In addition, OM induced significantly higher collagen production (5-fold) than MM at day 14 in BioRestore (Fig. 6a). In turn, the ALP activity of hASCs seeded in BioRestore was not significantly higher in OM than in MM (Fig. 5a).
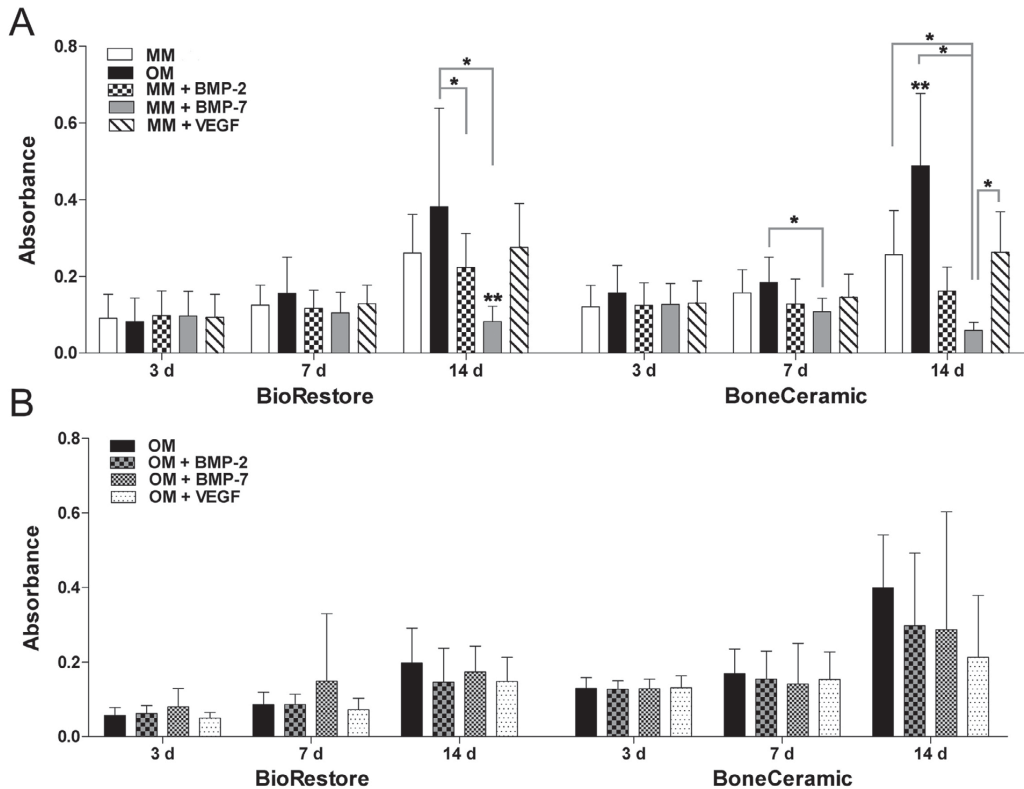
Fig. 5. ALP activity of hASCs at 3-, 7-, and 14-day time points on BioRestore or BoneCeramic. (**A**) Growth factors in MM: ALP activity of hASCs cultured with MM, OM or growth factors in MM. *$p < 0.05$ between the indicated groups. **$p < 0.05$ with respect to other groups within that time point. (**B**) Growth factors in OM*:* ALP activity of hASCs cultured with OM or growth factors in OM. No significant differences in panel B. Results are expressed as mean absorbance + SD.

In BoneCeramic, the cell number (Fig. 4a) was significantly higher in OM than in MM cultures (1.5-fold) on day 14. In contrast, Live/dead analysis showed slightly higher cell number in OM than MM on day 7, but no notable difference between OM and MM on day 14 in BoneCeramic (Fig. 3). The ALP activity (Fig. 5a) and collagen production (Fig. 6a) were induced 1.9-fold more with OM than MM in BoneCeramic at day 14 ($p < 0.05$).

Comparison of growth factor induction to MM
In general, all the growth factors tested in the present study supported the viability (Fig. 2 and 3) and proliferation of hASCs (Fig. 4a). BMP-2 and VEGF did not increase but rather supported similar levels of proliferation as MM (Fig. 4a). The result was similar with ALP activity (Fig. 5a) and collagen production (Fig. 6a), where BMP-2 and VEGF resulted in comparable levels as MM in both biomaterials. In contrast to BMP-2 and VEGF, BMP-7 resulted in two times lower cell number than MM in BioRestore ($p < 0.001$). Consistently, ALP activity (Fig. 5a) was three times lower in BMP-7 group than in MM in BioRestore ($p = 0.002$). Equally low amounts of collagen

(Fig. 6a) were produced by all growth factors and MM in hASCs cultured in BioRestore.

The effects of growth factors in BoneCeramic were mostly similar to BioRestore, i.e., no enhancement in comparison to MM. However, in BoneCeramic BMP-7 did not significantly inhibit proliferation. In turn, the adverse effect of BMP-7 was significant in ALP activity; four times lower values than with MM were detected on day 14 (Fig. 5a). Some differences in collagen production (Fig. 6a) were detected between the growth factor groups in BoneCeramic. On day 7, BMP-2 exhibited significantly higher collagen amount than MM and OM ($p < 0.05$), although there was no difference from MM on day 14. Furthermore, VEGF exhibited significantly higher ALP activity and collagen content than BMP-7 (4.4-fold and 1.8-fold, respectively), but not higher in comparison to MM.

Comparison of OM induction to growth factors
Overall, OM showed superior capacity to induce osteogenic differentiation and proliferation of hASCs than the growth factors tested in the study. In BioRestore,
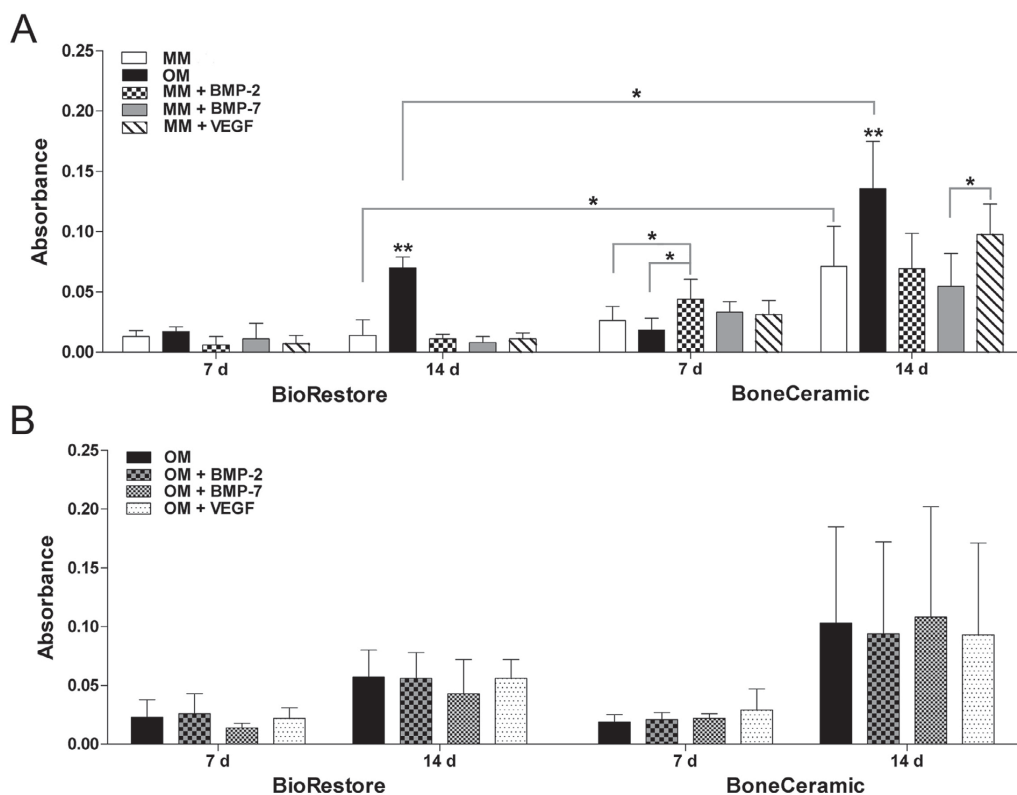
Fig. 6. Collagen production of hASCs at 7- and 14-day time points on BioRestore or BoneCeramic. (**A**) Growth factors in MM: Collagen production of hASCs cultured with MM, OM or growth factors in MM. *$p < 0.05$ between the indicated groups. **$p < 0.05$ with respect to other groups within that time point. (**B**) Growth factors in OM: Collagen production of hASCs cultured with OM or growth factors in OM. No significant differences in panel B. Results are expressed as mean absorbance + SD.

Live/dead analysis (Fig. 2) showed increased viability and cell number by the OM group when compared with growth factor groups at day 7 and 14. This was confirmed by the quantitative analysis of cell numbers (Fig. 4a); OM induced significantly higher cell numbers than growth factors (1.4- to 2.2-fold) in BioRestore. In a similar way, the collagen production was enhanced 6- to 9-fold by OM when compared to growth factors in BioRestore (Fig. 6a). OM also induced significantly higher ALP activity than BMP-2 (1.7-fold) and BMP-7 (4.6-fold) in BioRestore (Fig. 5a). VEGF resulted in comparable level of ALP activity to MM and OM in BioRestore. The OM-induced ALP activity was donor dependent, and hence was not as consistent as the OM-induced collagen production.

In BoneCeramic, the growth factors supported comparable levels of viability to OM and MM (Fig. 3). However, according to the quantitative analysis of cell number (Fig. 4a), OM did result in significantly higher numbers of cells on day 14 than the growth factor groups ($p < 0.05$). The effect of OM on ALP activity (Fig. 5a) and collagen production (Fig. 6a) in BoneCeramic was significantly higher than with any of the growth factors.

In ALP activity, the effects of OM were 2- to 8-fold, and in collagen production 1.4- to 2.5-fold in comparison to growth factors. In particular, the negative effect of BMP-7 was evident in ALP activity of hASCs seeded on BoneCeramic (Fig. 5a), as the ALP activity of BMP-7 group decreased with time ($p = 0.006$, day 7 *versus* day 14).

Combination of growth factors with OM
As osteogenic differentiation was detected mostly with OM, in the second part of the study growth factors were added to OM to determine whether greater osteo-induction could be achieved by their combination. The viability (Fig. 2 and 3) and cell number (Fig. 4b) of OM + growth factors were comparable to that of plain OM, although slightly higher than with MM + growth factors. In BioRestore the inhibitory effect of BMP-7 on cell number could be detected even when combined with OM, but the difference was not significant to other groups.

Overall, combining growth factors with OM did not result in enhanced ALP activity or collagen production when compared to plain OM. However, in ALP activity,

the negative effect detected by BMP-7 (Fig. 5a) was rescued when combined with OM (Fig. 5b); in some donor cells OM + BMP-7 increased ALP activity on day 7 in BioRestore and on day 14 in BoneCeramic, although the difference to plain OM was not significant.

When comparing the effects of OM + growth factors between the two biomaterials, the results were comparable to those obtained with MM + growth factors; BioRestore stimulated higher cell number than BoneCeramic, whereas BoneCeramic induced higher ALP activity and collagen production.

Discussion

Every year, over 2 million bone graft operations are carried-out world-wide (Giannoudis *et al.*, 2005). Due to the limitations of the traditional bone-grafting, alternative approaches such as tissue engineering are emerging in order to meet the increasing need for bone substitutes (Betz, 2002). To date, much reliance has been put on the osteo-inductive effect of BMPs (Garrison *et al.*, 2007; Clokie and Sandor, 2008; Mesimaki *et al.*, 2009). However, the cost, safety and effectiveness of growth factors have been the subject of controversy lately (Alarmo *et al.*, 2009; Garrison *et al.*, 2010; Zuk *et al.*, 2011). Due to the several risks and disadvantages related to the use of growth factors, we studied OM as an alternative method to enhance osteogenic differentiation of hASCs. OM containing AsA2-P, Dex and β-GP is a cost-effective osteo-inducer of hASCs *in vitro* as well as *in vivo*. In several *in vivo* studies, the osteogenic commitment of ASCs has been enhanced by OM during the *in vitro* culture prior to implantation (Cui *et al.*, 2007; Di Bella *et al.*, 2008; Bohnenblust *et al.*, 2009; Schubert *et al.*, 2011). For clinical bone tissue engineering it is critical to reduce the total time required to regenerate functional bone tissue. The pre-implantation expansion of hASCs takes several days to weeks, and bone formation after implantation of the construct takes from several weeks to months. In this respect, induction by OM would be a highly cost-effective way to enhance both osteogenic differentiation and proliferation of hASCs during the *in vitro* culture preceding implantation of the construct. Although the feasibility of OM-induction has been illustrated in several *in vivo* studies, the effect of OM has not been systematically compared to BMP-2, BMP-7 and VEGF *in vitro*.

Consequently, the current study demonstrated significantly greater osteogenic differentiation of hASCs by OM over BMP-2, BMP-7 and VEGF treatment in 3D culture, when the growth factors were added to MM. In fact, MM + BMP-2 or MM + VEGF treatment did not enhance the osteogenic differentiation of hASC more than MM alone with either biomaterial. In addition, it was discovered that BMP-7 significantly decreases proliferation and ALP activity of hASCs, an adverse effect that was detected consistently with both biomaterials. As osteogenic differentiation was detected solely with OM, in the second part of the study we tested whether OM could sensitise hASCs to growth factors in order to yield greater osteo-induction. However, the combination of BMP-2, BMP-7 or

VEGF with OM resulted in similar level of osteo-induction to OM alone, suggesting that OM induction is sufficient, and that differentiating hASCs may not respond to growth factor stimulation. Interestingly, the inhibitory effect of BMP-7 was rescued when BMP-7 was combined with OM. Hence, OM showed superiority over BMP-2, BMP-7 and VEGF added to MM, and these growth factors added to OM hold no advantage over plain OM induction *in vitro*.

Some studies have suggested that exogenously added BMP-2 (Knippenberg *et al.*, 2006; Song *et al.*, 2011), BMP-7 (Al-Salleeh *et al.*, 2008) and VEGF (Behr *et al.*, 2011) could have an osteo-inductive effect on ASCs, but in the current study these growth factors did not enhance osteogenic differentiation of hASC more than MM with either biomaterial. Out of these three growth factors, BMP-2 is the most studied with ASCs (Knippenberg *et al.*, 2006; E *et al.*, 2010; Song *et al.*, 2011; Zuk *et al.*, 2011; Mehrkens *et al.*, 2012; Overman *et al.*, 2012). Although BMP-2 concentrations from 50 to 100 ng/mL have successfully induced osteogenic differentiation of ASCs in some studies (Song *et al.*, 2011; Knippenberg *et al.*, 2006), Zuk and co-workers found no effect with doses in the range of 10-100 ng/mL (Zuk *et al.*, 2011). Similar to the findings of the present study and those reported by Zuk and co-workers, a recent study showed no effect by BMP-2 with 50 ng/mL (Mehrkens *et al.*, 2012). However, Mehrkens and co-workers suggested that a 10 times higher concentration, 500 ng/mL, is able to stimulate osteogenic differentiation of hASCs *in vitro* (Mehrkens *et al.*, 2012). In turn, this is in contrast to two studies, where a short, only 15 min treatment with 10 ng/mL BMP-2 was able to support osteo-induction of ASCs for 14-21 days (Knippenberg *et al.*, 2006; Overman *et al.*, 2012). Hence, there is no consensus on the effect of BMP-2 on osteo-induction of ASCs, and further systematic *in vitro* and *in vivo* studies are required.

Several factors may explain the great variation in the outcomes of BMP-2 studies, including use of animal-derived ASCs (Knippenberg *et al.*, 2006; E *et al.*, 2010), differential effects of 3D biomaterials (E *et al.*, 2010; Overman *et al.*, 2012) to 2D culture, and the use of various cell densities and culture media. Nevertheless, various explanations have been suggested for the failure of BMP induction in ASCs and bone marrow stromal cells (BMSCs), including up-regulation of BMP antagonists such as noggin and gremlin (Pereira *et al.*, 2000; Diefenderfer *et al.*, 2003; Sutherland *et al.*, 2004; Zuk *et al.*, 2011). On the other hand, the problem may originate from an insufficient activation of downstream signalling related to phosphorylation and nuclear translocation of certain Smads, the intracellular target proteins of *e.g.* BMP-2 signalling, as proposed by Zuk and co-workers (Zuk *et al.*, 2011). It is obvious that several aspects of cell signalling including timing, dosage, and complex interplay between different effectors and inhibitors need further elucidation to master the effect of growth factors.

The expanding literature on *in vivo* experiments conducted with ASCs suggests two critical requirements for successful bone formation; firstly, the osteogenic commitment of ASCs, and secondly, the presence of a mineral component in a scaffold (Scherberich *et al.*, 2010). The biomaterials used in the current study were

chosen because they represent prospective candidates for hASC-based bone tissue engineering approaches. As such, osteoconductivity and ability to heal bony defects has been reported in clinical and *in vivo* studies for both BioRestore (Moimas *et al.*, 2006; Clozza *et al.*, 2012a; Clozza *et al.*, 2012b) and BoneCeramic (Jensen *et al.*, 2007; Jensen *et al.*, 2009; Frenken *et al.*, 2010; Rokn *et al.*, 2011). Although capable of orthotopic bone formation, BoneCeramic failed to form ectopic bone together with BMSCs in subcutaneous rodent models (Zimmermann *et al.*, 2011; Mrozik *et al.*, 2012) indicating a need for enhanced osteo-induction. Recently, a similar biomaterial to BoneCeramic, except in a porous block format, was shown to increase bone formation in segmental femoral defects significantly more when seeded with hASCs than without cells (Choi *et al.*, 2011). In a clinical study of 13 patients, BioRestore alone was able to induce formation of woven bone in tooth extraction sockets, although no mature lamellar bone was detected within a 6 months healing period (Clozza *et al.*, 2012b). However, the bone formation capacity of BioRestore could be enhanced significantly by hASC transplantation in the future. Promising *in vitro* results have been reported previously for culturing hASCs in BioRestore scaffolds under control conditions (Haimi *et al.*, 2009b). Previous *in vitro* studies with BoneCeramic have been conducted with fibroblasts (Kauschke *et al.*, 2006), periodontal ligament fibroblasts (Mrozik *et al.*, 2012) and BMSCs (Mrozik *et al.*, 2012), but this is the first study to report hASC response on BoneCeramic and BioRestore when combined with osteo-induction by growth factors or OM.

The aim of the current study was to compare the efficiency of OM and growth factors for the osteo-induction of hASCs using two clinically prospective biomaterial carriers. Importantly, our findings indicate that the 3D biomaterial plays a notable role in hASC behaviour. The most significant difference between the 3D hASC-carriers, BioRestore and BoneCeramic, was detected in their ability to stimulate collagen production by hASCs. BoneCeramic induced a significantly larger amount of collagenous matrix than BioRestore under control conditions, and the effect was further enhanced with OM. Although different types of collagens are present in several tissues, the onset of osteoblastic differentiation is strongly related to the formation of organic matrix, mainly consisting of collagen type I, which will be subsequently mineralised – a process that is in turn facilitated by the accumulation of phosphate as a function of ALP enzyme. The differential behaviour of hASCs may be dependent on differences between the chemistry, topography, or 3D structure of the biomaterials.

The other major difference between the biomaterials was detected in their capacity to support cell proliferation, as BioRestore resulted in a significantly higher hASC number than BoneCeramic, an effect likely related to the 3D structure of the biomaterials. The fibre structure of BioRestore provides large surface area and allows the cells to spread more easily throughout the scaffold, whereas the granular format in BoneCeramic provides less contact area between the granules, hindering the spreading of the cells. This hypothesis was further supported by the viability assay, as some BoneCeramic granules were fully populated by hASCs whereas other granules in the same well had no

or very few cells. Based on these results, a larger initial cell seeding concentration would be recommended for BoneCeramic when considering clinical approaches to guarantee sufficient and evenly distributed cell population over the biomaterial. Although the comparison of these two biomaterials is challenging, due to the major differences in their 3D structures, based on our results both carriers represent viable alternatives for hASC-based bone tissue engineering as such, although combined stimulation with OM is suggested for efficient osteo-induction.

Based on the valuable *in vitro* findings of the present study, a corresponding *in vivo* study to demonstrate the utility of OM over growth factors has been planned. In order to reduce the number of animal experiments to be performed, it was critical to evaluate the hASCs response to growth factors and OM *in vitro*. For example, based on our results, there is no point in testing growth factors with OM, because there was no extra benefit from OM + growth factors in comparison to OM alone. Therefore, it is not necessary to test all the groups used in the current study *in vivo*. However, in the future *in vivo* study, effectiveness of OM over growth factors in MM should be demonstrated.

Conclusions

To conclude, this is the first study to demonstrate that OM enhances hASC differentiation towards bone-forming cells in 3D culture significantly more than the traditionally used growth factors BMP-2, BMP-7 and VEGF. Both biomaterials tested in this study, BioRestore and BoneCeramic, supported the hASC viability and proliferation during 14 days of culture. The most significant osteogenic differentiation of hASCs was achieved by BoneCeramic combined with OM. In contrast, combining growth factors with either biomaterial did not increase osteogenic differentiation or proliferation when compared to MM. Moreover, BMP-7 consistently inhibited proliferation and osteogenic differentiation of hASCs in 3D culture. Combining OM with BMP-7 eliminated the adverse effect of BMP-7. Otherwise, there was no significant benefit from adding growth factors to OM. Our results indicate that instead of BMP-2, BMP-7 or VEGF, OM should be used to obtain successful osteogenic commitment of hASCs *in vitro*.

Acknowledgements

References

Al-Salleeh F, Beatty MW, Reinhardt RA, Petro TM, Crouch L (2008) Human osteogenic protein-1 induces osteogenic differentiation of adipose-derived stem cells harvested from mice. Arch Oral Biol **53**: 928-936.

Alarmo EL, Parssinen J, Ketolainen JM, Savinainen K, Karhu R, Kallioniemi A (2009) BMP7 influences proliferation, migration, and invasion of breast cancer cells. Cancer Lett **275**: 35-43.

Axelrad TW, Steen B, Lowenberg DW, Creevy WR, Einhorn TA (2008) Heterotopic ossification after the use of commercially available recombinant human bone morphogenetic proteins in four patients. J Bone Joint Surg Br **90**: 1617-1622.

Barr T, McNamara AJ, Sandor GK, Clokie CM, Peel SA (2010) Comparison of the osteoinductivity of bioimplants containing recombinant human bone morphogenetic proteins 2 (Infuse) and 7 (OP-1). Oral Surg Oral Med Oral Pathol Oral Radiol Endod **109**: 531-540.

Behr B, Tang C, Germann G, Longaker MT, Quarto N (2011) Locally applied vascular endothelial growth factor a increases the osteogenic healing capacity of human adipose-derived stem cells by promoting osteogenic and endothelial differentiation. Stem Cells **29**: 286-296.

Betz RR (2002) Limitations of autograft and allograft: new synthetic solutions. Orthopedics **25**: 561-570.

Bohnenblust ME, Steigelman MB, Wang Q, Walker JA, Wang HT (2009) An experimental design to study adipocyte stem cells for reconstruction of calvarial defects. J Craniofac Surg **20**: 340-346.

Choi HJ, Kim JM, Kwon E, Che JH, Lee JI, Cho SR, Kang SK, Ra JC, Kang BC (2011) Establishment of efficacy and safety assessment of human adipose tissue-derived mesenchymal stem cells (hATMSCs) in a nude rat femoral segmental defect model. J Korean Med Sci **26**: 482-491.

Choi YS, Vincent LG, Lee AR, Dobke MK, Engler AJ (2012) Mechanical derivation of functional myotubes from adipose-derived stem cells. Biomaterials **33**: 2482-2491.

Clokie CM, Sandor GK (2008) Reconstruction of 10 major mandibular defects using bioimplants containing BMP-7. J Can Dent Assoc **74**: 67-72.

Clozza E, Biasotto M, Cavalli F, Moimas L, Di Lenarda R (2012a) Three-dimensional evaluation of bone changes following ridge preservation procedures. Int J Oral Maxillofac Implants **27**: 770-775.

Clozza E, Pea M, Cavalli F, Moimas L, Di Lenarda R, Biasotto M (2012b) Healing of fresh extraction sockets filled with bioactive glass particles: histological findings in humans. Clin Implant Dent Relat Res, in press.

Cowan CM, Shi YY, Aalami OO, Chou YF, Mari C, Thomas R, Quarto N, Contag CH, Wu B, Longaker MT (2004) Adipose-derived adult stromal cells heal critical-size mouse calvarial defects. Nat Biotechnol **22**: 560-567.

Cui L, Liu B, Liu G, Zhang W, Cen L, Sun J, Yin S, Liu W, Cao Y (2007) Repair of cranial bone defects with adipose derived stem cells and coral scaffold in a canine model. Biomaterials **28**: 5477-5486.

D'Alimonte I, Nargi E, Mastrangelo F, Falco G, Lanuti P, Marchisio M, Miscia S, Robuffo I, Capogreco M, Buccella S, Caputi S, Caciagli F, Tete S, Ciccarelli R (2011) Vascular endothelial growth factor enhances *in vitro* proliferation and osteogenic differentiation of human dental pulp stem cells. J Biol Regul Homeost Agents **25**: 57-69.

De Girolamo L, Sartori MF, Albisetti W, Brini AT (2007) Osteogenic differentiation of human adipose-derived stem cells: comparison of two different inductive media. J Tissue Eng Regen Med **1**: 154-157.

Di Bella C, Farlie P, Penington AJ (2008) Bone regeneration in a rabbit critical-sized skull defect using autologous adipose-derived cells. Tissue Eng Part A **14**: 483-490.

Diefenderfer DL, Osyczka AM, Garino JP, Leboy PS (2003) Regulation of BMP-induced transcription in cultured human bone marrow stromal cells. J Bone Joint Surg Am **85**-A Suppl 3: 19-28.

Dominici M, Le Blanc K, Mueller I, Slaper-Cortenbach I, Marini F, Krause D, Deans R, Keating A, Prockop D, Horwitz E (2006) Minimal criteria for defining multipotent mesenchymal stromal cells. The International Society for Cellular Therapy position statement. Cytotherapy **8**: 315-317.

Dudas JR, Marra KG, Cooper GM, Penascino VM, Mooney MP, Jiang S, Rubin JP, Losee JE (2006) The osteogenic potential of adipose-derived stem cells for the repair of rabbit calvarial defects. Ann Plast Surg **56**: 543-548.

E LL, Xu LL, Wu X, Wang DS, Lv Y, Wang JZ, Liu HC (2010) The interactions between rat-adipose-derived stromal cells, recombinant human bone morphogenetic protein-2, and beta-tricalcium phosphate play an important role in bone tissue engineering. Tissue Eng Part A **16**: 2927-2940.

Frenken JW, Bouwman WF, Bravenboer N, Zijderveld SA, Schulten EA, ten Bruggenkate CM (2010) The use of Straumann Bone Ceramic in a maxillary sinus floor elevation procedure: a clinical, radiological, histological and histomorphometric evaluation with a 6-month healing period. Clin Oral Implants Res **21**: 201-208.

Garrido CA, Lobo SE, Turibio FM, Legeros RZ (2011) Biphasic calcium phosphate bioceramics for orthopaedic reconstructions: clinical outcomes. Int J Biomater **2011**: 129727.

Garrison KR, Donell S, Ryder J, Shemilt I, Mugford M, Harvey I, Song F (2007) Clinical effectiveness and cost-effectiveness of bone morphogenetic proteins in the non-healing of fractures and spinal fusion: a systematic review. Health Technol Assess **11**: 1-150, iii-iv.

Garrison KR, Shemilt I, Donell S, Ryder JJ, Mugford M, Harvey I, Song F, Alt V (2010) Bone morphogenetic protein (BMP) for fracture healing in adults. Cochrane Database Syst Rev **6**: CD006950.

Ghanaati S, Barbeck M, Detsch R, Deisinger U, Hilbig U, Rausch V, Sader R, Unger RE, Ziegler G, Kirkpatrick CJ (2012) The chemical composition of synthetic bone substitutes influences tissue reactions *in vivo*: histological and histomorphometrical analysis of the cellular inflammatory response to hydroxyapatite, beta-tricalcium phosphate and biphasic calcium phosphate ceramics. Biomed Mater **7**: 015005.

Giannoudis PV, Dinopoulos H, Tsiridis E (2005) Bone substitutes: an update. Injury **36 Suppl 3**: S20-27.

Giannoudis PV, Kanakaris NK, Einhorn TA (2007) Interaction of bone morphogenetic proteins with cells of the osteoclast lineage: review of the existing evidence. Osteoporos Int **18**: 1565-1581.

Giusta MS, Andrade H, Santos AV, Castanheira P, Lamana L, Pimenta AM, Goes AM (2010) Proteomic analysis of human mesenchymal stromal cells derived from adipose tissue undergoing osteoblast differentiation. Cytotherapy **12**: 478-490.

Haimi S, Gorianc G, Moimas L, Lindroos B, Huhtala H, Raty S, Kuokkanen H, Sandor GK, Schmid C, Miettinen S, Suuronen R (2009a) Characterization of zinc-releasing three-dimensional bioactive glass scaffolds and their effect on human adipose stem cell proliferation and osteogenic differentiation. Acta Biomater **5**: 3122-3131.

Haimi S, Moimas L, Pirhonen E, Lindroos B, Huhtala H, Raty S, Kuokkanen H, Sandor GK, Miettinen S, Suuronen R (2009b) Calcium phosphate surface treatment of bioactive glass causes a delay in early osteogenic differentiation of adipose stem cells. J Biomed Mater Res A **91**: 540-547.

Hattori H, Masuoka K, Sato M, Ishihara M, Asazuma T, Takase B, Kikuchi M, Nemoto K (2006) Bone formation using human adipose tissue-derived stromal cells and a biodegradable scaffold. J Biomed Mater Res B Appl Biomater **76**: 230-239.

Hench LL (1998) Biomaterials: a forecast for the future. Biomaterials **19**: 1419-1423.

Hicok KC, Du Laney TV, Zhou YS, Halvorsen YD, Hitt DC, Cooper LF, Gimble JM (2004) Human adipose-derived adult stem cells produce osteoid *in vivo*. Tissue Eng **10**: 371-380.

Jensen SS, Bornstein MM, Dard M, Bosshardt DD, Buser D (2009) Comparative study of biphasic calcium phosphates with different HA/TCP ratios in mandibular bone defects. A long-term histomorphometric study in minipigs. J Biomed Mater Res B Appl Biomater **90**: 171-181.

Jensen SS, Yeo A, Dard M, Hunziker E, Schenk R, Buser D (2007) Evaluation of a novel biphasic calcium phosphate in standardized bone defects: a histologic and histomorphometric study in the mandibles of minipigs. Clin Oral Implants Res **18**: 752-760.

Kauschke E, Rumpel E, Fanghanel J, Bayerlein T, Gedrange T, Proff P (2006) The *in vitro* viability and growth of fibroblasts cultured in the presence of different bone grafting materials (NanoBone and Straumann Bone Ceramic). Folia Morphol (Warsz) **65**: 37-42.

Kim H, Kim HW, Suh H (2003) Sustained release of ascorbate-2-phosphate and dexamethasone from

porous PLGA scaffolds for bone tissue engineering using mesenchymal stem cells. Biomaterials **24**: 4671-4679.

Kim H, Suh H, Jo SA, Kim HW, Lee JM, Kim EH, Reinwald Y, Park SH, Min BH, Jo I (2005) *In vivo* bone formation by human marrow stromal cells in biodegradable scaffolds that release dexamethasone and ascorbate-2-phosphate. Biochem Biophys Res Commun **332**: 1053-1060.

Knippenberg M, Helder MN, Zandieh Doulabi B, Wuisman PI, Klein-Nulend J (2006) Osteogenesis *versus* chondrogenesis by BMP-2 and BMP-7 in adipose stem cells. Biochem Biophys Res Commun **342**: 902-908.

Kokubo T, Kim HM, Kawashita M (2003) Novel bioactive materials with different mechanical properties. Biomaterials **24**: 2161-2175.

Lindfors NC, Koski I, Heikkila JT, Mattila K, Aho AJ (2010) A prospective randomized 14-year follow-up study of bioactive glass and autogenous bone as bone graft substitutes in benign bone tumors. J Biomed Mater Res B Appl Biomater **94**: 157-164.

Lindroos B, Aho KL, Kuokkanen H, Raty S, Huhtala H, Lemponen R, Yli-Harja O, Suuronen R, Miettinen S (2010) Differential gene expression in adipose stem cells cultured in allogeneic human serum *versus* fetal bovine serum. Tissue Eng Part A **16**: 2281-2294.

McCullen SD, McQuilling JP, Grossfeld RM, Lubischer JL, Clarke LI, Loboa EG (2010) Application of low-frequency alternating current electric fields via interdigitated electrodes: effects on cellular viability, cytoplasmic calcium, and osteogenic differentiation of human adipose-derived stem cells. Tissue Eng Part C Methods **16**: 1377-1386.

McIntosh K, Zvonic S, Garrett S, Mitchell JB, Floyd ZE, Hammill L, Kloster A, Di Halvorsen Y, Ting JP, Storms RW, Goh B, Kilroy G, Wu X, Gimble JM (2006) The immunogenicity of human adipose-derived cells: temporal changes *in vitro*. Stem Cells **24**: 1246-1253.

Mehrkens A, Saxer F, Güven S, Hoffmann W, Müller AM, Jakob M, Weber FE, Martin I, Scherberich A (2012) Intraoperative engineering of osteogenic grafts combining freshly harvested, human adipose-derived cells and physiological doses of bone morphogenetic protein-2. Eur Cell Mater **24**: 308-319.

Mesimaki K, Lindroos B, Tornwall J, Mauno J, Lindqvist C, Kontio R, Miettinen S, Suuronen R (2009) Novel maxillary reconstruction with ectopic bone formation by GMP adipose stem cells. Int J Oral Maxillofac Surg **38**: 201-209.

Moimas L, Biasotto M, Di Lenarda R, Olivo A, Schmid C (2006) Rabbit pilot study on the resorbability of three-dimensional bioactive glass fibre scaffolds. Acta Biomater **2**: 191-199.

Mrozik KM, Gronthos S, Menicanin D, Marino V, Bartold PM (2012) Effect of coating Straumann(R) Bone Ceramic with Emdogain on mesenchymal stromal cell hard tissue formation. Clin Oral Investig **16**: 867-878.

Ogawa R, Mizuno H, Watanabe A, Migita M, Shimada T, Hyakusoku H (2004) Osteogenic and chondrogenic differentiation by adipose-derived stem cells harvested from GFP transgenic mice. Biochem Biophys Res Commun **313**: 871-877.

Overman JR, Farré-Guasch E, Helder MN, Ten Bruggenkate CM, Schulten EA, Klein-Nulend J (2012) Short (15 minutes) BMP-2 treatment stimulates osteogenic differentiation of human adipose stem cells seeded on calcium phosphate scaffolds *in vitro*. Tissue Eng Part A, in press. doi:10.1089/ten.tea.2012.0133.

Park A, Hogan MV, Kesturu GS, James R, Balian G, Chhabra AB (2010) Adipose-derived mesenchymal stem cells treated with growth differentiation factor-5 express tendon-specific markers. Tissue Eng Part A **16**: 2941-2951.

Peltola M, Aitasalo K, Suonpaa J, Varpula M, Yli-Urpo A (2006) Bioactive glass S53P4 in frontal sinus obliteration: a long-term clinical experience. Head Neck **28**: 834-841.

Peltola M, Kinnunen I, Aitasalo K (2008) Reconstruction of orbital wall defects with bioactive glass plates. J Oral Maxillofac Surg **66**: 639-646.

Pereira RC, Economides AN, Canalis E (2000) Bone morphogenetic proteins induce gremlin, a protein that limits their activity in osteoblasts. Endocrinology **141**: 4558-4563.

Rada T, Reis RL, Gomes ME (2011) Distinct stem cells subpopulations isolated from human adipose tissue exhibit different chondrogenic and osteogenic differentiation potential. Stem Cell Rev **7**: 64-76.

Rokn AR, Khodadoostan MA, Reza Rasouli Ghahroudi AA, Motahhary P, Kharrazi Fard MJ, Bruyn HD, Afzalifar R, Soolar E, Soolari A (2011) Bone formation with two types of grafting materials: a histologic and histomorphometric study. Open Dent J **5**: 96-104.

Roldan JC, Detsch R, Schaefer S, Chang E, Kelantan M, Waiss W, Reichert TE, Gurtner GC, Deisinger U (2010) Bone formation and degradation of a highly porous biphasic calcium phosphate ceramic in presence of BMP-7, VEGF and mesenchymal stem cells in an ectopic mouse model. J Craniomaxillofac Surg **38**: 423-430.

Samartzis D, Khanna N, Shen FH, An HS (2005) Update on bone morphogenetic proteins and their application in spine surgery. J Am Coll Surg **200**: 236-248.

Scherberich A, Muller AM, Schafer DJ, Banfi A, Martin I (2010) Adipose tissue-derived progenitors for engineering osteogenic and vasculogenic grafts. J Cell Physiol **225**: 348-353.

Schubert T, Xhema D, Veriter S, Schubert M, Behets C, Delloye C, Gianello P, Dufrane D (2011) The enhanced performance of bone allografts using osteogenic-differentiated adipose-derived mesenchymal stem cells. Biomaterials **32**: 8880-8891.

Shen B, Wei A, Whittaker S, Williams LA, Tao H, Ma DD, Diwan AD (2010) The role of BMP-7 in chondrogenic and osteogenic differentiation of human bone marrow multipotent mesenchymal stromal cells *in vitro*. J Cell Biochem **109**: 406-416.

Song I, Kim BS, Kim CS, Im GI (2011) Effects of BMP-2 and vitamin D3 on the osteogenic differentiation of adipose stem cells. Biochem Biophys Res Commun **408**: 126-131.

Sutherland MK, Geoghegan JC, Yu C, Winkler DG, Latham JA (2004) Unique regulation of SOST, the sclerosteosis gene, by BMPs and steroid hormones in human osteoblasts. Bone **35**: 448-454.

Thesleff T, Lehtimaki K, Niskakangas T, Mannerstrom B, Miettinen S, Suuronen R, Ohman J (2011) Cranioplasty with adipose-derived stem cells and biomaterial. A novel method for cranial reconstruction. Neurosurgery **68**: 1535-1540.

Tirkkonen L, Halonen H, Hyttinen J, Kuokkanen H, Sievanen H, Koivisto AM, Mannerstrom B, Sandor GK, Suuronen R, Miettinen S, Haimi S (2011) The effects of vibration loading on adipose stem cell number, viability and differentiation towards bone-forming cells. J R Soc Interface **8**: 1736-1747.

Wysocki RW, Cohen MS (2007) Ectopic ossification of the triceps muscle after application of bone morphogenetic protein-7 to the distal humerus for recalcitrant nonunion: a case report. J Hand Surg Am **32**: 647-650.

Xynos ID, Hukkanen MV, Batten JJ, Buttery LD, Hench LL, Polak JM (2000) Bioglass 45S5 stimulates osteoblast turnover and enhances bone formation *In vitro*: implications and applications for bone tissue engineering. Calcif Tissue Int **67**: 321-329.

Yoon E, Dhar S, Chun DE, Gharibjanian NA, Evans GR (2007) *In vivo* osteogenic potential of human adipose-derived stem cells/poly lactide-co-glycolic acid constructs for bone regeneration in a rat critical-sized calvarial defect model. Tissue Eng **13**: 619-627.

Zimmermann CE, Gierloff M, Hedderich J, Acil Y, Wiltfang J, Terheyden H (2011) Survival of transplanted rat bone marrow-derived osteogenic stem cells *in vivo*. Tissue Eng Part A **17**: 1147-1156.

Zuk P, Chou YF, Mussano F, Benhaim P, Wu BM (2011) Adipose-derived stem cells and BMP2: part 2. BMP2 may not influence the osteogenic fate of human adipose-derived stem cells. Connect Tissue Res **52**: 119-132.

Zuk PA, Zhu M, Ashjian P, De Ugarte DA, Huang JI, Mizuno H, Alfonso ZC, Fraser JK, Benhaim P, Hedrick MH (2002) Human adipose tissue is a source of multipotent stem cells. Mol Biol Cell **13**: 4279-4295.

Zuk PA, Zhu M, Mizuno H, Huang J, Futrell JW, Katz AJ, Benhaim P, Lorenz HP, Hedrick MH (2001) Multilineage cells from human adipose tissue: implications for cell-based therapies. Tissue Eng **7**: 211-228.

Discussion with Reviewers

Reviewer I: Fig. 6 compares collagen content among different groups, what is the collagen normalised to among different groups?

Authors: Fig. 6 shows the absolute values obtained as absorbance; hence the results have not been normalised. Absorbance is directly proportional to the amount of collagen in the samples; therefore, a reliable comparison among different groups can be obtained using absolute values. Unfortunately, with the collagen assay, it was not possible to determine cell number from the same samples.

Reviewer I: Authors need to provide *in vivo* data to demonstrate that ADSC preconditioned in osteogenic medium are better at forming bone *in vivo* than ADSCs exposed to BMP-2 or any other growth factors. Results from these studies would enhance the data being reported.

Authors: The authors agree that *in vivo* study is important to further demonstrate the efficiency of OM over BMP-2, BMP-7 and VEGF. However, the authors feel that the present study in its current form provides valuable information on the effects of BMP-2, BMP-7, VEGF and OM on hASC proliferation and osteogenic differentiation in 3D scaffolds, and behaviour of hASCs in two clinically relevant biomaterials. These valuable findings can be utilised to better plan the corresponding *in vivo* study. In order to reduce the number of animal experiments to be performed, it is critical to evaluate the hASCs response to growth factors and OM *in vitro*. For example, based on our results, there is no point in testing growth factors with OM, because there was no extra benefit from OM + growth factors in comparison to OM alone. Therefore, it is not necessary to test all of the groups used in the current study *in vivo*. However, in the future *in vivo* study, effectiveness of OM over growth factors in MM should be demonstrated. It is clear that systematic *in vitro* data is of fundamental importance before it is reasonable to conduct *in vivo* studies. The *in vitro* results also facilitate the correct interpretation of the *in vivo* results.

Reviewer I: The present report concludes that osteogenic medium is superior in enhancing adipose derived stem cells differentiation toward osteogenic lineage than bone morphogenetic proteins. Although, the data reported is valid, use of osteogenic medium to assess osteogenic differentiation is an established protocol. There are controversies regarding response of adipose derived stem cells to BMP-2 to induce osteoblasts differentiation; some reports have shown positive response others have shown reduced response. The findings reported in this manuscript thus confirm original observations. Please comment.

Authors: We would like to note that the OM used in our study is not that traditionally used, but specifically optimised for hASCs. The modified OM with low Dex (5 nM) and high AsA2-P (250 μM) concentration used in this study may have contributed to the superior effect of the OM over the tested growth factors. Because the traditional OM with high Dex (100 nM) and low AsA2-P (50 μM) was originally developed based on studies with BMSCs (Jaiswal *et al.*, 1997, additional reference), it has been reported that OM with lower Dex and higher AsA2-P is more optimal for ASCs (De Girolamo *et al.*, 2007, text reference; Kyllönen *et al.*, unpublished results). However, our study, where the efficiency of the modified OM over the traditional OM has been reported, is under submission (Kyllönen *et al.*, unpublished results). This modified OM has been used successfully for the efficient osteo-induction of hASCs previously (Tirkkonen *et al.*, 2011, text reference). Although several studies have been conducted with BMP-2, there is still no consensus on the effect of BMP-2 on osteo-induction of hASCs. In addition, the effects of BMP-7 and VEGF have been even less reported on hASCs than BMP-2. Furthermore, in the present study, these growth factors were systematically compared in control medium and OM.

Additional Reference

Jaiswal N, Haynesworth SE, Caplan AI, Bruder SP (1997) Osteogenic differentiation of purified, culture-expanded human mesenchymal cells *in vitro*. J Cell Biochem **64**: 295-312.

PUBLICATION
II

Engineering pre-vascularized bone grafts with adipose stem cells and supercritical carbon dioxide processed composites

Pitkänen S., Paakinaho K., Vuornos K., Poot A., Leijiten J., Grijpma D., Seppänen-Kaijansinkko R., Kääriäinen M., Kellomäki M., Miettinen S., Kyllönen L.*, Haimi S*.

PUBLICATION
III

Characterisation and *in vitro* and *in vivo* evaluation of supercritical-CO₂-foamed β-TCP/PLCL composites for bone applications

Pitkänen S., Paakinaho K., Pihlman H., Ahola N., Hannula M., Asikainen S., Manninen M., Morelius M., Keränen P., Hyttinen J., Kellomäki M., Laitinen-Vapaavuori O., Miettinen S.

CHARACTERISATION AND *IN VITRO* AND *IN VIVO* EVALUATION OF SUPERCRITICAL-CO$_2$-FOAMED B-TCP/PLCL COMPOSITES FOR BONE APPLICATIONS

S. Pitkänen[1,2,*], K. Paakinaho[1,3,4], H. Pihlman[5], N. Ahola[3], M. Hannula[6], S. Asikainen[7], M. Manninen[4], M. Morelius[5], P. Keränen[5], J. Hyttinen[6], M. Kellomäki[3], O. Laitinen-Vapaavuori[5] and S. Miettinen[1,2]

[1] Adult Stem Cell Group, BioMediTech, Faculty of Medicine and Health Technology, Tampere University, Tampere, Finland
[2] Research, Development and Innovation Centre, Tampere University Hospital, Tampere, Finland
[3] Biomaterials and Tissue Engineering Group, BioMediTech, Faculty of Medicine and Health Technology, Tampere University, Tampere, Finland
[4] Orton Orthopaedic Hospital, Helsinki, Finland
[5] Department of Equine and Small Animal Medicine, Faculty of Veterinary Medicine, University of Helsinki, Helsinki, Finland
[6] Computational Biophysics and Imaging Group, BioMediTech, Faculty of Medicine and Health Technology, Tampere University, Tampere, Finland
[7] Polymer Technology Research Group, Department of Chemical and Metallurgical Engineering, Aalto University, Espoo, Finland

Abstract

Most synthetic bone grafts are either hard and brittle ceramics or paste-like materials that differ in applicability from the gold standard autologous bone graft, which restricts their widespread use. Therefore, the aim of the study was to develop an elastic, highly porous and biodegradable β-tricalciumphosphate/poly(L-lactide-co-ε-caprolactone) (β-TCP/PLCL) composite for bone applications using supercritical CO$_2$ foaming. Ability to support osteogenic differentiation was tested in human adipose stem cell (hASC) culture for 21 d. Biocompatibility was evaluated for 24 weeks in a rabbit femur-defect model. Foamed composites had a high ceramic content (50 wt%) and porosity (65-67 %). After 50 % compression, in an aqueous environment at 37 °C, tested samples returned to 95 % of their original height. Hydrolytic degradation of β-TCP/PLCL composite, during the 24-week follow-up, was very similar to that of porous PLCL scaffold both *in vitro* and *in vivo*. Osteogenic differentiation of hASCs was demonstrated by alkaline phosphatase activity analysis, alizarin red staining, soluble collagen analysis, immunocytochemical staining and qRT-PCR. *In vitro*, hASCs formed a pronounced mineralised collagen matrix. A rabbit femur defect model confirmed biocompatibility of the composite. According to histological Masson-Goldner's trichrome staining and micro-computed tomography, β-TCP/PLCL composite did not elicit infection, formation of fibrous capsule or cysts. Finally, native bone tissue at 4 weeks was already able to grow on and in the β-TCP/PLCL composite. The elastic and highly porous β-TCP/PLCL composite is a promising bone substitute because it is osteoconductive and easy-to-use and mould intraoperatively.

*Address for correspondence: Sanna Pitkänen, BioMediTech, Faculty of Medicine and Health Technology, FI-33014 Tampere University, Tampere, Finland.
Telephone number: +358 401901789   Email: sanna.pitkanen@tuni.fi

Introduction

Bone is the second most commonly transplanted tissue, with approximately 2.2 million orthopaedic surgeries carried out worldwide (Campana *et al.*, 2014; Kinaci *et al.*, 2014; Van der Stok *et al.*, 2011). As people age, this number is expected to rise. Among bone transplants, autologous bone is considered

the gold standard, while allogenic bone and bone substitutes are also used. Important patient groups affected by problems concerning bone transplants are young children, who do not have enough bone tissue to be harvested, and elderly people, whose bone quality is weak. In addition, several problems are related to the use of autologous bone transplants, such as morbidity of the harvesting site, insufficiency and viability of the harvested bone and infection (Freeman and McNamara, 2017; Van der Stok *et al.*, 2011). Furthermore, even though allograft bone may provide enough bone, transplanted tissue might be rejected; also, proteins and osteoinductive factors might be denatured following sterilisation (Boyce *et al.*, 1999). Moreover, when using allografts, disease transmission and infection are recurring problems, as 18 % of donated femoral heads have been shown to be affected by bacterial or fungal infections (Barbour and King, 2003; Boyce *et al.*, 1999; Freeman and McNamara, 2017). Therefore, there is an evident and growing need for safe, synthetic bone transplants and tissue engineering strategies.

Even though various biomaterials have been proposed for bone replacement, the study and development of these structures have rarely proceeded to clinical applications (de Misquita *et al.*, 2016). Before a bone substitute can become a clinically used product, its efficacy and safety has to be demonstrated both *in vitro* and *in vivo* as well as in a clinical trial. According to the regulation (EU) 2017/745 of the European Parliament and of the Council of 5 April 2017 on medical devices, a product cannot receive a CE mark without clinically proven data (Web ref. 1). An ideal bone substitute should be osteoconductive or osteoinductive, biocompatible, biodegradable (Van der Stok *et al.*, 2011) and highly porous, with a pore size larger than 250 μm to allow cell and tissue ingrowth (Mathieu *et al.*, 2005; Turnbull *et al.*, 2017; Zadpoor, 2015) and vascularisation (Rouwkema *et al.*, 2008). Furthermore, the implant should not induce the formation of fibrotic tissue (Van der Stok *et al.*, 2011) or infection. Cost-effective, large-scale manufacturing is also important when designing a new bone substitute for clinical use.

Ceramics, such as hydroxyapatite and other calcium phosphates, are highly compatible with bone tissue and, therefore, the most widely used synthetic bone substitute materials for treating large bone defects. Among calcium phosphates, β-tricalciumphosphate (β-TCP) induces significantly more bone in an ectopic site *in vivo* as compared to hydroxyapatite (Chatterjea *et al.*, 2013; Yuan *et al.*, 2010) and, therefore, β-TCP was chosen as the calcium phosphate phase of the composite. However, there has been conflicting results concerning the osteoinductive properties of β-TCP and speculation that they might vary according to the surface properties of the material (Bohner and Miron, 2019; Duan *et al.*, 2018). Calcium phosphate materials are hard and brittle, making them difficult to shape intraoperatively and implant. Synthetic

polymers such as polylactide, polyglycolide, poly-ε-caprolactone and their copolymers are biocompatible and support osteogenic differentiation of stem cells *in vitro* (Campana *et al.*, 2014; Jeong *et al.*, 2008; Temple *et al.*, 2014; Wang *et al.*, 2016). Poly(L-lactide-co-ε-caprolactone) (PLCL) is a copolymer of L-lactide and ε-caprolactone with highly desirable characteristics as an implant material: elasticity, flexibility, high tensile strength, controllable degradation rate and good biocompatibility (Holmbom *et al.*, 2005; Wang *et al.*, 2016). PLCL scaffolds have been used in bone tissue engineering although, as PLCL is inert, hydrophobic and lacks biological recognition sites, the interaction with tissue and cells is not good enough either *in vitro* or *in vivo* (Jeong *et al.*, 2008; Wang *et al.*, 2016). By using supercritical CO_2 (scCO_2) processing, it was possible to create a homogenous, porous composite of the bioactive β-TCP and elastic PLCL. scCO_2 foaming was chosen as the processing technique as it is easy, cost-effective and non-toxic. Furthermore, the technique enables the production of polymeric structures with different pore sizes and total porosities. Briefly, CO_2 becomes a supercritical fluid above its critical temperature and pressure (31.10 °C, 73.9 bar), adapting characteristics between a liquid and a gas. Polymeric materials can be dissolved in scCO_2 and, as the pressure is decreased controllably, the CO_2 gas nucleation and expansion creates the wanted porous structure inside the polymeric material (Mathieu *et al.*, 2005).

Multipotent human adipose stem cells (hASCs) are easily available. Furthermore, hASCs have been widely studied in the field of bone tissue engineering *in vitro* (Kyllönen *et al.*, 2013a; Kyllönen *et al.*, 2013b; Ojansivu *et al.*, 2015; Tirkkonen *et al.*, 2013; Vanhatupa *et al.*, 2015) and *in vivo* (Jeon *et al.*, 2008; Wilson *et al.*, 2012). Therefore, hASCs are a relevant cell type for studying both the cytocompatibility of a potential bone substitute and the ability of a scaffold to support osteogenic differentiation *in vitro*.

The aim of the current study was to overcome the major limitations of previous bone-application-intended materials, to develop an elastic, highly porous, biodegradable and biocompatible β-TCP/PLCL composite for bone applications by using scCO_2 and to test its performance both *in vitro* and *in vivo*. Furthermore, the aim was to create a composite mimicking the mechanical properties of cartilaginous soft callus, which serves as the natural scaffold for bone regeneration during bone healing. For the first time, it was shown that scCO_2 processing of β-TCP/PLCL composite with a high ceramic content (50 wt%) could be used to produce scaffolds with porosity as high as 65-67 %. Furthermore, β-TCP granules were brought to the surface of the composites by a dynamic compression treatment. *In vitro* studies with hASCs demonstrated both cytocompatibility and osteogenic capacity of the scaffold. Furthermore, biocompatibility, osteoconductivity and bone tissue ingrowth were shown *in vivo* in a rabbit femur defect model.

Materials and Methods

Composite manufacturing and characterisation

Composites were manufactured by melt-mixing PLCL-polymer (70L/30CL; Purasorb PLC7015, Corbion Purac Biomaterials, Gorinchem, the Netherlands) with 50 wt% β-TCP, having a particle size range between 100 and 300 μm (Plasma Biotal Ltd., Buxton, UK). Composites were foamed using $scCO_2$, as described in the granted patent (Web ref. 2), by using a Supercritical Carbon Dioxide Reactor System (SFE250, Waters Ltd., MA, USA). The residual lactide monomer content was measured by gas chromatography (DC8000, CE Instruments, Rodano, Italy) after post-melting. Foamed blocks were cut into discs for *in vitro* studies [diameter (Ø) = 8 mm, height (h) = 3 mm)] and into cylinders for *in vivo* studies for cancellous bone (Ø = 3.2 mm, h = 10 mm) and intramuscular implantation (Ø = 4.0 mm, h = 10 mm). All samples were sterilised by γ-irradiation with a minimum dose of 25 kGy.

Prior to *in vitro* and *in vivo* studies, elastic scaffolds were treated by dynamically pre-compressing them repeatedly in an aqueous environment at 37 °C for a minimum of 20 cycles and compression level of at least 50 %. Composites were imaged by using a scanning electron microscope (SEM; Philips XL-30) and Xradia MicroXCT-400 X-ray imaging system with a voxel size of 5.6 μm (Carl Zeiss X-ray Microscopy Inc.) before and after the compression treatment. Porosities and pore sizes were calculated from micro-computed tomography (μCT) images with Fiji (Schindelin *et al.*, 2012) using BoneJ (Doube *et al.*, 2010) plugin. All the visualisations were conducted with Avizo 9.3.0 Software (Thermo Fisher Scientific).

Mechanical testing of composites

Mechanical testing was performed for both intact and pre-compressed samples (Ø = 8 mm, h = 3.5 ± 0.6 mm), as dry at room temperature (RT) and in an aqueous environment at 37 °C using the Instron Electropuls E1000 (High Wycombe, UK) by compressing unconfined samples 1 mm/min until a 50 % strain was reached. Used crosshead speed was adapted from the standard ISO 604. Elastic modulus was determined from linear section of the stress-strain curve, between 0 and 20 % strain.

Hydrolytic degradation of composites *in vitro* and *in vivo*

Hydrolytic degradation of the porous composites *in vitro* was studied at 4, 12 and 24 weeks at 37 °C in Sörensen buffer solution (*n* = 6) and *in vivo* as intramuscular implantation on underside of the supraspinatus muscle (*n* = 6 at 4 and 12 weeks; *n* = 1 at 24 weeks due to strong scaffold degradation). A porous PLCL (70/30) polymer scaffold was used as a reference. Degradation was monitored by size exclusion chromatography (SEC) utilising a Waters Associates system equipped with a Waters 717Plus Satellite autosampler, a Waters 510 HPLC solvent pump, two linear PL gel 5 μm columns connected in series and a Waters 2414 differential refractometer. The number-average molecular weight (M_n), weight-average molecular weight (M_w) and polydispersity of the samples were determined against polystyrene standards at RT. Chloroform was used as the eluent and was delivered at a flow rate of 1 mL/min. Samples were dissolved in chloroform at a polymer concentration of 13.5 ppm. The injection volume was 100 mL.

Isolation, characterisation and seeding of hASCs *in vitro*

hASCs were isolated from adipose tissue samples obtained from three female donors (40 ± 11 years old) undergoing surgical procedures at the Department of Plastic Surgery, Tampere University Hospital after patients gave their consent. The study was conducted in accordance with the Ethics Committee of the Pirkanmaa Hospital District, Tampere (R15161).

Isolation of hASCs was conducted using a mechanical and enzymatic protocol as described previously (Lindroos *et al.*, 2009). Isolated hASCs were expanded in basic medium (BM) consisting of Dulbecco's modified Eagle's medium: nutrient mixture F-12 (DMEM/F-12 1 : 1; Thermo Fischer Scientific), 5 % human serum (HS; BioWest, Nuaillé, France), 1 % antibiotics (100 U/mL penicillin; 100 U/mL streptomycin; Lonza) and 1 % L-glutamine (GlutaMAX I; Thermo Fischer Scientific). hASCs were cultured at 37 °C in 5 % CO_2 and medium was changed twice a week. Cells were detached with TrypLE Select (Life Technologies). Experiments were carried out at passage 3.

To verify the mesenchymal origin of the cells, surface marker expression of hASCs at passage 1 was characterised by fluorescent-activated cell sorter (FACSAria; BD Biosciences) as described previously (Lindroos *et al.*, 2009). Monoclonal antibodies against CD14-PE-Cy7, CD19-PE-Cy7, CD45RO-APC, CD73-PE, CD90-APC (BD Biosciences), CD34-APC, HLA-DR-PE (Immunotools, Friesoythe, Germany) and CD105-PE (R&D Systems) were used. The analysis was performed on 10,000 cells per sample and unstained hASC samples were used to compensate for the background autofluorescence levels. The expression of the surface markers CD73, CD90 and CD105 was positive, the expression of CD14, CD19, CD45 and human leukocyte antigen DR isotype (HLA-DR) was negative and that of CD34 was moderate (Table 1). The surface markers' expression of hASCs confirmed the mesenchymal origin of the cells (Dominici *et al.*, 2006).

Before cell seeding, sterile composites were pre-compressed in BM and incubated for 24 h in BM at 37 °C. hASCs were seeded in a 50 μL medium drop at a density of 510 cells/mm³ into the scaffolds. Cells were allowed to attach for 2-3 h before 500 μL of BM or osteogenic medium (OM) were added. OM consisted of BM with the addition of 250 μM ascorbic acid 2-phosphate (Sigma-Aldrich), 10 mM

Table 1. Surface marker expression of hASCs at passage 1. Positive > 98 %; negative < 2 %; moderate < 50 % > 2 %. SD: standard deviation.

	Surface marker	mean ± SD	expression
CD14	Serum lipopolysaccharide binding protein	0.6 ± 0.6	negative
CD19	B lymphocyte-lineage differentiation antigen	0.4 ± 0.2	negative
CD34	Sialomucin-like adhesion molecule	34.8 ± 32.2	moderate
CD45	Leukocyte common antigen	1.6 ± 0.3	negative
CD73	Ecto-50-nucleotidase	98.2 ± 1.3	positive
CD90	Thy-1 (T-cell surface glycoprotein)	99.8 ± 0.1	positive
CD105	SH-2, endoglin	98.3 ± 1.2	positive
HLA-DR	Major histocompatibility class II antigens	0.6 ± 0.1	negative

β-glycerophosphate (Sigma-Aldrich) and 5 nM dexamethasone (Sigma-Aldrich). As a 2-dimensional (2D) control for alizarin red staining, 500 cells were seeded in 1 mL of BM or OM in a 24-well plate (Nunc, Roskilde, Denmark).

Cell viability and proliferation
Cell viability was evaluated qualitatively by staining hASCs with fluorescent live/dead-staining probes (Molecular Probes) after 7, 14 and 21 d. hASCs were incubated for 45 min at RT with a mixture of 0.5 μM calcein acetoxymethyl ester (Molecular Probes) and 0.25 μM ethidium homodimer-1 (Molecular Probes). Images of living cells (green fluorescence) and dead cells (red fluorescence) were acquired using an Olympus IX51 phase contrast microscope with fluorescence optics and Olympus DP30BW camera (Olympus).

Cell number was analysed quantitatively after at 7, 14 and 21 d by analysing the total amount of DNA by CyQUANT Cell Proliferation Assay Kit (Molecular Probes), according to manufacturer's protocol, as reported previously (Kyllönen *et al.*, 2013a). Samples were analysed after two freeze-thaw cycles and fluorescence was measured at 480/520 nm with a microplate reader (Victor 1420 Multilabel Counter; Wallac, Turku, Finland).

Analysis of osteogenic differentiation *in vitro*
Alkaline phosphatase (ALP) activity was determined after 7, 14 and 21 d, as described previously (Kyllönen *et al.*, 2013a). ALP activity was determined from the same cell lysates as total DNA content. Absorbance was measured at 405 nm (Victor 1420).

Soluble total collagen was analysed at 7, 14 and 21 d by Soluble Collagen Assay Sircol™ (Biocolor, Carrickfergus, UK), as described previously (Tirkkonen *et al.*, 2013). Briefly, collagen was dissolved for 2 h at 4 °C with 0.5 M acetic acid (Merck) containing 0.1 mg/mL pepsin (Sigma-Aldrich), while gently shaking. Thereafter, 100 μL samples were dyed with 500 μL of Sircol™ Dye Reagent (Sirius red in picric acid; Biocolor) for 30 min at RT, while gently

shaking. Then, samples were centrifuged for 10 min at 13,400 ×*g* and the dyed collagen pellets were washed with 750 μL of ice-cold Acid-Salt Wash Reagent (Biocolor). After another 10 min centrifugation at 13,400 ×*g*, the dye was diluted by adding 250 μL of Alkali Reagent (Biocolor) on top of the dyed collagen pellet. Intensity of the dye was measured from two parallel 100 μL samples in a 96-well plate (Nunc) using a microplate reader (Viktor 1420).

Mineralisation was studied by alizarin red S staining after 14 and 21 d, as described previously (Kyllönen *et al.*, 2013a). In brief, paraformaldehyde (Sigma-Aldrich)-fixed cell-scaffold constructs were stained with filtered 2 % alizarin red S (pH 4.2; Sigma-Aldrich) and photographed after several washing steps. Dye was extracted with cetylpyridinium chloride (100 mM, Sigma-Aldrich) and its intensity was determined by measuring the absorbance at 540 nm (Victor 1420).

Quantitative real-time reverse transcription polymerase chain reaction (qRT-PCR) analysis was used to compare the relative expression of osteogenic genes in different experimental groups. Total RNA was isolated from hASCs at 14 and 21 d using the NucleoSpin RNA II kit reagent (Macherey-Nagel) according to the manufacturer's protocol. Single-strand cDNA was synthesised from total RNA using the High-Capacity cDNA Reverse Transcriptase Kit (Applied Biosystems). Data were normalised to the expression of the housekeeping gene human acidic ribosomal phosphoprotein large P0 (*hRPLP0*). Primer sequences and accession numbers for *RPLP0* and osteogenic genes *RUNX2a*, *OSTERIX* and *DLX5* are listed in Table 2. The qRT-PCR mixture contained cDNA, primers and SYBR Green PCR Master Mix (Applied Biosystems). Reactions were conducted with ABI PRISM® 7300 Sequence Detection System as reported previously (Kyllönen *et al.*, 2013a). Results were processed with ABI PRISM® 7300 Sequence Detection System-software (Applied Biosystems).

Osteogenic marker proteins collagen type I (COL-I) and osteocalcin (OCN) were detected with an indirect immunocytochemical staining method. At 7, 14 and

Table 2. Primer sequences and accession numbers of genes analysed by qRT-PCR.

Name	Full name	Accession number		Sequence	Product size (bp)
hRPLP0	Ribosomal protein, large, P0	NM_001002	Forward	5'-AAT CTC CAG GGG CAC CAT T-3'	70
			Reverse	5'-CGC TGG CTC CCA CTT TGT-3'	
hALP	Alkaline phosphatase	NM_000478.4	Forward	5'-CCC CCG TGG CAA CTC TAT CT-3'	73
			Reverse	5'-GAT GGC AGT GAA GGG CTT CTT-3'	
hRUNX2A	Runx2A, variant 1	NM_001024630.3	Forward	5'-CTT CAT TCG CCT CAC AAA CAA C-3'	62
			Reverse	5'-TCC TCC TGG AGA AAG TTT GCA-3'	
hOSX	Osterix	AF_477981	Forward	5'-TGA GCT GGA GCG TCA TGT G-3'	79
			Reverse	5'-TCG GGT AAA GCG CTT GGA-3'	
hDLX5	Distal-less homeobox 5	NM_005221.5	Forward	5'-ACC ATC CGT CTC AGG AAT CG-3'	75
			Reverse	5'-CCC CCG TAG GGC TGT AGT AGT-3'	

21 d, hASCs were fixed with 4 % paraformaldehyde (Sigma Aldrich) in Dulbecco's phosphate-buffered saline (DPBS) with 0.05 % Triton-X 100 (Sigma Aldrich) for 10 min followed by washing steps. Cells were blocked in 1 % bovine serum albumin (BSA) in DPBS for 1 h at 4 °C. Primary antibodies mouse monoclonal anti-COL-I (dilution 1 : 2,000; Abcam) and mouse monoclonal anti-OCN (dilution 1 : 100; Abcam) were diluted in 1 % BSA and incubated over night at 4 °C. As a negative control, 1 % BSA without primary antibody was used. After washing steps, secondary antibody donkey anti-mouse AlexaFluor 488 IgG (dilution 1 : 1,000; Invitrogen) diluted in 1 % BSA was added and incubated for 45 min at RT. Cells were washed repeatedly and treated with 0.1 % 4, 6-diamidino-2-phenylindole (DAPI) (Sigma Aldrich) in DPBS for 5 min at RT. Finally, cells were washed and imaged using an Olympus IX51 phase contrast microscope with fluorescence optics and Olympus DP30BW camera (Olympus). Images were edited with Adobe Photoshop version CS4.

Animal experiments
The Finnish Animal Experiment Board (ESAVI/5398/04.10.07/2014) approved the animal study and used protocols. 20 female New Zealand white rabbits were used.

Anaesthesia was induced by subcutaneous injection of ketamine (35 mg/kg, Ketador vet® 100 mg/mL, Richter Pharma, Wels, Austria) and medetomidine (0.3 mg/kg, Domitor® 1 mg/mL, OrionPharma, Espoo, Finland). Intravenous propofol boluses (2-5 mg/rabbit, Vetofol® 10 mg/mL, Norbrook Laboratories, Newry, Ireland), ketamine bolus (10 mg/kg) or mask anaesthesia with 1.5 % isoflurane (IsoFlo® vet 100%, Abbott Laboratories, Chicago, IL, USA) were used during the surgical procedure if needed. Intravenous trimethoprim/sulfamethoxazole (15 mg/kg, Duoprim® 200/40 mg/mL, Intervet International, Boxmeer, the Netherlands) was used as an antibiotic prophylaxis. Intravenous carprophen (4 mg/kg, Norocarp® 50 mg/mL, Norbrook Laboratories) and buprenorphine (0.03 mg/kg, Bupaq® 0.3 mg/mL, Richter Pharma) were used as a pain medication.

A 20 mm skin incision was made on the lateral aspect of the right femoral condyle and a 3.2 mm diameter and 10 mm deep drilling hole was made above the lateral collateral ligament. Composites were moistened and pre-compressed in blood collected from the drilling hole prior to implantation. The drilling hole was filled with 3.2 × 10 mm cylinder-shaped β-TCP/PLCL composite implant and periosteum and skin were closed.

For the degradation study, a skin incision was made midline over the spine between the scapulae and two 4 × 10 mm β-TCP/PLCL composites were inserted through an applicator tube to the right supraspinatus muscle and two 4 × 10 mm polymer implants to the left supraspinatus muscle. Subcutaneous atipametzole (0.75 mg/kg, Antisedan® 5 mg/mL, OrionPharma) was used to reverse the sedative effect of the medetomidine after the procedure. For postoperative pain, subcutaneous buprenorphine (0.03 mg/kg) and carprophen (4 mg/kg) were used. Subcutaneous metoclopramide (0.2 mg/kg, Primperan® 5 mg/mL, Sanofi Oy, Espoo, Finland) was used to increase the intestinal motility. Rabbits were in a cage rest for 2 weeks after the surgery and, then, in a large-group housing area. They had access to hay and water *ad libitum*. One rabbit died during the procedure due to anaesthesia-related causes and one died 3 d after the operation as a result of a complication unrelated to the femoral defect.

The 18 rabbits were randomly divided in groups of 6 animals and euthanised 4, 12 and 24 weeks after the procedure. Subcutaneous injection of medetomidine (0.3 mg/kg) and ketamine (35 mg/kg) was followed by intracardial injection of pentobarbital (300 mg/rabbit, Mebunat® vet 60 mg/mL, Orion Pharma Oy, Espoo, Finland). The intramuscular implants were collected for further analysis.

μCT analysis (MicroXCT-400, Zeiss) was performed on all the harvested femoral condyles

before histological preparation. Tube voltage of 120 kV and tube current of 83 µA were selected. From each sample, 1,600 projections were taken with a 13.4 µm voxel size. Exposure time was 4 s. Projections were reconstructed with the manufacturer's XMReconstructor software. Image processing and analysis were done with Avizo Software (Thermo Fisher Scientific). Thereafter, the femoral condyles were fixed in 10 % buffered formalin solution

followed by routine ascending ethanol series and methyl methacrylate embedding. A hard-tissue microtome (Leica, SM2500) was used to cut 5 µm-thick slice. Masson-Goldner's Trichrome (MGT) staining was performed.

Statistical analysis
Statistical analysis was performed with SPSS version 23 (IBM) using a non-parametric test, due to the small
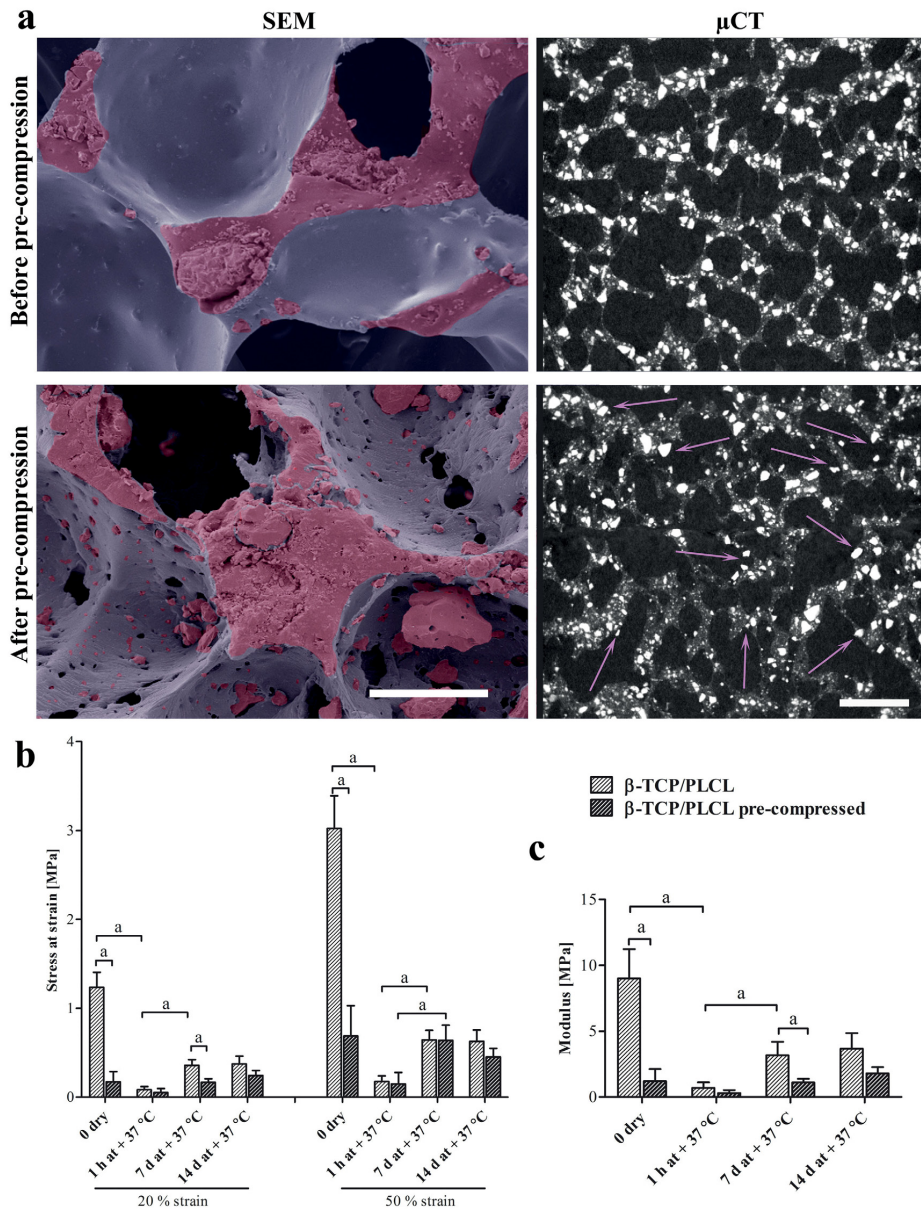

Fig. 1. β-TCP/PLCL composite characteristics before and after pre-compression treatment. (**a**) Representative SEM (scale bar: 200 µm; PLCL coloured violet; β-TCP coloured pink) and µCT (arrows indicate the granules released from under the polymer film; scale bar: 1,000 µm) images. (**b**) Compressive stress at 20 and 50 % strain when dry and 1 h, 7 or 14 d at 37 °C in aqueous environment. (**c**) Modulus when dry and 1 h, 7 or 14 d at 37 °C in aqueous environment. Statistical significances indicated as [a] $p ≤ 0.05$ ($n = 6$).

sample size. The effects of stress and strain ($n = 6$) on intact and pre-compressed composites and of pre-compressing and incubation at 37 °C on modulus ($n = 6$) of composites were compared using Mann-Whitney U-test with Bonferroni correction. Effects of BM or OM in combination with the composite on cell number, ALP activity, mineralisation, soluble collagen amount and gene expression were compared using Mann-Whitney U-test with Bonferroni correction. Results were considered significant when $p < 0.05$. Experiments for cell number, ALP activity, mineralisation and soluble collagen amount were repeated with 3 donor lines each with 3 parallel samples ($n = 9$). Experiments for gene expression were repeated with 3 donor lines each with 2 parallel samples ($n = 6$).

Results

Characteristics of the composite

Scaffold porosity was 65-67 %, with an average pore size of 380 ± 130 μm. In addition, compressive stress at 20 and 50 % strain and modulus were analysed at different time points. SEM images (Fig. 1**a**) showed that before pre-compression treatment, β-TCP (coloured pink) was mainly on the cutting surface of the composite, while the surfaces of the pores were smooth and a PLCL film (coloured violet) mainly covered the β-TCP granules. However, the effect of the pre-compression was evident, as after the protocol the PLCL surface of the pores had ruptured and β-TCP granules protruded through it. Furthermore, SEM images demonstrated that the treatment tore additional holes in the pores of the composite. μCT images agreed with SEM images as they revealed that after the treatment more β-TCP granules were on display on the pore surfaces or even detached from the polymer phase in contrast to intact composite (Fig. 1**a**).

Both the compression treatment and warming at 37 °C had a significant effect on the mechanical properties of the composite. The compression treatment of a dry composite decreased the modulus significantly in contrast to an intact composite, but 1 h at 37 °C aqueous solution treatment erased such a difference (Fig. 1**c**). The same phenomenon was seen in the compressive stress analysis at both 20 and 50 % strain (Fig. 1**b**). Moreover, warming and wetting of the intact composite significantly decreased the modulus in comparison to dry intact composite (Fig. 1**c**). Intriguingly, both modulus and strength increased between 1 h and 7 d in an aqueous environment at 37 °C (Fig. 1**b**,**c**). No samples were broken during the compression analysis and samples tested in an aqueous environment at 37 °C returned to 95 % of their original height after the 50 % compression.

Hydrolytic degradation of the composite *in vitro* and *in vivo*

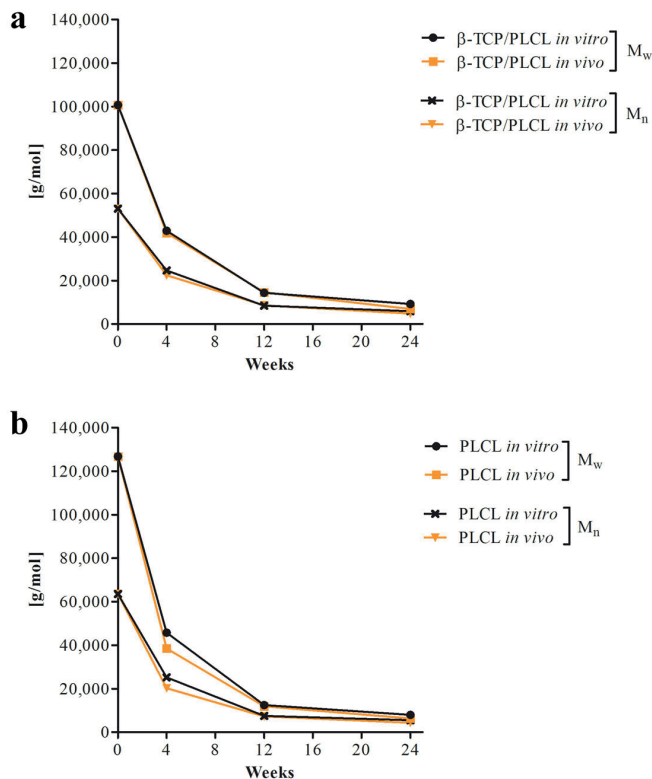Molecular weight (M_n and M_w) change, caused by hydrolytic degradation of the polymer chains in

Fig. 2. Hydrolytic degradation analysis results. M_n and M_w of (**a**) β-TCP/PLCL composites and (**b**) PLCL scaffolds were analysed *in vitro* and *in vivo* after 4, 12 and 24 weeks.

both β-TCP/PLCL composites (Fig. 2**a**) and PLCL polymer scaffolds (Fig. 2**b**), was analysed both *in vitro* and *in vivo*. M_n and M_w of the samples were determined at 4, 12 and 24 weeks and the results showed that the degradation *in vitro* was similar to that *in vivo* for both materials. Furthermore, scaffold molecular weight had already decreased significantly during the first 4 weeks. In addition, M_n and M_w of the composite scaffold decreased by approximately 90 % during the 24-week follow-up. The neat polymer scaffold had initial M_n and M_w values higher than the composite but the difference in the degradation profile was evened out in 4 weeks, after which no clear differences were seen between the materials or the *in vitro* and *in vivo* environments. The residual L-lactide content after melt-extrusion and scCO₂-foaming for the PLCL scaffold was 0.09 wt% and for the β-TCP/PLCL composite 0.06 wt%.

Viability and proliferation of hASCs *in vitro*
Cell viability was very good since only single dispersed dead cells were observed in cultures. In BM, cell number was clearly less than that in OM at 7 d (Fig. 3) and the difference was evident also at 14 and 21 d. Cell number was similar in OM at 7 d and BM at 21 d.

Cell proliferation was analysed by fluorescent CyQUANT proliferation assay after 7, 14 and 21 d in culture. In concordance with the live/dead staining, cell number was significantly larger in OM in contrast to BM at all time points (Fig. 4**a**). Moreover, cell number as indicated by live/dead staining was similar in OM at 7 d and BM at 21 d. Variation among the different donor cell lines was evident in proliferation analysis, as OM did not increase the proliferation of hASCs in comparison to BM from one of the donors as it did for the other two.

Osteogenic differentiation of hASCs *in vitro*
ALP activity (Fig. 4**b**) was significantly greater in OM, in contrast to BM at 7 and 14 d. Furthermore, ALP activity in both BM and OM increased significantly from 7 to 14 d. However, ALP activity did not rise significantly from 14 to 21 d in either BM or OM. ALP activity varied between different donor cell lines and especially one donor cell line had higher ALP activity in comparison to the others.

Total collagen amount did not vary notably among BM and OM groups at 7, 14 or 21 d (Fig. 4**c**). Collagen amount increased in both study groups slightly from 7 to 14 d; however, collagen amount seemed to decline from 14 to 21 d.

hASCs produced a pronounced mineralised matrix on the composite in both BM and OM at 14 and 21 d (Fig. 4**e**). Furthermore, they produced notably more mineralised matrix on the scaffold in comparison to hASCs seeded on cell culture plastic (2D) at 21 d (Fig. 4**e**). At 14 d there was no difference between BM and OM. However, at 21 d, the mineral amount in OM was significantly larger than that in BM (Fig. 4**d**).

Immunocytochemical staining of COL-I was conducted at 7, 14 and 21 d. In BM, COL-I expression was modest at all time points (Fig. 5**a**). However, in OM, a clear development of a collagenous matrix was seen during the 3-week experiment: at 7 d, cells were producing COL-I; at 14 d, cells were still producing COL-I and had also excreted COL-I to the extracellular matrix (ECM); at 21 d, there was a strong extracellular COL-I matrix seen in the representative image (Fig. 5**a**). In addition to COL-I, OCN was also stained at 14 and 21 d. OCN was expressed in both BM and OM at both time points; however, the staining was slightly stronger in OM at both time points (Fig. 5**b**).
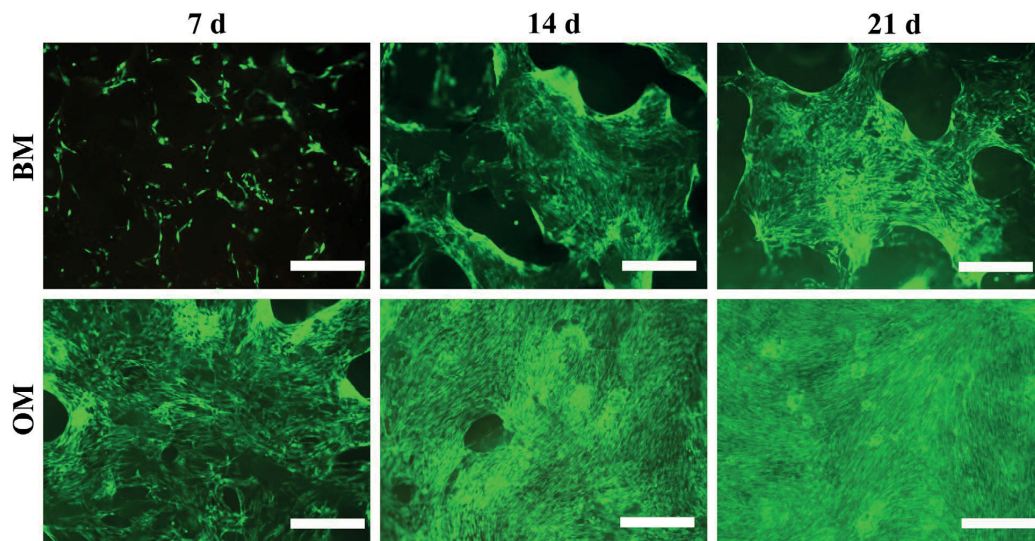

Fig. 3. Viability of hASCs in β-TCP/PLCL composites. Representative images of live/dead stained hASCs cultured in β-TCP/PLCL composites in BM or OM after 7, 14 and 21 d in culture. Scale bar: 500 µm.

qRT-PCR analysis for osteogenic genes *ALP*, *RUNX2a*, *OSX* and *DLX5* was conducted at 7, 14 and 21 d. Relative gene expression did not significantly differ in BM in comparison to OM during the experiment, although, the expression of *RUNX2a* (p values between groups at 7 d: 0.394; 14 d: 0.078; 21 d: 0.310) and *OSTERIX* (p values between groups at 7 d: 0.394; 14 d:0.123; 21 d: 0.240) was higher in OM as compared to BM at all time points (Fig. 6).

Bone regeneration within composites in rabbit femur defects

Bone was already able to grow on the surface as well as form inside the composite at 4 weeks (Fig. 7). The increased bone growth was observed on the surface and inside the composite at 12 and 24 weeks. In the 4-week μCT and histological staining images, some bone formation could be seen beyond the original bone margins, which was most likely a periosteum-induced reaction and not bone formation induced by the implant. Histological staining showed no signs of fibrous tissue or formation of cysts during the 24 weeks. μCT imaging confirmed the histological staining results. In addition, especially the representative μCT images at 24 weeks showed that the composite had degraded as compared to 4- and 12-week images (Fig. 7).

Discussion

Composites consisting of calcium phosphates and synthetic polymers have presented promising results in bone engineering applications and it has been
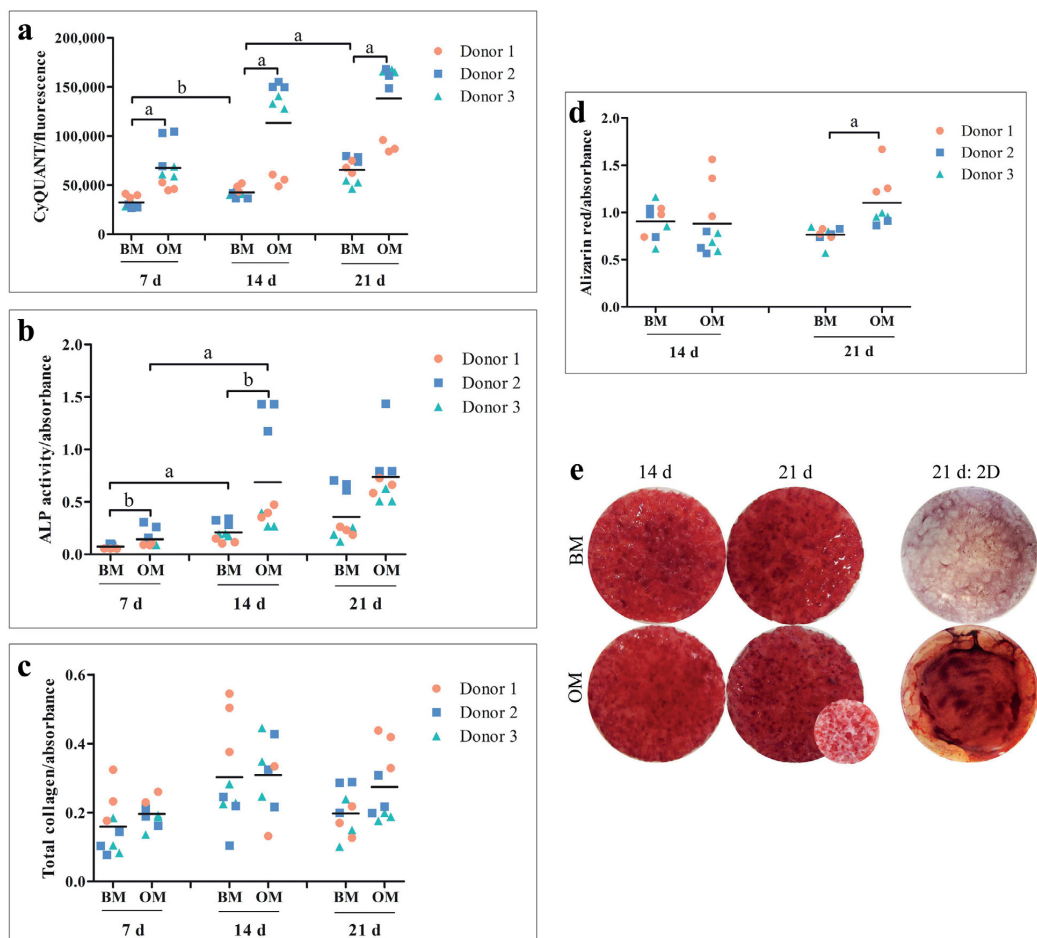

Fig. 4. hASC culture and differentiation in β-TCP/PLCL composites. (**a**) Cell numbers at 7, 14 and 21 d. (**b**) ALP activity at 7, 14 and 21 d. (**c**) Total soluble collagen amount at 7, 14 and 21 d. (**d**) Quantitative mineralisation results after 14 and 21 d. (**e**) Representative images of mineral-stained cell-scaffold constructs after 14 and 21 d and of hASC cultures on cell culture plastic (2D) after 21 d. Stained blank scaffold without seeded cells is presented on the left of 21 d OM scaffold (scaffold Ø = 8 mm; well Ø = 15.5 mm). Statistical significance indicated as [a] $p \leq 0.001$ or [b] $p < 0.05$ ($n = 9$).

suggested that among biomaterials, composites are the most promising strategy for bone regeneration (de Misquita *et al.*, 2016). ScCO$_2$ processing is a very interesting processing method for polymeric tissue engineering structures as it is totally non-toxic, cost effective and has low critical parameters (T_C: 304 K; P_C: 7.5 MPa) enabling the addition of biomolecules, such as bone morphogenetic protein 2 (BMP-2), into the structure during processing (Duarte *et al.*, 2013). The study aim was to manufacture a composite with high β-TCP content, with porosity similar to that of human cancellous bone. In scCO$_2$ processing, the higher ceramic content decreases the porosity and

increases the average pore size of the composite (Mathieu *et al.*, 2006). Moreover, 5 wt% β-TCP content has been suggested to be the upper limit in order to obtain a homogenous and interconnected pore structure (Mathieu *et al.*, 2006). In contrast to previous studies, it was possible, for the first time, to create a composite with 50 wt% β-TCP content with porosity as high as 65-67 % and average pore size of 380 μm by using scCO$_2$. Previously, Mathieu *et al.* (2006) manufactured polylactide (PLA)/β-TCP composites by scCO$_2$ with 74 % porosity but with only 10 % ceramic content. Moreover, Diaz-Gomez *et al.* (2017) reported PCL/fibroin/hydroxyapatite (70/20/10 %)
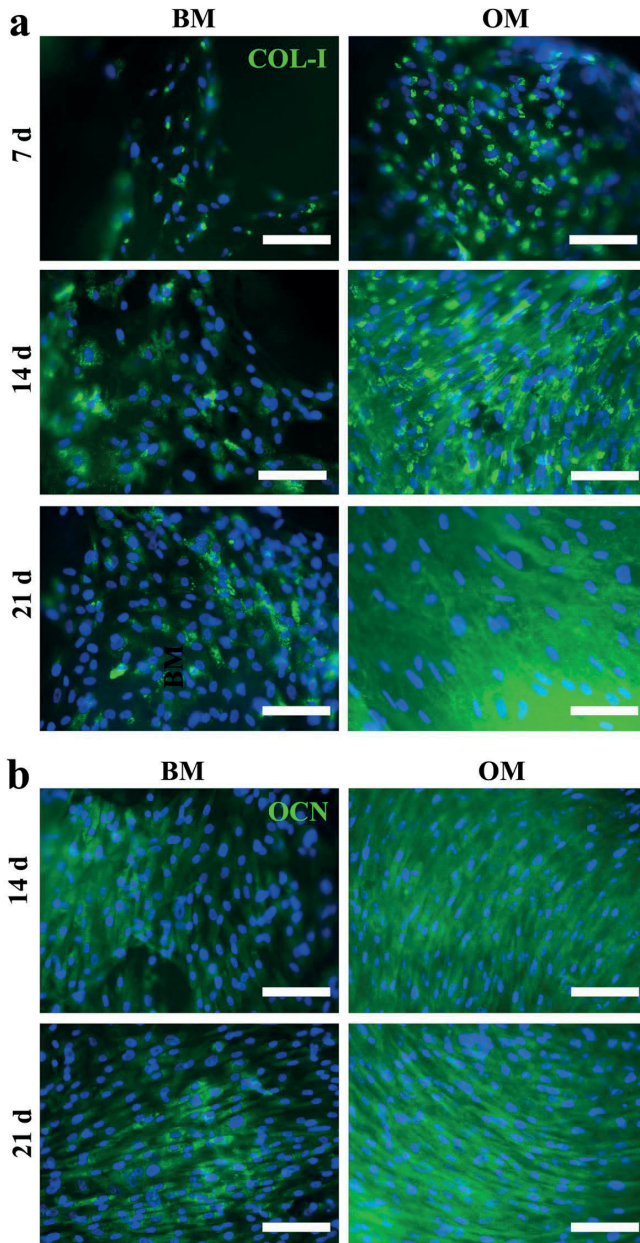
Fig. 5. Immunocytochemical staining of osteogenic markers in hASCs in β-TCP/PLCL composites. Representative images of immunocytochemical staining of (**a**) COL-I (green) after 7, 14 and 21 d in culture and (**b**) OCN (green) after 14 and 21 d in culture. Nuclei are stained in blue. Scale bar: 100 μm.

composites processed by using scCO$_2$ with average porosity of 69.7 %.

Another challenge related to manufacturing polymer-ceramic composites by using scCO$_2$ is that the otherwise homogeneously distributed ceramic granules are covered by a polymer surface. To the authors' knowledge, this was the first study overcoming this problem by using a dynamic compression treatment for the composites conducted in an aqueous environment at 37 °C. The treatment tore the polymer surface and β-TCP granules protruded on display as shown in the SEM images. The display of the β-TCP granules on the composite surface is highly important for the early interaction of the composite with cells and tissues, because PLCL lacks biological binding sites (Jeong *et al.*, 2008; Wang *et al.*, 2016) whereas β-TCP has the ability to bind to bone tissue (Barrere *et al.*, 2006; Chatterjea *et al.*, 2013) and induce osteogenic differentiation of mesenchymal stem cells (Marino *et al.*, 2010). In addition, as the compression treatment tore additional holes in the PLCL pore surfaces, it increased the micro porosity and interconnectivity of the composites.

The modulus of the composite was more similar to the modulus of cartilage (2.4-10 MPa) (Beck *et al.*, 2016) than to that of trabecular bone (10.75-13.66 GPa) (Peters *et al.*, 2018), thus mimicking the soft callus formed during natural bone healing. Therefore, a bone defect treated with this composite would still require additional fixation to restrain the defect site. The closest comparable clinically approved composite material to the study composite is the bone void filler chronOS™ Strip from DePuy Synthes, which comprise PLCL and β-TCP granules. The compression strength of the β-TCP/PLCL composite analysed dry at RT was 1.1 MPa at 20 % strain and 3 MPa at 50 % strain. The compressive strength of the chronOS® β-TCP granules is approximately 5 MPa (product manual of chronOS®), which is of the same order as the strength of the composite described in the current study. However, to the authors' knowledge, the strength of the composite chronOS™ Strip has not been reported. Shikinami *et al.* (2006) compared different P$_{(D/L)}$LA-based composites and reported the compression strength of 5.4 MPa for a porous β-TCP/ P$_{(D/L)}$LA (weight ratio 70/30) analysed at RT. Moreover, Mathieu *et al.* (2006) reported the compression strength of approximately 3.5 MPa for a porous P$_{(L)}$LA/β-TCP (weight ratio 90/10) composite also analysed dry at RT. As the requirements for an ideal bone substitute are highly demanding, the development of a scaffold may require compromising between achieving good cell and tissue response, desirable mechanical as well as user-friendly properties (Turnbull *et al.*, 2017).

The compression treatment significantly decreased both modulus and strength at 20 and 50 % strain, when samples were tested dry at RT. However, the aqueous
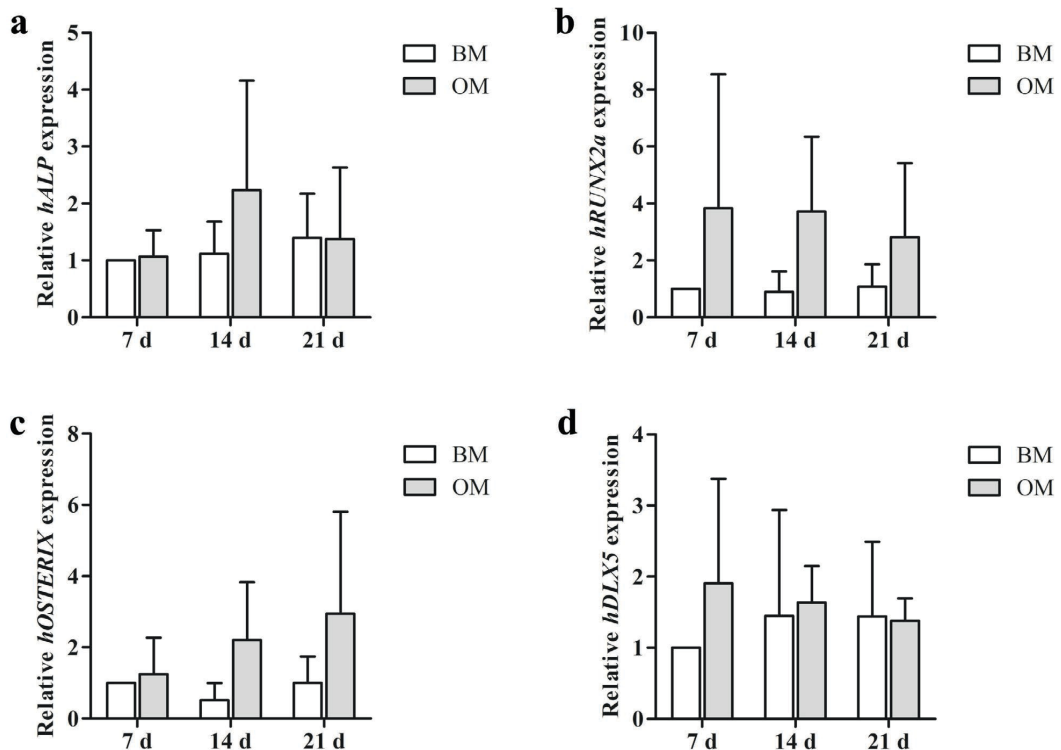

Fig. 6. Relative gene expression of osteogenic genes in hASCs in β-TCP/PLCL composites. (**a**) *ALP*, (**b**) *RUNX2a*, (**c**) *OSTERIX* and (**d**) *DLX5*. Results (*n* = 6) are expressed relative to *hRPLP0* and 7 d BM result.

environment at 37 °C, simulating the physiological environment, diminished these differences. This is due to PLCL's glass transition temperature, which is between 21 and 22 °C (Ahola *et al.*, 2013). β-TCP particles were not able to reinforce the porous composite matrix because the polymer chains seemed to be mobile at 37 °C, making the composite highly elastic. During incubation at 37 °C, both intact and pre-compressed composites started to recover from the initial drop of modulus and strength, as there was a rise from 1 h to 7 d at 37 °C. van der Pol *et al.* (2010) proposed that increasing the amount of β-TCP over 5 wt% in a scCO₂-processed composite would make the composite more brittle and make it lose its ability to sustain any deformation. However, present results contradicted this suggestion. The increase in modulus between 1 h and 7 d at 37 °C was likely to be related to the reorganisation of the polymer matrix, *e.g.* crystallisation or an aging type phenomenon in aqueous environment at 37 °C, enabling the polymer chains to organise towards energetically more stable conformations (Pan *et al.*, 2007; Zong *et al.*, 1999). However, within limits of the present study, the true mechanism could not be determined.

By monitoring the hydrolytic degradation both *in vitro* and *in vivo*, the aim was to define how accurately the *in vitro* degradation extrapolated to the situation *in vivo*. Because the degradation characteristics may depend *e.g.* on the polymer or the manufacturing method, the molecular degradation profile *in vitro* may model relatively accurately the degradation *in vivo* (Weir *et al.*, 2004) or differ significantly (Koepp *et al.*, 2004). The results showed that the hydrolytic degradation of the scCO₂-foamed β-TCP/PLCL composite and the following degradation-dependent structural changes could be studied with very good

accuracy in the *in vitro* model. The small differences in the degradation rate during the first 4 weeks could be related to the β-TCP content, which slows down the hydrolytic degradation by neutralising the acidic degradation products of lactide-based polymers (Niemelä, 2005). Previously, the same polymer and composite with β-TCP content were studied *in vitro* as non-foamed blocks (Ahola *et al.*, 2013). Despite the different initial molecular weight but similar residual monomer content, the molecular weight was similar after 12 weeks of incubation at 37 °C (Ahola *et al.*, 2013) to that of the present foamed scaffolds.

Results showed that the composites were cytocompatible *in vitro*, as hASC viability was very high, with only some dead cells, as observed by live/dead staining. Both live/dead staining and cell proliferation analysis showed that hASCs proliferated more when cultured in OM as compared to BM, as expected according to previous results with hASCs (Kyllönen *et al.*, 2013a; Tirkkonen *et al.*, 2013; Vanhatupa *et al.*, 2015).

Osteogenic differentiation of hASCs in composites was demonstrated by using various methods. Induction of ALP activity clearly occurred in BM and OM, even though the level of ALP activity was significantly higher in OM than in BM at 7 and 14 d. ALP activity as well as *ALP* expression peaked at 14 d, as ALP expression is related to the matrix maturation phase of bone ECM development (Lian *et al.*, 2012). Moreover, total soluble collagen amount was generally very similar in both BM and OM. Collagen amount was only slightly larger in OM at 7 and 21 d as compared to BM. The slight decrease in soluble collagen from 14 to 21 d might be due to the development of osteogenic ECM. Mineralised collagen fibrils are the elementary building blocks
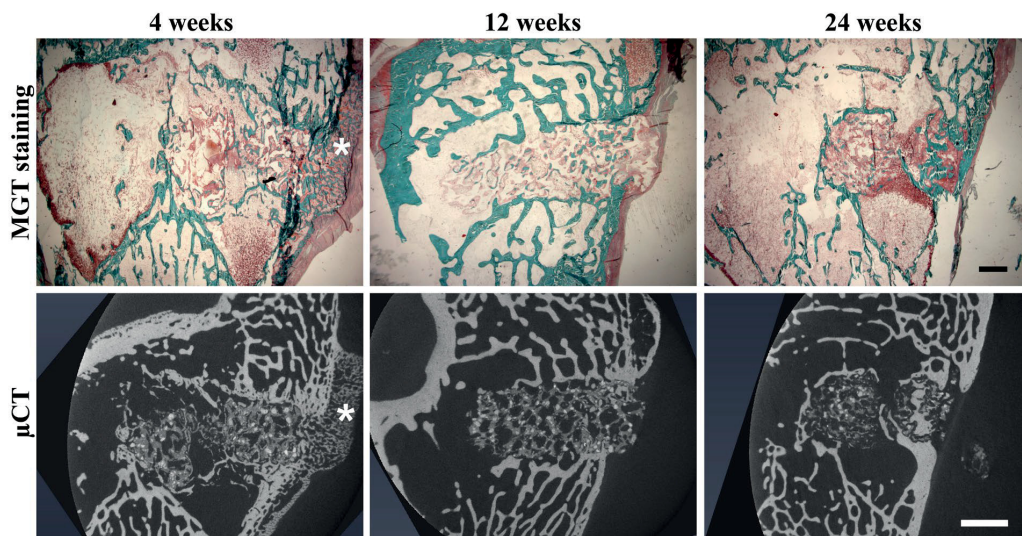

Fig. 7. Bone formation in rabbit femora. Representative images of MGT-stained histological samples (scale bar 1 mm) from rabbit femora with implanted composites and corresponding μCT imaging (scale bar 2 mm) 4, 12 and 24 weeks after implantation. * indicating periosteum-induced bone formation.

of bone (Nair *et al.*, 2013) and the mineralisation of collagen fibrils may affect the solubility of collagen during soluble collagen analysis. Moreover, dense COL-I matrix promotes the osteogenic differentiation of mesenchymal stem cells attaching to it (Buxton *et al.*, 2008). As alizarin red staining already confirmed the formation of a strong mineralised matrix in both BM and OM at 14 d and the immunocytochemical staining of COL-I was especially strong in OM at 14 and 21 d, it is possible that mineralised collagen matrix, typical of bone development, had developed in cell cultures. In addition, the detection of the late osteogenic marker OCN by immunocytochemical staining confirmed the late osteogenic differentiation of hASCs in the composites (Lian *et al.*, 2012). The expression of osteogenic genes was in line with the literature concerning bone development, as *ALP* and *RUNX2a* expression peaks are related to the early phase of differentiation whereas *OSTERIX* expression peaks to the late phase of differentiation (Lian *et al.*, 2012). Moreover, when comparing the formed mineralised matrix on the scaffold in BM to that on the 2D control in BM, the composite itself seemed to induce osteogenic differentiation of hASCs even without the addition of osteogenic supplements.

Bone regeneration within composites implanted in a rabbit distal femur defect model was demonstrated in a 24-week study. During implantation, the composite proved to be easy to handle and implant due to its elasticity and ability to recover after compression. Poly(L-lactide) implants (Pihlajamäki *et al.*, 2006) and composites (van der Pol *et al.*, 2010) have been shown to induce an inflammatory reaction due to acidic degradation products leading to the development of a fibrous capsule around the implant. However, the femur defect model demonstrated that the biocompatibility of the β-TCP/PLCL composite was good, as no formation of fibrous layer, cysts or infection was detected in any of the animals during the 24-week study. Moreover, the composite was shown to be osteoconductive as, according to the MGT staining and μCT images, bone was already able to grow on the surface of the composite and infiltrate inside the porous structure at 4 weeks. In contrast to the present results, van der Pol *et al.* (2010) showed that a PLA/β-TCP (95/5 wt%) composite manufactured by scCO₂ processing induces the formation of a clear fibrous layer between the implant and mineralised tissue at 8 and 16 weeks in sheep femur defects. In concordance with the present results, Pihlman *et al.* (2018) studied the same porous β-TCP/PLCL composites and demonstrated the osteoconductivity and ingrowth of bone and vascular tissue in a rabbit calvarial defect model. Moreover, the β-TCP/PLCL composite gives structural support and blocks the surrounding soft tissues from bulging into the defect (Pihlman *et al.*, 2018). Also, Pihlman *et al.* (2018), in their *in vivo* study, concluded that the mouldable and resilient composite is easier to use in clinics in contrast to most available products used for bone substitutes.

Conclusions

A highly porous, biodegradable, elastic and easy-to-handle β-TCP/PLCL composite to serve as a bone substitute was created. To the authors' knowledge, the present study was the first one reporting a composite manufactured by scCO₂ processing with a high ceramic content (50 wt%) and porosity as high as 65-67 %. Furthermore, β-TCP particles in the processed composites were uncovered by using a dynamic compression treatment.

The β-TCP/PLCL composite was cytocompatible and supported osteogenic differentiation of hASCs *in vitro*. The formation of a collagenous mineralised matrix already after 3 weeks *in vitro* was an especially clear indication of the composite's potential as a bone substitute. Furthermore, the rabbit femur defect model showed that the β-TCP/PLCL composite was biocompatible, as it did not elicit the formation of fibrous capsule, cysts or infection. Finally, the β-TCP/PLCL composite was osteoconductive, as bone tissue was already able to grow on the surface and inside the scaffold at 4 weeks. To conclude, the β-TCP/PLCL composite foamed by using scCO₂ is a very promising bone substitute material and a potential candidate for use in clinics.

References

Ahola N, Veiranto M, Rich J, Efimov A, Hannula M, Seppala J, Kellomäki M (2013) Hydrolytic degradation of composites of poly(L-lactide-co-epsilon-caprolactone) 70/30 and beta-tricalcium phosphate. J Biomater Appl **28**: 529-543.

Barbour SA, King W (2003) The safe and effective use of allograft tissue – an update. Am J Sports Med **31**: 791-797.

Barrere F, van Blitterswijk CA, de Groot K (2006) Bone regeneration: molecular and cellular interactions with calcium phosphate ceramics. Int J Nanomedicine **1**: 317-332.

Beck EC, Barragan M, Tadros MH, Gehrke SH, Detamore MS (2016) Approaching the compressive modulus of articular cartilage with a decellularized cartilage-based hydrogel. Acta Biomater **38**: 94-105.

Bohner M, Miron RJ (2019) A proposed mechanism for material-induced heterotopic ossification. Materials Today **22**: 132-141.

Boyce T, Edwards J, Scarborough N (1999) Allograft bone. The influence of processing on safety and performance. Orthop Clin North Am **30**: 571-581.

Buxton PG, Bitar M, Gellynck K, Parkar M, Brown RA, Young AM, Knowles JC, Nazhat SN (2008) Dense collagen matrix accelerates osteogenic differentiation and rescues the apoptotic response to MMP inhibition. Bone **43**: 377-385.

Campana V, Milano G, Pagano E, Barba M, Cicione C, Salonna G, Lattanzi W, Logroscino G (2014) Bone substitutes in orthopaedic surgery: from basic science to clinical practice. J Mater Sci Mater Med **25**: 2445-2461.

Chatterjea A, van der Stok J, Danoux CB, Yuan H, Habibovic P, van Blitterswijk CA, Weinans H, de Boer J (2013) Inflammatory response and bone healing capacity of two porous calcium phosphate ceramics in critical size cortical bone defects. J Biomed Mater Res A **102**: 1399-1407.

de Misquita MR, Bentini R, Goncalves F (2016) The performance of bone tissue engineering scaffolds in *in vivo* animal models: a systematic review. J Biomater Appl **31**: 625-636.

Diaz-Gomez L, Garcia-Gonzalez CA, Wang J, Yang F, Aznar-Cervantes S, Cenis JL, Reyes R, Delgado A, Evora C, Concheiro A, Alvarez-Lorenzo C (2017) Biodegradable PCL/fibroin/hydroxyapatite porous scaffolds prepared by supercritical foaming for bone regeneration. Int J Pharm **527**: 115-125.

Dominici M, Le Blanc K, Mueller I, Slaper-Cortenbach I, Marini F, Krause D, Deans R, Keating A, Prockop D, Horwitz E (2006) Minimal criteria for defining multipotent mesenchymal stromal cells. The International Society for Cellular Therapy position statement. Cytotherapy **8**: 315-317.

Doube M, Klosowski MM, Arganda-Carreras I, Cordelieres FP, Dougherty RP, Jackson JS, Schmid B, Hutchinson JR, Shefelbine SJ (2010) BoneJ: free and extensible bone image analysis in ImageJ. Bone **47**: 1076-1079.

Duan R, Barbieri D, de Groot F, de Bruijn JD, Yuan H (2018) Modulating bone regeneration in rabbit condyle defects with three surface-structured tricalcium phosphate ceramics. ACS Biomater Sci Eng **4**: 3347-3355.

Duarte ARC, Santo VE, Alves A, Silva SS, Moreira-Silva J, Silva TH, Marques AP, Sousa RA, Gomes ME, Mano JF (2013) Unleashing the potential of supercritical fluids for polymer processing in tissue engineering and regenerative medicine. J Supercrit Fluids **79**: 177-185.

Freeman FE, McNamara LM (2017) Endochondral priming: a developmental engineering strategy for bone tissue regeneration. Tissue Eng Part B Rev **23**: 128-141.

Holmbom J, Sodergard A, Ekholm E, Martson M, Kuusilehto A, Saukko P, Penttinen R (2005) Long-term evaluation of porous poly(epsilon-caprolactone-co-L-lactide) as a bone-filling material. J Biomed Mater Res A **75**: 308-315.

Jeon O, Rhie JW, Kwon IK, Kim JH, Kim BS, Lee SH (2008) *In vivo* bone formation following transplantation of human adipose-derived stromal cells that are not differentiated osteogenically. Tissue Eng Part A **14**: 1285-1294.

Jeong SI, Lee AY, Lee YM, Shin H (2008) Electrospun gelatin/poly(L-lactide-co-epsilon-caprolactone) nanofibers for mechanically functional tissue-engineering scaffolds. J Biomater Sci Polym Ed **19**: 339-357.

Kinaci A, Neuhaus V, Ring DC (2014) Trends in bone graft use in the United States. Orthopedics **37**: e783-788.

Koepp HE, Schorlemmer S, Kessler S, Brenner RE, Claes L, Günther K, Ignatius AA (2004) Biocompatibility and osseointegration of β-TCP: histomorphological and biomechanical studies in a weight-bearing sheep model. J Biomed Mater Res B Appl Biomater **70B**: 209-217.

Kyllönen L, Haimi S, Mannerström B, Huhtala H, Rajala KM, Skottman H, Sandor GK, Miettinen S (2013a) Effects of different serum conditions on osteogenic differentiation of human adipose stem cells *in vitro*. Stem Cell Res Ther **4**: 17. DOI: 10.1186/scrt165.

Kyllönen L, Haimi S, Säkkinen J, Kuokkanen H, Mannerström B, Sandor GK, Miettinen S (2013b) Exogenously added BMP-6, BMP-7 and VEGF may not enhance the osteogenic differentiation of human adipose stem cells. Growth Factors **31**: 141-153.

Lian JB, Stein GS, van Wijnen AJ, Stein JL, Hassan MQ, Gaur T, Zhang Y (2012) MicroRNA control of bone formation and homeostasis. Nat Rev Endocrinol **8**: 212-227.

Lindroos B, Boucher S, Chase L, Kuokkanen H, Huhtala H, Haataja R, Vemuri M, Suuronen R, Miettinen S (2009) Serum-free, xeno-free culture media maintain the proliferation rate and multipotentiality of adipose stem cells *in vitro*. Cytotherapy **11**: 958-972.

Marino G, Rosso F, Cafiero G, Tortora C, Moraci M, Barbarisi M, Barbarisi A (2010) Beta-tricalcium phosphate 3D scaffold promote alone osteogenic differentiation of human adipose stem cells: *in vitro* study. J Mater Sci Mater Med **21**: 353-363.

Mathieu LM, Montjovent MO, Bourban PE, Pioletti DP, Manson JA (2005) Bioresorbable composites prepared by supercritical fluid foaming. J Biomed Mater Res A **75**: 89-97.

Mathieu LM, Mueller TL, Bourban PE, Pioletti DP, Muller R, Manson JA (2006) Architecture and properties of anisotropic polymer composite scaffolds for bone tissue engineering. Biomaterials **27**: 905-916.

Nair AK, Gautieri A, Chang SW, Buehler MJ (2013) Molecular mechanics of mineralized collagen fibrils in bone. Nat Commun **4**: 1724. DOI: 10.1038/ncomms2720.

Niemelä T (2005) Effect of β-tricalcium phosphate addition on the *in vitro* degradation of self-reinforced poly-L,D-lactide. Polym Degrad Stab **89**: 492-500.

Ojansivu M, Vanhatupa S, Björkvik L, Häkkänen H, Kellomäki M, Autio R, Ihalainen JA, Hupa L, Miettinen S (2015) Bioactive glass ions as strong enhancers of osteogenic differentiation in human adipose stem cells. Acta Biomater **21**: 190-203.

Pan P, Zhu B, Inoue Y (2007) Enthalpy relaxation and embrittlement of poly(l-lactide) during physical aging. Macromolecules **40**: 9664-9671.

Peters AE, Akhtar R, Comerford EJ, Bates KT (2018) The effect of ageing and osteoarthritis on the mechanical properties of cartilage and bone in the human knee joint. Sci Rep **8**. DOI: 10.1038/s41598-018-24258-6.

Pihlajamäki H, Böstman O, Tynninen O, Laitinen O (2006) Long-term tissue response to bioabsorbable poly-l-lactide and metallic screws: an experimental study. Bone **39**: 932-937.

Pihlman H, Keranen P, Paakinaho K, Linden J, Hannula M, Manninen IK, Hyttinen J, Manninen M, Laitinen-Vapaavuori O (2018) Novel osteoconductive β-tricalcium phosphate/poly(L-lactide-co-e-caprolactone) scaffold for bone regeneration: a study in a rabbit calvarial defect. J Mater Sci Mater Med **29**. DOI: 10.1007/s10856-018-6159-9.

Rouwkema J, Rivron NC, van Blitterswijk CA (2008) Vascularization in tissue engineering. Trends Biotechnol **26**: 434-441.

Schindelin J, Arganda-Carreras I, Frise E, Kaynig V, Longair M, Pietzsch T, Preibisch S, Rueden C, Saalfeld S, Schmid B, Tinevez JY, White DJ, Hartenstein V, Eliceiri K, Tomancak P, Cardona A (2012) Fiji: an open-source platform for biological-image analysis. Nat Methods **9**: 676-682.

Shikinami Y, Okazaki K, Saito M, Okuno M, Hasegawa S, Tamura J, Fujibayashi S, Nakamura T (2006) Bioactive and bioresorbable cellular cubic-composite scaffolds for use in bone reconstruction. J R Soc Interface **3**: 805-821.

Temple JP, Hutton DL, Hung BP, Huri PY, Cook CA, Kondragunta R, Jia X, Grayson WL (2014) Engineering anatomically shaped vascularized bone grafts with hASCs and 3D-printed PCL scaffolds. J Biomed Mater Res A **102**: 4317-4325.

Tirkkonen L, Haimi S, Huttunen S, Wolff J, Pirhonen E, Sandor GK, Miettinen S (2013) Osteogenic medium is superior to growth factors in differentiation of human adipose stem cells towards bone-forming cells in 3D culture. Eur Cell Mater **25**: 144-158.

Turnbull G, Clarke J, Picard F, Riches P, Jia L, Han F, Li B, Shu W (2017) 3D bioactive composite scaffolds for bone tissue engineering. Bioact Mater **3**: 278-314.

van der Pol U, Mathieu L, Zeiter S, Bourban PE, Zambelli PY, Pearce SG, Boure LP, Pioletti DP (2010) Augmentation of bone defect healing using a new biocomposite scaffold: an *in vivo* study in sheep. Acta Biomater **6**: 3755-3762.

Van der Stok J, Van Lieshout EM, El-Massoudi Y, Van Kralingen GH, Patka P (2011) Bone substitutes in the Netherlands – a systematic literature review. Acta Biomater **7**: 739-750.

Vanhatupa S, Ojansivu M, Autio R, Juntunen M, Miettinen S (2015) Bone morphogenetic protein-2 induces donor-dependent osteogenic and adipogenic differentiation in human adipose stem cells. Stem Cells Transl Med **4**: 1391-1402.

Wang Z, Lin M, Xie Q, Sun H, Huang Y, Zhang D, Yu Z, Bi X, Chen J, Wang J, Shi W, Gu P, Fan X (2016) Electrospun silk fibroin/poly(lactide-co-epsilon-caprolactone) nanofibrous scaffolds for bone regeneration. Int J Nanomedicine **11**: 1483-1500.

Weir NA, Buchanan FJ, Orr JF, Dickson GR (2004) Degradation of poly-L-lactide. Part 1: *in vitro* and *in vivo* physiological temperature degradation. Proc Inst Mech Eng H **218**: 307-319.

Wilson SM, Goldwasser MS, Clark SG, Monaco E, Bionaz M, Hurley WL, Rodriguez-Zas S, Feng L, Dymon Z, Wheeler MB (2012) Adipose-derived mesenchymal stem cells enhance healing of mandibular defects in the ramus of swine. J Oral Maxillofac Surg **70**: e193-203.

Yuan H, Fernandes H, Habibovic P, de Boer J, Barradas AM, de Ruiter A, Walsh WR, van Blitterswijk CA, de Bruijn JD (2010) Osteoinductive ceramics as a synthetic alternative to autologous bone grafting. Proc Natl Acad Sci U S A **107**: 13614-13619.

Zadpoor AA (2015) Bone tissue regeneration: the role of scaffold geometry. Biomater Sci **3**: 231-245.

Zong X, Wang Z, Hsiao BS, Chu B, Zhou JJ, Jamiolkowski DD, Muse E, Dormier E (1999) Structure and morphology changes in absorbable poly(glycolide) and poly(glycolide-co-lactide) during *in vitro* degradation. Macromolecules **32**: 8107-8114.

Web Reference

1. https://eur-lex.europa.eu/legal-content/EN/TXT/?uri=CELEX%3A32017R0745 [05-08-2019]

2. https://worldwide.espacenet.com/publicationDetails/originalDocument?FT=D&date=20190215&DB=&locale=en_EP&CC=FI&NR=127762B&KC=B&ND=4 [12-07-2019]

Discussion with Reviewers

Ryan Porter: Much attention has been paid to the compressive strength of potential bone graft

substitutes. However, existing composite scaffolds with the porosity needed for osteoconduction do not approach the modulus required to replace lost bone function and avoid the need for bone fixation – particularly for lower extremity defects. If immediate restoration of bone mechanical properties is not a design goal, what factors determine the strength needed of candidate scaffolds for bone repair? Would this differ for grafts used in maxillofacial *versus* long bone defects?
Authors: The main aims in composite development are optimal porosity, biocompatibility and osteoconductivity. In addition, easy intra-operative tailoring is highly important, as, for instance, ceramics are not easy to handle or tailor during a surgery, which hinders surgeons' work. With that said, future efforts aim to improve composite mechanical properties to create a composite with similar modulus to subchondral spongiosa. The requirements for mechanical strength of the scaffold are, of course, lower in maxillofacial defects in comparison to long bone defects and, therefore, the composite described in the study is suitable for non-load bearing sites.

Ryan Porter: Supercritical CO$_2$ has also been used for biomaterial sterilisation processes, including bone allografts. Was the γ-irradiation step included for precautionary measures? Would both steps be required in a good manufacturing practice (GMP) manufacturing protocol for the proposed composite?
Authors: It is true that the processing method can also be used as a sterilisation method. γ-irradiation sterilisation was used for precautionary measures and because it is the commonly used and highly trusted sterilisation method among clinical products. The composite is classified as a medical device and, therefore, there is no need for a GMP-level manufacturing protocol but an ISO13485 manufacturing protocol is sufficient.

Ryan Porter: What might be the challenges to clinically translate bone graft alternatives manufactured using supercritical CO$_2$?
Authors: These are highly important matters when developing a clinical product. The challenges in clinical translation of scCO$_2$-processed structures are related to producing a homogenous pore structure in a reproducible manner. Furthermore, the scalability of the processing is another challenge to overcome in case of a large-scale production.

Pamela Habibovic: A problem of the *in vitro* experiments is the (partially strong) osteogenic differentiation in BM samples. This could indicate pre-differentiation of the used cells, pointing towards an activation of differentiation by the material itself or problems in the assays. This could be clarified by including data of suitable control groups in the results section, *e.g.* cells cultured in BM and OM on tissue culture plastic *etc.*.
Authors: The reason for not using a 2D well plate control was the challenge related to the differences between experimental setups in 3D and 2D. Due to these differences, *e.g.* notable differences in cell seeding density and cell attachment, the results between the two setups would not be fully comparable.

Editor's note: The Scientific Editor responsible for this paper was Joost de Bruijn.

PUBLICATION
IV

3D scaffolds of PCL/copper-doped bioactive glass: architecture engineering with additive manufacturing and cellular assessments in a co-culture of hBMSCs and endothelial cells

Wang X.*, Zhang B.*, Pitkänen S.*, Ojansivu M., Xu C., Hannula M., Hyttinen J., Miettinen S., Hupa L., Wallace G.

3D Scaffolds of Polycaprolactone/Copper-Doped Bioactive Glass: Architecture Engineering with Additive Manufacturing and Cellular Assessments in a Coculture of Bone Marrow Stem Cells and Endothelial Cells

Xiaoju Wang,*,[†,#] Binbin Zhang Molino,[‡,#] Sanna Pitkänen,[§,‖,#] Miina Ojansivu,[§,‖] Chunlin Xu,[†] Markus Hannula,[⊥] Jari Hyttinen,[⊥] Susanna Miettinen,[§,‖] Leena Hupa,[†] and Gordon Wallace[‡]

[†]Johan Gadolin Process Chemistry Centre, Åbo Akademi University, Piispankatu 8, 20500 Turku, Finland

[‡]ARC Centre of Excellence for Electromaterials Science, Intelligent Polymer Research Institute, University of Wollongong, Northfields Avenue, Wollongong, New South Wales 2522, Australia

[§]Adult Stem Cell Group, BioMediTech, Faculty of Medicine and Health Technology, Tampere University, Arvo Ylpön katu 34, P.O. BOX 100, FI-33014 Tampere, Finland

[‖]Research, Development and Innovation Centre, Tampere University Hospital, Arvo Ylpön katu 6, P.O. BOX 2000, FI-33521 Tampere, Finland

[⊥]Computational Biophysics and Imaging Group, BioMediTech, Faculty of Medicine and Health Technology, Tampere University, FI-33014 Tampere, Finland

Ⓢ Supporting Information

ABSTRACT: The local delivery of Cu^{2+} from copper-doped bioactive glass (Cu-BaG) was combined with 3D printing of polycaprolactone (PCL) scaffolds for its potent angiogenic effect in bone tissue engineering. PCL and Cu-BaG were, respectively, dissolved and dispersed in acetone to formulate a moderately homogeneous ink. The PCL/Cu-BaG scaffolds were fabricated via direct ink writing into a cold ethanol bath. The architecture of the printed scaffolds, including strut diameter, strut spacing, and porosity, were investigated and characterized. The PCL/Cu-BaG scaffolds showed a Cu-BaG content-dependent mechanical property, as the compressive Young's modulus ranged from 7 to 13 MPa at an apparent porosity of 60%. The ion dissolution behavior in simulated body fluid was evaluated, and the hydroxyapatite-like precipitation on the strut surface was confirmed. Furthermore, the cytocompatibility of the PCL/Cu-BaG scaffolds was assessed in human bone marrow stem cell (hBMSC) culture, and a dose-dependent cytotoxicity of Cu^{2+} was observed. Here, the PCL/BaG scaffold induced the higher expression of late osteogenic genes *OSTEOCALCIN* and *DLX5* in comparison to the PCL scaffold. The doping of Cu^{2+} in BaG elicited higher expression of the early osteogenic marker gene *RUNX2a* but decreased the expression of late osteogenic marker genes *OSTEOCALCIN* and *DLX5* in comparison to the PCL/BaG scaffold, demonstrating the suppressing effect of Cu^{2+} on osteogenic differentiation of hBMSCs. In a coculture of hBMSCs and human umbilical vein endothelial cells, both the PCL/BaG and PCL/Cu-BaG scaffolds stimulated the formation of a denser tubule network, compared to the PCL scaffold. Meanwhile, only slightly higher gene expression of *vWF* was observed with the PCL/Cu-BaG scaffold than with the PCL/BaG scaffold, indicating the potent angiogenic effect of the released Cu^{2+}.

KEYWORDS: *3D printing, tissue engineering scaffold, angiogenesis, polycaprolactone, copper-doped bioactive glass, gradient porosity, coculture of mesenchymal stem cells and endothelial cells*
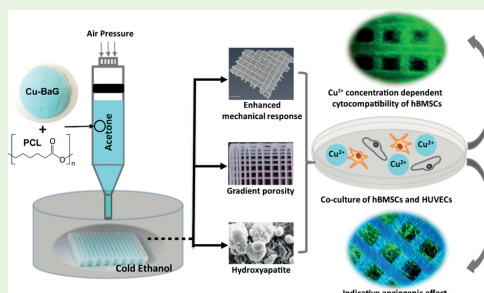
■ INTRODUCTION

Synthetic bone grafts that resemble the architecture and composition of the bone extracellular matrix are always sought by biomaterial scientists and surgeons to overcome the limitations of bone autografts and allografts in the treatments of large bone defects in patients.[1−3] The application of tissue engineering (TE) scaffolds has emerged as a strategic approach for bone reconstitution, as it combines the engineered biomaterial structure, soluble/mechanical factors (e.g., release of stimulating bio(macro)molecules/ions), and regenerative cells to provide a structural and physiological support to the spatial tissue growth.[4,5]

As the first man-made biomaterial capable of forming chemical bonding to bone,[6] bioactive glasses (BaGs) have been extensively explored during the past several decades in bone TE because of their osteostimulative capability to guide and stimulate the bone growth.[7−9] However, successful neovascularization (the sprouting of blood vessels) in the bone TE constructs remains challenging.[10,11] Several well-established compositions of silicate BaGs, such as 45S5 and S53P4, are capable of inducing angiogenic differentiation of mesenchymal stem cells (MSCs).[12,13] This is attributed to their ionic dissolution products of soluble Ca, Si, and P that can upregulate the genes related to angiogenesis, such as those encoding vascular endothelial growth factor (VEGF) and basic fibroblast growth factor (bFGF).[13,14] Moreover, the essential participation of Cu^{2+} in angiogenesis has been acknowledged: Cu^{2+} in a proper dosage has a clear proangiogenic function by activating a group of proangiogenic growth factors, including VEGF and platelet-derived growth factor (PDGF), therefore promoting endothelial cell proliferation and tubule formation.[15−17] At present, the local delivery of Cu^{2+} from the Cu-doped BaG to induce angiogenesis has been investigated in various forms, e.g., porous scaffold of Cu-doped mesoporous BaG,[18] composite hydrogel containing Cu-doped mesoporous BaG,[19] functional coating of Cu-doped BaG nanoparticles and electrospun nanofibers of Cu-doped BaG.[20−22] Strategically, the incorporation of Cu-doped BaG in bone TE scaffolds may offer a straightforward approach to address the neovascularization challenge in bone tissue regeneration.

The critical aspects to be taken into consideration when designing a bone TE scaffold are the selection of suitable biomaterials to support cell adhesion and proliferation as well as the definitive structural parameters of the scaffold to mimic the native bone tissue. Polycaprolactone (PCL), a bioresorbable polymer extensively used in various biomedical applications, offers excellent material properties and cytocompatibility.[23] The extrusion-based 3D printing (3DP) techniques offer a high-level control of the scaffold architecture, including pore size, distribution, and interconnectivity.[24] Previously, the TE scaffolds for bone regeneration manufactured by the 3DP using PCL or its composites with inorganic minerals such as the microparticles of tricalcium phosphate,[25] hydroxyapatite, and calcium polyphosphate have been studied.[26,27] Conventionally, the melted PCL is used as the carrier phase for the mineral microparticles, and the printed constructs keep the shape fidelity through fast cooling after being extruded through the nozzle in 3DP.

In the current study, a solvent-based approach was proposed to prepare the well-dispersed BaG microparticles of Cu-doped S53P4 (S53P4−Cu1) in PCL solution (in acetone) as a homogeneous ink fed in the direct ink writing (DIW), and the printed struts solidified rapidly in the cold ethanol due to the solubility change of PCL, thus facilitating the fabrication of the PCL/Cu-BaG composite scaffolds. This method offers a facile printing as no heating is needed and also extends the possibility to incorporate other bioactive molecules, such as growth factors, within the scaffold during the printing process. Then, the ion dissolution behavior and bioactivity (in terms of supporting the hydroxyapatite precipitation) of the composite scaffolds were evaluated in simulated body fluid (SBF). Furthermore, the cytocompatibility of the composite scaffolds as well as the impact of the ion release on the early osteogenic differentiation of human bone marrow stem cells (hBMSCs) were evaluated *in vitro*. Finally, we studied whether the Cu^{2+} released from the 3D scaffolds could promote the angiogenesis in a coculture of hBMSCs and human umbilical vein endothelial cells (HU-VECs). The observations are indicative for utilizing the Cu-doped BaG aiming at enhancing the vascularization in TE scaffolds.

■ MATERIALS AND EXPERIMENTAL

Glass Melting of BaGs (S53P4 and S53P4−Cu1) and Preparation of BaG Microparticles. Two BaGs, S53P4 (53% SiO_2−4%P_2O_5−20%CaO−23%Na_2O wt %) and S53P4−Cu1 (53% SiO_2−4%P_2O_5−19%CaO−23%Na_2O−1%CuO wt %), were prepared using the melt-quenching method. The batches consisted of analytical grade reagents Na_2CO_3, $CaCO_3$, $CaHPO_4\cdot2H_2O$, $Cu(NO_3)_2\cdot2.5H_2O$ (all purchased from Sigma-Aldrich), and Belgian glass quality quartz sand (0.32 mm, Varnia Oy). The batches were melted in a Pt crucible at 1360 °C for 3 h, cast, annealed, crushed, and remelted to ensure the homogeneity. The annealed glass block was crushed and gradually fractionated with a set of woven wire mesh sieves with #mm from 500 μm down to 45 μm (laboratory test sieves, Retsch GmbH) to give several powdered fractions. The finest powder fraction, which could pass through the #mm = 45 μm sieve, was further milled for 10 min using a benchtop planetary ball mill (MinMill, Philips) to obtain the fine particles of BaG for the DIW ink formulation.

Scaffolds Fabrication via DIW. A 30 g portion of PCL (M_w = 80 000, Aldrich) was dissolved in 100 mL of acetone overnight in a 50 °C water bath to obtain a viscous solution, which was then used as the carrier phase for the BaG particles in the ink formulation. The BaG particles were homogeneously dispersed into the viscose PCL solution using a planetary centrifugal mixer (ARE-250, Thinky Corporation) at a rotation speed of 2000 rpm. The compositional ratio between the PCL and BaG was adjusted to 4:1, 2:1, or 1:1, according to the content of PCL and BaG in wt %.

The scaffold fabrication via DIW was carried out using an adapted Korean Institute for Machinery and Materials (KIMM) Bioplotter. The KIMM Bioplotter software was used to produce a G-code tooling path for printing. Square block models (x = 10 mm, y = 10 mm, and z = 1, 2, or 4 mm) were designed with the Bioplotter software, and the strut spacing (SS) was defined as either 400 or 800 μm between the center of the struts. For the scaffolds with a gradient porosity, the SS was decreased from the center to the edge of the scaffold, from 800 to 200 μm. The viscous ink as formulated was loaded into a fluid dispensing system (Optimum by Nordson EFD), with the syringe barrel installed onto the KIMM printer and connected to an air pressure regulator. A precision tip made of stainless steel (25GA, Nordson EFD) was used as the dispensing nozzle. The scaffolds were printed layer-by-layer through extruding the ink into a cold ethanol bath. The feed rate was kept constant at 2 mm s^{-1}, and the extrusion pressure was then manually adjusted in the range 1.5−3.0 bar according to the viscosity of the ink for an optimal printing process. The scaffolds were then soaked in absolute ethanol for 24 h, and the ethanol was replaced every 8 h to complete the phase exchange of PCL from acetone to ethanol. Finally, the scaffolds were collected and dried in air before further characterizations.

Scaffold Imaging with Optical Microscopy, Scanning Electron Microscopy (SEM), and Micro Computed Tomography (μ-CT). The microscopic features of scaffolds were observed by using a LEICA M205A optical microscope. The reported strut diameter and strut spacing were assessed in triplicate (n = 3). The morphological features of the scaffold strut were characterized by using SEM. To assess the macroporosity, μ-CT was used to analyze the inner structure of the scaffolds. The imaging was performed with an Xradia MicroXCT-400 (Zeiss, Pleasanton, CA) device: 1600 projections were taken with a pixel size of 19.70 μm. The source voltage was set to 80 kV, and the source current was 125 μA. To achieve the desired image quality, a 3 s exposure time was used. The device manufacturer's XMReconstructor software was used to reconstruct the 3D volumes. Image segmentation was done with Avizo software (Thermo Fisher Scientific, Waltham, MA) using manual thresholding. Approximately 8.2 × 8.2 × 2.4 mm

volumes were selected, and the porosity, strut size, and pore size of the 3D scaffolds were calculated with the BoneJ plugin in the Fiji program.

Thermogravimetric (TG) Analysis. TG analysis of the scaffolds was performed using a differential thermal analysis instrument (Netzsch STA 449F1) in the gas flow of synthetic air at a speed of 100 mL min^{-1}. The temperature ramped up to 850 °C at an elevating rate of 10 °C min^{-1}. The BaG wt % of the scaffold was determined as relative to the residue content in the TG analysis.

Mechanical Tests. The compressive response of the printed scaffolds was measured with a Shimadzu EZ-L Universal Mechanical Tester. Scaffolds were compressed at 1 mm min^{-1} and a maximum loading of 500 N was applied. When calculating the strength, the dimensions along the x, y, and z-axes measured with a digital caliper were used. Strain was registered as a function of stress for an applied and increasing force and the measurements were conducted in triplicate to elaborate the compressive modulus based on the stress vs strain curves.

Ion Release Study of PCL/Cu-BaG Scaffolds in SBF. The SBF was prepared according to the protocol of Kokubo, and the exact composition is presented in the Supporting Information S1.[28] The 3D scaffolds were immersed in 10 mL of SBF in airtight polyethylene containers that were placed in an incubating orbital shaker held at 37 °C and agitated at 100 rpm. The samples were incubated for a total period of 30 days and sampled at intervals of 6 h, 24 h, 3 days (3 d), 7 d, 14 d, 22 d, and 30 d. At each time point, 0.5 mL of the immersion solution was sampled, and 0.5 mL of fresh SBF was additionally replenished for a continued immersion. The ionic concentrations of Ca, P, Si, and Cu ions in the sampled solution were analyzed with an inductively coupled plasma optical emission spectrometer (ICP-OES) (Optima 5300 DV, PerkinElmer, Shelton, CT). For the ICP-OES measurements, the sampled aliquots were diluted 10 times with deionized H$_2$O. At the end of the immersion test, the scaffolds were carefully collected, washed extensively with ethanol, and dried in the air. The surface morphology and elemental analysis of the scaffolds were characterized with an SEM-EDXA instrument (EDXA, LEO Gemini 1530 with a Thermo Scientific UltraDry Silicon Drift Detector, X-ray detector by Thermo Scientific).

Isolation and Characterization of hBMSCs and HUVECs. The hBMSCs were isolated from a bone marrow aspirate sample obtained from a surgical procedure at the Department of Orthopedics and Traumatology, Tampere University Hospital, with the patient's consent. The hBMSCs used in the study were harvested from a female donor of 80 years of age. The study was conducted in accordance with the Ethics Committee of the Pirkanmaa Hospital District, Tampere (R15174). hBMSCs were isolated using centrifugation through a Ficoll gradient. First, the bone marrow aspirate was suspended in Dulbecco's phosphate buffered saline (DPBS), and the solution was pushed through a 100 μm cell strainer. The bone marrow aspirate solution was centrifuged, and the fat layer was removed. Thereafter, the bone marrow aspirate solution was pipetted carefully on top of a Ficoll gradient (Histopaque-1077; 1.077 g mL^{-1}; Sigma-Aldrich; St. Louis, MO). A 2.6 mL portion of Ficoll (Histopaque; Sigma-Aldrich) per 1 mL of bone marrow aspirate sample was used. The bone marrow aspirate solution was centrifuged for 20 min at 800g, and the mononucleated hBMSCs were harvested from an interphase between the Ficoll and plasma phases. The cells were washed twice with 5 mL of MEM Alpha medium (Thermo Fisher Scientific, Waltham, MA) per 1 mL of collected interphase, and the suspension was centrifuged for 15 min at 400g. The cell pellet was suspended in basic medium (BM) consisting of MEM Alpha medium (Thermo Fisher Scientific), 5% human serum (HS; BioWest, Nuaillé, France), and 1% antibiotics (100 U mL^{-1} penicillin; 100 U mL^{-1} streptomycin; Lonza, Basel, Switzerland) with 5 ng mL^{-1} human FGF-2 (Miltenyi Biotec; Bergisch Gladbach, Germany). Isolated hBMSCs were expanded in BM at 37 °C in 5% CO$_2$, and medium was changed twice per week. Cells were detached with TrypLE Select (Thermo Fisher Scientific). The experiments were carried out at passage 3.

HUVECs were extracted from the umbilical cord acquired from scheduled Cesarean section at the Department of Obstetrics and Gynecology, Tampere University Hospital, with the donor's consent according to Hamilton et al.[29] The study was conducted in accordance with the Ethics Committee of the Pirkanmaa Hospital District,

Tampere (R13019). Briefly, the cord was separated from the placenta; the umbilical vein was cannulated with a 20G needle, and the needle was secured by clamping the cord over the needle with a clamp. The vein was perfused with PBS to wash out blood, and then, the opposing end of the umbilical vein was clamped. Subsequently, the vein was infused with collagenase II (Sigma). The umbilical cord was incubated in a water bath at 37 °C for 15 min. After incubation, the collagenase solution containing HUVECs was flushed from the cord into a 50 mL polypropylene tube. The cells were centrifuged at 1200 rpm for 6 min and resuspended in EGM-2 BulletKit (Lonza) medium supplemented with 2% HS and seeded into 25 cm^3 flasks. The HUVECs were cultured at 37 °C in 5% CO$_2$, and the medium was changed twice per week. Cells were detached with TrypLE Select (Thermo Fisher Scientific). The experiments were carried out at passage 3.

To verify the mesenchymal origin of the hBMSCs and the endothelial phenotype of HUVECs, surface marker expression was characterized by flow cytometry (FACSAria; BD Biosciences, Erembodegem, Belgium) as described previously, as documented in Supporting Information S2.[30]

Cell Seeding and Culture on Scaffolds. In the cell culture study, the PCL scaffolds were used as a control to the composite scaffolds; the scaffolds PCL/S53P4 were also included as a Cu-free control to the scaffolds of PCL/S53P4–Cu1. All the tested scaffolds (10 mm × 10 mm × 1 mm) were sterilized by incubating the scaffolds 2 × 10 min in 70% ethanol, and then, the scaffolds were left to dry for 2 h in a biosafety cabinet. Thereafter, the scaffolds were incubated in BM for 48 h prior to cell seeding.

All scaffolds' ability to support hBMSC viability, proliferation, and early osteogenic differentiation was evaluated in hBMSC culture. hBMSCs were seeded, 50 000 per scaffold, in a 50 μL OM (BM with 200 μM ascorbic acid 2-phosphate (Sigma-Aldrich), 10 mM β-glycerophosphate (Sigma-Aldrich), and 5 nM dexamethasone (Sigma-Aldrich)) drop on to the scaffolds. Cells were allowed to attach for 3 h before adding 2 mL of OM per well. The medium was changed to a fresh one twice per week during the experiment.

The scaffolds' ability to support vascularization was assessed in the coculture experiment with hBMSCs and HUVECs. Only PCL, PCL/S53P4 = 4:1, and PCL/S53P4–Cu1 = 4:1 scaffolds were used in the coculture experiment due to the observed cytotoxicity of higher S53P4–Cu1 content with the other compositional ratios. The originally printed scaffolds (10 mm × 10 mm × 1 mm and d = 400 μm) were cut into four quarters for further use. hBMSCs were seeded, 20 000 per scaffold, and cultured for 6 d before seeding an equal amount of HUVECs. After seeding the HUVECs, the medium was changed to EGM-2 (Lonza, Basel, Switzerland). hBMSCs alone were used as a control group and cultured in OM throughout the experiment.

Cell Viability and Proliferation. Cell viability was evaluated qualitatively by staining the hBMSCs with fluorescent live/dead-staining probes (Thermo Fisher Scientific) after 1 d and 14 d of culture. The samples were incubated for 45 min at room temperature in a mixture of 0.5 μM calcein-AM and 0.25 μM ethidium homodimer-1. Images of viable cells (green fluorescence) and dead cells (red fluorescence) were taken using an Olympus IX51 phase contrast microscope with fluorescence optics and Olympus DP30BW camera (Olympus, Tokyo, Japan).

Cell viability was quantitatively analyzed by a lactate dehydrogenase (LDH) activity assay (Abcam, Cambridge, UK). The LDH reduces NAD to NADH, which then interacts with a specific probe to produce a color. The medium samples were collected at every medium change and stored at −20 °C until analysis. The analysis was conducted according to the manufacturer's protocol. After 30 min of incubation at room temperature, the absorbance, i.e., the intensity of the color, was determined at 450 nm with a microplate reader (Victor 1420 Multilabel Counter; Wallac; Turku, Finland).

Cell number was determined quantitatively after 7 d and 14 d of hBMSC culture by analyzing the total amount of DNA by a CyQUANT cell proliferation assay kit (Thermo Fisher Scientific) as reported previously.[31] CyQUANT GR dye emits fluorescence when bound to nucleic acids. Samples were analyzed after two freeze–thaw cycles, and

Table 1. Primer Sequences and Accession Numbers of Genes Analyzed by qRT-PCR

name		5′-sequences-3′	product size (bp)	accession number
hRPLP0	Frw	AATCTCCAGGGGCACCATT	70	NM_001002
	Rev	CGCTGGCTCCCACTTTGT	70	NM_001002
hOSTEOCALCIN	Frw	AGCAAAGGTGCAGCCTTTGT	63	NM_000711
	Rev	GCGCCTGGGTCTCTTCACT	63	NM_000711
hRUNX2a	Frw	CTTCATTCGCCTCACAAACAAC	62	NM_001024630.3
	Rev	TCCTCCTGGAGAAAGTTTGCA	62	NM_001024630.3
hDLX5	Frw	ACCATCCGTCTCAGGAATCG	75	NM_005221.5
	Rev	CCCCCGTAGGGCTGTAGTAGT	75	NM_005221.5

fluorescence was measured at 480/520 nm with a microplate reader (Victor 1420, Wallac).

Cu^{2+} Concentration in Culture Medium of hBMSCs. In the culture of hBMSCs, the medium samples were collected from 3 parallel wells at 2 d, 6 d, and 13 d while the medium was changed and pooled as one sample per time point. The concentration of Cu^{2+} in the sample was analyzed by the ICP-OES analysis using the same protocol as described in the earlier Ion Release Study of PCL/Cu-BaG Scaffolds in SBF section.

Alkaline Phosphatase Activity. Alkaline phosphatase (ALP) activity was determined after 7 d and 14 d of hBMSC culture as described previously.[31] The ALP activity was determined from the same cell lysates as the total DNA content. Absorbance was measured at 405 nm (Victor 1420, Wallac).

Quantitative Real-Time PCR. The relative expression of endothelial marker genes PECAM and vWF was evaluated with quantitative real-time reverse transcription polymerase chain reaction (qRT-PCR) at 6 d (hBMSCs only), 11 d, and 20 d (hBMSCs only and hBMSCs+HUVECs coculture) time points as previously described.[32] The relative expression of osteogenic genes RUNX2a, OSTEOCAL-CIN, and DLX5 was analyzed with qRT-PCR at 11 d and 20 d time points (hBMSCs only and hBMSCs+HUVECs coculture). The data was normalized to the expression of a housekeeping gene RPLP0 (human acidic ribosomal phosphoprotein P0), and the calculations were conducted using a previously described mathematical model.[33] For vWF and PECAM, the QuantiTect primer assays were used (Qiagen, Hilden, Germany). The primer sequences and accession numbers for RPLP0 and osteogenic genes RUNX2a, OSTERIX, and DLX5 are listed in Table 1. The qRT-PCR mixture contained cDNA, primers, and SYBR Green PCR Master Mix (Applied Biosystems). The reactions were carried out with an ABIPRISM 7300 sequence detection system, and the results were analyzed with AbiPrism 7300 sequence detection system software (Applied Biosystems).

Immunocytochemical Staining. The expression of endothelial marker proteins vWF and CD31 (the product of the PECAM gene) was characterized with immunocytochemical staining after 13 d and 20 d of culture (hBMSCs only and hBMSCs+HUVECs coculture). The protocol was conducted as previously described.[32] The following primary antibodies were used: CD31 monoclonal mouse antihuman antibody (dilution 1:20, Dako, Agilent, Santa Clara, CA) and rabbit polyclonal anti-vWF antibody (dilution 1:100, Abcam). The primary antibodies were incubated overnight at +4 °C. The secondary antibodies goat antimouse Alexa Fluor 488 (for CD31 staining; dilution 1:200; Thermo Fisher Scientific) and goat antirabbit Alexa Fluor 568 (for vWF staining; dilution 1:500; Thermo Fisher Scientific) were incubated for 1 h at room temperature. The images were acquired with an Olympus IX51 phase contrast microscope with fluorescence optics and Olympus DP30BW camera.

Statistical Testing. Statistical testing was conducted with SPSS version 23 (IBM, Armonk, NY) using a nonparametric test due to small sample size. The effects of the scaffolds on cell viability, cell amount, ALP activity, and gene expression were compared using the Kruskal–Wallis test with Mann–Whitney U post hoc test and Bonferroni correction. The results were considered significant when $p < 0.05$. The cell culture experiments were repeated with 1 donor line with 3 or 4 parallel samples ($n = 3$ or $n = 4$). However, most likely due to the small

sample size, no significant differences between the test groups were detected.

RESULTS

Scaffolds Fabrication via DIW and Morphological Features. In this work, we used a viscous solution of PCL dissolved in acetone as the carrier phase to disperse the BaG microparticles to formulate a homogeneous ink. Up to 50% of BaGs calculated as the dry weight in PCL/BaG could be mixed into the ink with the aid of orbital mixing. In DIW, the printing nozzle was immersed in a cold ethanol bath, and the printed struts solidified as extruded due to the solubility change of PCL in acetone (soluble) and in ethanol (insoluble).

Figure 1 presents the optical and morphological images of the PCL/S53P4—Cu1 scaffolds with various compositional ratios at
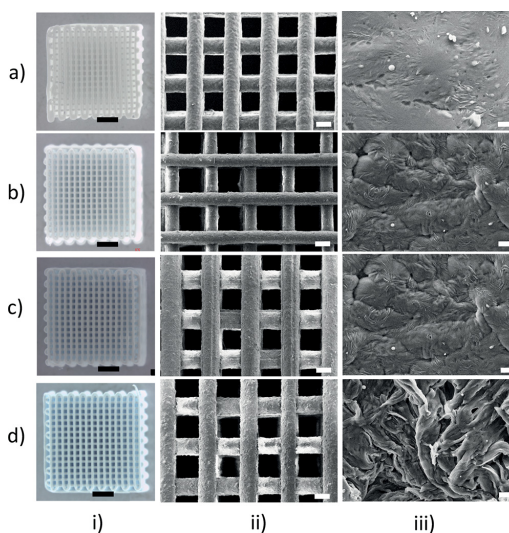

Figure 1. Optical images (column i) and SEM images of the scaffolds (column ii and column iii) of PCL ($d = 400\ \mu m$) (row a), PCL:S53P4—Cu1 = 4:1 ($d = 400\ \mu m$) (row b), PCL:S53P4—Cu1 = 2:1 ($d = 400\ \mu m$) (row c), and PCL:S53P4—Cu1 = 1:1 ($d = 400\ \mu m$) (row d). Scale bars: 2 mm (i), 200 μm (ii), 2 μm (iii).

4:1, 2:1, or 1:1 (wt %). Overall, the well-defined layouts of the struts were obtained in all the scaffolds, as seen in the first two columns. After the solvent exchange and drying, the printed scaffolds shrank compared to the designed model, more in the z-axis than the x- and y-axes (Table 2). The gravitational force was

Table 2. Structural Parameters of 3D Printed Scaffolds of PCL/S53P4−Cu1

scaffold	dimension (mm × mm × mm) mean ± SEM	axial shrinkage (%)	strut diameter (μm) mean ± SEM	spacing between struts (μm) mean ± SEM	BaG content in composite as revealed by TG[a]
PCL	8.65 (±0.03) × 8.72 (±0.02) × 3.20 (±0.03)	13−14% on x- and y-axes; ∼20% on z-axis	229 (±16)	297 (±9)	
PCL:S53P4−Cu1 = 4:1	8.86 (±0.07) × 8.88 (±0.05) × 3.28 (±0.06)	∼11% on x and y-axes; ∼18% on z-axis	207 (±8)	339 (±6)	20.2%
PCL:S53P4−Cu1 = 2:1	9.20 (±0.03) × 9.21 (±0.03) × 3.41 (±0.14)	∼8% on x and y-axes; ∼15% on z-axis	232 (±20)	323 (±12)	32.0%
PCL:S53P4−Cu1 = 1:1	9.58 (±0.01) × 9.61 (±0.01) × 3.49 (±0.01)	∼4% on x and y-axes; ∼12% on z-axis	231 (±3)	337 (±4)	57.4%

[a]Determined from the weight loss in the TG analysis curves as shown in Supporting Information S3.

assumed to cause the higher compaction along the z-axis during the solidification. Also, the content of S53P4−Cu1 in the composite affected the shrinkage rate. As seen from Table 2, less shrinkage occurred in the composite containing more BaG microparticles since the shrinkage is mainly caused by the condensation of PCL polymer after the removal of organic solvent. The shrinkage decreased from 13% to 14% for the PCL scaffold to 4% for the composite scaffold of PCL/S53P4−Cu1 = 1:1 on x- and y-axes while for the z-axis the difference in the shrinkage was from 20% compared to 12%. The strut diameter and strut spacing were confined within the range 200−230 μm and 300−340 μm, respectively, after the shrinkage upon solidification. As the content of S53P4−Cu1 in the composites increased, the composites showed a coarser surface morphology as revealed by the SEM images (Figure 1). The increased surface roughness in the composites containing more S53P4−Cu1 microparticles was probably due to the presence of more BaG microparticles that protruded the PCL matrix to a larger extent. In the scaffolds of PCL/S53P4−Cu1 = 2:1 and 1:1, small cavities and even microcracks were seen on the surface, indicating a disruption to the continuous phase of PCL in the struts.

TG analysis confirmed the compositional ratio of S53P4−Cu1 in the composite scaffolds, as displayed in Supporting Information S3 as well as listed in Table 2. The residual content was highly consistent with the inorganic content of BaG in the ink dispersion. Also, the cross-section image of the PCL/S53P4−Cu1 = 2:1 scaffold revealed a moderately homogeneous distribution of BaG microparticles through the PCL matrix (as seen in the SEM image in Supporting Information S3). This indicates that the dispersion of BaG microparticles in viscous PCL solution was rather homogeneous, which consequently facilitated the DIW fabrication of the scaffolds with good textural integrity and high resolution.

Compressive Response of the 3D Scaffolds of PCL and PCL/S53P4−Cu1. In a compressive mode, the mechanical responses of the PCL and PCL/S53P4−Cu1 scaffolds were analyzed. The stress−strain response curves for the scaffolds of PCL and PCL/S53P4−Cu1 = 4:1 and 2:1 with the SS = 400 μm are displayed in Figure 2a. The observed stress−strain response of the scaffolds is typical for the highly porous PCL-based scaffolds reported elsewhere.[26,34,35] Their stress−strain curves are characterized by three different regions: a linear region at lower strain values, suggesting an initial rigid mechanical response, associated with elastic behavior of the scaffolds; a region with lower stiffness; and lastly, a region where a rise of stress with increasing strain is recorded, which is related to
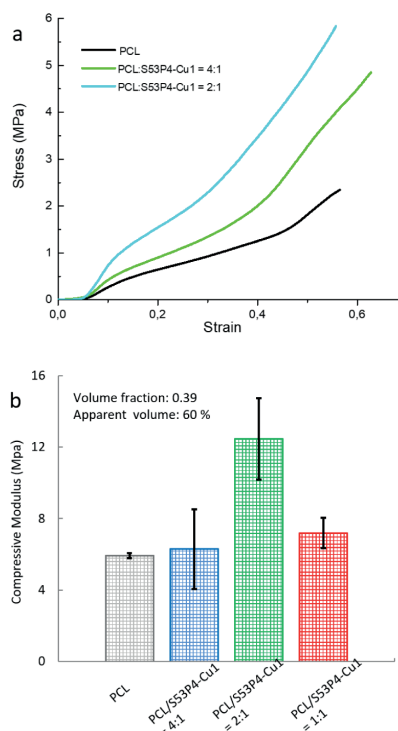

Figure 2. (a) Stress−strain curves for the 3D scaffolds. (b) Compressive Young's modulus vs the compositional ratio of PCL/S53P4−Cu1 in the scaffold. Error bar: SEM.

densification of the porous structure. Compared with the PCL scaffold, all the composite scaffolds exhibited reinforced mechanical properties as the strains were yielded at higher stress values. The compressive Young's moduli E of the scaffolds calculated from the slope of the stress−strain curves are displayed in Figure 2b with respect to the compositional ratio between the PCL and S53P4−Cu1. The PCL scaffold showed an E value of 5.9 MPa and a yield stress σ_y (at 0.2% strain) of 0.64 MPa. Among the compositional ratios at 4:1, 2:1, and 1:1 for PCL/S53P4−Cu1, the scaffold of PCL/S53P4−Cu1 = 2:1 exhibited the highest E value of 12.5 MPa and yield stress σ_y (at
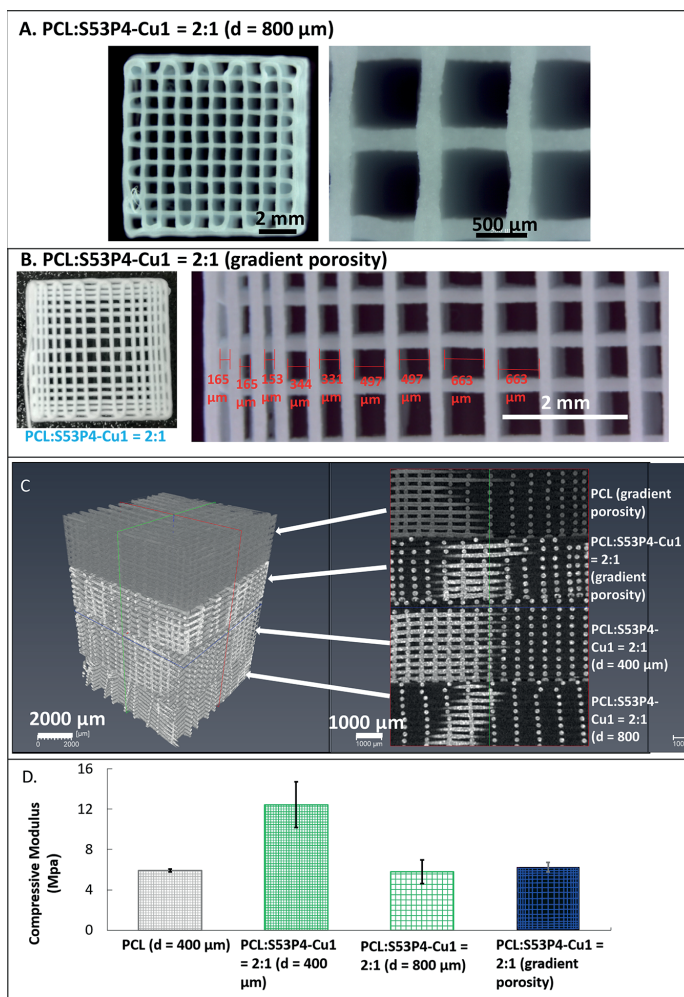
Figure 3. (A) Optical images of the scaffold of PCL/S53P4−Cu1 = 2:1 with strut spacing at d = 800 μm. (B) Optical images of the scaffold of PCL/S53P4−Cu1 = 2:1 with a dense outward gradient porosity. (C) μ-CT images of the scaffolds with different porosity parameter. (D) Young's modulus with respect to various porosity in scaffolds of PCL and PCL/S53P4−Cu1 = 2:1.

0.2% strain) of 1.54 MPa, more than 2 times higher than the PCL scaffold of similar porosity. As revealed by the μ-CT measurements, all the scaffolds printed with SS = 400 μm gave a volume fraction of approximately 0.39 as well as an apparent porosity of 60%. The scaffold of PCL/S53P4−Cu1 = 4:1 demonstrated a similar compressive modulus to the PCL scaffold with an E value of 6.29 MPa, while the scaffold of PCL/S53P4−Cu1 = 1:1 demonstrated an E value of 7.19 MPa, which is lower than that of the scaffold of PCL/S53P4−Cu1 = 2:1. The reduction in mechanical properties of the scaffold of PCL/S53P4−Cu1 = 1:1 can be attributed to the formation of BaG agglomerates, which may result in a heterogeneous dispersion of the inorganic fillers in the PCL matrix, as observed in the SEM images (Figure 1d,iii).

Porosity Control on the Printed Scaffold in DIW. As revealed by the μ-CT measurements, the scaffolds printed with

SS = 400 μm gave a volume fraction of about 0.393 as well as an apparent porosity of 60.64%. To demonstrate the precision control of the DIW process over the scaffold porosity with the developed ink system, the scaffolds with the SS = 800 μm (shown in Figure 3A) or with a dense outward gradient porosity (shown in Figure 3B) were, respectively, printed using the ink of the compositional ratio at PCL/S53P4−Cu1 = 2:1. It showed that, after solidification, the scaffolds with SS = 800 μm had the same strut diameters of 232 μm as the scaffolds with SS = 400 μm, but the SS remained around 610 μm. The μ-CT measurements gave a volume fraction of 0.274 with an apparent porosity of 72.53%. In the design of dense outward gradient porosity, the strut spacing was set with a linear change from edge to center on both x- and y-axes. As displayed in Figure 3B, this resulted in an almost linear change of the SS value from 165 to 663 μm in the scaffold after shrinkage.

Table 3. Pore Architecture Parameters in the Printed Scaffold of PCL/S53P4−Cu1 = 2:1

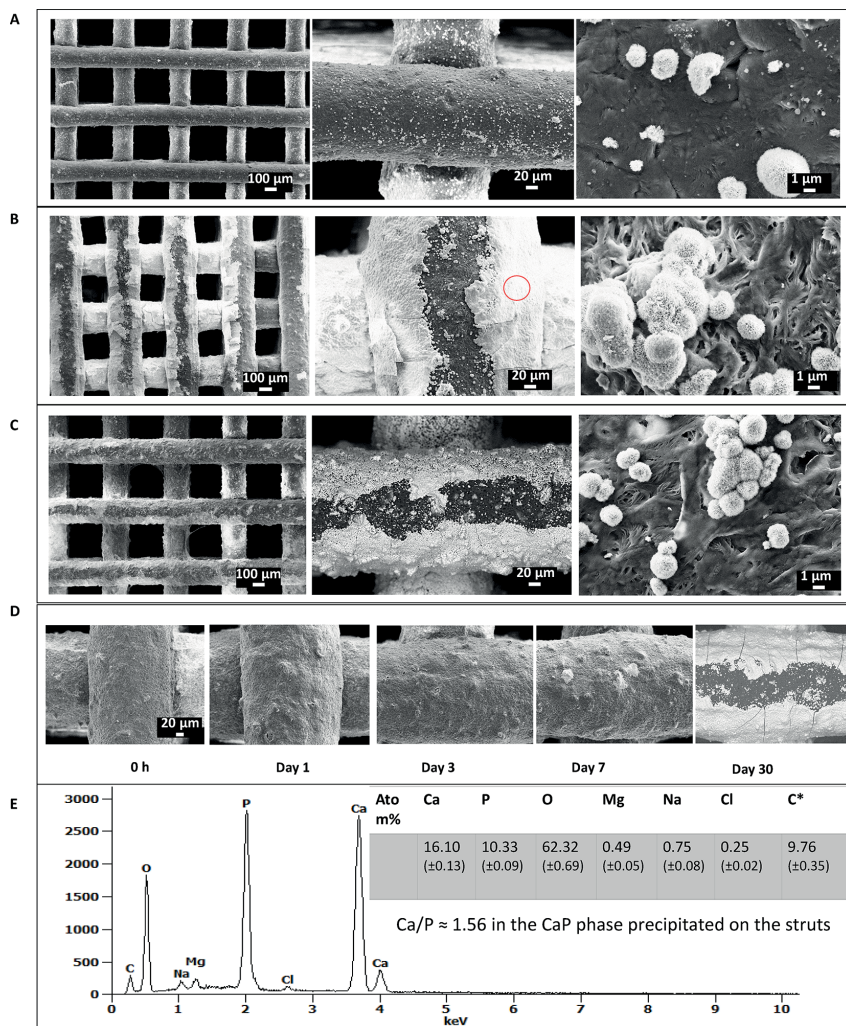| scaffold PCL:S53P4−Cu1 = 2:1	strut diameter (μm) mean ± SEM	spacing between struts (μm) mean ± SEM	volume fraction measured by μ-CT	porosity measured by μ-CT (%)
d = 400 μm	232 (±20)	323 (±12)	0.393	60.64
d = 800 μm	232 (±20)	610	0.274	72.53
gradient porosity	232 (±20)	gradient change	0.261	73.92

Figure 4. (A) SEM image of the strut surface in the scaffold of PCL/S53P4−Cu1 = 4:1 after 30 days of immersion in SBF in various resolutions. (B) SEM image of the strut surface in scaffold PCL/S53P4−Cu1 = 2:1 after 30 days of immersion in SBF in various resolutions. (C) SEM image of the strut surface in scaffold of PCL/S53P4−Cu1 = 1:1 after 30 days of immersion in SBF in various resolutions. (D) SEM image of the strut surface in scaffold of PCL/S53P4−Cu1 = 2:1 at various immersion time points. (E) EDXA performed on the precipitates on the strut surface in scaffold of PCL/S53P4−Cu1 = 2:1 after 30 days of immersion in SBF.

For the scaffolds with different porosity parameters, the μ-CT image on the left in Figure 3C demonstrates the 3D spatial space inside the printed scaffolds, and the image on the right presents the 2D distribution of struts in the scaffolds. In general, the 3D reconstruction of the scaffolds displayed as the "replicates" in accordance to the CAD designs, indicating good controllability of the developed DIW process. The pore architecture parameters in these scaffolds are summarized with respect to the varied porosity in Table 3. The Young's moduli of these scaffolds were also compared with respect to the porosity in
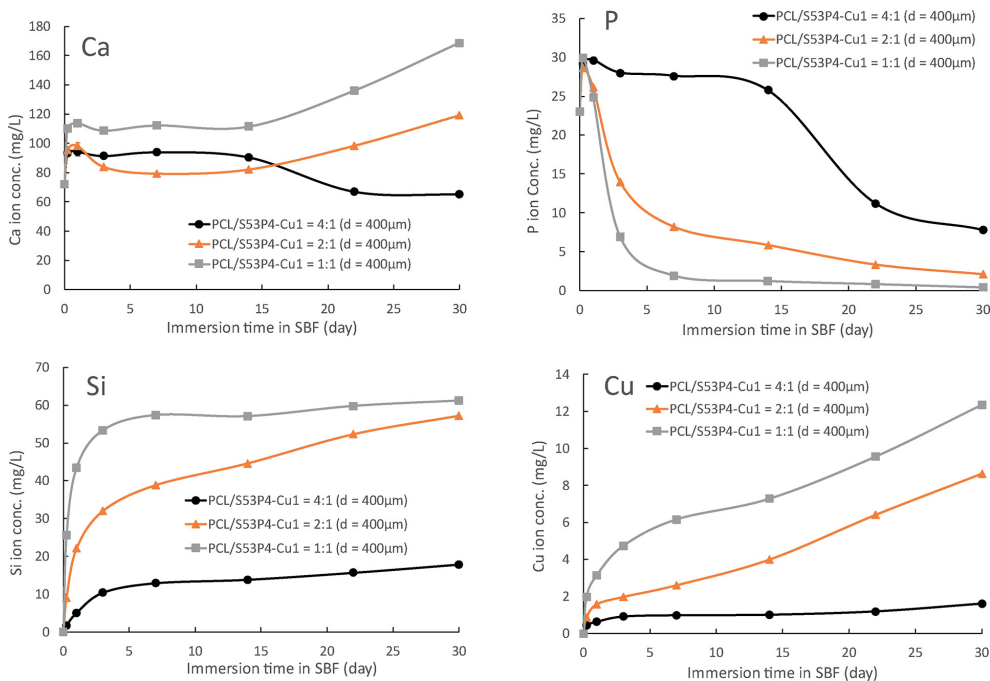
Figure 5. Ion concentration profiles of Ca, P, Si, and Cu ions in SBF with static immersion of PCL/S43P4-Cu1 scaffolds at various compositional ratios.

Figure 3D. Compared with the scaffold with SS = 400 μm, the compressive modulus decreased for both the scaffold with SS = 800 μm and the one with a gradient porosity, as the porosity in both types of scaffolds increased to ~73%. An increase of the total porous volume from 10% to 20% may result in a factor of 4 decrease in the mechanical strength.[36]

Ion Dissolution Profiles and Bioactivity of PCL/Cu-BaG Scaffolds in SBF *in Vitro*. The bioactivity and ion dissolution behaviors of the scaffolds of PCL/S53P4−Cu1 (SS = 400 μm) at various compositional ratios were evaluated in SBF for a total duration of 30 d. Figure 4A−C, respectively, displays the strut surface morphology in the scaffolds of PCL/S53P4−Cu1 = 4:1, 2:1, and 1:1 after static immersion in SBF for 30 d. In the scaffold of PCL/S53P4−Cu1 = 4:1, only small aggregates of calcium phosphate phase (CaP) decorated on the strut surface (Figure 4A), whereas heavy precipitation of CaP formed layers covered the strut surface in the scaffolds of both PCL/S53P4−Cu1 = 2:1 and PCL/S53P4−Cu1 = 1:1 (Figure 4B,C). The CaP precipitate demonstrated a characteristic cauliflower-like morphology consisting of numerous nanoflakes and gave a Ca/P = 1.56 as measured by the EDXA (Figure 4E), which was close to the Ca/P ratio of 1.67 in natural bone minerals, hydroxyapatite. Figure 4D reveals the morphological change of the strut surface in the scaffold of PCL/S53P4−Cu1 = 2:1 at various time points during the SBF immersion. Notable precipitation of the CaP phase on the strut surface was only observed after 7 d of immersion.

By analyzing the ion concentrations in SBF at various time points, the ion dissolution profiles of the scaffolds were acquired. Figure 5 displays the ion dissolution profiles for PCL/S53P4−

Cu1 scaffolds with compositional ratios at 4:1, 2:1, and 1:1, all with dimensions of 10 mm (x) × 10 mm (y) × 2 mm (z) and SS = 400 μm defined in DIW. With respect to the dissolution of Si, in all three types of scaffolds a burst release was initially detected within 3 d of immersion, which was most likely associated with the initial dissolution of Cu-BaG particles exposed on the most outer surface. After 3 d, the Cu-BaG dissolution slowed down when the ion diffusion from the inner of the particles might have been hindered by the formed silica-rich layer. Overall, a rather low amount of Si was detected for the scaffold of PCL/S53P4−Cu1 = 4:1 due to the low content of S53P4−Cu1. For the scaffold of PCL/S53P4−Cu1 = 2:1, a continuous release of Si at an almost constant rate was detected for the rest of the immersion period, whereas the Si released from the scaffold of PCL/S53P4−Cu1 = 1:1 reached a saturation level at ~60 mg L^{-1} in SBF after 7 d of immersion. With respect to the dissolution of Cu, in general the release trend was similar to that of Si. A higher concentration of Cu^{2+} was observed in SBF from the scaffold of PCL/S53P4−Cu1 = 1:1 due to the highest burst release in the initial dissolution. The ion concentration profiles of Ca and P in SBF are reflected both by the ion dissolution from the scaffold and by the precipitation of CaP phase on the strut surface. For the scaffold of PCL/S53P4−Cu1 = 4:1, apparent precipitation of CaP was only seen after 14 d of immersion due to the low concentration of Ca^{2+} accumulated in SBF, as indicated by the steep ramp in P concentration. For the scaffolds of PCL/S53P4−Cu1 = 2:1 and PCL/S53P4−Cu1 = 1:1, the CaP precipitation was readily indicated after 1 d of immersion by the steep ramp of P concentration in SBF as shown in Figure 5.
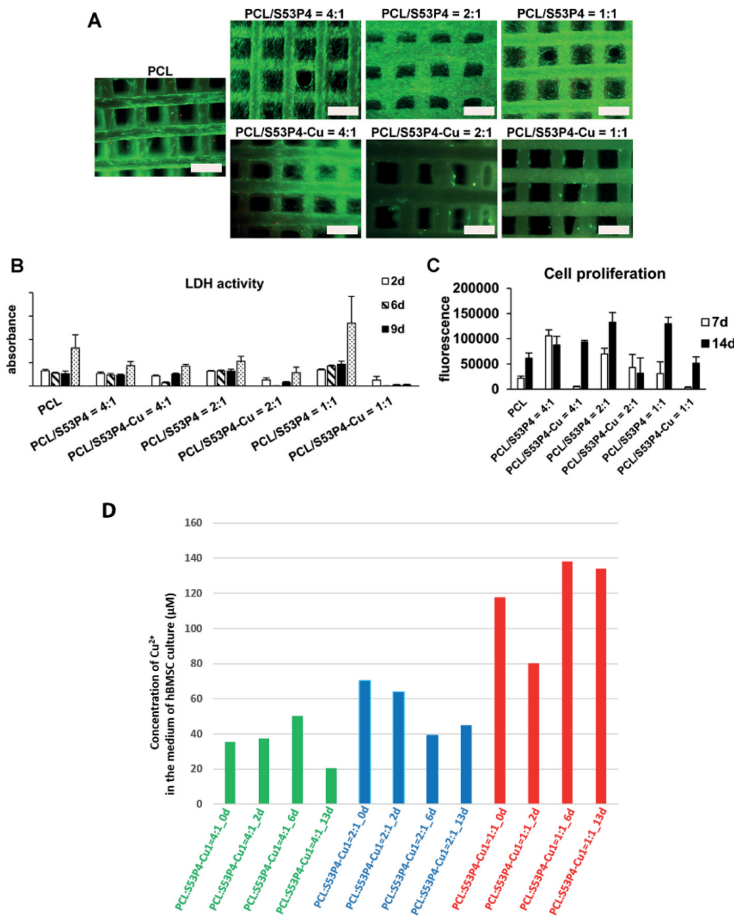
Figure 6. Results concerning viability and proliferation of hBMSCs in scaffolds. (A) Representative images of live/dead staining at the 14 d time point. Live cells are stained green and dead cells red. Scale bars: 500 μm. (B) LDH activity results at 2 d, 6 d, 9 d, and 13 d time points ($n = 3$, mean + SD). (C) Total DNA amount in samples at 7 d and 14 d time points, indicating hBMSC proliferation ($n = 4$, mean + SD). (D) ICP-OES analysis results on Cu^{2+} concentration in culture medium at 0 d, 2 d, 6 d, and 13 d time points ($n = 1$).

hBMSC Culture on the Scaffolds. To determine the viability of hBMSCs on the scaffolds, a qualitative live/dead staining as well as a quantitative LDH activity assay were conducted. As made evident in Figure 6A, the cells were viable on all the materials after 14 d of culture, and the number of dead cells was negligible. Increasing the content of S53P4 in the composite seemed to induce hBMSC proliferation more in comparison to the PCL control. However, apart from the scaffold of PCL/S53P4−Cu1 = 4:1, the high content of S53P4−Cu1 had a clear negative effect on the cell amount.

Cells release LDH enzyme to the culture medium upon cell death associated membrane rupture, making LDH a good quantitative indicator of cell viability. Figure 6B shows the LDH activity levels of the culture medium after 2 d, 6 d, 9 d, and 13 d of culture. Since the medium was changed at each of these time points, the LDH activity values are not cumulative. In general, the LDH activities remained at a relatively low and constant level with all the scaffolds until 9 d, indicating low cytotoxicity of the studied scaffolds. At 13 d the values increased slightly, which is likely due to the high cell density at this point, as observed in the live/dead staining (Figure 6A). Unexpectedly, the amount of Cu^{2+} released from the scaffolds of PCL/S53P4−Cu1 = 2:1 and PCL/S53P4−Cu1 = 1:1 did not induce elevated LDH levels in the culture medium, as expected based on the live/dead staining. Still, cell amount in the S53P4−Cu1-containing scaffolds was clearly less than that in the other samples, thus possibly explaining this observation.

The cell proliferation was quantitatively evaluated at time points of 7 d and 14 d as shown in Figure 6C. The integration of S53P4 in the composite showed an increasing effect on the hBMSC proliferation at both time points and with all the studied BaG contents. Regarding the role of Cu^{2+} released from S53P4−Cu1, the cell proliferation assay was in line with the live/dead staining, indicating the inhibitory effect of the increased concentration of Cu^{2+} on the growth of hBMSCs. Still, despite the very low cell amount on the scaffold of PCL/S53P4−Cu1 =

4:1 at 7 d, the cell amount at 14 d was comparable to that in the scaffold of PCL/S53P4 = 4:1. The Cu^{2+} concentration in the culture medium at time points of 0 d, 2 d, 6 d, and 13 d was further analyzed by ICP-OES, which are presented in Figure 6D with respect to the compositional ratio. During the preincubation in BM for 48 h (0 d at cell seeding), the concentration of Cu^{2+} in the culture medium, respectively, reached 35, 70, and 117 μM released from the scaffolds of PCL/S53P4—Cu1 = 4:1, 2:1, and 1:1. As seen in Figure 6C, the proliferation of hBMSCs on the scaffold of PCL/S53P4—Cu1 = 4:1 was first inhibited at the early time point of 7 d. When the concentration of Cu^{2+} decreased to 20 μM after the culture medium was changed several times, and the dissolution rate of Cu slowed down after the initial burst, the hBMSCs were able to retain their proliferative capacity at the later time point of 14 d, which was comparable to that on the scaffold of PCL/S53P4 = 4:1. However, at both time points of 7 d and 14 d, the proliferation of hBMSCs was restricted on the scaffolds of PCL/S53P4—Cu1 = 2:1 and PCL/S53P4—Cu1 = 1:1 due to the high concentration of Cu^{2+} in the culture media at these time points. Apparently, the concentration of Cu^{2+} is critical for retaining the proliferative capacity of hBMSCs.

To evaluate the early osteogenic commitment of hBMSCs on the scaffolds, ALP activity was quantitatively determined after 7 d and 14 d of culture. As seen in Figure 7, the ALP activity
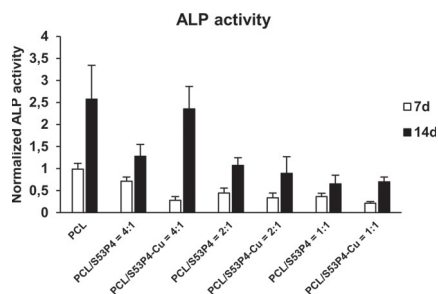
Figure 7. Alkaline phosphatase activity results of hBMSCs in scaffolds at 7 d and 14 d time points. Results are normalized to cell amount ($n = 4$, mean + SD).

increased on all the materials from 7 d to 14 d, indicating that all the scaffolds supported the early osteogenic differentiation. On one hand, the ALP activity decreased with increasing the BaG content (both for S53P4 and S53P4—Cu1), and the highest values were detected on the PCL control. On the other hand, a higher ALP activity was observed in the scaffold of PCL/S53P4—Cu1 = 4:1 in contrast to the scaffold of PCL/S53P4 = 4:1.

hBMSCs and hBMSCs+HUVECs Coculture on the Scaffolds. The ability of the PCL/BaG and PCL/Cu-BaG scaffolds to support the vascularization in both hBMSC culture and hBMSC+HUVEC coculture was analyzed by immunocytochemical staining of the endothelial proteins CD31 and vWF after 13 d and 20 d of culture. Moreover, the expression of these two markers was also evaluated in gene level with the qRT-PCR after 6 d, 11 d, and 20 d of culture. Due to the observed inhibitory effect of the scaffold of PCL/S53P4—Cu1 = 2:1 and PCL/S53P4—Cu1 = 1:1, only the scaffold of PCL/S53P4—Cu1 = 4:1 was chosen for the coculture experiments, along with the PCL scaffold as a control to the composite scaffold and the

PCL/S53P4 = 4:1 scaffold as a Cu-free composite control. As seen in Figure 8A,B, elevated production of CD31 protein was
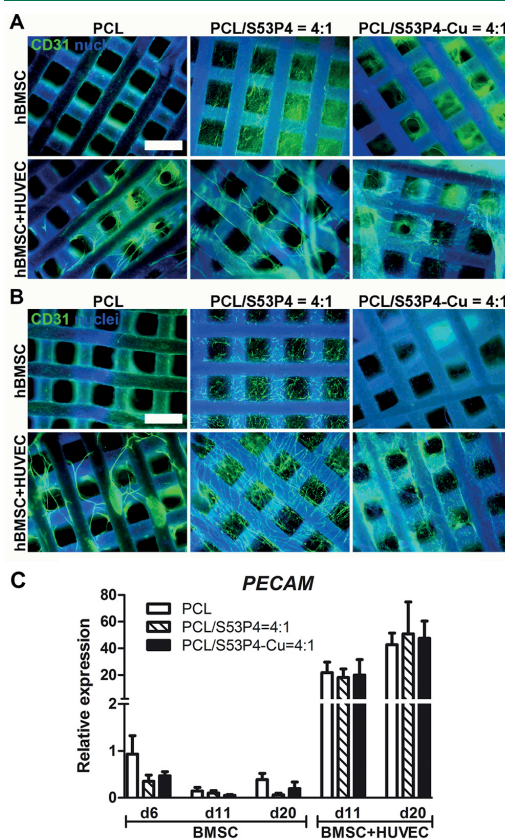
Figure 8. Immunocytochemical staining of endothelial marker protein CD31 (stained green) in hBMSCs and hBMSCs+HUVECs cultured in scaffolds at (A) 13 d and (B) 20 d time points. Nuclei are stained blue; scale bars: 500 μm. (C) Gene expression results of endothelial marker gene *PECAM* in hBMSC and hBMSC+HUVEC cultures at 6 d, 13 d, and 20 d time points. Results are expressed relative to hBMSCs cultured for 6 days on PCL scaffold ($n = 3$, mean + SD).

observed on all the scaffolds in the coculture. Importantly, extensive tubule formation was clearly visible. On the PCL scaffold, the tubular structures were thick but relatively sparse, whereas a denser network of thinner tubules was formed on the S53P4-containing scaffolds. However, the scaffold of PCL/S53P4—Cu1 = 4:1 did not stimulate tubule formation to a higher extent when compared with the Cu-free scaffold of PCL/S53P4 = 4:1. Notably, S53P4 in the composite scaffolds also stimulated the CD31 production in the hBMSC culture without HUVECs, although no tubular structures were detected. On the gene level, *PECAM* was notably upregulated in the coculture when compared with the hBMSC culture, but no clear differences among the material groups could be detected (Figure 8C). Still, in the coculture model, the expression increased from 11 d to 20 d in all the groups.

The production of vWF was in line with the immunological staining of CD31 as made evident in Figure 9. Tubular structures
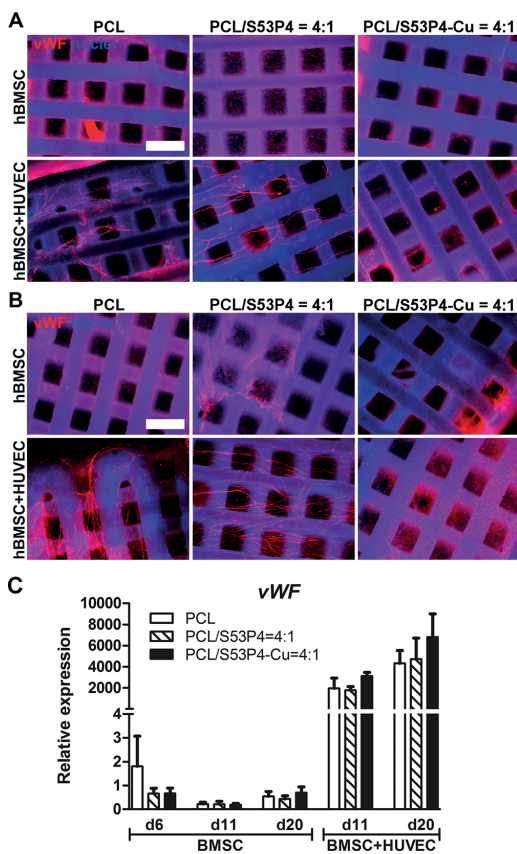

Figure 9. Immunocytochemical staining of endothelial marker protein vWF (stained red) in hBMSCs and hBMSCs+HUVECs cultured in scaffolds at (A) 13 d and (B) 20 d time points. Nuclei are stained blue; scale bars: 500 μm. (C) Gene expression results of endothelial marker gene *vWF* in hBMSC and hBMSC+HUVEC cultures at 6 d, 13 d, and 20 d time points. Results are expressed relative to hBMSCs cultured for 6 days on PCL scaffold ($n = 3$, mean + SD)

were evident in the coculture on the scaffold of PCL and the scaffold of PCL/S53P4 = 4:1 at 13 d (Figure 9A), and their amount had clearly increased at 20 d especially on the scaffold of PCL/S53P4 = 4:1 (Figure 9B). Still, the Cu^{2+} released from the scaffold of PCL/S53P4−Cu1 = 4:1 did not stimulate the vWF production or the tubular structure formation. There was a low level of vWF production also in the culture of hBMSC alone, but no tubular structures were observed. The relative *vWF* gene expression followed a highly similar pattern as *PECAM*; elevated expression levels were observed in the coculture, but the differences among the material groups were minimal (Figure 9C). In the coculture, the *vWF* gene expression increased from 11 d to 20 d, and at both time points the expression level was slightly higher in the scaffold of PCL:S53P4−Cu1 = 4:1 when compared with the other groups.

The effect of PCL, PCL/S53P4 = 4:1, and PCL/S53P4−Cu1 = 4:1 scaffolds on osteogenic differentiation in both hBMSC culture and hBMSC+HUVEC coculture was analyzed by qRT-PCR of osteogenic marker genes *RUNX2a*, *OSTEOCALCIN*, and *DLX5* after 11 d and 20 d of culture. The early osteogenic marker gene *RUNX2a* expression was elevated in hBMSCs when cultured in the scaffolds of PCL and PCL/S53P4−Cu1 = 4:1 in comparison to the scaffold of PCL/S53P4 = 4:1 at both time points (Figure 10A). In contrast, in hBMSC+HUVEC culture the scaffold of PCL/S53P4 = 4:1 promoted *RUNX2a* expression more at both time points in comparison to the other two scaffolds. The scaffold of PCL/S53P4−Cu1 = 4:1 seemed to have a decreasing effect on both *OSTEOCALCIN* and *DLX5* expression, whereas the scaffold of PCL/S53P4 = 4:1 elevated their expression at both time points and both culture setups (Figure 10B,C). Altogether, the expression of the osteogenic genes was more pronounced in hBMSC culture in contrast to the coculture setup.

■ DISCUSSION

Tuning the Architecture Parameters and Balancing the Mechanical Strength of PCL/BaG Scaffolds. The architecture parameters in scaffolds, including pore size and distribution, pore interconnectivity, and void volume, are important aspects to consider in designing TE scaffolds.[36] Optimal porosity in a scaffold allows the migration and proliferation of seeded cells, as well as the formation of a vascular network. A high porosity, greater than 80%, is desirable to enhance the osteogenesis.[36] An interconnected architecture of macropores has a decisive effect for the ingrowth of new bone, especially in long-term tissue interface maintenance. A pore size greater than 300 μm is of importance for the osteogenesis to occur as well as for the development of the vascularization network through the TE construct.[37,38] Furthermore, the TE scaffolds shall incorporate a similar structural complexity as the native tissues, which typically have a gradient porous structure.[39] The gradient porosity enables specific cell migration during tissue regeneration. The gradient porosity is also required for the treatment of articular cartilage defects in osteochondral TE.[37,40]

In this work, we have successfully fabricated 3D printed scaffolds with different pore sizes and porosities, as well as a gradient porous structure (Figure 3). In the early osteogenic differentiation culture of hBMSCs, the scaffolds of PCL/S53P4 = 2:1 and PCL/S53P4−Cu1 = 2:1 with different porosity parameters (SS = 400 μm, SS = 800 μm, and gradient porosity as in Figure 3B) were evaluated in terms of cell viability and proliferative capability. However, no significant differences were observed among the tested groups as shown in Supporting Information S4. As indicated by this set of data, the pore size ranging from 167 to 667 μm supports the proliferation of hBMSCs well.

TE scaffolds should have matching mechanical performance to ensure their mechanical integrity during the surgical implantations and to replenish the bone functions during the healing process. The modulus of the human cancellous bones varies in the range 10−1000 MPa with respect to the apparent density of the bone.[41] In this work, we have fabricated scaffolds with 60% apparent porosity, and the highest compressive modulus of 12.5 MPa was measured for the scaffolds of PCL/ S53P4−Cu1 = 2:1 with SS = 400 μm. This has determined that the composite scaffolds fabricated by this method are appropriate for the non-load-bearing sites in bone TE. Nevertheless, changing porosity and pore size also resulted in
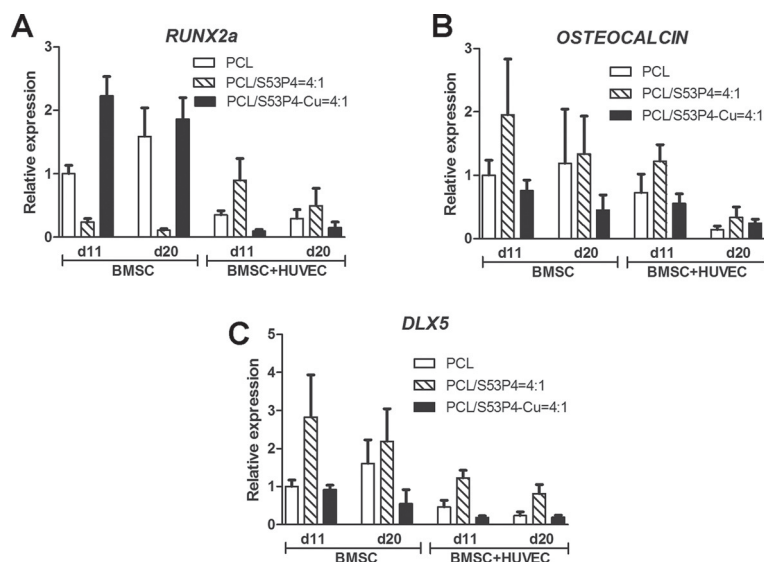
Figure 10. Gene expression results of osteogenic marker genes (A) *RUNX2a*, (B) *OSTEOCALCIN*, and (C) *DLX5* in hBMSC and hBMSC+HUVEC cultures at 13 d and 20 d time points. Results are expressed relative to hBMSCs cultured for 11 days on the PCL scaffold ($n = 3$, mean + SD).

changes in the mechanical properties, as it changes the density and the structural integrity of the scaffolds (as seen in Figure 3C). However, to achieve modulus in a much higher range, an alternative fabrication strategy and/or reinforcing component need to be considered to enhance the mechanical properties in future studies.

Effect of Cu^{2+} Released from BaG on hBMSCs and HUVECs. The surface reactions occurring on BaG involve ionic dissolution of critical concentrations of soluble Si, Ca, P, and Na ions. These ions give rise to both intracellular and extracellular responses in cells at the interface of the glass. The key phenomenon is the controlled release rates of ionic dissolution products, especially the critical concentrations of soluble Si and Ca ions. For example, 15−30 ppm of soluble Si and 60−90 ppm of soluble Ca ions are needed for osteoconduction or osteostimulation.[42] In the PCL/BaG composite, the primary role of BaG is to release the biologically active ions at the concentrations and rates needed for supporting cell proliferation and differentiation. As discussed in the Results section, the ion concentrations measured in SBF within 30 days were mainly from the dissolution of Cu-BaG microparticles exposed on the most outer strut surface since the degradation of PCL under physiological conditions is rather slow due to the low hydrolytic reactivity of PCL itself (expected to last for years).[43] Above all, the release of inorganic ions from these PCL/S53P4−Cu1 scaffolds can sustain over an extended period.

The physiologically relevant effects of Cu^{2+} as therapeutic ions, such as the antimicrobial properties, have been previously examined by applying the composite of PCL/Cu-BaG nano-particles as an anticorrosive surface coating onto magnesium implants, as reported by Yang et al.[20] Comparatively, doping of Cu into S53P4 was strategically set to release the Cu^{2+} locally for its therapeutic effect on promoting the angiogenesis in the present study. However, the specific mechanisms of Cu^{2+} affecting the cellular interactions in hBMSCs and HUVECs are complex as indicated by our results. The ion dissolution

products of S53P4 are not expected to greatly impact the proliferation of hBMSCs, as suggested in previous studies.[22,44] Regarding the proliferation and differentiation of hBMSCs, the surface wettability is also a key parameter for consideration. Feasibly, the hydrophilic BaG particulates alter the surface hydrophilicity in the composite struts in contrast to the hydrophobic PCL struts. The hydrophilic properties of biomaterials as bone substitutes are important for the induction of early cell attachment and growth.[45] Regarding the role of Cu^{2+} released from the S53P4−Cu1, the cell proliferation results were in line with the live/dead staining results, indicating that a high concentration of Cu^{2+} has an inhibitory effect on the hBMSC proliferation. The generation of reactive oxygen species is one of the main mechanisms by which the Cu^{2+} elicits cytotoxicity in cell monolayers *in vitro*. As recently investigated by Weng et al.,[22] a dose- and exposure-duration-dependent cytotoxicity of Cu^{2+} released from the nanofibers of Cu-BaG was also confirmed for the proliferation of multiple TE-related cell lines, including HUVECs, adipose-tissue-derived stem cells (ADSCs), as well as hBMSCs. In line with our previous results, a high concentration of Cu^{2+} released from the mesoporous Cu-doped BaG microparticles embedded in a nanocellulose hydrogel was cytotoxic for 3T3 fibroblasts.[19] Furthermore, Wu et al. compared mesoporous Cu-BaG scaffolds and their extracts containing varying amount of Cu^{2+} and concluded that a high concentration of Cu^{2+} significantly reduced the hBMSC proliferation.[18] In our study, the highest Cu^{2+} concentration in the culture medium varied from 50 μM (the scaffold of PCL:S53P4−Cu1 = 4:1) to 140 μM (the scaffold of PCL:S53P4−Cu1 = 1:1), and these levels are still less than the 100 mg mL^{-1} being equivalent to the 157 μM level, at which Wu et al. concluded that the Cu^{2+} inhibited the hBMSC growth.[18] According to the proliferation analysis, the hBMSCs retained their proliferative capacity when the concentration of Cu^{2+} was maintained under 20 μM. In a previous study, the Cu^{2+} concentration at 50 μM diminished the proliferate rate of

hBMSCs.[46] In the present study, the cell culture was carried out in a static model while the culture medium was only changed on fixed intervals. Under such conditions, the Cu^{2+} released from the scaffold has accumulated between medium changes. Depending on the content of S53P4−Cu1 in the composite, the accumulated Cu^{2+} showed a dose-dependent cytotoxicity on the proliferation of hBMSCs. Obviously, the concentration of Cu^{2+} is critical for retaining the proliferative capacity of hBMSCs.

All the scaffolds supported the ALP activity of hBMSCs, although the increase in the BaG or Cu-BaG content had a decreasing effect on the ALP activity. Previously, it was shown that the ALP activity of hBMSCs slightly increased as the Cu^{2+} concentration rose, however, the difference was not significant.[18] Also, the addition of Cu in BaG did not have a significant effect on the ALP activity of hBMSCs cultured in the Cu-doped 45S5 BaG scaffolds.[47] The high level of ALP activity may not be as important in the osteogenic differentiation as the fact that there is a clear level of ALP activity in samples, ensuring the presence of Pi and decreasing the concentration of pyrophosphate, to allow mineralization.[32] The osteogenic differentiation of hBMSCs was also analyzed by qRT-PCR in hBMSC culture and hBMSC+HUVEC coculture setups with the scaffolds of PCL, PCL:S53P4 = 4:1, and PCL:S53P4−Cu1 = 4:1. Interestingly, in the hBMSC culture setup the Cu-containing scaffold induced the expression of early osteogenic marker gene *RUNX2a* notably in contrast to the scaffold of PCL:S53P4 = 4:1. *RUNX2* expression is essential in the early differentiation of MSCs into osteoblastic lineage.[48] However, in order for the differentiation to proceed, the expression of *RUNX2* needs to decline, as high expression of *RUNX2* has been shown to inhibit osteoblast maturation keeping the cells in a premature stage.[48] Therefore, the high expression of *RUNX2a* as late as at 20 d combined with the low expression of late osteogenic marker genes *OSTEOCALCIN* and *DLX5* in the scaffold of PCL:S53P4−Cu1 = 4:1 is not optimal for osteogenic differentiation. Osteocalcin is only expressed in the late phase of osteogenic differentiation, and *DLX5* is an important activator of several osteogenic genes during maturation and mineralization phases.[49,50] The gene expression of *OSTEOCALCIN* and *DLX5* was higher in the scaffold of PCL:S53P4 = 4:1 in comparison to the scaffold of PCL:S53P4−Cu1 = 4:1 at both time points indicating the negative effect of Cu^{2+} on osteogenic differentiation of hBMSCs. In line with this, Li et al. demonstrated that Cu^{2+} ions inhibited the osteogenesis of rat BMSCs *in vitro*.[51] Furthermore, they showed that Cu^{2+} ions inhibited collagen formation and accumulation of collagen type I while inducing vascular formation *in vivo*. In contrast to OM supplemented hBMSC cultures, the cocultures were supplemented with EGM-2, which explains the lower expression of osteogenic genes in the coculture. Also, the expression of the osteogenic genes seemed to go down from 11 d to 20 d in the coculture setup.

According to the immunocytochemical staining of CD31 and vWF, both scaffolds of PCL:S53P4 = 4:1 and PCL:S53P4−Cu1 = 4:1 induced the secretion of these endothelial proteins and supported the formation of a denser tubular network in both hBMSC and hBMSC+HUVEC cultures in contrast to the PCL scaffold. Similarly, 45S5 BaG has been shown to support the formation of a tubular network in fibroblast and endothelial cell cultures.[14] Also, the S53P4 dissolution products have previously been reported to increase the VEGF secretion of human fibroblasts.[47] The secretion of both CD31 and vWF was stronger in the coculture setup in comparison to the hBMSC culture. In line with this, the Cu-doped 45S5 BaG scaffolds have been demonstrated to stimulate the secretion of VEGF and the formation of tubular networks in a coculture of hBMSCs with human dermal microvascular endothelial cells.[47] Interestingly, they also noticed that the Cu^{2+} alone did not increase the secretion of VEGF in these endothelial cells, but the presence of hBMSCs was also needed.[47] As expected, the gene expression of endothelial genes *PECAM* and *vWF* was notably higher in the coculture setup in comparison to the hBMSC culture with all the scaffolds (PCL, PCL:S53P4 = 4:1, and PCL:S53P4−Cu = 4:1). As several previous studies have suggested that the Cu^{2+} ions have an inductive effect on vascularization, we would have expected to see a more pronounced difference between the scaffolds of PCL:S53P4 = 4:1 and PCL:S53P4−Cu1 = 4:1.[18,19,47] However, only the gene expression of *vWF* in the coculture setup was slightly higher in the Cu-containing scaffold of PCL:S53P4−Cu1 = 4:1 in contrast to the scaffold of PCL:S53P4 = 4:1. These conflicting results may be related to the different experimental design on the Cu-mediated angiogenic or cytotoxic effect, such as the BaG composition, used cell type, or medium supplements. However, we may speculate whether the S53P4 BaG itself promotes angiogenesis, and the addition of Cu^{2+} that was released from the scaffold of PCL:S53P4−Cu1 = 4:1 does not suffice to produce observable differences in tubular network formation. A similar finding was reported in an *in vivo* evaluation of the angiogenetic effect of the Cu-doped 45S5 scaffolds in the AV loop model: a tendency toward an increased vascularization in the Cu-doped BaG group compared to the plain BaG group was observed in μ-CT and histological evaluations, but no statistical difference in vascularization could be measured between both groups.[52] Altogether, the PCL:S53P4 = 4:1 and PCL:S53P4−Cu1 = 4:1 scaffolds supported the vascularization and tubular formation in the coculture setup; however, the angiogenic effect of Cu^{2+} was not notable in contrast to the PCL/BaG composite. The key point to consider for future experimental design is to optimize the Cu^{2+} release and prevent the accumulation of Cu^{2+} in the culture medium, for instance, by using a dynamic culture system that would also simulate the *in vivo* environments better.

■ CONCLUSIONS

Using a viscous solution of PCL in acetone as the carrier phase for BaG microparticles to achieve a homogeneous ink in combination with the solidification of PCL in ethanol has enabled the DIW fabrication of the PCL/BaG composite scaffolds. Because of the excellent homogeneity of the DIW ink as prepared, the mechanical properties of the composite scaffolds were enhanced, compared to the PCL scaffold. The DIW technique allows a precise control of the scaffold architecture with high resolutions. The reinforced scaffolds of PCL/S53P4−Cu1 at various compositional ratios and with a strut diameter around 230 μm as well as an apparent porosity of 60% showed a compressive Young's modulus in the range 7−13 MPa. This indicates that the scaffolds would be appropriate to be used for non-load-bearing sites in bone TE. The bioactivity of S53P4−Cu1 in the composite scaffolds was confirmed by the CaP precipitation in SBF *in vitro*. The PCL/S53P4−Cu1 scaffolds as fabricated were able to provide a sustained release of biologically relevant inorganic ions over an extended period. The high content of S53P4−Cu1 in the scaffolds of PCL/S53P4−Cu1 = 2:1 and PCL/S53P4−Cu1 = 1:1 inhibited the proliferation of hBMSCs. However, in the scaffold of PCL/S53P4−Cu1 = 4:1, the hBMSCs retained their proliferative

capacity at a delayed culture time. Furthermore, the rising BaG and Cu content in the composite had a decreasing effect on ALP activity in hBMSCs. The PCL:S53P4 = 4:1 scaffold supported the osteogenic differentiation of hBMSCs whereas the addition of Cu suppressed the osteogenic effect of the composite. The scaffolds of PCL:S53P4 = 4:1 and PCL:S53P4−Cu1 = 4:1 supported the vascularization and tubule formation in the hBMSC+HUVEC coculture setup. Unexpectedly, the Cu^{2+} released from the scaffold of PCL:S53P4−Cu1 = 4:1 did not have an apparent effect on the tubule formation in comparison to the scaffold of PCL:S53P4 = 4:1.

■ ASSOCIATED CONTENT

Ⓢ Supporting Information

The Supporting Information is available free of charge on the ACS Publications website at DOI: 10.1021/acsbiomaterials.9b00105.

> Concentrations of inorganic ions in the SBF; surface marker expression of hBMSCs and HUVECs; homogeneity investigation of the 3D scaffolds of PCL/Cu-BaG; and cell viability and proliferation on scaffolds with different porosity control parameters (PDF)

■ AUTHOR INFORMATION

Corresponding Author

*E-mail: xwang@abo.fi.

ORCID ⊙

Xiaoju Wang: 0000-0002-1728-4164
Miina Ojansivu: 0000-0002-5493-3530
Chunlin Xu: 0000-0003-1860-9669
Jari Hyttinen: 0000-0003-1850-3055
Gordon Wallace: 0000-0002-0381-7273

Author Contributions

#X.W., B.Z.M., and S.P. contributed equally to this study as the cofirst authors. The manuscript was written through contributions of all the coauthors. All the coauthors have given approval to the final version of the manuscript.

■ REFERENCES

(1) Wang, W.; Yeung, K. W. K. Bone Grafts and Biomaterials Substitutes for Bone Defect Repair: A Review. *Bioactive Mater.* **2017**, *2*, 224−247.

(2) Yu, X.; Tang, X.; Gohil, S. V.; Laurencin, C. T. Biomaterials for Bone Regenerative Engineering. *Adv. Healthcare Mater.* **2015**, *4*, 1268−1285.

(3) Kolk, A.; Handschel, J.; Drescher, W.; Rothamel, D.; Kloss, F.; Blessmann, M.; Heiland, M.; Wolff, K.-D.; Smeets, R. Current Trends and Future Perspectives of Bone Substitute Materials − From Space Holders to Innovative Biomaterials. *J. Craniomaxillofac. Surg.* **2012**, *40*, 706−718.

(4) Oryan, A.; Alidadi, S.; Moshiri, A.; Maffulli, N. Bone Regenerative Medicine: Classic Options; Novel Strategies and Future Directions. *J. Orthop. Surg. Res.* **2014**, *9*, 18.

(5) Tang, D.; Tare, R. S.; Yang, L.-Y.; Williams, D. F.; Ou, K.-L.; Oreffo, R. O. C. Biofabrication of Bone Tissue: Approaches; Challenges and Translation. *Biomaterials* **2016**, *83*, 363−382.

(6) Hench, L. L. The Story of Bioglass. *J. Mater. Sci.: Mater. Med.* **2006**, *17*, 967−978.

(7) Rahaman, M. N.; Day, D. E.; Bal, B. S.; Fu, Q.; Jung, S. B.; Bonewald, L. F.; Tomsia, A. F. Bioactive Glass in Tissue Engineering. *Acta Biomater.* **2011**, *7*, 2355−2373.

(8) Jones, J. R. Review of Bioactive Glass: from Hench to Hybrids. *Acta Biomater.* **2013**, *9*, 4457−4486.

(9) El-Rashidy, A. A.; Roether, J. A.; Harhaus, L.; Kneser, U.; Boccaccini, A. R. Regenerating Bone with Bioactive Glass Scaffolds: A Review of in vivo Studies in Bone Defect Models. *Acta Biomater.* **2017**, *62*, 1−28.

(10) Almubarak, S.; Nethercott, H.; Freeberg, M.; Beaudon, C.; Jha, A.; Jackson, W.; Marcucio, R.; Miclau, T.; Healy, K.; Bahney, C. Tissue Engineering Strategies for Promoting Vascularized Bone Regeneration. *Bone* **2016**, *83*, 197−209.

(11) Mercado-Pagán, Á. E.; Stahl, A. M.; Shanjani, Y.; Yang, Y. Vascularization in Bone Tissue Engineering Constructs. *Ann. Biomed. Eng.* **2015**, *43*, 718−729.

(12) Day, R. M. Bioactive Glass Stimulates the Secretion of Angiogenic Growth Factors and Angiogenesis In Vitro. *Tissue Eng.* **2005**, *11*, 768−777.

(13) Detsch, R.; Stoor, P.; Grunewald, A.; Roether, J. A.; Lindfors, N. C.; Boccaccini, A. R. Increase in VEGF Secretion from Human Fibroblast Cells by Bioactive Glass S53P4 to Stimulate Angiogenesis in Bone. *J. Biomed. Mater. Res., Part A* **2014**, *102A*, 4055−4061.

(14) Gorustovich, A.; Roether, J. A.; Boccaccini, A. R. Effect of Bioactive Glasses on Angiogenesis: A review of In Vitro and In Vivo Evidences. *Tissue Eng., Part B* **2010**, *16*, 199−207.

(15) Sen, C. K.; Khanna, S.; Venojarvi, M.; Trikha, P.; Ellison, E. C.; Hunt, T. K.; Roy, S. Copper-Induced Vascular Endothelial Growth Factor Expression and Wound Healing. *Am. J. Physiol. Heart Circ. Physiol.* **2002**, *282*, 1821−1827.

(16) Gerard, C.; Bordeleau, L.-J.; Barralet, J.; Doillon, C. J. The Stimulation of Angiogenesis and Collagen Deposition by Copper. *Biomaterials* **2010**, *31*, 824−831.

(17) Kornblatt, A. P.; Nicoletti, V. G.; Travaglia, A. The Neglected Role of Copper Ions in Wound Healing. *J. Inorg. Biochem.* **2016**, *161*, 1−8.

(18) Wu, C.; Zhou, Y.; Xu, M.; Han, P.; Chen, L.; Chang, J.; Xiao, Y. Copper-Containing Mesoporous Bioactive Glass Scaffolds with Multifunctional Properties of Angiogenesis Capacity; Osteostimulation and Antibacterial Activity. *Biomaterials* **2013**, *34*, 422−433.

(19) Wang, X.; Cheng, F.; Liu, J.; Smått, J.-H.; Gepperth, D.; Lastusaari, M.; Xu, C.; Hupa, L. Biocomposites of Copper-containing Mesoporous Bioactive Glass and Nanofibrillated Cellulose: Biocompatibility and Angiogenic Promotion in Chronic Wound. *Acta Biomater.* **2016**, *46*, 286−298.

(20) Yang, Y.; Zheng, K.; Liang, R.; Mainka, A.; Taccardi, N.; Judith, A.; Roether, J. A.; Detscha, R.; Goldmann, W. H.; Virtanen, S.; Boccaccini, A. R. Cu-releasing BG/PCL Coating on Mg with Antibacterial and Anticorrosive Properties for Bone Tissue Engineering. *Biomed. Mater.* **2018**, *13*, 015001.

(21) Bari, A.; Bloise, N.; Fiorilli, S.; Novajra, G.; Vallet-Regí, M.; Bruni, G.; Torres-Pardo, A.; González-Calbet, J. M.; Visai, L.; Vitale-Brovarone, C. Copper-Containing Mesoporous Bioactive Glass

Nanoparticles as Multifunctional Agent for Bone Regeneration. *Acta Biomater.* **2017**, *55*, 493−504.

(22) Weng, L.; Boda, S. K.; Teusink, M. J.; Shuler, F. D.; Li, X.; Xie, J. Binary Doping of Strontium and Copper Enhancing Osteogenesis and Agiogenesis of Bioactive Glass Nanofibers while Suppressing Osteoclast Activity. *ACS Appl. Mater. Interfaces* **2017**, *9*, 24484−24496.

(23) Malikmammadov, E.; Tanir, T. E.; Kiziltay, A.; Hasirci, V.; Hasirci, N. PCL and PCL-Based Materials in Biomedical Applications. *J. Biomater. Sci., Polym. Ed.* **2018**, *29*, 863−893.

(24) Placone, J. K.; Engler, A. J. Recent Advances in Extrusion Based 3D printing for Biomedical Applications. *Adv. Healthcare Mater.* **2018**, *7*, 1701161.

(25) Nyberg, E.; Rindone, A.; Dorafshar, A.; Grayson, W. L. Comparison of 3D-printed Poly-e-caprolactone Scaffolds Functionalized with Tricalcium Phosphate; Hydroxyapatite; Bio-Oss; or Decellularized Bone Matrix. *Tissue Eng., Part A* **2017**, *23*, 503−514.

(26) Gómez-Lizárraga, K. K.; Flores-Morales, C.; Del Prado-Audelo, M. L.; Álvarez-Pérez, M. A.; Piña-Barba, M. C.; Escobedo, C. Polycaprolactone- and Polycaprolactone/Ceramic-based 3D-Bioplotted Porous Scaffolds for Bone Regeneration: A Comparative Study. *Mater. Sci. Eng., C* **2017**, *79*, 326−335.

(27) Neufurth, M.; Wang, X.; Wang, S.; Steffen, R.; Ackermann, M.; Haep, N. D.; Schröder, H. C.; Müller, W. E. G. 3D Printing of Hybrid Biomaterials for Bone Tissue Engineering: Calcium-Polyphosphate Micoparticles Encapsulated by Polycaprolactone. *Acta Biomater.* **2017**, *64*, 377−388.

(28) Kokubo, T.; Kushitani, H.; Ohtsuki, C.; Sakka, S. Chemical Reaction of Bioactive Glass and Glass-Ceramic with a Simulated Body Fluid. *J. Mater. Sci.: Mater. Electron.* **1992**, *3*, 79−83.

(29) Hamilton, R. D.; Leach, L. Isolation and Properties of An In Vitro Human Outer Blood-Retinal Barrier Model. *Methods Mol. Biol.* **2011**, *686*, 401−416.

(30) Lindroos, B.; Boucher, S.; Chase, L.; Kuokkanen, H.; Huhtala, H.; Haataja, R.; Vemuri, M.; Suuronen, R.; Miettinen, S. Serum-Free; Xeno-Free Culture Media Maintain the Proliferation Rate and Multipotentiality of Adipose Stem Cells In Vitro. *Cytotherapy* **2009**, *11*, 958−972.

(31) Tirkkonen, L.; Haimi, S.; Huttunen, S.; Wolff, J.; Pirhonen, E.; Sandor, G. K. Osteogenic Medium Is Superior to Growth Factors in Differentiation of Human Adipose Stem Cells towards Bone-Forming Cells in 3D Culture. *Eur. Cell. Mater.* **2013**, *25*, 144−158.

(32) Ojansivu, M.; Vanhatupa, S.; Björkvik, L.; Häkkänen, H.; Kellomäki, M.; Autio, R.; Ihalainen, J. A.; Hupa, L.; Miettinen, S. Bioactive Glass Ions as Strong Enhancers of Osteogenic Differentiation in Human Adipose Stem Cells. *Acta Biomater.* **2015**, *21*, 190−203.

(33) Pfaffl, M. W. A New Mathematical Model for Relative Quantification in Real-Time RT-PCR. *Nucleic Acids Res.* **2001**, *29*, No. 45e.

(34) Hutmacher, D. W.; Schantz, T.; Zein, I.; Ng, K. W.; Teoh, S. H.; Tan, K. C. Mechanical Properties and Cell Cultural Response of Polycaprolactone Scaffolds Designed and Fabricated via Fused Deposition Modeling. *J. Biomed. Mater. Res.* **2001**, *55*, 203−216.

(35) Morouço, P.; Biscaia, S.; Viana, T.; Franco, M.; Malça, C.; Mateus, A.; Moura, C.; Ferreira, F. C.; Mitchell, G.; Alves, N. M. Fabrication of Poly(ε-caprolactone) Scaffolds Reinforced with Cellulose Nanofibers; with and without the Addition of Hydroxyapatite Nanoparticles. *BioMed Res. Int.* **2016**, *2016*, 1596157.

(36) Hannink, G.; Arts, J. J. C. Bioresorbability; Porosity and Mechanical Strength of Bone Substitutes: What is Optimal for Bone Regeneration? *Injury* **2011**, *42*, S22−S25.

(37) Loh, Q. L.; Choong, C. Three-Dimensional Scaffolds for Tissue Engineering Applications: Role of Porosity and Pore Size. *Tissue Eng., Part B* **2013**, *19*, 485−502.

(38) Murphy, C. M.; O'Brien, F. J. Understanding the Effect of Mean Pore Size on Cell Activity in Collagen-Glycosaminoglycan Scaffolds. *Cell Adh. Migr.* **2010**, *4*, 377−381.

(39) Bracaglia, L. G.; Smith, B. T.; Watson, E.; Arumugasaamy, N.; Mikos, A. G.; Fisher, J. P. 3D printing for the Design and Fabrication of Polymer-Based Gradient. *Acta Biomater.* **2017**, *56*, 3−13.

(40) Rai, V.; Dilisio, M. F.; Dietz, N. E.; Agrawal, D. K. Recent Strategies in Cartilage Repair: A Systemic Review. *J. Biomed. Mater. Res., Part A* **2017**, *105A*, 2343−2354.

(41) Keaveny, T. M.; Morgan, E. F.; Yeh, O. C. Bone Mechanics. In *Standard Handbook of Biomedical Engineering and Design*; Kutz, M., Ed.; McGraw-Hill: New York, 2004; pp 8.1−8.23, ISBN:9780071356374.

(42) Hench, L. L. Genetic Design of Bioactive Glass. *J. Eur. Ceram. Soc.* **2009**, *29*, 1257−1265.

(43) Lam, C. X. F.; Teoh, S. H.; Hutmacher, D. W. Comparison of the Degradation of Polycaprolactone and Polycaprolactone−(β-Tricalcium Phosphate) Scaffolds in Alkaline Medium. *Polym. Int.* **2007**, *56*, 718−728.

(44) Qazi, T. H.; Hafeez, S.; Schmidt, J.; Duda, G. N.; Boccaccini, A. R.; Lippens, E. Comparison of the Effects of 45S5 and 1393 Bioactive Glass Microparticles on hMSC behavior. *J. Biomed. Mater. Res., Part A* **2017**, *105A*, 2772−2782.

(45) Yeh, C.-H.; Chen, Y.-W.; Shie, M.-Y.; Fang, H.-Y. Poly-(Dopamine)-Assisted Immobilization of Xu Duan on Printed Poly-(Lactic Acid) Scaffolds to Up-Regulate Osteogenic and Angiogenic Markers of Bone Marrow Stem Cells. *Materials* **2015**, *8*, 4299−4315.

(46) Rodríguez, J. P.; Ríos, S.; González, M. Modulation of the Proliferation and Differentiation of Human Mesenchymal Stem Cells by Copper. *J. Cell. Biochem.* **2002**, *85*, 92−100.

(47) Rath, S. N.; Brandl, A.; Hiller, D.; Hoppe, A.; Gbureck, U.; Horch, R. E.; Boccaccini, A. R.; Kneser, U. Bioactive Copper-Doped Glass Scaffolds Can Stimulate Endothelial Cells in Co-Culture in Combination with Mesenchymal Stem Cells. *PLoS One* **2014**, *9*, No. e113319.

(48) Komori, T.; Groner, Y.; Ito, Y.; Liu, P.; Neil, J. C.; Speck, N. A.; van Wijnen, A. Roles of Runx2 in Skeletal Development. *Adv. Exp. Med. Biol.* **2017**, *962*, 962.

(49) Lian, J. B.; Stein, G. S. Development of the Osteoblast Phenotype: Molecular Mechanisms Mediating Osteoblast Growth and Differentiation. *Iowa Orthop. J.* **1995**, *15*, 118−140 PMCID: PMC2329080 .

(50) Lian, J. B.; Stein, G. S.; van Wijnen, A. J.; Stein, J. L.; Hassan, M. Q.; Gaur, T.; Zhang, Y. MicroRNA Control of Bone Formation and Homeostasis. *Nat. Rev. Endocrinol.* **2012**, *8* (4), 212−227.

(51) Li, S.; Wang, M.; Chen, X.; Li, S.; Li-Ling, J.; Xie, H. Inhibition of Osteogenic Differentiation of Mesenchymal Stem Cells by Copper Supplementation. *Cell Proliferation* **2014**, *47*, 81−90.

(52) Bührer, G.; Rottensteiner, U.; Hoppe, A.; Detsch, R.; Dafinova, D.; Fey, T.; Greil, P.; Weis, C.; Beier, J. P.; Boccaccini, A. R.; Horch, R. E.; Arkudas, A. Evaluation of in vivo angiogenetic effects of copper doped bioactive glass scaffolds in the AV loop model. *Biomed. Glasses* **2016**, *2*, 111−117.